eman ta zabal zazu
Universidad del País Vasco
Euskal Herriko Unibertsitatea
MEDIKUNTZA ETA ERIZAINTZA FAKULTATEA
FACULTAD DE MEDICINA Y ENFERMERÍA

# Identifying alterations in RNA metabolism and translation dynamics of oligodendrocytes in Alzheimer´s disease

Adhara Gaminde Blasco
2023

Director:
Dra. Elena Alberdi Alfonso
Co-director:
Dra. Jimena Baleriola Gómez de Pablos

# Table of contents

# ABSTRACT

Oligodendrocyte dysfunction, myelin degeneration and alterations in the white matter structures are early events in Alzheimer's disease (AD) that might lead to cognitive deficits. One of the hallmarks of AD is the presence of extracellular aggregates of amyloid beta peptide (Aβ), and Aβ oligomers (Aβo) have been proposed to induce changes in oligodendrocytes and myelin. However, the effects of Aβo on oligodendrocytes are not fully understood. Here, we report that RNA metabolism and proteostasis regulation mechanisms significantly affected by Aβo in oligodendrocytes.

To gain more comprehensive insights into the impact of Aβo on oligodendrocytes, we performed RNA-seq in primary cultured cells treated with Aβo and controls. The differential expression analysis revealed that Aβo significantly altered signaling pathways associated with RNA metabolism. Likewise, by comparative analysis we showed that this pathway is also altered in triple transgenic AD (3xTg-AD) mice model and AD patient's oligodendrocytes. RNA-binding proteins (RBPs) are the main regulators of gene expression that control splicing, mRNA transport, translation and decay. Thus, to obtain a mechanistic understating of these cellular processes, we focus our study on heterogeneous nuclear ribonucleoprotein A2 (hnRNP A2), a key regulator of RNA metabolism that mediates intracellular trafficking of *Mbp* and *Mobp*, which are important proteins for oligodendrocytes and myelin formation. Indeed, western blot and immunocytochemistry analysis showed that hnRNP A2 was upregulated in oligodendrocytes of AD patients, 3xTg-AD mice and *in vitro* treated with Aβo. Using RNA-immunoprecipitation (RIP)-seq, we identified components of RNA-splicing, -processing and -binding, translational regulation and ribonucleoprotein complex biogenesis, as A2-interacting RNAs in oligodendrocytes. Upon Aβo treatment, the A2-interactome was significantly modified, suggesting that Aβo could be modulating the aforementioned pathways. Accordingly, we showed that overexpression of hnRNP A2 overlapped with an increase in number and dynamics of mRNA transport granules and local translation of MBP and MOBP. Interestingly, upregulation of MBP led to changes in calcium homeostasis, translation in cultured oligodendrocytes, and myelination in the 3xTg-AD mouse. Besides, we have also seen that Aβo are able to modify oligodendrocytes

morphology by altering its actin dynamics through a mechanism involving actin binding proteins. Finally, we also demonstrated that oligodendrocytes treated with Aβo secrete more extracellular vesicles (EVs), which consequently led to changes in neuron functions like, translation, synapsis and Aβ secretion.

Taken together, these results suggest that Aβo could alter oligodendrocyte basic functions through modification of hnRNP A2 interactome and MBP upregulation, with potential consequences in the oligodendrocyte-neuron interactions.

# ABBREVIATIONS

| | |
|---|---|
| **3xTg-AD** | Triple transgenic mouse model of AD |
| **3´UTR** | 3´untranslated region |
| **5XFAD** | Transgenic mouse model with five familial AD |
| **AAV** | Adenoassociated virus |
| **A2RE** | Cis-acting sequence A2-reponse element |
| **aCSF** | Artificial cerebrospinal fluid |
| **ACTB** | β-actin |
| **AD** | Alzheimer's disease |
| **AICD** | APP intracytoplasmic domain |
| **Akt** | Serine/threonine protein kinase |
| **ANOVA** | Analysis of variance |
| **ApoE** | Apolipoprotein E |
| **APP** | Amyloid precursor protein |
| **APP/PS1** | Double transgenic mouse model of AD |
| **ATP** | Adenosine triphosphate |
| **a.u.** | Arbitrary units |
| **Aβ** | Amyloid β peptide |
| **Aβo** | Amyloid–β oligomers |
| **BACE** | β-site amyloid precursor protein cleaving enzyme |
| **BP** | Biological processes |
| **bHLH** | Basic helix-loop-helix |
| **BSA** | Bovine serum albumin |
| **$Ca^{2+}$** | Calcium |
| **CAP** | Compound action potential |
| **Caspr** | Contactin associated protein 1 |
| **cDNA** | Complementary DNA |
| **CERAD** | Consortium to establish a registry for Alzheimer's disease |
| **CNPase** | 2´, 3´-Cyclic nucleotide-3´-phosphodiesterase |
| **CNS** | Central nervous system |
| **CNTF** | Ciliary neurotrophic factor |
| **COP** | Differentiation-committed oligodendrocyte precursor |
| **CSF** | Cerebrospinal fluid |
| **Ct** | Threshold cycle |
| **DAPI** | 4'-6-diamidino-2-phenylindale |
| **DEG** | Differentially expressed gene |
| **DG** | Dentate gyrus |
| **DIV** | Days *in vitro* |
| **DMEM** | Dulbecco's modified Eagle´s medium |
| **DMSO** | Dimethyl sulfoxide |
| **DNA** | Deoxyribonucleic acid |
| **DPF** | Days post fertilization |
| **EDTA** | Ethylenediamine tetraacetic acid |
| **ELISA** | Enzyme-linked immunosorbent assay |
| **EM** | Electron microscopy |

| | |
|---|---|
| **ER** | Endoplasmic reticulum |
| **EV** | Extracellular vesicle |
| **F-actin** | Filamentous actin |
| **FBS** | Fetal bovine serum |
| **FRAP** | Fluorescence recovery after photobleaching |
| **FTH1** | Ferritin heavy chain |
| **G-actin** | Globular actin |
| **GAPDH** | Glyceraldehyde-3-phosphate dehydrogenase |
| **GM** | Grey matter |
| **GO** | Gene ontology |
| **HBSS** | Hank's balanced salt solution |
| **HEPES** | 4-(2-hydroxyethyl)-1-piperazineethanesulfonic acid |
| **HFIP** | Hexafluoroisopropanol |
| **hnRNP** | Heterogeneous nuclear ribonucleoprotein |
| **Hp** | Hippocampus |
| **HPF** | Hours post fertilization |
| **HRP** | Horseradish peroxidase |
| **IP** | Immunoprecipitation |
| **Itgβ1** | Integrin β1 |
| **KCl** | Potassium chloride |
| **kDa** | Kilodalton |
| **LatB** | Latrunculin B |
| **lnRNA** | Long non-coding RNA |
| **MAG** | Myelin associated glycoprotein |
| **MBP** | Myelin basic protein |
| **MCI** | Mild cognitive impairment |
| **MCT** | Monocarboxylate transporter |
| **MOBP** | Myelin associated oligodendrocyte basic protein |
| **MOG** | Myelin oligodendrocyte glycoprotein |
| **MRI** | Magnetic resonance imaging |
| **mRNA** | Messenger ribonucleic acid |
| **Myrf** | Myelin regulatory factor |
| **NFT** | Neurofibrillary tangles |
| **NGS** | Normal goat serum |
| **NMDA** | N-methyl-D-aspartate |
| **NT-3** | Neurotrophin 3 |
| **OL** | Oligodendrocyte |
| **Olig1 and 2** | Oligodendrocyte transcription factor 1 and 2 |
| **OPC** | Oligodendrocyte progenitor cell |
| **ORG** | Organotypic culture |
| **PB** | Phosphate buffer |
| **PBS** | Phosphate saline buffer |
| **PCL** | Polycaprolactone |
| **PDGFR-α** | Platelet-derived growth factor receptor-α |
| **PDL** | Poly-D-Lysine |
| **PFA** | Paraformaldehyde |
| **PLA** | Proximity ligation assay |

| | |
|---|---|
| **PLP** | Myelin proteolipid protein |
| **P/S** | Penizilin and streptomycin |
| **PSD95** | Postsynaptic density protein 95 |
| **PSN 1 and 2** | Presenilin 1 and 2 |
| **RIP** | RNA-immunoprecipitation |
| **RNA** | Ribonucleic acid |
| **ROI** | Region of interest |
| **RT** | Room temperature |
| **RT-qPCR** | Real Time Quantitative Polymerase Chain Reaction |
| **S.E.M.** | Standard error of the mean |
| **SDS** | Sodium dodecyl sulfate |
| **SDS-PAGE** | SDS polyacrylamide gel electrophoresis |
| **SFK** | Src family kinase |
| **siRNA** | Small interfering RNA |
| **SIRT2** | Deacetylase sirtuin 2 |
| **sncRNA** | Small non-coding RNA |
| **T3** | Triiodotironine |
| **T4** | L-Tryroxine |
| **TBS** | Tris-buffered saline |
| **TSG 101** | Tumor susceptibility gene 101 |
| **VGCC** | Voltage gated calcium channel |
| **WB** | Western blot |
| **WM** | White matter |
| **WT** | Wild type |

# INTRODUCTION

## 1. Oligodendrocytes

More than half of the human brain volume is made up of white matter (WM), which enables fast and efficient nerve conduction, required for a proper cognitive function in the central nervous system (CNS). White matter refers to areas of the CNS that are mainly made up of myelinated axons, also called tracts. Oligodendrocytes (OL) extend membrane processes to wrap the axons of multiple neurons and generate and maintain highly specialized multilamellar lipid structure around axons, known as myelin, which gives the WM its colour. Thus, OL provide neurons with trophic and metabolic support essential for their survival and promote rapid saltatory conduction by concentrating voltage-dependent sodium channels at the periodic gaps in the insulating myelin sheath called nodes of Ranvier (Moore et al., 2020; Nave, 2010).

Myelin formation starts in rodents at about birth and is completed around 2 months after birth. In humans, it takes place largely within the first 2 years of life, but white matter volume increases up until around mid-life as new axonal projections become myelinated. Myelin is continuously exchanged and renewed being highly plastic, modifiable by experience, and seems to play important roles in learning and memory, and normal cognitive function (Fields, 2008).

### 1.1 Oligodendrocyte differentiation

Oligodendrocytes are one of the major glial cell types in the CNS along with microglia and astroglia. They derive from specific neural progenitor cells; oligodendrocyte progenitor cells (OPCs; also called NG2-glia). During development, OPCs migrate to populate the developing white matter, where they proliferate and form an evenly spaced network of processes. After migrating and establishing in a suitable region, some OPCs remain in a precursor state and others differentiate into myelin-forming oligodendrocytes providing a continuous source of new mature oligodendrocytes. This process called oligodendrogenesis, undergoes three canonical stages: the OPCs, the premyelinating oligodendrocytes (preOL) and the myelinating oligodendrocytes (OL).

The specific phenotypic stages are defined by the sequential expression of molecular markers and morphology (Baumann & Pham-Dinh, 2001) **(Figure 1)**. OPCs migrate and proliferate, and are mainly characterized by expressing platelet-derived growth factor receptor-α (PDGFR-α) and have a bipolar or stellate shape. Following lineage progression, OPCs differentiate into premyelinating or immature oligodendrocytes which develop a highly branched morphology aiming to reach axons. At this differentiation stage, pre-oligodendrocytes are characterised by the expression of three main myelin associated markers, 2', 3'-cyclic-nucleotide 3'-phosphodiesterase (CNPase) and the cell surface markers O4 and O1. Finally, these cells differentiate into myelinating or mature oligodendrocytes, which are characterised by the production of myelin and myelin proteins including myelin basic protein (MBP), proteolipid protein (PLP), myelin-associated oligodendrocyte basic protein (MOBP), myelin associated glycoprotein (MAG) as well as myelin-oligodendrocyte glycoprotein (MOG). They contain myelin sheaths, rod-like processes that orientate parallel in the white matter and randomly in the grey matter (Young et al., 2013).

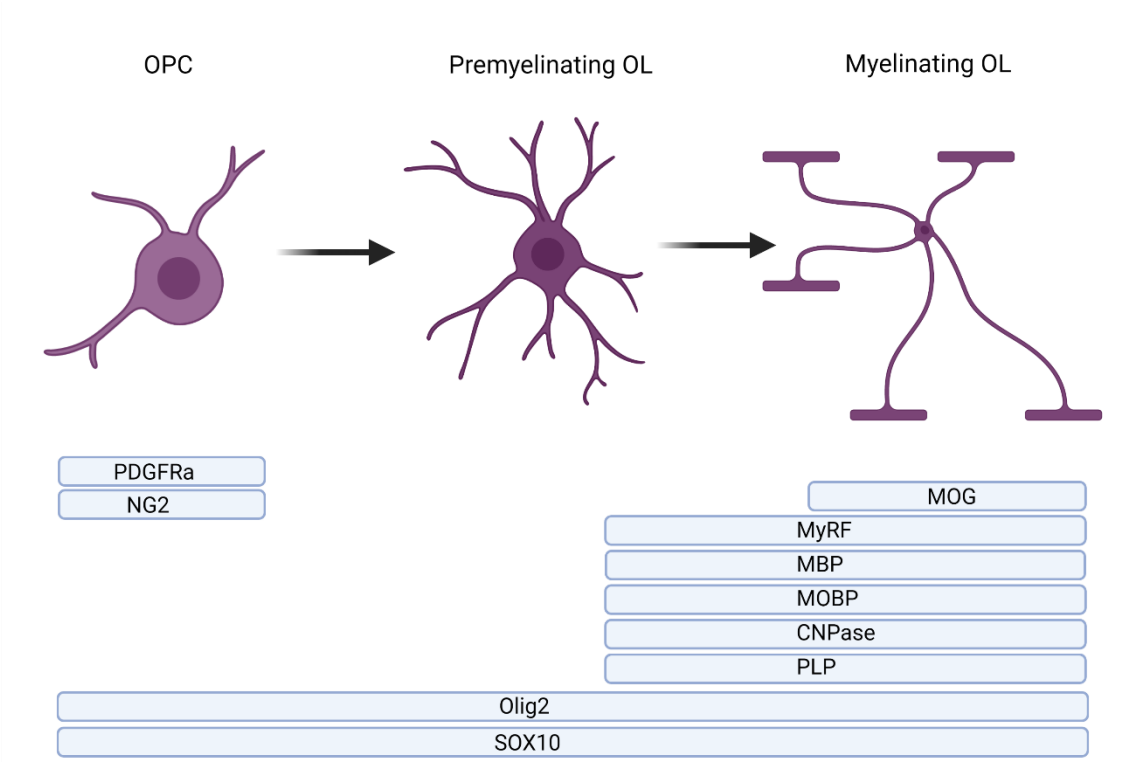


***Figure 1. Oligodendrocyte differentiation stages.*** *Cells of oligodendroglial lineage can be subdivided into three stages of differentiation based on protein expression: oligodendrocyte progenitor cells (OPCs), premyelinating oligodendrocytes and myelinating oligodendrocytes. Essentially all OPCs co-express the*

*NG2 proteoglycan and PDGFRα. Premyelinating oligodendrocytes upregulate Myelin Regulatory Factor (MyRF). Myelinating oligodendrocytes express myelin-related proteins including MBP, MOBP, PLP, CNPase and MOBP. MOG is the last one to be expressed by oligodendrocytes. All cells of the oligodendroglial lineage express the transcription factors OLIG2 and SOX10. Adapted from Pepper et al., 2018. Illustration done in BioRender.*

Nevertheless, the molecular and cellular mechanisms underlying these phenotypic differences are unclear. Recent advances in single-cell transcriptomics have revealed that there are distinct oligodendrocyte populations, suggesting possible functional heterogeneity (Marisca et al., 2020; Marques et al., 2016). In total, 12 different populations, representing a continuum from OPC to mature OLs have been reported: OPCs, differentiation-committed oligodendrocyte precursors (COPs), newly-formed oligodendrocytes (NFOLs 1-2), myelin-forming oligodendrocytes (MFOLs 1-2), and mature oligodendrocytes (MOLs 1-6). Whereas OLs at early maturation stages are found sequentially and uniformly across CNS regions, mature OLs show regional specificity, being present in unique proportions in each brain region (Marques et al., 2016).

Oligodendrocyte differentiation is actively regulated by various transcription factors that control all the stages of the process. Positive regulators are myelin regulatory factor (Myrf), Olig1/2, Sox2/3/10 and Nkx2.2 that interact synergistically to drive the maturation process (Elbaz & Popko, 2019). Olig2 is expressed through all oligodendrocyte lineage, being its levels progressively decreased at mature stages (Kitada & Rowitch, 2006), whereas Myrf is specifically induced during OL differentiation. It has been shown that Hes family basic helix-loop-helix (BHLH) transcription factors-1/5 (Hes1/5) and Id2/4 act as negative regulators binding directly to pro-differentiation factors such as oligodendrocyte transcription factor 1 (Olig1) and Sox10 to inhibit their function (Liu et al., 2006; Samanta & Kessler, 2004).

### 1.2 Oligodendrocyte morphology

Morphologically, OLs are one of the most versatile and complex cells of the CNS. OPCs evolve into myelinating OLs, which extend a complex and expanded process network that leads to myelin sheath formation. Mechanical transitions during OPC differentiation

into myelinating OLs represent one of the most significant shifts in cell remodelling, which is tightly regulated spatially and temporally by a dynamic interplay between actin, myosin-II motors and microtubules, and cell membrane adhesion complexes. Filamentous actin (F-actin) is more dynamic than microtubules and have a higher turnover rate and faster reorganization potential, enabling cells to rapidly change their shape and migrate. The restructuration of the actin cellular network governs morphological plasticity in oligodendrocytes (Song, Goetz, Baas, & Duncan, 2001), which is important for their development and maturation.

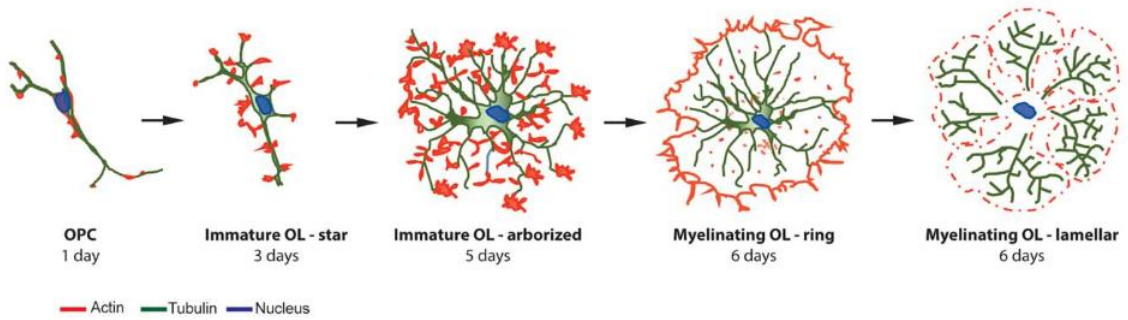


***Figure 2. Spatiotemporal distribution and dynamics of the cytoskeleton during in vitro OL differentiation and myelination.*** *Organization of actin and microtubules in developing OL. In vitro differentiation of a mouse/rat OPC into myelinating OL takes approximately 6 days and requires extensive remodelling of the actin and tubulin cytoskeleton. Adapted from Domingues et al., 2017.*

*In vitro*, during the first days of OL differentiation of murine cells, extension of membrane protrusions and arborization seem to be highly dependent on actin and tubulin polymerization. Actin filaments are mainly present at the protrusion´s leading edge while microtubules are also present in the cell body **(Figure 2)**. *In vitro* OL maturation is usually reached between 5–7 days of culture, where more distal interbranch connections of actin are established with fewer invasions of microtubules. In this phase, an increased actin depolymerization rate allows the conversion of protrusions into sheets accompanied by significant changes in cell stiffness (Domingues et al., 2018; Thomason, Escalante, Osterhout, & Fuss, 2020).

### 1.3 Oligodendrocytes functions

The main function of OLs is the formation of the myelin sheath around the axon **(Figure 3)**. Functionally, myelin enables maximum conduction velocity and reduces axonal energy consumption (Crotty, Sangrey, & Levy, 2006; Waxman, 1997). In fact, axonal insulation by myelin membrane restricts their energy requirements and accelerates nerve conduction 20-100-fold in comparison with non-myelinated axons. Moreover, oligodendrocytes generate up to 80 different myelin sheaths on various axonal areas (internodes), depending on several factors as axon calibre and length (Snaidero & Simons, 2014). In this regard, most oligodendrocytes myelinating large calibre axons develop fewer internodes, which are longer and have thicker myelin sheath.

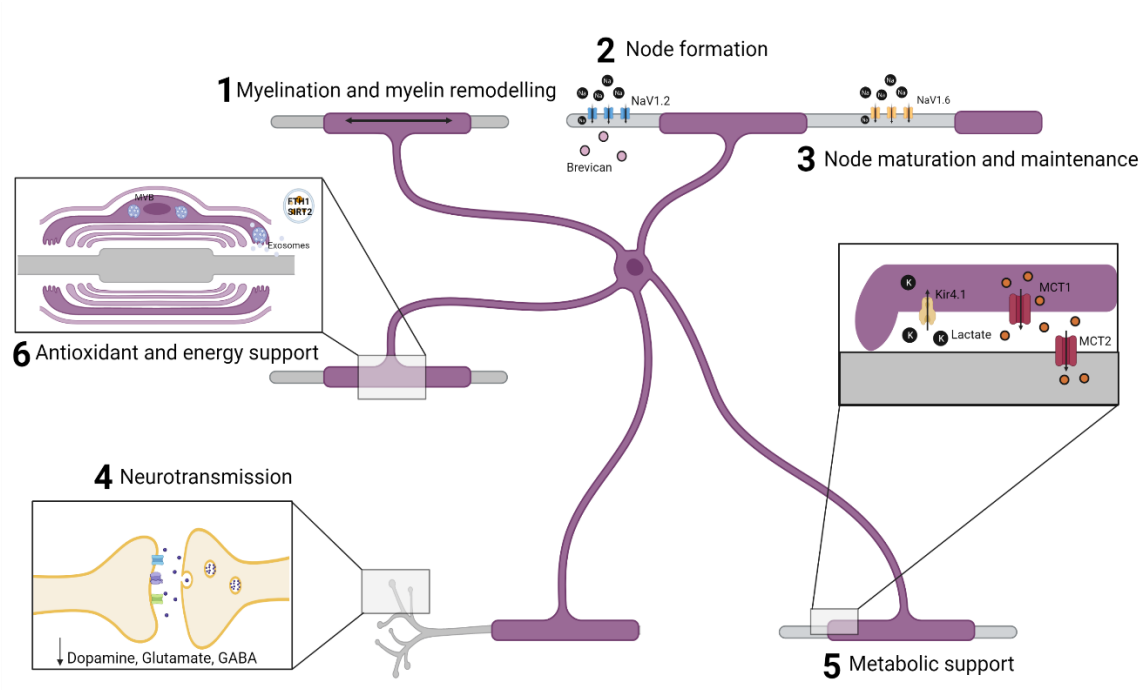


***Figure 3. Oligodendrocytes perform multiple functions in the developing and adult CNS.*** *(1) Oligodendrocytes elaborate and remodel myelin internodes. (2, 3) Oligodendrocytes secrete extracellular matrix molecules, such as brevican, which trigger the clustering of NaV1.2 into pre-nodes. Myelination is also important for nodal maturation (NaV1.2 is exchanged for NaV1.6) and nodal maintenance. (4) Oligodendrocytes and their myelin modulate neuronal excitability and neurotransmitter release. (5) Oligodendrocytes provide lactate to axons via the periaxonal space and remove K+ ions. (6) Oligodendrocytes secrete EVs containing molecules like FTH1 and SIRT2 to provide them with energy and antioxidant support. Adapted from Pepper et al., 2018. Illustration done in BioRender.*

In addition to electrical insulation of axons, oligodendrocytes and myelin sheaths metabolically support axons **(Figure 3)**. Oligodendrocytes can generate lactate or pyruvate and transfer them to neurons through monocarboxylate transporter 1 (MCT1) located at the uncompacted inner tongue of the myelin sheath. Then, lactate is taken up by neurons, which catabolize it to generate ATP. Other metabolites, nutrients and signalling molecules are transported from oligodendrocyte somata to axons through non-compacted areas, called myelin cytoplasmatic channels, in order to support axonal activity (Nave & Werner, 2014). In fact, loss of cytoplasmatic channels is observed in CNPase-null mice, which develop a progressive axonal degeneration with a far more compacted myelin. In contrast, MBP-null mice (shiverer mice) develop a severe demyelination but preserve the axonal integrity and function, likely due to the maintenance of the glia-driven metabolic support from the thin, uncompacted myelin process. These observations in knockout mice for specific oligodendrocyte proteins suggest that the absence of myelin is better than the presence of defective one for sustaining proper axonal functions, as defective myelin is associated with oligodendrocyte-axon metabolic support disconnection (Philips & Rothstein, 2017).

It has also been recently described that oligodendrocytes provide axonal support via transcellular delivery of EVs **(Figure 3)**. In fact, oligodendrocytes provide antioxidant defence for neurons by secreting exosomal ferritin heavy chain (FTH1) into the extracellular space. This secretion is thought to be a protective mechanism against oxidative stress in aging (Mukherjee et al., 2020). What´s more, they also deliver NAD-dependent deacetylase sirtuin 2 (SIRT2), which enhances neuronal ATP production by deacetylating mitochondrial proteins boosting axonal bioenergetics under pathological conditions (Chamberlain et al., 2021).

## 2. Oligodendrocyte myelination

Myelination is a precise and coordinated multi-step process that supports the smooth functioning and development of the CNS. In order to ensure the optimal function of this process, myelination is tightly regulated by several signals that control both initial formation and maintenance of myelin sheaths.

Equipped with molecules needed for myelination, mature oligodendrocytes extent their processes to contact axons and then ensheath and wrap around them. Various models have been proposed to explain the mechanism underlying myelin wrapping. The most accepted model is described as oligodendrocytes first forming a triangular membrane that simultaneously expands around and along the axon in a coordinated bi-directional movement. In this process, oligodendrocytes rapidly reorganize their cytoskeleton and increase microfilament polymerization and branching in response to axon-oligodendrocyte recognition (Snaidero et al., 2014). Data from the last decade demonstrate that actin polymerization drives the early stages of cell differentiation and that its depolymerization is a crucial element driving myelination.

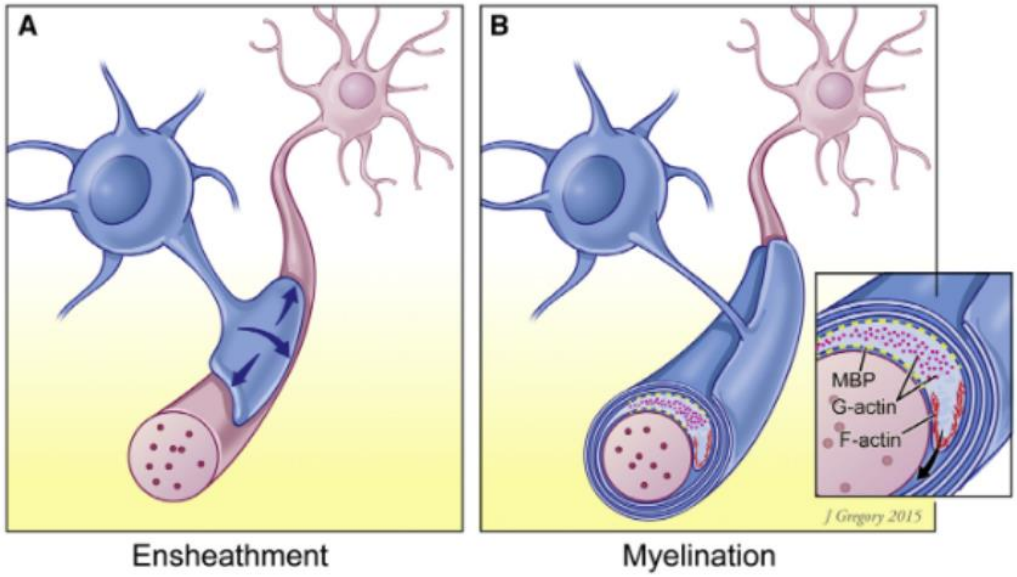


***Figure 4. Ensheathment and myelination by actin dynamics.*** *Schematic representation of (A) an oligodendrocyte process at an early stage of axon ensheathment, when F-actin predominates and promotes ensheathment, and (B) a process actively myelinating an axon in which actin depolymerization, mediated by gelsolin and ADF/cofilin, predominates. The leading edge of the inner turn is shown as expressing F-actin subcortically, whereas in regions enriched in MBP (shown in yellow), G-actin predominates, which is proposed to result from indirect activation of depolymerisation. Adapted from Samanta and Salzer, 2015.*

First, the contact with axons and process expansion is driven by Arp2/3-dependent actin polymerization at the leading edge of lamellipodium-like structures of oligodendrocyte protrusions. Then, actin depolymerization via ADF/cofilin1 at the backside of protrusions decreases surface tension on the membrane promoting lateral expansion of myelin

sheaths during wrapping and compaction. In the mature myelin sheath, MBP in the membrane competes with ADF/cofilin1 for binding to PI(4,5)P2, triggering the release of this protein into the cytosol and activating actin disassembly that promotes membrane deformation and compaction. Finally, the F-actin rich inner-tongue pushes under pre-existing membrane. This way, the axon is wrapped in progressive membrane layers where the outermost layer is closer to oligodendrocyte cell body and innermost layer is in direct contact with the axon (Nawaz et al., 2015; Samanta & Salzer, 2015; Zuchero et al., 2015) **(Figure 4)**. In the last years additional mechanisms which control myelination have emerged. A recent study demonstrates that VAMP2/3-mediated exocytosis is necessary for myelin membrane expansion and formation of Nodes of Ranvier (Lam et al., 2022).

*In vitro*, oligodendrocytes have the intrinsic property to wrap myelin in a neuron-independent manner on nanofibers (Bechler, Byrne, & Ffrench-Constant, 2015; Lee et al., 2012). However, *in vivo*, myelin is targeted with remarkable specificity only to certain axons depending on their biophysical properties (e.g axon size), and on permissive and repulsive signals **(Figure 5)**. The amount of myelin adapts to the size and requirement of axons by responding to signalling pathways induced in the latter. (Almeida, 2018; Snaidero & Simons, 2014). All these signals are integrated by oligodendrocytes and in turn control neuronal responses. A key neuronal signal integrator is Fyn, a member of the Src family of cytoplasmic nonreceptor tyrosine kinase family, whose expression is predominant and upregulated during oligodendrocyte differentiation and is essential for myelination and MBP translation (Krämer-Albers & White, 2011; Osterhout, Wolven, Wolf, Resh, & Chao, 1999) Moreover, *in vivo* studies have demonstrated the importance of Fyn as a mediator of myelin formation, since Fyn-deficient transgenic mice are characterized by impaired myelination and abnormal oligodendrocyte development (Sperber & McMorris, 2001). In addition, analysis in the zebrafish model showed that activation and reduction of Fyn kinase in oligodendrocytes increases and decreases sheath number per cell, respectively (Czopka, Ffrench-Constant, & Lyons, 2013).

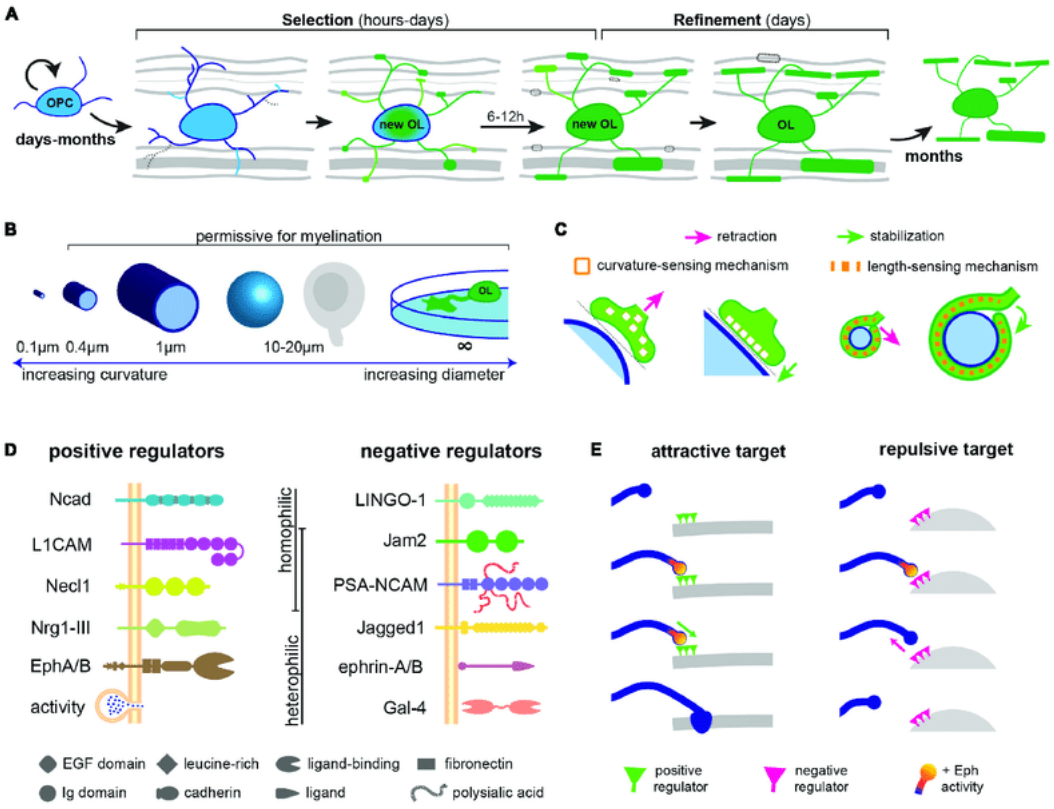


***Figure 5. Regulation of CNS myelin targeting. (A)*** *Myelin is targeted in a short period in the life of an oligodendrocyte and appears to include two stages: (1) a target selection stage during differentiation and formation of nascent sheaths and (2) a target refinement stage after differentiation, when some sheaths are retracted. Then, oligodendrocytes and their myelin are stable for many months.* ***(B)*** *Biophysical properties such as axon diameter and/or curvature determine the permissiveness of a target for myelination.* ***(C)*** *Curvature or length-sensing proteins in oligodendrocyte processes may sense appropriately sized targets.* ***(D)*** *Attractive and repulsive cell-adhesion molecules on prospective targets regulate CNS myelination.* ***(E)*** *Similar to synapse formation, the temporal dynamics of key signalling pathways may determine the fate of OPC processes during myelin target selection. Adapted from Almeida et al., 2018.*

Nevertheless, the complex structural organization of myelin is not easily coordinated and is prone to errors. Recent studies have documented a number of ultrastructural myelin abnormalities, such as outfoldings, bulging, fragmentation, and splitting, that arise during early myelination but are rapidly resolved as development progresses. This is done by microglia that modulate myelin organization, and correct errors in myelin formation during development (Hughes & Appel, 2020) but also preserve myelin health and integrity in adulthood (McNamara et al., 2022).

## 2.1 Myelin

The myelin sheath is an extension of the oligodendrocyte plasma membrane that wraps axons in the CNS. The multi-layered myelin membrane displays a distinct and complex multi-protein structure. The term myelin was coined by Rudolf Virchow in 1864 and comes from Greek word for marrow (myelos).

Electron microscopy studies show that myelin spiralling pattern around axons generates two periodic morphological features; (1) the electro-dense layer (major dense line), which represents the tight condensed zone of the cytoplasmic leaflets, and (2) the electron-light layer (intraperiod line), which is in apposition to the extracellular leaflets (Hartline, 2008). The compaction between the membranes in each of these layers results in repeated patterns of 12 nm and provides high electrical resistance and low capacitance, essential for propagation of axon potentials.

The myelinated segments along axons have periodic gaps (nodes of Ranvier), small areas lacking myelin exposed to the extracellular space and enriched in sodium channels. The action potential propagated by one node of Ranvier jumps to and is regenerated at the next node along the axon, thereby enabling the action potential to travel rapidly along the fibre (Waxman & Ritchie, 1993). At the edges of each myelin segment, individual myelin lamellae attach to the axon by forming specialized septate-like junctions, known as paranodes. Paranodes are maintained by the adhesion of a tripartite complex of cell adhesion molecules, composed of contactin-1 and Caspr proteins on the axonal surface and Neurofascin-155 at the glial side (Stadelmann, Timmler, Barrantes-Freer, & Simons, 2019) **(Figure 6)**.

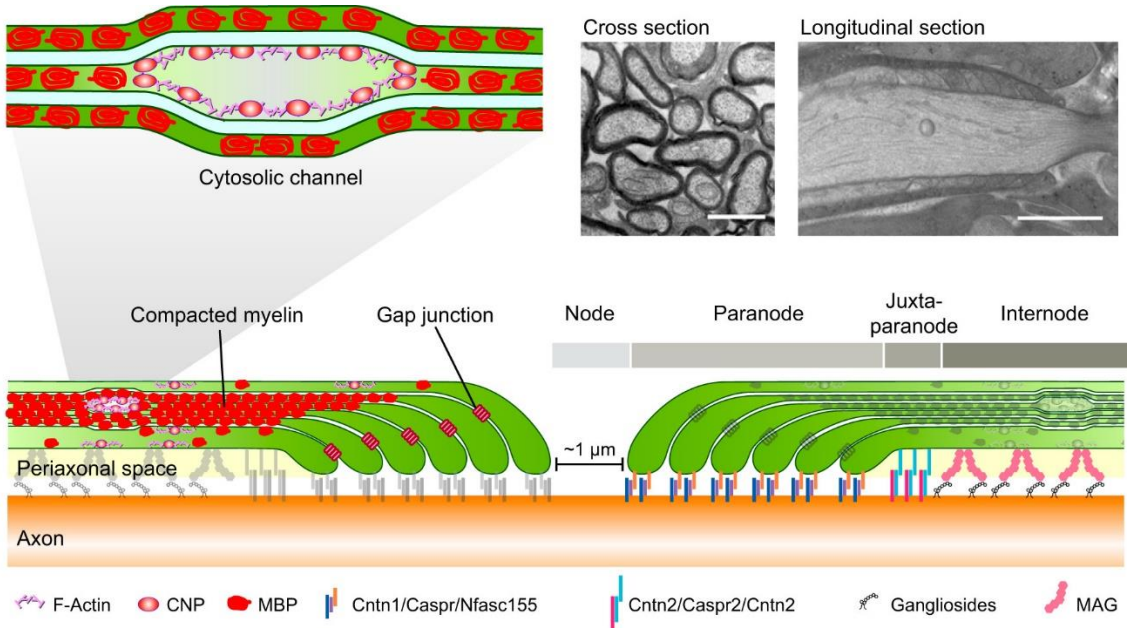


***Figure 6. CNS myelin structure.*** *Graphical illustration of myelin structure including the different domains of myelinated axons. MBP is essential in generating compacted myelin membrane stacks by zippering the cytoplasmic surfaces closely together. CNPase interacts with the actin cytoskeleton and counteracts the polymerizing forces of MBP, thereby generating cytoplasmic channels within the myelin sheath. Gap junctions connect the paranodal loops of myelin at the lateral edges of myelin. Adapted from Stadelmann et al., 2019.*

In addition to myelin membrane ultrastructure, its specialized composition makes myelin a unique membrane in the CNS. While most plasma membranes are composed of 50% proteins and 50% lipids in dry weight, the myelin sheath is poorly hydrated containing high proportion of lipids (70%–85%) and consequently a low proportion of small proteins (15%–30%), being MBP and PLP the major ones. The high lipid/protein ratio in myelin contributes to the compaction and tight organization of the myelin sheath through non-covalent interactions between lipids and myelin proteins (Min et al., 2009). Myelin membrane components, like myelin proteins and lipids, have half-lives of approximately several weeks to months making it a highly stable structure. Apart from proteins, myelin is also enriched in mRNAs encoding for myelin related proteins, components of the translational machinery and molecules required for protein transport and localization. The existence of this transcript pool may suggest that local translation at myelin sheath enables efficient turnover without the need of using the slower intracellular protein transport (Thakurela et al., 2016).

## 2.2 Myelin compaction

The formation of tight barriers and compacted layers of insulating membrane are needed to prevent ion leakage. Myelin compaction is mediated by MBP and occurs early in development. The compaction starts in the outermost layers and progresses inward both radially and longitudinally in parallel with membrane growth. *Mbp* mRNA is transported from the nucleus to the innermost layers and there, close to the axons, it is translated. To prevent premature compaction at the inner tongue, the myelin membrane-associated enzyme CNPase, antagonizes MBP activity by acting as a spacer between two adjacent cytoplasmatic membranes and preventing excessive membrane compaction. This way, cytoplasmic regions are maintained intact in the adult myelin sheath (Snaidero et al., 2017).

## 2.3 Myelin turnover and plasticity

Myelin is a dynamic structure with adaptive capacity to respond to neuronal activity changes. Interestingly, the behaviour of OPCs can be controlled by neurotransmitters and by surrounding neuronal demands. For example, in the presence of higher neural activity, oligodendrocytes change the amounts of myelin sheaths, which affects the electrical transmission of the neuronal network (Fields, 2015). This plasticity enables myelin to modulate information processing and network activity during adult life (Fields, 2008). Myelin synthesized during development is continuously exchanged and renewed and removal of modified toxic components or myelin disposal is considered as a part of myelin turnover. Recently, Aber *et al*., 2022 reported that OLs use macroautophagy for myelin turnover enabling functional neuronal circuitry maintenance and CNS health (Aber et al., 2022). The maintenance of pre-existing myelin sheaths by mature oligodendrocytes involves slow but constant replenishment and degradation of myelin constituents and thus life-long turnover of myelin sheaths (Williamson & Lyons, 2018).
It has been recently shown that mature oligodendrocytes persist life-long in mice as well as in humans (Tripathi et al., 2017; Yeung et al., 2014) and that myelin sheaths are remarkably stable once formed with little fluctuation in length. Accordingly, myelin proteins are characterized by slow turnover, with lifetimes in the range of weeks or months (Fornasiero et al., 2018). The newly synthesized myelin sheaths by adult-born

oligodendrocytes are suggested to be incorporated into the pre-existing myelin sheath through myelin sheath replacement or myelin remodelling or they can be used for *de novo* myelination of previously naked axons (Wang & Young, 2014). A study recent has shown that continuous myelin synthesis at the inner tongue is needed to maintain the integrity of the white matter, (Meschkat et al., 2022).

# 3. Myelin basic protein

MBP is one of the major structural components in the CNS myelin; it makes up about 30% of total protein and about 10% of the dry weight of myelin. So far, it is the only essential protein needed for the formation of myelin in the CNS and that is why it has been referred to as an "executive molecule" (Moscarello, M.A. et al., 1997). This essential role was first demonstrated in the naturally occurring mutant *shiverer* mice, where a large proportion of MBP is absent and consequently severe hypomyelination can be observed (Boggs, 2006).

*Mbp* sequence is very highly conserved among several species and the transcript variants can be categorized into two main families, Classic and Golli-MBP (Genes of oligodendrocyte Lineage). Classic-MBP isoforms are found in mature oligodendrocytes and myelin sheaths, and plays a key role in compaction and stability of myelin around axons. In contrast, Golli-MBP isoforms, are ubiquitously expressed through early developing oligodendrocytes, neurons and immune cells (Boggs, 2006).
In classic MBP, alternative splicing of a single *Mbp* primary transcript leads to various isoforms in the 14-21 KDa range in rodents and 17-21.5 KDa in humans. The classic 18.5 kDa MBP variant is the predominant isoform in adult humans and bovines, whereas the 14 KDa variant is predominantly found in rats and mice. These diverse, complex and dynamic spectrum of variants give rise to the MBP proteome, from which protein isoform plays a specific role in oligodendrocytes.

## 3.1 MBP function

MBP is a multifunctional protein whose main role is to control the proper compaction of the forming myelin sheaths around the axons in the CNS. It acts as a zipper by bringing

the cytoplasmic leaflets together. To do so, MBP carries positive electrostatic charges that interacts with the negatively charged headgroups of phospholipids in the inner leaflet, leading to the compaction of the two opposing cytoplasmic membrane layers (Bakhti, Aggarwal, & Simons, 2014; Boggs, 2006; Harauz & Boggs, 2013). Notably, MBP undergoes various post-transcriptional modifications which are important for its multifunctionality (Harauz & Musse, 2007). Moreover, increasing evidence of other important functions of MBP has more recently emerged. These include a role in regulating the composition and organization of the myelin membrane (Fitzner et al., 2006; Aggarwal et al., 2011; Steshenko et al., 2016), reorganization of the actin cytoskeleton during the myelination process (Zuchero et al., 2015), calcium homeostasis (Smith et al., 2011) and a suggested role in cell signalling pathways through interactions with SH3 domain-containing proteins (Harauz, Ladizhansky, & Boggs, 2009).

### 3.2 MBP synthesis: mRNA transport and translation

The synthesis of MBP protein is an essential step during oligodendrocyte maturation and myelin formation and has been shown to be precisely regulated on the posttranscriptional level. *Mbp* mRNA was one of the first mRNAs described to be transported and locally translated in the myelin compartment (Ainger et al., 1993; Colman, Kreibich, Frey, & Sabatini, 1982). To ensure the rapid and efficient transport of MBP to the myelin compartment, *Mbp* mRNA is transported into granules from the nucleous into the most distal regions of oligodendrocytic processes and into the myelin membrane where it is locally translated. mRNA localization is considered an efficient mechanism used to spatially and temporally control the expression of certain proteins and to avoid ectopic translation elsewhere within the cell. In oligodendrocytes, this process starts with the binding of the transacting factor heterogeneous nuclear ribonucleoprotein A2/B1 (hnRNP A2/B1) to cis-acting sequence A2-reponse element (A2RE) (Hoek, Kidd, Carson, & Smith, 1998). This binding is needed for the co-assembly of *Mbp* mRNA into granules. Furthermore, homotypic hnRNP A2 interactions provide the driving force for co-assembly of multiple RNA copies into the same granule (Carson, Worboys, Ainger, & Barbarese, 1997), increasing the efficiency of the transport system. Once in the cytoplasm, different transacting factors interact simultaneously with the RNA granule via hnRNP A2 or RNAto regulate controlled and localized protein synthesis

(Table 1 AND Figure). hnRNP A2 binds to the microtubule associated tumor overexpressed gene (TOG) protein which might serve as a hub for multiplexing several hnRNP A2 proteins into the granule (Kosturko, Maggipinto, D'Sa, Carson, & Barbarese, 2005). Alike, the A/B type hnRNP CBF-A binds to *Mbp* mRNA and plays a role in the control of *Mbp* mRNA transport and localization (Raju et al., 2008). hnRNE1 (or PCBP1) together with the small non-coding RNA 175 ( sncRNA 175) inhibits translation during transport by binding to a specific region in the 3´UTR of *Mbp* (Bauer et al., 2012; Kosturko et al., 2006) Finally, hnRNPF binds to hnRNPA2 and is involved in the modulation of MBP translation once the mRNA reaches its final destination (Torvund-Jensen, Steengaard, Reimer, Fihl, & Laursen, 2014; White et al., 2012).

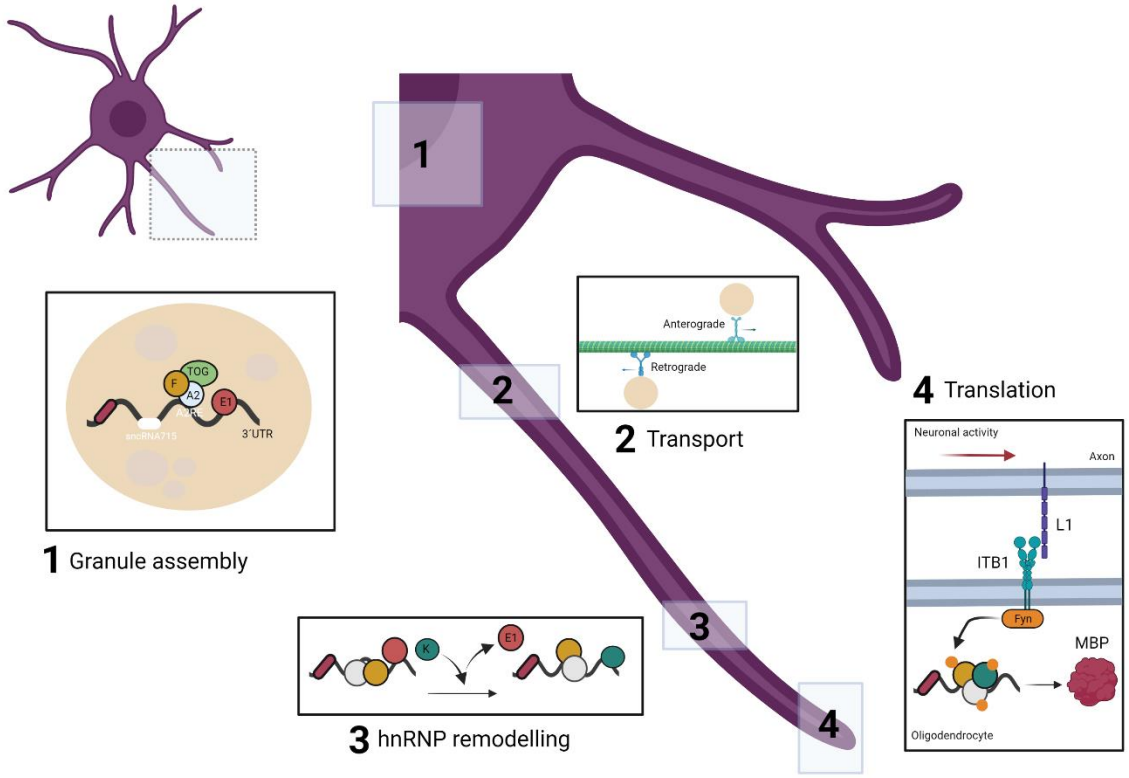


***Figure 7. Transport and localized translation of MBP.*** *Mbp mRNA is assembled into granules containing RNA binding proteins, motor proteins and parts of the protein synthesis machinery (1), then it is transported by microtubules toward the oligodendroglial periphery (2). Before translation, the RNA granule complex undergoes a remodelling exchanging E1 for K (3). Finally, at the plasma membrane, Fyn kinase transduces axonal signals leading to MPB localized translationin oligodendrocytesP (4). Illustration done in BioRender.*

All the elements aforementioned **(Table 1)** form a supramolecular membraneless complex that is transported by microtubules through the major oligodendrocyte processes in a bidirectional manner (anterograde and retrograde) associating with motor proteins kinesin and dynein/dynactin (Carson et al., 1997; Herbert et al., 2017; Lyons, Naylor, Scholze, & Talbot, 2009). Once in the periphery, hnRNP E1 exchanges for hnRNP K, which is a prerequisite for the targeting of the mRNA to the myelin sheath and ttranslation initiation (Torvund-Jensen et al., 2014). Specifically, hnRNP K competes with hnRNPE1 for *Mbp* mRNA binding to counteracting its effect. Then, neuronal activity stimulates MBP synthesis by a mechanism that involves upregulation of adhesion molecule laminin-1 on the axonal surface that causes Fyn activation. The activation of Fyn induces the phosphorylation of hnRNP A2 and hnRNP F leading to *Mbp* translation at the axon-glia contact site **(Figure 7)**.

MBP synthesis is also regulated by transcription factors as cAMP response element-binding (CREB) which may be phosphorylated by CaMKII, PKC and growth factor-induced kinases like ribosomal S6 kinase (Afshari, Chu, & Sato-Bigbee, 2001).

***Table 1.*** *Summary of the Mbp RNA granule components.*

| Molecule | Binding region | Function | References |
|---|---|---|---|
| hnRNP A2 | A2RE within RTS in 3´UTR | Granule assembly and cytoplasmic transport | Hoek et al. (1998) |
| hnRNP K | Specific recognition site in 3´UTR | Translation | Laursen et al. (2011) & Torvund-Jensen et al. (2014) |
| hnRNP F | Presumably via hnRNPA2 | Translation | White et al., (2012) |
| hnRNP E1 | Presumably via hnRNPA2 and specific site important for the tranlation in 3´UTR, shared with hnRNPK | Translation repression during transport | Kosturko et al., (2005) & Torvund-Jensen et al. (2014) |
| hnRNP CBF-A | RTS in 3´UTR | | Raju et al 2008 |
| SncRNA 715 | Specific recognition site in 3´UTR | Translation repression during transport | Bauer et al., (2012) |
| TOG | Presumably via hnRNPA2 | Transport, regulation of kynesin activity, Translation | Kosturko et al. (2006) |
| Ago2 | Via hnRNPA2 | Translation | Muller et al. (2015) |
| DDX5 | | Splicing | Hoch-Kraft et al. (2018) |

# 4. Alzheimer´s disease

Alzheimer´s disease (AD) is the leading cause of dementia and accounts for an estimated 60-80% of all cases. AD has been well-characterized as a disease involving primary pathologies of intracellular neurofibrillary hyperphosphorylated tau tangles and extracellular insoluble aggregates of the amyloid beta (Aβ) peptide called senile plaques **(Figure 8)**. At present, there is no cure, although there are palliative treatments available that may improve some symptoms. Pharmaceuticals have been developed to target these hallmark pathologies, but even therapeutics successful at reducing Aβ plaque load have been unable to sufficiently halt disease progression. Recently, it was proposed that the only FDA-approved amyloid-targeting drug, Aducanumab, might be more efficacious when combined with drugs that target oligodendrocytes and promote remyelination (Fessel, 2022).

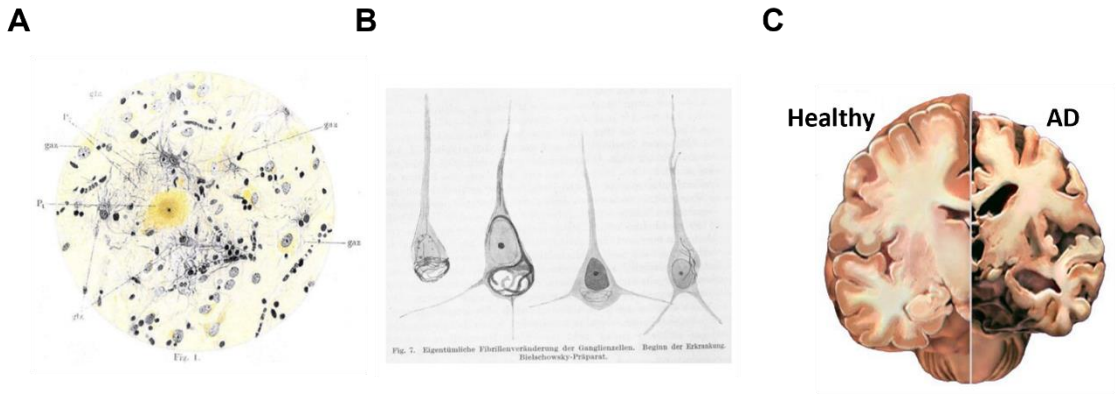


***Figure 8. AD pathological features.*** *Drawings of Alois Alzheimer showing senile plaques composed by amyloid β peptide* ***(A)*** *and neurons with intracellular tangles* ***(B)*** *present in AD patients.* ***(C)*** *Brain atrophy in AD brain compared with healthy brain.*

AD is a neurodegenerative disorder characterized by a profound cognitive decline occurring as a consequence of a progressive and irreversible neuronal loss. These neurodegenerative events developed in AD patients follow a well-established anatomical pattern. Amyloid deposits spreads from neocortex to allocortical regions to brainstem, eventually reaching the cerebellum (Thal, Rüb, Orantes, & Braak, 2002). Conversely, neurofibrillary tangles spreading starts in the transenthortinal region, all the way into the neocortex (Braak & Braak, 1995). The degeneration of these specific areas

is related to deficits in learning and formation of new memories. Several studies have suggested that tau tangles do not spread into the neocortex in the absence of Aβ (Long & Holtzman, 2019), suggesting that Aβ may be a prerequisite to develop tau pathology.

There are two types of AD, namely (i) early-onset (familial AD), occurring before 65 years of age, and (ii) late-onset (sporadic AD), which affects patients older than65 years of age. Both AD types show have a multifactorial nature and are associated with multifaceted toxicity. Although it only accounts for a small percentage of AD cases, early onset AD is the most severe form of the disaese, with the majority of cases caused by mutations in genes responsible for Aβ formation such as the amyloid precursor protein (APP) and the γ-secretase complex proteins presenilin-1 and -2 (PSEN1/2). However, late-onset AD accounts for the vast majority of AD cases (95%). Age is the major risk factor, and it is well established that possession of an apolipoprotein ε4 allele (APOEε4) is a risk factor as well, which is the main cholesterol transporter in the brain.

### 4.1 Amyloid-β peptide

Aβ is a 4.5 kDa peptide originating from the proteolytic processing of the APP, a transmembrane glycoprotein with a large extracellular domain that carries out a wide range of biological functions in the CNS (Zheng & Koo, 2011). The detection of Aβ as main constituent of the plaques and the identification of gene mutations related to Aβ formation in familial AD have led to formulate the amyloid cascade hypothesis (Hardy & Higgins, 1992; Selkoe, 1991). This hypothesis postulates that the abnormal accumulation of Aβ in the brain, due to the unbalance between its generation and elimination, leads to neurodegeneration and subsequent dementia.

The sequential proteolytic processing of APP occurs mainly in two ways, (1) non-amylogenic cascade and (2) amylogenic cascade **(Figure 9)**. The non-amyloidogenic processing of APP is carried out by the α-secretase protease and generates soluble fragments APPsα (N-terminus) and CTFα (C-terminus), the latter remaining anchored to the cell membrane. CTFα is subsequently cleaved by a second enzyme, γ-secretase, producing two soluble peptides, namely p3, and AICD (APP intracytoplasmic domain)

which functions as a transcriptional regulator of several genes such as glycogen synthase kinase 3β or p53 (Kimberly, Zheng, Guénette, & Selkoe, 2001; von Rotz et al., 2004).

In contrast, in the amyloidogenic cascade the first cleavage is performed by the protease β-secretase, generating APPsβ and CTFβ fragments. Further processing of CTFβ by γ-secretase produces AICD and the Aβ peptide, which is released extracellularly. Remarkably, while the non-amyloidogenic cascade is predominant in physiological conditions -presumably to avoid excessive production of Aβ peptide- the equilibrium between the two pathways seems altered in AD patients. In addition, there are several non-canonical pathways through which APP can be processed, some of them also contributing to Aβ peptide generation (Müller, Deller, & Korte, 2017).

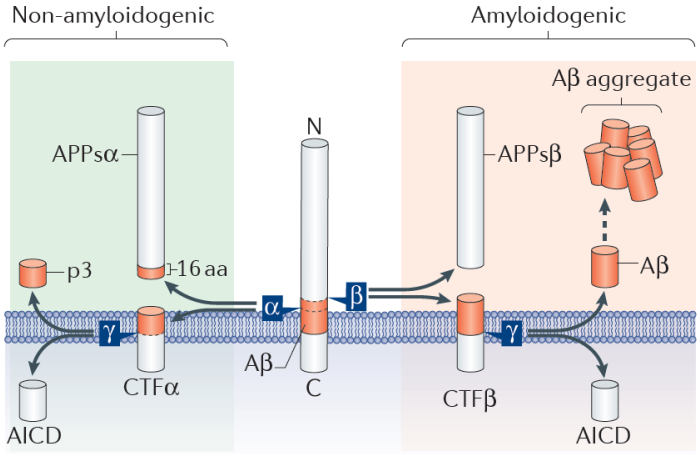


***Figure 9. Schematic representation of canonical APP processing****. The non-amyloidogenic (green background) and amyloidogenic (red background) pathways are shown. The proteolytic cleavage of APP by α- or β-secretase, and subsequently by γ-secretase, generates AICD, and p3 or Aβ peptides, respectively. Adapted from Müller et al., 2017.*

Following APP processing, Aβ monomers, especially $A\beta_{1-42}$, tend to aggregate into a variety of species, including dimers, trimers, high-n oligomers, protofibrils, or fibrils that deposit in the brain, and eventually generate senile plaques (Recuero, Serrano, Bullido, & Valdivieso, 2004). The complexity of Aβ peptide biochemistry makes it prone to aggregation and it acts as promiscuous molecules able to signal through a repertoire of receptors, promoting a wide range of effects in neurons and other cell types (Viola & Klein, 2015).

# 5. Alzheimer´s disease and white matter

Because of the prominent feature of neuronal loss, AD has been traditionally considered as a grey matter (GM) disease. However, emerging evidence suggest that white matter degeneration and demyelination are important pathophysiological features as well. WM is an essential component of neuronal networks, and it is crucial for many high order cognitive processes including attention, executive functioning, non-verbal/visual-spatial processing, and generalized processing speed, all of which are impaired in AD. Myelin loss and the inability of the oligodendrocytes to repair myelin damage may be additional central features of AD. Furthermore, at early stages of AD pathology it has been observed that WM atrophy occurs before GM degeneration as well as neuronal loss, plaque formation or cognitive decline, suggesting that axonal or myelin chemical abnormalities provoke neuronal loss (Nasrabady, Rizvi, Goldman, & Brickman, 2018; Sachdev, Zhuang, Braidy, & Wen, 2013). Moreover, a recent theory proposed that Aβ and tau are secondary, rather than primary pathologies and may result from the brain attempting to maintain myelin homeostasis through a cycle of damage, repair, and maintenance (Bartzokis, 2011).

## 5.1 Oligodendrocytes and amyloid β peptide

Despite the relevance that the WM and myelin seem to have in AD pathology, little is known about the effect of Aβ peptide in oligodendrocytes in the context of AD. In fact, oligodendrocytes show a high expression of APP as well as BACE1, the secretase involved in the amyloidogenic pathway. BACE1 and APP play important and distinct roles in CNS myelination, demyelination and remyelination events. While BACE1 regulates myelin sheath thickness (Hu et al., 2006), APP ensures normal myelination and remyelination in adult nerves (Truong et al., 2019). Interestingly, oligodendrocytes are able to produce Aβ that may exacerbate the development of the disease (Skaper et al., 2009).

*In vitro* studies showed that Aβ turns into toxic when it oligomerizes (Zhao, Long, Mu, & Chew, 2012) and can directly damage oligodendrocytes and myelin (Xu et al., 2001). In fact, $A\beta_{1\text{-}40}$ or $A\beta_{25\text{-}35}$ causes dose-dependent cell death, characterized by nuclear and cytoskeletal disintegration, DNA fragmentation, and mitochondrial dysfunction in

oligodendrocytes (Xu et al., 2001). In addition, injection of high concentrations of $A\beta_{1-42}$ in rat corpus callosum results in considerable axonal damage, and loss of myelin and oligodendrocytes (Jantaratnotai, Ryu, Kim, & McLarnon, 2003).

On the other hand, contradictory results have been reported when analysing whether differentiation stage in oligodendroglial lineage plays a role in cell susceptibility. It has been observed that after $A\beta_{1-42}$ treatment (0.5, 1, 2, 4 µM for 4 h) both immature and mature oligodendrocyte population present an increased abundance of cells with pyknotic nuclei (Desai et al., 2010). Additionally, it has been also described that soluble $A\beta_{1-42}$ (10 µM for 48 h) inhibits the survival of mature OLs but not of OPCs and prevents myelin sheath formation by inhibiting F-actin distribution without changing the number of MBP+ cells or MBP/PLP expression (Horiuchi et al., 2012). In the same line, another study has shown decreased number of MBP+ cells and membrane expansion upon $A\beta_{1-42}$-treatement (10 µM for 96 h) (Zhang et al., 2018). Conversely, $A\beta_{1-42}$ treatment at low doses (200 nM for 24 h) increases cell viability and additionally promotes oligodendrocyte differentiation and induces MBP expression via integrin β1 and Fyn kinase signalling (Quintela-Lopez et al., 2019).

### 5.2 Oligodendrocytes and AD models

The generation of AD animal models has been extremely useful to expand the knowledge about the disorder. Moreover, they have allowed analysing and examining in detail the progression of WM pathology and understanding the direct role of AD-related mutations in the onset and progression of the disease. In this sense, Aβ pathology has been linked to WM abnormalities in animal models such as Tg2576, 3xTg-AD, APP/PS1 and 5XFAD mice, which overproduce Aβ peptide. In these animals, focal demyelination areas associated with Aβ plaques have been observed, similar to those described in human patient samples (Behrendt et al., 2013; Mitew et al., 2010). Interestingly, plaque-free tissues of transgenic mice have no significant loss of myelin or oligodendrocyte number (Mitew et al., 2010). However, electron microscopy images of myelin in APP/PS1 revealed higher number of fibers with myelin aberrations in transgenic mice (Behrendt et al., 2013).

In addition, APP/PS1 transgenic mice exhibit an increased density of proliferating progenitor cells and newly generated mature cells at 6 and 11 months of age compared to wild-type mice. Notably, the generation of mature oligodendrocytes in WM areas is higher than in the cortical grey matter (Behrendt et al., 2013). Interestingly, a study in APP/PS1 mice at early stages of AD demonstrated alterations of myelin integrity in the hippocampus of 2-month-old transgenic mice. APP/PS1 present an increased MBP expression accompanied by thicker myelin sheaths and shorter internodal distance (Wu et al., 2017). In same line, in a recent study, $APP^{Sw.Ind}$ (APP mice), exhibited increased oligodendrogenesis in the 2- and 4-month-old hippocampus, fimbria and entorhinal cortex. However, this phenotype is lost in older animals. Moreover, these mice present shorter nodes of Ranvier and longer paranodes in the hippocampus at 3 months of age and thicker myelin (Ferreira et al., 2020). In another study, decreased OPC density was observed in the hippocampus of 9-month-old APP/PS1 but not at 14 months of age. Authors associated these changes with a reduction in MBP between 9 and 14 months compared to controls, which suggests impaired myelination (Chacon-De-La-Rocha et al., 2020). Curiously, OPCs exhibit a senescent phenotype in the Aβ plaque environment in APP/PS1 mice, suggesting a role for cell senescence in the cascade of events by which Aβ accumulation causes cognitive impairment in AD (Zhang et al., 2019). Another study showed that APP/PS1 mice have increased rate of new myelin formation (Chen et al., 2021).

More interestingly, Desai and co-workers (2009) also observed changes in myelin in hippocampal CA1 and entorhinal cortex in 3xTg-AD mice. Moreover, levels of MBP were found decreased in both areas, although axonal integrity was maintained intact. Likewise, another study also reported OPC atrophy and MBP decrease in the hippocampus of 3xTg-AD mice (Vanzulli et al., 2020). Imaging studies in the 3xTg-AD model show pronounced myelin changes in the fimbria, which acts as the major output tract of the hippocampus (Nie et al., 2019).

In the last few years, transcriptomic analysis performed in different AD animal models pointed out oligodendrocytes as one of the most deregulated cells in the disease. Zhou et al., 2020 reported that 5xFAD mice contain more oligodendrocytes than their

wildtype counterparts, and oligodendrocytes harbour the most strikingly upregulated genes. Additionally, oligodendrocytes adopt a reactive state and increase the expression of the complement component C4b, the serine protease inhibitor Serpina3n, and MHC-I (H2-D1), which may facilitate Aβ aggregation. Moreover, a recent study showed an increase with age in the expression of oligodendrocyte associated genes in the hippocampus of 3xTg-AD mice (Balderrama-Gutierrez et al., 2021).

The discrepancies in the oligodendrocyte response in AD models have not yet been explained, but they could be associated with when and how fast the pathology develops in different models.

### 5.3 Oligodendrocytes and myelin in AD

WM progressively deteriorates with normal aging (Damoiseaux et al., 2009; Inano, Takao, Hayashi, Abe, & Ohtomo, 2011), and whole brain imaging studies suggest that this natural tendency is exacerbated and accelerated in AD (Bartzokis et al., 2003; de la Monte, 1989; Stricker et al., 2009). *Post mortem* and *in vivo* magnetic resonance imaging (MRI) studies have largely demonstrated a substantiated WM impairment in AD, finding reduced WM volume and alterations of WM microstructure (Bartzokis, 2011; Roher et al., 2002), as well as differences in the physical organization of the myelin lipid bilayer (Chia, Thompson, & Moscarello, 1984). In a recent study, in which several imaging measurements of myelin status and psychological test are combined, it was demonstrated that age-related demyelination is associated with memory impairment, especially in dementia states (Kavroulakis et al., 2018). In same line, an MRI study done with Aβ positive AD patients compared to Aβ negative controls, showed that white matter hyperintensities (WMH) in the corpus callosum region were larger in positive patients and were associated with worse cognitive performance (Garnier-Crussard et al., 2022). Accordingly, AD patients present loss of myelin in specific regions of the brain, such as cortical GM and WM (Roher et al., 2002), and a large decrease in the number of Olig2+ cells in the WM and GM of the superior temporal gyrus and the sensory motor cortex. In contrast, the WM of the middle frontal gyrus exhibits increased density of Olig2+ cells (Behrendt et al., 2013). In turn, the corpus callosum is also affected in AD

brains and its impairment correlates with the progression and severity of the disease (Teipel et al., 2002).

Interestingly, several studies have reported WM disruption in asymptomatic individuals with increased risk for AD and in patients with mild cognitive impairment (MCI) (Bartzokis et al., 2006; Parente et al., 2008). Bartzokis and colleagues correlated age-related slow cognitive processing speed with myelin breakdown in late-myelinating WM areas in these subjects. In this regard, a recent exhaustive study of asymptomatic individuals with genetic risk factors for AD shows that these individuals present brain alterations of myelin content which correlate with well-established AD markers in the cerebrospinal fluid (CSF). Interestingly, a strong association between myelin content reduction and soluble Aβ concentration in the CSF is observed. This study also revealed that age-related changes in myelin are particularly evident in late-myelinating areas, such as the frontal WM and the genu of the corpus callosum, corroborating the facts previously described (Dean et al., 2017). These results indicate that myelin plays an important role in preclinical stages in AD, which may be related to the onset of the cognitive decline.

The underlying causes of oligodendrocyte and myelin dysfunction in AD have not been fully clarified. However, several studies propose Aβ as a candidate to promote WM dysfunction. In AD patients, increased levels of Aβ peptide have been correlated with brain regions exhibiting myelin abnormalities (Roher et al., 2002), being these Aβ deposits mainly in late-myelinating areas (Bartzokis et al., 2007). Moreover, WM changes including demyelination have been also documented in MCI and are potentially related to Aβ and tau pathology (Bartzokis et al., 2003; Dean et al., 2017; Selkoe & Hardy, 2016). Specifically, focal demyelination is observed in plaque-associated myelinated axons from AD temporal cortex, whereas plaque-free cortical GM of AD patients have no significant loss of myelin or oligodendrocyte density (Mitew et al., 2010).

Consistent with those findings, biochemical analysis of total myelin fraction in AD patients revealed increased $A\beta_{1-42}$ levels accompanied by a significant decrease in the amount of MBP, PLP and CNPase. In addition, myelin lipid content was also altered, observing a marked decrease in cholesterol levels, while total fatty acid content was

increased (Roher et al., 2002). Noteworthy, a recent study has shown that APOE4, one of the strongest genetic risk factors for AD, impairs myelination by altering cholesterol metabolism (Blanchard et al., 2022).

While MBP in the AD brain´s frontal WM is significantly lower in comparison with MCI (Wang et al., 2004a), increased levels of MBP are observed in cortical GM of AD patients (Selkoe, Brown, Salazar, & Marotta, 1981; Zhan et al., 2015). Interestingly, in these patients the high ratio of degraded MBP over total MBP reveals a strong rate of MBP degradation (Zhan et al., 2015). Increase of degraded MBP and myelin components such as galactocerebroside is also observed within vesicles in the periventricular WM of AD patients (Zhan et al., 2014), suggesting a high myelin damage. Furthermore, an increase in degraded MBP associated with autophagy specific markers has been described (Zhan et al., 2015). These findings are consistent with previous studies documenting myelin and lipid changes in GM and WM in AD (Han et al., 2002; Han, 2007; Pernber et al., 2012). However, the mechanisms by which MBP levels are higher in AD patients (and mouse models) compared to healthy individuals remains unclear. Surprisingly, it was recently shown that MBP binds to Aβ and inhibits its fibril formation, possibly playing a role in regulating its deposition and senile plaque formation in the parenchyma (Hoos et al., 2009; Liao et al., 2009; Dean et al., 2017).

Transcriptomic studies performed in the last few years have shown dysregulated OL functions in AD, including changes in differentiation, myelination and metabolic adaptation to neuronal degeneration. OLs have been accepted as important players in disease progression, showing sexual dimorphism (Mathys et al., 2019), dysregulation of AD susceptible genes (Grubman et al., 2019), and expression of potential targets for novel AD therapeutics (Morabito et al., 2021). Interestingly, Lau and colleagues showed that oligodendrocytes adopt a remyelinating state in AD, suggesting a potential cell-intrinsic recovery mechanism (Lau, Cao, Fu, & Ip, 2020).

Overall, oligodendrocyte and myelin, away from being secondary characters in the disease, they respond to injury and have important implications in the onset and development of AD. Thus, understanding the role of oligodendrocyte failure and myelin

loss may be key factors for developing innovative strategies, which might provide effective therapeutic options to prevent or treat AD.

# HYPOTHESIS AND OBJECTIVES

Accumulation in the brain of soluble Aβ oligomers and myelin and white matter atrophy, are relevant early events in Alzheimer´s disease pathogenesis and are related to the cognitive impairment associated with this disease. Several studies have shown that oligodendrocytes are vulnerable to Aβ peptide. Results from our laboratory have revealed that Aβo increase levels of MBP, the major component of myelin in addition to being essential for many aspects of oligodendrocyte homeostasis. Given the importance of MBP, we hypothesize that the alteration of this protein can lead to dysfunctional oligodendrocyte and thus, contribute to an aberrant myelination of CNS regions. These alterations may lead to axonal conduction and function impairment, contributing to cognitive deterioration in AD. In order to investigate this hypothesis, we plan to characterize the effects of Aβo in oligodendrocyte and myelination *in vitro* and in animal models of AD. To test our hypothesis, the following specific objectives were addressed:

**Aim 1.** To study the effect of Aβ peptide oligomers in RNA alterations in primary oligodendrocyte culture, in 3xTg-AD mouse model and in AD oligodendrocytes.

**Aim 2.** To define the role of Aβ peptide oligomers in the synthesis of myelin proteins in primary oligodendrocyte cultures and in 3xTg-AD mouse model.

**Aim 3.** To analyse the effect Aβ peptide oligomers in hnRNPs of *Mbp* and *Mobp* mRNA in primary oligodendrocyte cultures and in 3xTg-AD mouse model.

**Aim 4.** To evaluate the implication of the upregulation of MBP in oligodendrocytes functions.

**Aim 5.** To study the effect of Aβ peptide oligomers in cytoskeleton dynamics.

**Aim 6.** To evaluate the role of Aβ peptide oligomers in myelination *in vivo*

**Aim 7.** To study the role of Aβ peptide in oligodendrocyte exosome secretion and their impact in neurons

# MATERIAL AND METHODS

## 1. Animals

All experimental procedures with mice and rats were approved by the Animal Ethic Committees of the University of the Basque Country (UPV/EHU) and followed the European Communities Council Directive 2010/63/EU. In particular, all protocols were approved by the "Ethics Committee on Animal Experimentation" (CEEA) which is a collegiate authority in the operational structure of the Ethics Commission for Research and Teaching (CEID) of the UPV/EHU. In the case of zebrafish, all procedures were approved by the University of Colorado Anschutz Medical Campus Institutional Animal Care and Use Committee (IACUC) and performed to their standards.

### 1.1 Mice

Animals were housed in standard conditions with 12 h light cycle and with ad libitum access to food and water. All possible efforts were made to minimize animal suffering and the number of animals used. Experiments were performed in Sprague Dawley rats and in the triple transgenic mouse model of Alzheimer´s disease (3xTg-AD), which harbours the Swedish mutation in the human amyloid precursor protein ($APP^{Swe}$), presenilin knock-in mutation ($PS1^{M146V}$), and tau P301L mutant transgene ($Tau^{P301L}$) (Oddo et al., 2003).

### 1.2 Zebrafish

All nontransgenic embryos were obtained from pairwise crosses of male and females from the AB strain. Embryos were raised at 28.5°C in E3 media (5 mM NaCl, 0.17 mM KCl, 0.33 mM CaCl, 0.33 mM MgSO4 (pH 7.4), with sodium bicarbonate) and sorted for good health and normal developmental patterns.

# 2. Cell culture

## 2.1 Primary cortical oligodendrocyte culture

Purified OPCs were prepared from mixed glial cultures obtained from the forebrain of newborn (P0-P2) Sprague-Dawley rats according to the protocol of McCarthy and de Vellis, 1980 with modifications (Canedo-Antelo et al., 2018; Chen et al., 2007; Sánchez-Gómez, Serrano, Alberdi, Pérez-Cerdá, & Matute, 2018). Briefly, forebrains were removed from the skulls, and after careful removal of the meninges, cortices were isolated and digested by incubation (15 min, 37°C) in Hank's balanced salt solution (without $Ca^{2+}$ and $Mg^{2+}$, $HBSS^{-/-}$) containing 0.25% trypsin and 0.004% deoxyribonuclease (DNAse) (all from Sigma-Aldrich). Then, the enzymatic reaction was stopped by adding Iscove's modified Dulbecco's medium (IMDM) supplemented with 10% fetal bovine serum (FBS, Hyclone; both from Gibco) and the cell suspension was centrifuged at 1,000 x g for 5 min. The pellet was resuspended in 1 ml of the same solution and cells were dissociated by passage through needles (21G and 23G), centrifuged at 1,000 x g, 5 minutes and resuspended again in IMDM +10% Hyclone.

Afterwards, cells were seeded into 75 cm2 flasks coated with poly-D-lysine (PDL; 1 µg/ml; Sigma-Aldrich) and maintained in culture at 37°C and 5% CO2 with a medium change every 3 days. After 7 days in culture, flasks were shaken (400 rpm, 1 h, at 37°C) to remove adherent microglia. In some occasions, flasks were reused after 14 days, by re-shaking the same flask. The remaining OPCs present on top of the confluent monolayer of astrocytes were detached by shaking overnight at 250 rpm. The resulting cell suspension was filtered through a 10 µm pore size nylon mesh and pre-plated in 100 mm coated Petri dishes (ThermoFisher Scientific) for 1 hour at 37°C and 5% CO2, allowing microglia to firmly attach to the dish while OPCs were loosely attached and could be collected with a gentle shaking of the Petri dishes. The collected forebrain OPC cell suspension was filtered again through a 10 µm pore size nylon mesh.

Cell number was determined by trypan blue staining (Sigma-Aldrich) with 20 µl of sample and the remaining cell suspension was centrifuged at 1,000 x g for 10 min and the pellet was resuspended to a final concentration of 1.000 cell/µl in chemically defined

Sato medium consisting of a supplemented (4.5 g/l glucose and 0.11 g/l sodium piruvate) DMEM base with several factors that favour oligodendrocyte survival and development **(Table 2)**. Cells were plated onto poly-D-Lysine-coated (PDL) 14-mm-diameter or 12-mm-diameter coverslips resting in 24-well plates or without coverslips directly onto a PDL-coated 6-well plates at densities between 1,5 x $10^4$ and 5 x $10^6$ cells per well maintained at 37°C and 5% $CO_2$ in chemically defined Sato medium (SATO+) **(Table 2)**. Cultured oligodendrocytes were allowed to grow for 3 days *in vitro* (DIV). The purity of oligodendroglial cultures was confirmed by immunostaining with cell type-specific antibodies. After 1 day in culture, PDGFRα+ OPCs represented 97 ± 5% of the total cells, and after 3 days in OL differentiation medium, at least 98% were MBP+ cells (Sánchez-Gómez et al., 2018).

***Table 2.*** *Oligodendrocytes SATO+ medium components.*

| *Reagent* | *Concentration* | *Company* |
|---|---|---|
| *Dubelcco´s Modified Eagle Medium (DMEM)* | Base medium | Sigma-Aldrich |
| *Insulin* | 5 µg/ml | Lonza |
| *Penicillin/Streptomycin* | 100 U/ml | Sigma-Aldrich |
| *Bovine serum albumin (BSA)* | 1 mg/ml | Sigma-Aldrich |
| *L-Glutamine* | 2 mM | Sigma-Aldrich |
| *N-Acetyl L-Cystein* | 6.3 mg/ml | Sigma-Aldrich |
| *Transferrin* | 100 µg/ml | Sigma-Aldrich |
| *Putrescin* | 16 ng/ml | Sigma-Aldrich |
| *Progesterone* | 60 ng/ml | Sigma-Aldrich |
| *Sodium selenite* | 40 ng/ml | Sigma-Aldrich |
| *Triiodothyronine (T3)* | 30 ng/ml | Sigma-Aldrich |
| *L-Thyroxine (T4)* | 40 g/ml | Sigma-Aldrich |
| *Cilliary neurotrophic factor (CNTF)* | 10 ng/ml | Prepotech |
| *Neurotrophin 3 (NT-3)* | 1 ng/ml | Prepotech |

## 2.2 Primary hippocampal neuron culture

Hippocampal neurons were prepared from embryonic day 18 rat embryos (E18) as described (Banker & Goslin, 1988). Briefly, hippocampi were dissected from embryonic brains and dissociated in TrypLE Express (Gibco, Thermo Fisher Scientific) for 10 min at 37°C. Cells were washed twice with $HBSS^{-/-}$ (Gibco) and resuspended in plating medium containing 10% fetal bovine serum, 2 mM L-glutamine and 50 U/ml penicillin-streptomycin in Neurobasal (all from Gibco). Cells were homogenized with a Pasteur pipette and centrifuged for 5 min at 800 x g. Cells were resuspended in plating medium. Hippocampal neurons were cultured on PDL-coated coverslips in 24-well plates at low

density (20.000 cells/well). Cultures were maintained at 37°C in a 5% $CO_2$ humidified incubator. After 1 DIV the medium was replaced with growth medium (1× B27, 2 mM glutamine, and 50 U/ml penicillin-streptomycin in Neurobasal). To avoid the growth of glia, half of the medium was replaced with fresh medium containing 20 µM of 5-fluorodeoxyuridine and uridine (Sigma Aldrich) every 3 days. Treatments were performed at 10 and 21 DIV.

### 2.3 Organotypic hippocampal slice culture

Organotypic hippocampal slice culture were prepared from brain sections of P5-P7 Sprague Dawley rat pups according to previously described procedures (Stoppini, Buchs, & Muller, 1991). Briefly, after decapitation, brains were extracted and cut into 350 µm coronal slices using a tissue chopper (McIlwain), hippocampi were then separated and meninges were removed. Slices were transferred to 0.22 µm culture membranes inserts (Millipore), each containing two to three slices. Slices were maintained in 6-well plates for nine days in 25% basal medium with Earle´s balanced salts (Life technologies, EBSS), 44% Minimal Essential Medium (Life technologies, MEM), 25% inactivated horse serum (Life technologies), 35.2% glucose solution (Panreac), 50 µg/ml fungisone, B-27 supplement (Gibco), Glutamax (Gibco), 1% Penycilin/Streptomycin (Lonza) and AraC 4.4 µM (only at 2 DIV) at 37°C with 5% $CO_2$. After two days, organotypic slices were infected with 1 µL of $10^{12}$ pAAV-8 carrying MBP promoter (AAV-MBP-GFP) bound to GFP. After two days, media was changed. Slices were kept in culture for 9 days before performing the experiments.

## 3. Human Samples

Patients gave informed consent to all clinical investigations, which were performed in accordance with the principles embodied in the Declaration of Helsinki.

Formalin-fixed paraffin-embedded sections from hippocampus of x subject controls and x AD patients were obtained from the Neurological Tissue Bank Hospital Clinic-IDIBAPS Biobank (Table 3). AD samples were grouped by Braak and Braak (Braak & Braak, 1995)

into AD-II, AD-III, AD-IV and AD-V-VI stages, and by CERAD classification (Mirra et al., 1991) into AD-A, AD-B and AD-C stages **(Table 3)**.

***Table 3.*** *Characteristic of controls and AD subjects, categorized as stages I to VI of Braak and Braak and A, B or C of CERAD criteria.*

| Case nº | Ref. nº | Braak stage NFT | CERAD Senile plaque | Gender | Age | Region analyzed | Postmortem delay* |
|---|---|---|---|---|---|---|---|
| **1** | 695 | I | | M | 80 | Hp | 10:00 |
| **2** | 1378 | - | | M | 78 | Hp | 6:00 |
| **3** | 1648 | - | | M | 73 | Hp | 6:10 |
| **4** | 1357 | II | | F | 79 | Hp | 10:30 |
| **5** | 1912 | II | B | F | 72 | Hp | 13:35 |
| **6** | 1937 | II | B | F | 83 | Hp | 7:20 |
| **7** | 1247 | III | A | F | 80 | Hp | 8:00 |
| **8** | 1345 | III | A | M | 78 | Hp | 8:00 |
| **9** | 1112 | III | B | F | 83 | Hp | 7:30 |
| **10** | 608 | IV | - | M | 78 | Hp | 7:00 |
| **11** | 1040 | IV | C | M | 76 | Hp | 8:25 |
| **12** | 1417 | IV | - | F | 79 | Hp | 4:30 |
| **13** | 977 | VI | C | M | 75 | Hp | 10:00 |
| **14** | 999 | VI | C | F | 76 | Hp | 10:00 |
| **15** | 1135 | VI | C | M | 79 | Hp | 6:25 |

# 4. Preparation of Aβ oligomers

$A\beta_{1-42}$ oligomers were prepared as reported previously (Dahlgren et al., 2002). Briefly, $A\beta_{1-42}$ (ABX) was initially dissolved to 1 mM in hexafluoroisopropanol (Sigma-Aldrich) and separated into aliquots in sterile microcentrifuge tubes. Hexafluoroisopropanol was totally removed under vacuum in a speed vac system and the peptide film was stored desiccated at -80°C. For the aggregation protocol, the peptide was first resuspended in dry DMSO (Sigma-Aldrich) to a concentration of 5 mM, and Hams F-12 (PromoCell) was added to bring the peptide to a final concentration of 100 µM and incubated at 4°C for 24 h.

Labelled $A\beta_{1-42}$ was prepared as previously described (Jungbauer, Yu, Laxton, & LaDu, 2009). After 24 h incubation at 4°C, labelling was performed using the Alexa Fluor®488 TFP ester Microscale Labelling Kit (A30006, Invitrogen) according to manufacturer´s

instructions. Briefly, 50 µl of 100 µM Aβ oligomer solution was pH adjusted to pH 9 with 5 µl of 1 M NaHCO3, followed by addition of 4 µl of the $H_2O$ solubilized reactive dye. Incubation at room temperature (RT) was performed for 15 min followed by immediate addition of 55 µl of the labelling reaction mixture onto a spin column packed with a 425 µl slurry of Biogel P-6 resin for removal of unincorporated dye. The resulting eluant (pH 7.4) was stored for up to 2 days at 4°C or used immediately for injection experiments.

# 5. Drugs and gene silencing by siRNAs

The following drugs and inhibitors were used by directly added to the medium: Latrunculin B (5 µM; Santa Cruz Biotechnology), Jasplaklinolide (5 µM; Santa Cruz Biotechnology) and Puromycin dyhidrocloride (2 µM *in vitro* and 10 µM *in vivo* Santa Cruz Biotechnology).

Oligodendrocytes were transfected with 5 µL of scramble siRNA and *Mbp-targeting* siRNA (5 nmol; HorizonDiscovery) using Amaxa™ Basic Nucleofector™ Kit (Lonza) for Primary Mammalian Glial cells following the manufacturer's instructions. After, cells were treated with either vehicle or 1 µM Aβ for 24 h and subsequently protein extraction was carried out.

# 6. Protein extract preparation and detection by western blot

## 6.1 Oligodendrocyte protein preparation

After each treatment, cultured cortical OLs were washed in cold phosphate buffered saline (142 mM NaCl, 2,5 mM $NaH_2PO_4$, 75 Mm $Na_2HPO_4$; PBS) twice and cells were scraped in sample buffer (62.5 mM Tris pH 6.8, 10% glycerol, 2% SDS, 0.002% bromophenol blue and 5.7% β-mercaptoethanol in $dH_2O$). At least 3 wells/treatment and 90.000-120.000 cells/well were used. Extraction was performed on ice to enhance the lysis process and avoid protein degradation. Samples were then boiled at 95°C for 5 min.

### 6.1.1 G and F-actin extraction

Oligodendrocytes were treated 24 h with Aβ or vehicle and as negative control, 30 minutes before extraction with LatrunculinB (10 µM). Subsequently, cells were washed once in ice-cold PBS before lysis with actin stabilization buffer (5 mM Tris, pH 7.4, 300 mM sacarose, 2 mM EGTA, 0.3% TX-100, 2 mM phalloidin) supplemented with protease and phosphate inhibitor cocktail (ThermoFisher Scientific) on ice for 5 minutes. Then supernatant containing G-actin was collected and cells attached to the plastic were dislodged by scraping with RIPA (Thermofisher Scientific) buffer obtaining F-actin. Then sample buffer was added and samples were boiled at 95°C for 5 min.

### 6.1.2 Puromycilation assay

Puromicyn is a tRNA analog, which is incorporated into the nascent polypeptide chain in a ribosome-catalyzed reaction. This technique allows the *in situ* detection of protein synthesis with an anti-puromicyn antibody. At 3 DIV, DMSO- and Aβ-treated oligodendrocytes were exposed to 2 µM puromycin (Sigma Aldrich) for 10 minutes. To verify that puromycin labels newly synthesized proteins, 40 µM of the protein synthesis inhibitor anisomycin (Sigma Aldrich) was co-incubated with puromycin. Cells were washed with cold PBS with 3 µg.ml–1 digitonin (Sigma Aldrich).

## 6.2 Protein preparation from animal tissue samples

Mice were anesthetized with isofluorane (Schering-Plough) and hippocampus were extracted, placed on dry ice and stored at -80°C. For myelin-enriched fractions, brains were triturated and homogenised and myelin was extracted with a %22.5 Percoll gradient.

Animal tissue samples were resuspended in 200 µl of RIPA buffer (ThermoFisher) supplemented with protease and phosphatase inhibitor cocktail (ThermoFisher), and were homogenized with a douncer. Afterwards, they were sonicated for 25 cycles at 80% amplitude (Labsonic M, Sartorius), centrifuged for 10 min, at 2,000 x g and 4°C, and then supernatants were collected. Total protein content was quantified through Bradford assay (Bio-Rad).

### 6.3 Western Blot (WB)

Protein samples were separated by SDS-PAGE in 4-20% (Any KD) Tris-Glycine polyacrylamide precast gels (Bio-Rad). Electrophoresis was conducted in a Tris-Glycine buffer (25 mM Tris, 192 mM glycine, 0.1 % SDS in dH2O, pH 8.3) by using the Criterion cell system (Bio-Rad). Gels were transferred onto nitrocellulose membrane by using a Trans-Blot® Turbo™ Transfer System (Bio-Rad). Membranes were blocked for 1 h at RT in blocking solution, which consisted of TBST buffer (20 mM Tris, 137 mM NaCl, 0.1% Tween-20 in $dH_2O$, pH 7.4) supplemented with 5% BSA (Nzytech). Then, the membrane was incubated with specific primary antibodies **(Table 4)** in the same solution overnight (O/N) at 4°C with gentle shaking. Afterwards, membranes were washed three times with TBST and incubated in blocking solution containing secondary antibody conjugated to horseradish peroxidase (HRP) or fluorescence secondary antibodies (1:5000) for 1 h at RT.

Immunoreactive bands were detected by using enhanced electrochemical luminescence (NZY standard ECL and NZY advanced ECL) and ChemiDoc XRS Imaging System (Bio-Rad). Signals were quantified using Image Lab® software (Bio-Rad) and values were normalized to β-actin or GAPDH signal and provided as the mean ± S.E.M. of at least three independent experiments.

When needed, membranes were stripped of antibodies using Restore Western Blot Stripping Buffer (Thermo Fisher Scientific) for 20 min at RT. Membranes were then washed in TBST for three times, blocked and incubated again with other primary antibodies.

***Table 4.*** *Antibodies used for Western blot analysis.*

| Antibody | Host | Molecular weight (kDa) | Dilution | Reference |
|---|---|---|---|---|
| Anti-MBP | Mouse | 21.5-14 | 1:1000 | BioLegend SMI-99 |
| Anti-PLP | Rabbit | 23-25/20 | 1:1000 | Millipore MAB388 |
| Anti-MOG | Mouse | 28 | 1:1000 | Millipore MAB5680 |
| Anti-MAG | Mouse | 100 | 1:500 | Santa Cruz sc-166849 |
| Anti-CNP | Mouse | 48 | 1:1000 | Sigma C5922 |
| Anti-MOBP | Mouse | 17 | 1:1000 | Santa Cruz sc-517016 |
| Anti-hnRNPA2 | Mouse | 36/38 | 1:1000 | Santa Cruz sc-374053 |
| Anti-hnRNPE1 | Rabbit | 43 | 1:1000 | MBL RN024P |
| Anti-hnRNPF | Mouse | 48 | 1:1000 | Santa Cruz sc:32310 |
| Anti-hnRNPK | Rabbit | 51/65 | 1:1000 | MBL RN019P |
| Anti-Cofilin | Rabbit | 19-21 | 1:1000 | Cell signalling #5175 |
| Anti-pCofilin | Mouse | 19-21 | 1:1000 | Santa Cruz sc-3658882 |
| Anti-Dynactin | Mouse | 135 | 1:1000 | Santa Cruz sc-365274 |
| Anti-Dynein | Mouse | 10 | 1:1000 | Santa Cruz sc-136287 |
| Anti-Puromycin | Mouse | | 1:1000 | Millipore MABE343 |
| Anti-TSG101 | Rabbit | 50 | 1:1000 | Abcam ab30871 |
| Anti-6E10 | Mouse | | 1:1000 | BioLegend SIG-39320 |
| Anti-α-Tubulin | Mouse | 50 | 1:5000 | Abcam ab7291 |
| Anti-β-Actin | Rabbit | 43 | 1:5000 | Sigma A2228 |
| Anti-GAPDH | Mouse | 36 | 1:5000 | Millipore MAB374 |

# 7. Immunoprecipitation

## 7.1 Co-Immunoprecipitation

Co-Immunoprecipitation assays were performed to determine the changes in the dynamics of RNA granules in Aβ-triggered signalling in cultured oligodendrocytes. Briefly, 40 µl of agarose conjugated mouse anti-hnRNPA2 antibody (Santa Cruz Biotechnology) and 10 µl mouse anti-$IgG_{2b}$ (Santa Cruz Biotechnology) were used. ≈1x$10^6$ OPCs were harvested per condition and treated with Aβ at 1 µM for 3 h or 24 h. Cells were washed with cold PBS twice and scraped in 1 mL non-denaturing lysis (50 Mm Tris-HCl pH 8, 150 nM NaCl, 1% NP40) buffer supplemented with protease and phosphate inhibitor cocktail (ThermoFisher Scientific). Then, they were placed on ice for 10 min and centrifuged 5 min at 12,000 x g. The supernatant was added (1/10 was saved for input) to 40 µL of agarose conjugated anti-hnRNPA2 or anti-IgG2b and incubated for 2 h at 4°C to avoid unspecific interactions. The lysate-antibody-beads complex was centrifuged at 2,000 x g for 2 min and washed three times with non-denaturing lysis buffer and once by PBS 1X followed by centrifugation to obtain the immunocomplex.

Finally, protein elution was carried out in 40 µl of 2x sample buffer after boiling the sample at 95°C for 5 min and centrifuged at 12,000 x g for 1 min.

### 7.2 Immunoprecipitation

Immunoprecipitation assays were performed to determine the changes in hnRNP A2 phosphorylation. Briefly, 40 µl of agarose conjugated mouse anti-pTyr (PY99) antibody (Santa Cruz Biotechnology) and 10 µl mouse anti-IgG (Santa Cruz Biotechnology) were used. ≈1x$10^6$ OLs were harvested per condition and treated with Aβ at 1 µM for 15 min. Cells were washed with cold PBS twice and scraped in 1 mL ND lysis buffer supplemented with protease and phosphate inhibitor cocktail (ThermoFisher Scientific). Samples were placed on ice for 10 min and centrifuged 5 min at 12,000 x g. The supernatant was added (1/10 was saved for input) to 30 µL of agarose conjugated anti-pTyr or anti-IgG and incubated for 2 h at 4°C to avoid unspecific interactions. The lysate-antibody-beads complex was centrifuged at 2,000 x g for 2 min and washed three times with ND lysis buffer and once by PBS 1X followed by centrifugation to obtain the immunocomplex. Finally, protein elution was carried out in 30 µl of 2x sample buffer after boiling the sample at 95°C for 5 min and centrifuged at 12,000 x g for 1 min.

### 7.3 RNA immunoprecipitation (RIP)

For RIP assays, 40 µl of agarose conjugated mouse anti-hnRNPA2 antibody (Santa Cruz Biotechnology) and 10 µl mouse anti-IgG2b (Santa Cruz Biotechnology) were used. Briefly, 2x$10^6$ OLs were harvested per condition, whose lysate was obtained by scpraping the cells in an appropriate polysome lysis buffer. Lysates were centrifuged twice 30 min at 14,000 x g 4 $^{o}$C, and part of the supernatants, which corresponds to total RNA, were stored for the later use as “input”. The remaining sample was used for the IP. Part of the “input” and precipitate was kept for Western blot analysis.

RNA was isolated following a TRIzol RNA isolation protocol (ThermoFisher Scientific). RNA concentration was measured with Nano DropTM 2000 and diethylpyrocarbonate (DEPC) treated water was added in to bring all samples to the same concentration.

Data were normalized to a normalization factor obtained in geNorm Software through the analysis of the expression of two housekeeping genes: Glyceraldehyde-3-Phosphate Dehydrogenase (*Gapdh*) and β-actin (*Actb*) genes. *Mbp*, *Mobp* and *Tau* mRNA enrichment was examined relativizing RIP fraction values to normalized input values:

$$X\ mRNA\ enrichment = \frac{X\ mRNA\ RIP\ fraction}{normalized\ X\ mRNA\ input}$$

# 8. Immunofluorescence

## 8.1 Primary oligodendrocyte and neuronal cell cultures

Cells were fixed in 4% paraformaldehyde (PFA) and 4% of sucrose for 15 min, washed in 1X PBS for three times and then stored at 4°C. Cells were permeabilized and blocked in 4% normal goat serum (NGS, Palex), 0.1% Triton X-100 (Sigma-Aldrich) for OLs and 0.1% saponin for neurons in 1X PBS (blocking buffer) for 1 h and incubated with primary antibodies O/N at 4°C. Then, cells were washed in 1X PBS and incubated with the fluorochrome conjugated antibodies in blocking solution for 1 h at RT. Then, cells were washed and incubated with DAPI (4 µg/ml, Sigma-Aldrich) for 8 min. Cells were washed again twice and coverslips were mounted on glass slides with Fluoromount-G mounting medium (SouthernBiotech). Prepations were kept at 4°C until examination.

## 8.2 Organtypic slices

Organotypic slices were fixed in 4% PFA for 1 h at RT followed by three washes in 0.1 M PBS and stored in 0.1 M PBS at 4°C. Then they were permeabilized and blocked with 4% NGS (Palex), 0.2% Triton X-100 (Sigma-Aldrich) in TBS 1X (blocking solution) for 1 h at RT and thereafter rinsed twice with TBS 1X. Then, slices were incubated with primary antibodies dissolved in 1% BSA (Nzytech), 0.2% Triton X-100 (Sigma-Aldrich) in TBS 1X (incubation solution) O/N at 4°C with gentle shaking. Following incubation with primary antibodies, slices were washed four times in TBS 1X and incubated with incubation solution containing fluorescent secondary antibodies at RT for 2 h. Then, slices were washed three times in TBS 1X, the second wash containing DAPI (4 µg/ml, Sigma-

Aldrich). Slices were finally mounted on glass slides using Mowiol® mounting medium (Calbichem). Images were acquired by Leica Stellaris 5 confocal microscope using a 20X objective.

### 8.3 Acute slices

Mice were anesthesized with isofluorane and sacrificed. Brains were processed with a Leica VT 1200S vibratome (Leica microsystems) to obtain 150 µm-thick coronal sections. Sections were place in a chamber with continuous oxygenation in aCSF solution (NaCl 140 mM, KCl 2.5 mM, $NaH_2PO_4.H_2O$ 1.2 Mm, HEPES 10 Mm, Glucose 10 Mm, $NaHCO_3$ 26 mM, Sodium Pyrubate 1 Mm, N-acetylcysteine 12 mM, pH 7.3) for 1 h at 37°C to stabilize them. Then, they were treated 20 minutes with puromycin (10 µM), and negative controls were also treated with anysomycin (40 µM) for 45 minutes (25 minutes before puromycin). Samples were then fixed in 4% PFA for 1 h at RT and blocked with 10% NGS, 0.3% Triton X-100 in PB 0.1 M. Then, slices were incubated with primary antibodies dissolved in blocking solution O/N at 4°C with gentle shaking. Slices were washed three times in PB 0.1 M and incubated with incubation solution containing fluorescent secondary antibodies at RT for 1 h. Then,, slices were washed three times in 0.1 M PB, the second wash containing DAPI (4 µg/ml, Sigma-Aldrich). Slices were finally mounted on glass slides using Fluoromount-G mounting medium (SouthernBiotech).

### 8.4 Flouting mouse tissue

Mouse tissues were sectioned using a Leica VT 1200S vibratome (Leica microsystems) to obtained 40 µm-thick coronal sections. Slices were washed in 0.1 M PB and subjected to heat-induced treatment (121°C for 20 min) in R-Universal buffer (Aptum) for epitope recovery. The sections were then washed three time in 0.1 M PBS and treated with ice-col 100% EtOH for 10 minutes. Afterwards, they were washed three times with 0.1 M PB and permeabilized and blocked with 10% NGS, 0.1% Triton X-100 in PBS pH 7.4 for 30 min at RT. Slices were washed three times with 0.1 M PBS pH 7.4 and incubated with blocking solution-containing fluorochrome-conjugated secondary antibodies for 1 h at RT. Thent, slices were washed three times with 0.1 M PBS, incubated with DAPI (4 µg/ml, Sigma-Aldrich) for 8 min and washed again twice in 0.1 M PB. 18 months-old mouse

tissues were treated with Autofluorescence Eliminator Reagent according to the manufacturer's instructions (Millipore) to reduce lipofuscin-like autofluorescence and mounted on glass slides with Fluoromount-G mounting medium (Southern Biotech).

### 8.5 Paraffin-embedded human sections

Paraffin-embedded human sections (10 µM-thick) were deparaffinised and rehydratated by immersing in xylene followed by incubations with alcohol solutions (100%, 96% and 75% diluted in $H_2O$) in TBS for 10 min each. Samples were then boiled in R-Universal Buffer (Aptum) by using antigen retriever for 20 min and allowed to cool down for 30 min to promote epitope unmasking. After retrieval, samples were washed in TBS 3 times and blocked in 4% BSA in TBS for 1 h at RT and were incubated with primary antibodies in blocking solution O/N at RT. Then, samples were washed in TBS twice and incubated with fluorochrome-conjugated secondary antibodies and DAPI (4 µg/ml, Sigma-Aldrich) for 1 h at RT. Samples were washed in TBS and treated with Autofluorescence Eliminator Reagent according to the manufacturer's instructions (Millipore) to reduce lipofuscin-like autofluorescence. Finally, sections were washed and mounted with Fluoromont-G mounting medium.

***Table 5**. Antibodies used for immunofluorescence.*

| *Antibody* | *Host* | *Dilution* | *Reference* |
|---|---|---|---|
| Anti-MBP | Ms/ch/rb | 1:1000/1:200/1:200 | Biolegend Smi-99/Millipore ab9348/ Abclonal a1664 |
| Anti-MOG | Mouse | 1:1000 | Millipore MAB5680 |
| Anti-MOBP | Rabbit | 1:100 | Bioss bs-11184r |
| Anti-hnRNPA2 | Mouse | 1:1000 | Santa Cruz sc-374053 |
| Anti-hnRNPE1 | Rabbit | 1:1000 | MBL RNP024P |
| Anti-hnRNPF | Mouse | 1:1000 | Santa Cruz sc-32310 |
| Anti-hnRNPK | Rabbit | 1:1000 | MBL RNP019P |
| Anti-Puromycin | Mouse | 1:500 | Millipore MABE343 |
| Anti-Olig2 | Mouse | 1:1000 | Millipore MABN50 |
| Anti-Synaptophysin | Chicken | 1:500 | Synaptic systems #101006 |
| Anti-Homer1 | Rabbit | 1:500 | Synaptic systems #160003 |
| Anti-α-Tubulin | Mouse | 1:5000 | Abcam ab7291 |

## 8.6 Analysis of fluorescently-labelled samples

Images were acquired using a Leica TCS STED CW SP8X confocal microscope (Leica), a Leica Stellaris 5 confocal microscope (Leica) and a Zeiss Apotome 2 epifluorescence microscope (Zeiss). In experiments with multiple fluorophores, channels were scanned sequentially to avoid crosstalk. The same settings were applied to all the images within the same experiment. All analysis were carried out using the ImageJ/Fiji software (NIH).

### 8.6.1 Primary oligodendrocytes and neurons cultures

hnRNPs images were acquired with a Leica TCS STED CW SP8X confocal microscope using a 63X oil-immersion objective; 10 cells per condition were acquired in each experiment. First, a Gaussian filter was applied to the signal to discriminate background and improve the image. Then, the nuclei were deleted and a default threshold available in Fiji-ImageJ was applied. “Image Calculator” function was used with the channels for hnRNPA2 and hnRNPF to measure the doble-colocalization. Finally, “Analyze particles” function was used to identify the colocalized area. F-actin (phalloidin-TexasRed) and G-actin (DNAase I-Alexa 488) were acquired using a Zeiss Apotome 2 (Zeiss) epifluorescence microscope with a 40X oil-immersion objective. 10 different areas were taken per condition. Cells were outlined with the F-actin labelling to define a region of interest (ROI). Then, the mean intensity of both channels was quantified.

For hippocampal neurons, images were acquired with a Stellaris 5 confocal microscope using a 40X (for puromycin experiments) and a 63X oil-immersion objective (for synapsis analysis). 10 cells or areas for each condition were acquired in each experiment. The cell soma was outlined manually and puromycin integrated density was measured at the ROI. A macro designed by Dr. Jorge Valero was used to quantify synaptic marker staining in distal neuronal processes or neurites in primary neurons as a measure of synaptic damage. 20x4 µm ROIs were fixed in the image with the help of a routable tool to localize properly the ROI in the corresponding neurite orientation and then, area was calculated for each ROI.

### 8.6.2 Mouse tissue

Acute slices and flouting tissue images were acquired in a Leica TCS STED CW SP8X confocal microscope using a 40X oil-immersion objective to generate z-stack projections. Image analysis was carried out in 1-2 sections per subject. For puromycin fluorescence intensity analysis, cells were outlined manually and integrated density within oligodendrocytes was quantified. For, hnRNP A2 and Olig2 one z-stack images were acquired and hnRNP A2 mean intensity of $Olig2^{+}$cells nuclei was analysed.

### 8.6.3 Human samples

Human samples sections images were scanned by 3D Histech Pannoramic MIDI II slide scanner. 3 different areas in the hippocampus of each individual were used. hnRNP A2 fluorescence intensity was measured in $Olig2^{+}$ nuclei. Representative images were acquired by Leica TCS STED CW SP8X confocal microscope using a 40X oil-immersion objective to generate z-stack projections.

## 9. Proximity ligation assay using puromycin (Puro-PLA)

At 3 DIV, control and Aβ-treated oligodendrocytes ($2x10^4$ cells/well) were exposed to puromycin (2 µM) for 10 min in the absence or presence of the protein synthesis inhibitor anisomycin (40 µM) for 25 min. Negative controls with no puromycin received only fresh growth medium (vehicle). Cells were washed with cold PBS with digitonin and fixed in 4% PFA, 4% sucrose in PBS for 15 min.

PLA was conducted following Duolink® PLA Protocol (Sigma Aldrich). Briefly, as soon as cells were permeabilized and blocked, these were incubated with primary antibodies O/N; rabbit anti-MBP/mouse anti-puromycin (1:500) and rabbit anti-MOBP/mouse anti-puromycin (1:500). Coverslips were washed with an appropriate wash buffer and incubated with the corresponding PLA probes for 1 h. The ligation solution from the kit was applied and cells were incubated for 30 min. Then, signal amplification was achieved incubating cells with a polymerase for 100 min. All four incubation steps were conducted in a humidity chamber at 37 ºC and alternated with the subsequent washing steps. Finally, cells were washed and treated with Alexa 488-conjugated phalloidin in 1% BSA

in order to make the cytoskeleton visible. Coverslips were mounted on glass slides with Duolink® In situ Mounting Media with DAPI.

Images were taken with a Zeiss Apoteome 2 (Zeiss) epifluorescence microscope using 63X oil-immersion objective. Image analysis was performed using ImageJ/Fiji software. Phalloidin signal was processed with a Gaussian Blur plugin to create a mask. Employing a "Concentric Circles" plugin, concentric circles at 10 µm intervals emerging from the centre of the cell body were generated and mean values of fluorescence intensity of PLA probes were obtained.

## 10. Oligodendrocyte differentiation assay in nanofibers

After 14 DIV, control and Aβ-treated oligodendrocytes ($2x10^4$ cells/well) adhered to PDL-coated nanofibers (Sigma) were fixed in 4% PFA, 4% sucrose in PBS for 20 min, washed in 0.1 M PBS three times and then stored at 4°C.

Cells were permeabilized and blocked in 20% NGS, 0.1% Triton X-100 in 0.1 M PBS (blocking buffer) for 1 h and incubated with primary antibodies, chicken anti-MBP (1:200) and mouse anti-MOG (1:200) O/N at 4°C. Then, cells were washed with 0.1 M PBS and incubated with fluorochrome-conjugated secondary antibodies (1:500) in blocking buffer for 1 h at RT. Cells were washed and incubated with DAPI for 10 min. Then, cells were washed again twice and coverslips were mounted on glass slides with Fluoromount-G mounting medium. Images were acquired with a Leica TCS SP8 confocal microscope using a 63X oil-immersion objective to generate z-stack projections. ImageJ/Fiji software was used to measure the longitudinal MBP extension (the distance of the cellular MBP signal from the cell nucleus to the tip of the process in parallel to the nanofiber orientation) of all cell processes. The mean intensity MBP and MOG staining was also determined for each cell (the 3 most intense Z-stacks projections were considered).

## 11. Electron microscopy (EM)

Mice were perfused with 4% PFA, 2.5% glutaraldehyde (Electron microscopy Sciences) and 0.5% NaCl in phosphate buffer, pH 7.4, as previously described (Möbius et al., 2010). 8 dpf zebrafish were fixed with 2% glutaraldehyde, 4% PFA in 0.1 M cacolydate buffer, ph 7.4 for at least 5 days. The brains of mice and spinal cords of zebrafish were postfixed with the same fixative solution O/N at 4°C. The tissue was sagitally cut using Leica VT 1200S vibrating blade microtome (Leica) to obtain 200 µm-thick sections. Tissue sections were postfixed in 2% OsO4, dehydratated in ethanol abd propylenoxide and embedded in EPON (Serva) for 24 h at 60°C. Ultrathin sections (50 nm thickness) were obtained by Leica Ultracut S ultramicrotome (Leica) and contrasted 30 min with 4% uranyl acetate and 6 min with lead citrate.

EM pictures were taken with Zeiss EM900 electron microscope (Zeiss). *g*-ratio (100 myelinated axons per animal) was calculated as the ratio of the axon (A) plus the inner tongue (I) divided by the diameter of the whole fiber (M). The diameters for each region was measured using ImageJ/Fiji software from 8000x magnification images. The number of myelinated axons were quantified using 4000x magnification images.

## 12. Intrahippocampal injection in adult mice

10-week-old male mice (C57BL6/J) were subjected to intrahippocampal injections in the right dentate gyrus (DG). For the surgery, animals were anesthetized with 0.3 ml of Avertin, with addition of 0.1 ml if needed. Mice were immobilized with a stereotaxis apparatus and injected with the corresponding preparations: vehicle or 3 µL of Aβo at 10 µM. Coordinates for the injection were Bregma -2.2 mm, lateral 1.5 mm and DV 2 mm. After injection and before removal, the needle was left on site for 5 min to avoid reflux.

Mice were anesthetized with ketamine /xylacine (100/10 mg/kg) and perfused with 30 ml of phosphate buffer followed by 30 ml of 4% PFA IN 0.4 M PB. The brains were extracted and postfixed with the same fixative solution for 4 h at RT, placed in 30%

sucrose in 0.1 M PBS ph 7.5 at 4°C, and then kept in cryoprotectant solution (30% ethylene glycol, 30% glycerol and 10% 0.4 M PB in $dH_2O$) at -20°C.

# 13. Magnetic activated cell sorting (MACS)

Animals were anesthetized by isofluorone and sacrified by decapitation. Then oligodendrocytes were isolated as described before (de la Fuente et al., 2020). Briefly, the brains were removed from the skull, put in to Hibernate A (Gibco) and cut into small pieces (about 1 mm3). The brains were digested with a papain solution containing papain (33 U/ml) and DNase (0.04 mg/ml) in Hibernate A for 30 min at 37°C. Following tissue digestion papain was washed out with $HBSS^{-/-}$ (Gibco) via centrifugation. The tissue was then triturated with a polished glass Pasteur pipette in Hibernate A with 1×B27 (Gibco) and 2 mM sodium pyruvate (Gibco). After trituration, the single cell suspension was passed through a 70 µm strainer (VWR) and centrifuged for 20 min at 800 × g in a 22.5% Percoll (GE Healthcare) solution with DMEM Glutamax (Gibco). Following centrifugation Percoll was removed by aspiration and the cells were washed with $HBSS^{-/-}$ (Gibco). Cells were incubated with anti-O4 antibody (Milteny Biotech) for 15 min on ice. Excess antibody was again removed by washing with $HBSS^{-/-}$ and cells were magnetically sorted following the manufacturer's instructions (Milteny Biotech). Cells were eluted in Sato+ medium.

# 14. RNA extraction and quantification

## 14.1 RNA isolation

For cultured oligodendrocytes, total RNA was isolated using RNA Mini Kit (Quiagen) or TRIzol (ThermoFisher Scientific) according to manufacturer’s instructions. For MACS isolated oligodendrocytes, total RNA was isolated using RNA Micro Kit (Quiagen) according to manufacturer´s instructions. RNA concentration and integrity was measured by a spectrophotometer Nano Drop™ 2000 (ThermoFisher Scientific).

## 14.2 Retrotranscription and quantitative Real time-Polymerase Chain Reaction (RT-qPCR)

RNA was reverse transcribed in a 20 µl reaction containing 5X Buffer, 0.1 M DTT, random primers, dNTPs, RNase OUT and Superscript III retrotranscriptase following manufacturer's instructions in a Verity Thermal Cycler (Applied Biosystems). Resulting complementary DNA (cDNA) samples were diluted in sterile Mili-Q H2O. Then, RT-qPCR was performed in 3.5 µl RNAse-free water, 5 µl Sybr Green Master Mix 1 µl properly diluted primers and 0.5 µl cDNA sample. All reaction were performed by triplicates and carried out in cDNA CFX96 Touch Real-Time PCR Detection System (Bio-Rad). Amplification reactions were optimized and 3 min 95°C, and 40 cycles of 10 s at 95°C, 30 s at 60°C.

Primers were designed using Primer3 software and synthesized by integrated DNA Technologies (IDT) or commercially available primers from QIAGEN were used. PCR product specificity was checked by melting curves. Data were normalized to a normalization factor obtained in geNorm Software through the analysis of the expression of three different housekeeping genes. Primer sequences are detailed in **Table 5**.

***Table 5.*** *Sequences of primers used in the transcriptional analysis grouped in different categories.*

| Category | Gene | Sequence | Reference |
|---|---|---|---|
| Myelin-related proteins | MBP | | Quiagen QT00199255 |
| | MOG | | Quiagen QT00177149 |
| | MAG | | Quiagen QT00195391 |
| | MOBP- 81A | Fwd CGCTCTCCAAGAACCAGAAG<br>Rev GCTTGGAGTTGAGGAAGGTG | IDT |
| | PLP | Fwd CGACATCCCGACAAGTTTGTG<br>Rev CTAGGGAAGGCAATAGACTGGC | Eurofins |
| | CNP | Fwd CGCCCACTCATCATGAGCAC<br>Rev CCTGAGGATGACATTTTTCTGAAGA | Eurofins |
| hnRNPs | HNRNPA2B1 | | Quiagen QT01826545 |
| | HNRNPF | | Quiagen QT00453110 |
| | HNRNPK | | Quiagen QT00381626 |
| | HNRNPE1 | | Quiagen QT00507206 |
| Microtubules | TAU | Fwd CGCTCTCCAAGAACCAGAAG<br>Rev GCTTGGAGTTGAGGAAGGTG | IDT |
| | Dynlt1 | Fwd TTACACACCGCAAGTTCCTG<br>Rev GACTAGAAACGCTGGAACCG | IDT |
| | DNT1 | Fwd TTGACGTGGGTGGTAGCTGT<br>Rev TCTGCGTCATACTCGCCTTC | IDT |
| | DNT2 | Fwd CAGATGCTGCAATCAACCTT<br>Rev CAACTTTGGCAGCTTGAGAG | IDT |
| Housekeeping | GAPDH | Fwd GAAGGTCGGTGTCAACGGATTT<br>Rev CAATGTCCACTTTGTTCACAAGAGAA | Eurofins |
| | BM2 | Fwd CACCGAGACCGATGTATATGCTT<br>Rev TTACATGTTCTCGGTCCCAGG | Eurofins |
| | CICA | Fwd CAAAGTTCCAAAGACAGCAGAAAA<br>Rev CCACCCTGGCACATGAATC | Eurofins |
| | ACTB | Fwd TGTCACCAACTGGGACGATA<br>Rev GGGGTGTTGAAGGTCTCAAA | IDT |

## 15. RNA-seq

To perform RNA-seq samples were sent to the Genomic Platform at CICbioGUNE (Derio, Spain). The RNA quantity and quality was assessed using Qubit RNA assay kit (Invitrogen) and Agilent 2100 Bioanalyzer (Agilent RNA 6000 Pico Chips). All samples presented enough concentration and integrity to perform the experiments.

Sequencing libraries were prepared using "SMARTer Stranded Total RNA-seq Kit v2 – Pico Input Mammalian" kit (Takara Bio USA, Cat.# 634411), following "SMARTer Stranded Total RNA-seq Kit v2 – Pico Input Mammalian User Manual (Rev. 050619)". The protocol was started with 4-10 ng of total RNA. Briefly, RNA was fragmented and 1st strand cDNA synthesis was performed using SMARTScribe reverse Transcriptase, for 90 min at 42°C, 10 min at 70°C and pause at 4°C. Afterwards, Illumina Adapters containing Indexes were added, and a preamplification PCR reaction was performed (60 sec at 94°C, 5 cycles of 15 sec at 98°C, 15 sec at 55°C 30 sec at 68°C; and pause at 4°C). Then, Ribosomal cDNA was depleted with ZapR v2 and R-Probes v2. Finally, enrichment of libraries was achieved by PCR (60 sec at 94°C; 12 or 16 cycles of 15 sec at 98°C, 15 sec at 55°C, 30 sec at 68°C; and pause at 4°C). Libraries were visualized on an Agilent 2100 Bioanalyzer using Agilent High Sensitivity DNA kit (Agilent Technologies, Cat. # 5067-4626 ) and quantified using the Qubit dsDNA HS DNA Kit (Thermo Fisher Scientific, Cat. #Q32854). The Illumina sequencer generates raw images utilizing sequencing control software for system control and base calling through an integrated primary analysis software called RTA (Real Time Analysis). The BCL (base calls) binary is converted into FASTQ files utilizing Illumina Inc.'s package bcl2fastq and quality control analysis is performed (FastQC; Andrews, 2010).

The posterior bioinformatic analysis was then carried out in collaboration with Rodrigo Senovilla Ganzo, predoctoral researcher at Dr. Fernando García-Moreno (Achucarro BCN, Leioa, Spain). The alignment was carried out with STAR v2.7.1 (Dobin et al., 2013) against Ensembl genome of *Rattus norvegicus* (BN7.2.toplevel ang gtf v105), so not trimming was necessary. To obtain the count matrix, htseq-count (-s reverse) (Anders, Pyl, & Huber, 2015) was run with strand specificity and imported to R v4.2.2, where it was analysed with DESeq2 (Love, Huber, & Anders, 2014).

DESeq2 provides methods for differential expression tests based on negative binomial generalized linear models. Therefore, the factors involved in the analysis must be modelled beforehand in a sample table entry **(Table 6)**. This metadata allows DESeq2 to group samples by factors of interest (e.g. Experiment and Condition) to detect differentially expressed genes depending the biological question (contrast selection), but also to correct batch effect (e.g. Pair, blocking factor).

***Table 6. Sample Table**. Each sample (row name) is assigned a level of a factor (column names). IgG samples were a mix of both of control and Aβo treated cells, so it was used for regressing out noise in both conditions.*

| Sample Name | Experiment | Pair | Condition |
|---|---|---|---|
| **IgG2** | IgG | 2 | Control/Aβ |
| **IgG3** | IgG | 3 | Control/Aβ |
| **IgG4** | IgG | 4 | Control/Aβ |
| **InputC2** | Input | 2 | Control |
| **InputC3** | Input | 3 | Control |
| **InputC4** | Input | 4 | Control |
| **InputAβ2** | Input | 2 | Aβ |
| **InputAβ3** | Input | 3 | Aβ |
| **InputAβ4** | Input | 4 | Aβ |
| **RIPC2** | RIP | 2 | Control |
| **RIPC3** | RIP | 3 | Control |
| **RIPC4** | RIP | 4 | Control |
| **RIPAβ2** | RIP | 2 | Aβ |
| **RIPAβ3** | RIP | 3 | Aβ |
| **RIPAβ4** | RIP | 4 | Aβ |

The initial step of DESeq2 pipeline is to filter low expressed genes. The threshold was set to > 2 counts for the interactome analysis and > 5 counts for the Aβ-treatment impact analysis. These differences in the threshold for each analysis are due to the different amount of RNA obtained in the input and immunoprecipitated samples.

Moreover, we performed an additional filtering to avoid technical bias due to detection errors (gene not sequenced or aligned). For each condition and experiment, a gene was not considered if its expression was not over the selected threshold in at least two samples of the experiment/condition group.

For the different analysis, we selected different sample types to obtain a DESeq2 compatible matrix factors (as IgGs were a mix of both of wild-type and Aβ treated cells, they were common for both conditions). In the A2 interactome analysis, only control samples were selected (IgG, Input Control, RIP Control). Following similar pipelines (Moore et al, 2019 ; Tichy et al, 2018 ; Rossi et al, 2017 ; Gagliardi et al, 2016), the linear model design used were: ~ Pair + Experiment and contrast: list ("Experiment_RIP_vs_Input", "Experiment_IgG_vs_Input"), respectively. Those genes with p-adjusted value < 0.05 were identified as significantly interacting with A2. To analyse how Aβ treatment impaired A2 interactome, a similar workflow as above was carried out, but selecting those Aβ treated samples. Results obtained from the Aβ-treated interactome were compared to the control interactome.

Similarly, the impact of Aβ in oligodendrocytes transcriptome was explored with the following design: ~ SV1 + SV2 + Pair + Experiment + Condition + Experiment:Condition. However, due to the complexity of the model, we removed the IgG samples. SV1 and SV2 factors have computed based on Surrogate Variable Analysis (Leek et al, 2022) to extract variability due to unknown noisy factors as Aβ oligomerization and others. To explore the effect of Aβ in the whole-cell transcriptome, the following contrast was used: "Condition_Ab_vs_C".

For data visualization and functional enrichment: *ggplot2* (Wickham et al, 2016), clusterProfiler (Wu et al, 2021; Yu et al, 2012) and *ggVennDiagram* (Gao et al, 2021) were used. The code used can be found in https://github.com/rodrisenovilla/AlberdiLab. Analysed data will be uploaded conveniently at GEO repository (https://www.ncbi.nlm.nih.gov/geo/) once they are published.

## 16. RNA *in situ* hybridisation

Fluorescent *in situ* RNA hybridisation was performed using the RNAScope Multiplex Fluorescent V2 Assay Kit (Advanced Cell Diagnostics; ACD) on 15 µm thick paraformaldehyde-fixed and agarose embedded cryosections according to

manufacturer's instructions with the following modification: slides were covered with parafilm for all 40°C incubations to maintain moisture and disperse reagents across the sections. The zebrafish *mbpa*, *myrf*, and *sox10* transcript probes were designed and synthesized by the manufacturer and used at 1:50 dilutions except for *mbpa* that was not diluted. Transcripts were labelled by TSA-based Opal fluorophores Opal520 (1:1500), Opal570 (1:500) and Opal650 (1:1500) using the Opal 7 Kit (PerkinElmer). The images were acquired on a Zeiss Cell Observer Spinning Disk confocal system at 40×/1.20 NA water immersion objective. 28 z-stack tiles (z-step= 0.28 µm) of 10 sections of spinal cord were acquired from each animal. Total area occupied for each channel was determined in ImageJ/Fiji.

## 17. Enzyme-linked immunosorbent assay (ELISA)

The levels of human $A\beta_{1-42}$ were determined in homogenates using the High Sensitivity Human Amyloid β42 ELISA kit (Millipore, #EZHS42). Concentrations were quantified according to the manufacturer's instructions in triplicates. Triplicates were averaged and normalized to the total number of living cells.

50 µl of antibody conjugate solution was added into all wells. Then, 50 µl of standards solutions and samples (prediluted) were added into a 96-well plate pre-coated incubated for 5 min at RT with gentle shaking and incubated O/N without shaking at 4°C. Next day, the plate was washed with washing solution 5 times, and 100 µl of Enzyme Conjugate Solution was added and incubated for 30 min at RT with gentle shaking. Then, the plate was washed again 5 times, and 100 µl of substrate solution was added and incubated for 7 min at RT shaking in darkness. Finally, 100 µl of stop solution was added and the plate was read immediately in a fluorimeter at 450 and 590 nm. The standard curve was obtained plotting the standard concentration (pg/mL) on the x-axis and absorbance on the y-axis.

# 18. Extracellular vesicle (EVs) purification

Cultured oligodendrocytes were exposed to Aβ 1 µM for 24 h (250.000 cells/condition to treat neurons and $1x10^6$ cells/condition for WB) and then, oligodendrocyte viability assay was performed (to quantify living cells) and culture media was collected for EVs isolation. Proteins were extracted from the remaining cells and were used as whole-lysate controls. Culture media were then centrifuged at 1,500 x g for 5 min to remove lifted cells and cellular debris. The resultant supernatant was ultracentrifuged at 315,000 x g for 75 min and the final pellets containing EVs (mainly EVs and microvesicles) were resuspended in 15 µL of PBS 1X pH 7.4. Cell treatments and EV analyses were performed adjusting the VEs to the same amount of secreting (living) cells. Whole-cell lysates and vesicles were analysed by Western blot.

# 19. *In vivo* live imaging

## 19.1. Fluorescent recovery after photobleaching (FRAP)

FRAP experiments were performed in cultured oligodendrocytes (2 and 3 DIV) infected with a 1:100 dilution of the Sindbis virus carrying Life-Act for at least 16 hours. Each experiment was performed with two different conditions: control cells without treatment and cells treated with 1 µM of the Aβ peptide 30 minutes before the experiment. After these 30 minutes, the medium was replaced with “Live Cell Imaging Solution" (Thermofisher Scientific) for microscope visualization and 1 µM of the Aβ peptide was added back to be present during the FRAP assay. Images were obtained with a Leica TCS STED CW SP8 super-resolution confocal microscope following the Leica "FRAP with TCS SP8" protocol. F-actin-GFP was recorded for 20 seconds before photobleaching, which was performed at a wavelength of 405 nm. The consequent fluorescence recovery was measured for 280 seconds. The analysis of the fluorescent signal was carried out with the Leica Application Suite X (LAS X) program.

By using this technique, we wanted to adress the effect of Aβ peptide on the polymerization of fluorescently labeled F-actin in cultured oligodendrocytes. It should

be noted that the observed fluorescence recovery may be due to not only actin polymerization, as there may be some degree of diffusion of the fluorophore. For this reason, fluorescence was also recorded in a non-photobleached region of the same cell as a control. Thus, a correction factor calculated as the ratio of each value of the control region to the initial value of the same region was introduced in the data processing. The photobleached zone data were divided by their corresponding correction factor to compensate for fluorescence oscillations due to fluorophore diffusion rather than polymerization. After correction, data were plotted and normalized to the mean fluorescence before photobleaching (defined as 1). Fluorescence after of photobleaching was defined as 0. For the analysis of the results, the "Fast Half Life" parameter was chosen, which gives a measure of the rate of fluorescence recovery in the fast stage. Specifically, it corresponds to the time at which half of the fluorescence is recovered in this stage. The values of this parameter were obtained using nonlinear regression (two-phase decay model) using GraphPad Prism 8 software.

### 19.2 Cytosolic calcium imaging in cultured oligodendrocytes

Measurement of cytosolic $Ca^{2+}$ was carried out as previously described (Ruiz, Alberdi, & Matute, 2014). Briefly, oligodendrocytes were loaded with Fluo-4 AM (1 µM; Molecular Probes, Invitrogen) in SATO+ culture medium for 30 min at 37°C. Then, culture medium was removed and cells were maintained 20 min in extracellular solution (NaCl 140 mM, KCl 5 mM, MgCl2 2 mM, CaCl2 2 mM, Glucose 10 mM and HEPES 10 mM; pH 7.4) to allow de-esterification. Oligodendrocytes were exposed to KCl (25 mM) and images were acquired through a 40X oil objective with an inverted LCS SP2 confocal microscope (Leica, Germany) at an acquisition rate of 1 frame/15 s during 5 min. For data analysis, a homogeneous population of 10-20 cells was selected in the field of view and cell somata were selected as ROIs. Background values were always subtracted and data are expressed as $F/F0 \pm$ SEM (%) in which $F$ represents the fluorescence value for a given time point and $F0$ represents the mean of the basal fluorescence level.

### 19.3 Cytosolic calcium imaging in hippocampal organotypic slices

Organotypic slices were loaded with Fura 2-AM (5 µM; Molecular Probes, Invitrogen) and 0,01% Pluronic TM F-127 (Invitrogen) in culture medium for 30 min at 37°C. Then, cells were washed in HEPES-Hank´s solution (incubation buffer) (HBSS, MgCl2 1 mM, CaCl2 2 mM, Glucose 10 mM, NaHCO3 4 mM and HEPES 20 Mm; pH 7.4) 10 minutes at RT. Experiments were performed in a coverslip chamber continuously perfused (1.5 ml/min) with the incubation buffer. The perfusion chamber was mounted on the stage of a Leica DMLFSA epifluorescence microscope (Leica, Germany) equipped with a Polychrome V monochromator (Till Photonics, Germany). Organotyic cultures were exposed to a local application of KCl (50 mM) through a microinjector (Eppendorf) with an applied pressure of 160 hPa (duration of the pulse 10 s). Images were acquired through a 40X water objective at an acquisition rate of 1 frame/1 s during 2 min with Aquacosmos imaging software (Hamamatsu, Japan). Intracellular calcium levels were estimated by the 340/380 ratio method.

### 19.4 Myelin Sheath visualization in zebrafish larvae

Zebrafish larvae at 5 dpf were anesthetized with 0.4% tricaine and embedded laterally in 1.2% low-melt agarose containing 0.4% tricaine for immobilization on a glass bottom dish. The images were acquired on a Zeiss Cell Observer Spinning Disk confocal system at 63× water immersion objective. Images were collected from 1-2 field of view from each animal in 40 z-stack tiles (z-step= 0.28 µm). Sheath length and total number of sheaths per oligodendrocytes were analysed in maximum intensity projections using Fiji/ImageJ in a blind mode.

## 20. Statistical analysis

All data are expressed as mean ± S.E.M (Standard error of the mean) with sample size indicated in the figure by dots. Statistical analyses were performed using absolute values and GraphPad Prism 8 software. Paired and not paired two-tailed Student´s t-test, one-way ANOVA and two-way ANOVA tests were used and multiple-comparison corrections (Dunnett, Tukey and Sidak) were applied in *post-hoc* tests depending on the sample

characteristics. Statistical significance was represented as $p<0.05$ (*), $p<0.01$ (**), $p<0.001$ (***) and $p<0.0001$ (****).

# RESULTS

# PART I: Differential transcriptomic response of oligodendrocytes to AD pathology

It the recent years, single-cell genomics has highlighted common signalling pathways perturbed across multiple cell types in AD such as inflammation and immune response, lipid signalling and metabolism, metabolic stress and protein folding, DNA damage and cellular senescence and interactions with vascular cells (Murdock and Tsai, 2023). Insights into Alzheimer´s disease with single-cell genomic approaches reflect alterations in the diverse functional repertoire of oligodendrocytes, including myelination, sensing neural activity and immune function. In addition, spatial transcriptomic analyses performed in transgenic AD mice reveal that amyloid plaques alter the expression of oligodendroglial genes (Chen et al., 2020). However, little is known about the effect that Aβo can have in the oligodendrocytes and in the myelination processes, and how this can contribute to the development and progression of the disease.

## 1.1 $A\beta_{1-42}$ oligomers alter oligodendrocytes transcriptome *in vitro*

To investigate the transcriptional responses of oligodendrocytes to Aβo, we performed RNA sequencing (RNA-seq) on control and Aβo-treated primary-oligodendrocyte cultures. After 24 hours of Aβo-treatment, we found 3204 differentially expressed genes (DEGs), where 2002 genes were significantly upregulated, and 1202 were significantly downregulated (DeSeq2, adjusted P value<0.05) **(Figure 10A)**. To gain insight into the gene expression differences, we performed Gene Ontology (GO) term enrichment analyses (Cluster profiler software) and pathway analyses using WikiPathways (tool from webgestalt online software). We chose WikiPathways in addition to the classic GO analysis because it is continuously updated and curated and because it includes other pathway databases such as Reactome.

Clustering GO terms into biological processes (BPs) revealed a group of upregulated DEGs involved in RNA metabolism (such as *hnrnpu, hnrnpk, hnrnpm, hnrnpa2b1, App,* and *Dhx9*), as well as in chromosome regulation (such as *Upf1, Atrx, Parp1* and *Top2a*) and nuclear transport (*Ctnna1, Xpo, Htt, Nup133,* and *Stat3*). Other notable enriched

biological processes such as vesicle localization, Golgi vesicle transport and morphogenesis were also significantly enriched **(Figure 10C)**. Conversely, strongly downregulated genes were associated mainly with the mitochondria respiratory chain (such as different *Ndufs, Tfam,* and *Cos19*), and oxidative phosphorylation and ATP synthesis (such as *Uqcrq, Cox1, Cycs, Cytb,* and *Park7*) **(Figure 10D)**.

The significantly enriched pathways associated with upregulated DEGs included cholesterol metabolism and biosynthesis, hexose metabolism, TNF-alpha NF-kB signalling pathway and focal adhesion **(Table 7)**, all of which are key pathways in myelination. In contrast, the pathways associated with downregulated DEGs included cytoplasmic ribosomal proteins and eukaryotic transcription initiation, which are related to translation. Noteworthy, there are different pathways deregulated related to energy metabolism which would suggest a change in energetic demands and the sources of energy **(Table 7).**

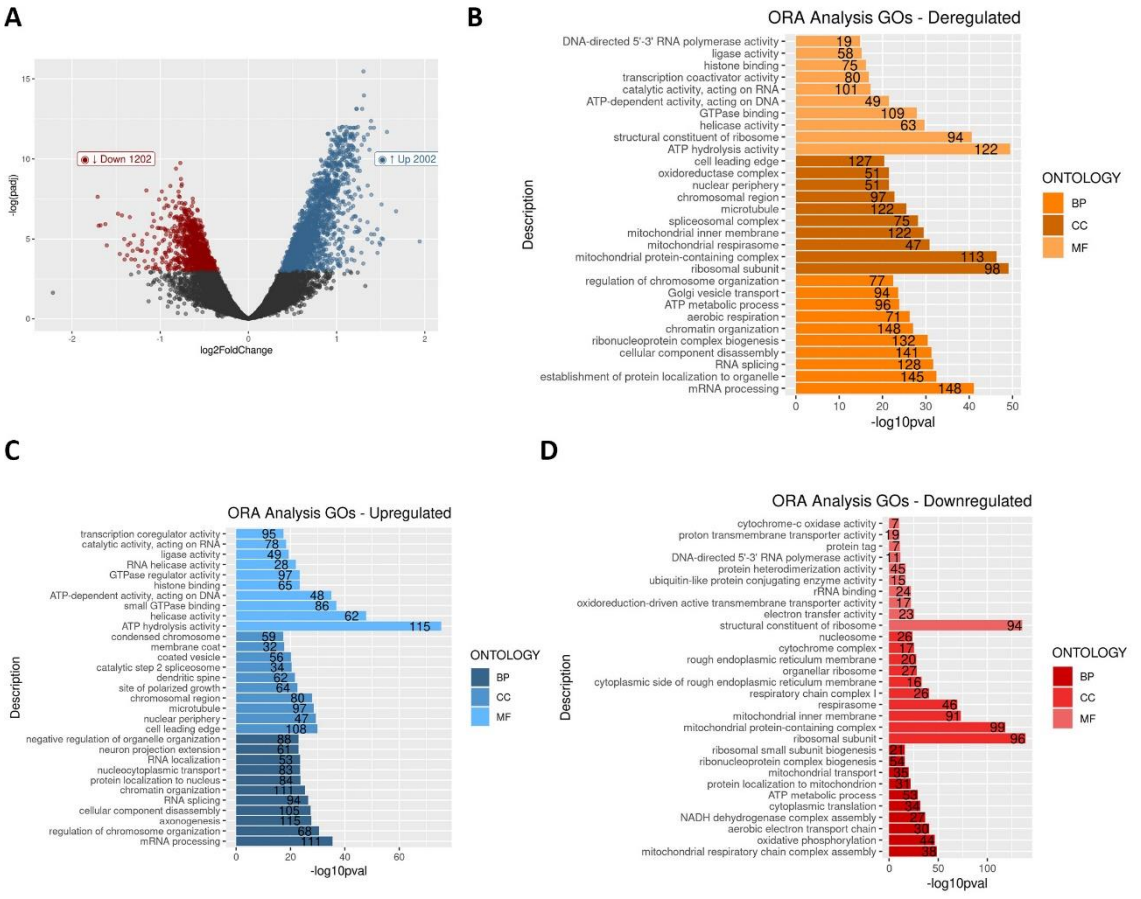


***Figure 10. Transcriptomic analysis of Aβ-treated compared to vehicle-treated oligodendrocytes. (A)*** *Volcano plots showing distribution of significantly up- and down-regulated genes.* ***(B)*** *GO analysis of*

*biological process (BP), cellular component (CC) and molecular function (MF) of DEGs and number of genes associated in each GO term.* ***(C)*** *GO analysis of upregulated genes and number of genes associated in each GO term.* ***(D)*** *GO analysis of downregulated genes and number of genes associated in each GO term.*

Interestingly, genes with the highest expression levels are related to important functions of oligodendrocytes and have a direct link to AD, such as myelination, iron homeostasis and APP pathway. The most remarkable ones among upregulated genes are *Actb, Nfasc, Cnp, Mag, Apoe, hnrnpa2b1* and *App* whereas *Fth1, Ftl1* and *Mobp* are downregulated.

***Table 7.*** *Pathway of upregulated (blue) and downregulated (red) genes in cultured oligodendrocytes treated with Aβo.*

| geneSet | description | size | overlap | pValue |
|---|---|---|---|---|
| **WP529** | *mRNA Processing* | *112* | *43* | *8.13E-03* |
| **WP632** | *Cholesterol metabolism* | *23* | *13* | *2.30E-09* |
| **WP3916** | *Hexoses metabolism in proximal tubules* | *55* | *18* | *3.38E-12* |
| **WP439** | *Insulin Signalling* | *152* | *36* | *8.73E-11* |
| **WP457** | *TNF-alpha NF-kB Signalling Pathway* | *174* | *39* | *0.001659* |
| **WP145** | *Statin Pathway* | *18* | *8* | *0.001800* |
| **WP1292** | *One Carbon Metabolism* | *26* | *10* | *0.001852* |
| **WP461** | *Cholesterol Biosynthesis* | *15* | *7* | *0.002502* |
| **WP188** | *Focal Adhesion* | *190* | *41* | *0.002720* |
| **WP372** | *Beta Oxidation Meta Pathway* | *32* | *10* | *0.010198* |
| **WP30** | *Cytoplasmic Ribosomal Proteins* | *108* | *47* | *<2.2E-16* |
| **WP59** | *Electron Transport Chain* | *93* | *35* | *<2.2E-16* |
| **WP1283** | *Oxidative phosphorylation* | *60* | *23* | *7.12E-02* |
| **WP491** | *Eukaryotic Transcription Initiation* | *40* | *11* | *3.63E-11* |
| **WP1279** | *Estrogen Signalling* | *69* | *12* | *0.0016441* |
| **WP1293** | *Selenium metabolism Selenoolproteins* | *34* | *7* | *0.0059846* |
| **WP294** | *p38 MAPK Signalling Pathway* | *37* | *7* | *0.0096622* |
| **WP1310** | *Selenium Micronutrient Network* | *23* | *5* | *0.0155700* |
| **WP1311** | *Folic Acid Network* | *25* | *5* | *0.0220634* |
| **WP4229** | *Insulin induced PI3K-Akt and MAPK in hepatocytes* | *34* | *5* | *0.0713909* |

## 1.2 Comparative analysis of DEGs between Aβo-treated oligodendrocytes *in vitro* and isolated oligodendrocytes from 3xTg-AD

Next, to gain a broader view we sought to verify the alterations shown *in vitro* in the 3xTg-AD mouse model (carrying $APP_{Swe}$, $MAPT_{P301L}$, and $PSEN1_{M146V}$ mutations). As we were interested in analysing perturbed pathways in early stages, we used MACS to selectively isolate immature and mature oligodendrocytes ($O4^+$) from the brain of 6-

months-old 3xTg-AD and WT mice and performed bulk RNA-seq to determine gene expression changes. We found 5537 DEGs, where 2392 genes were significantly upregulated, and 3145 were significantly downregulated (DeSeq2, adjusted *P* value<0.05) **(Figure 11A).** When comparing the DEGs between *in vitro* and *in vivo*, we observed that 1395 (%19) were altered in both cases. These DEGs are mainly involved in RNA metabolism (mRNA splicing and mRNA processing), Golgi vesicle transport, ribonucleoprotein complex biogenesis, autophagy and energy metabolism **(Figure 11B, C)**.

Then, from all the DEGs observed *in vitro* and *in vivo* we wanted to determine which ones follow the same pattern, that is to say, which genes are up or downregulated in both situations. Out of the 1395, only 193 genes were upregulated and conversely, 74 downregulated **(Figure 11D, F).** We performed GO term enrichment and Wikipathways analysis. When focusing on the upregulated BPs, we mainly observed those related to RNA metabolism (mRNA processing, RNA transport, RNA localization and mRNA binding), positive regulation of protein localization or microtubule cytoskeleton organization **(Figure 11E)**.

On the other hand, Wikipathway analyses revealed the top 10 enriched pathways in both models. Pathways associated with upregulated DEGs are related to insulin signalling, mRNA processing or mechanisms associated with pluripotency, while pathways associated with downregulated DEGs include MAPK and Akt signalling pathways. Moreover, as in the *in vitro* model we observe several pathways linked with energy metabolism like fatty acid beta-oxidation, oxidative stress and glycogen metabolism **(Table 8)**.

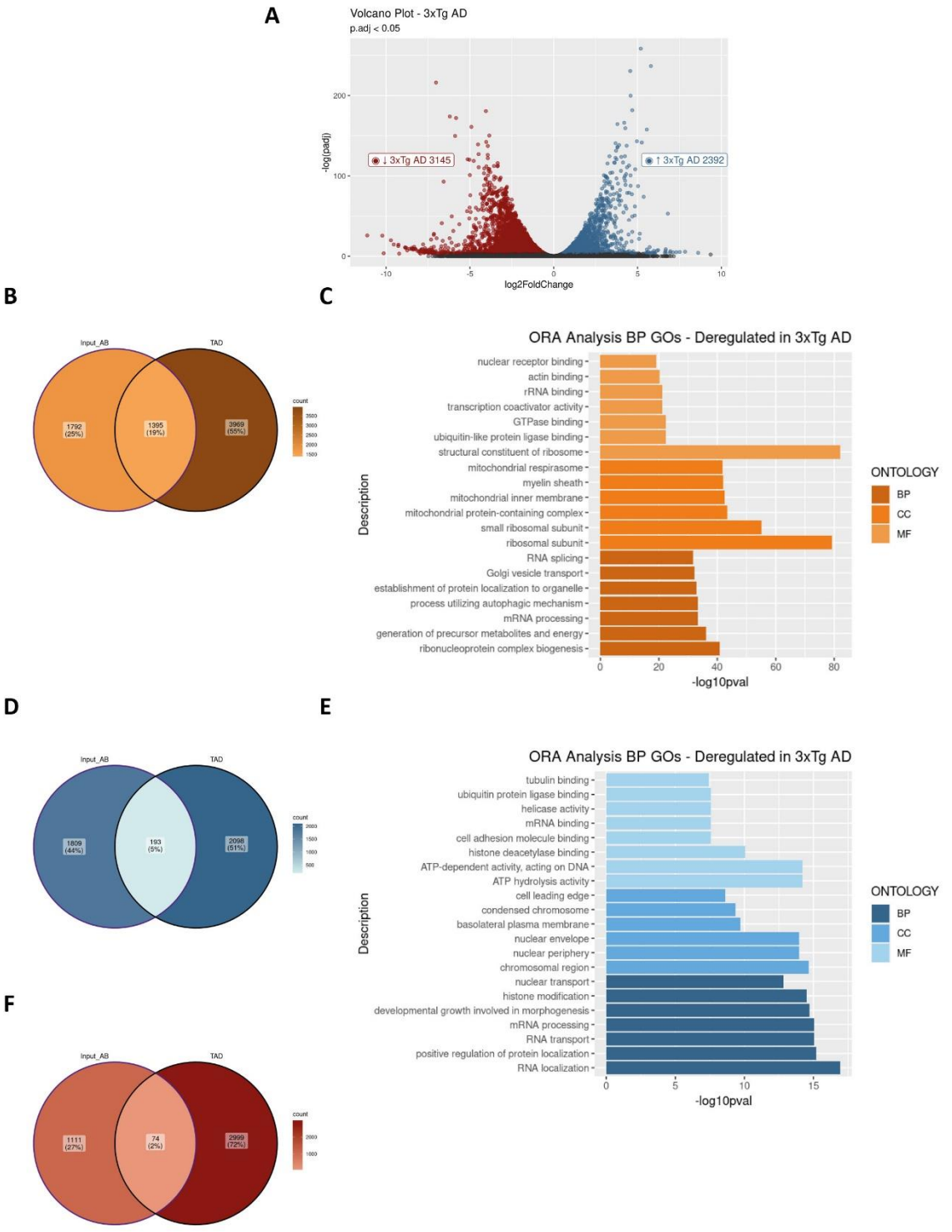


***Figure 11. Comparative transcriptomic analysis of oligodendrocytes in vitro and in 3xTg-AD mice (A)*** *Volcano plots showing the distribution of significantly up- and down-regulated genes in oligodendrocytes isolated from WT and 3xTg-AD mice.* ***(B)*** *Venn diagram depicting the overlap of DEGs in vitro vs 3xTg-AD. Percentage indicates the proportion of common genes.* ***(C)*** *GO analysis of biological process (BP), cellular component (CC) and molecular function (MF) of DEGs.* ***(D)*** *Venn diagram depicting the overlap of DEGs upregulated in vitro vs 3xTg-AD. Percentage indicates the proportion of common.* ***(E)*** *Analysis of top 10 BPs of commonly upregulated DEGs.* ***(F)*** *Venn diagram depicting the overlap of DEGs downregulated in*

*vitro vs 3xTg-AD. Percentage indicates the proportion of common genes.* ***(G)*** *Analysis of top 10 BPs of commonly downregulated DEGs.*

Interestingly, genes involved in myelination (*Mobp, Itgb1, App, Cnp, hnrnpa2b1 and Vamp2/3), cytoskeleton (Actb, Dnt1, Limk1, Rock1, Mapt, and Dyn)* and iron homeostasis *(Fth1, Ftl1 and Iscu)* are some of the most remarkable deregulated genes both in cultured and in 3xTg-AD-derived oligodendrocytes.

***Table 8.****Pathway of upregulated (blue) and downregulated (red) genes in cultured oligodendrocytes and 3xTg-AD mice oligodendrocytes.*

| geneset | Description | size | overlap | pvalue |
|---|---|---|---|---|
| **WP1763** | Mechanism associated with pluripotency | 293 | 16 | 3,29E-09 |
| **WP65** | Insulin Signalling | 159 | 7 | 0.008329 |
| **WP571** | FAS pathway and Stress induction of HSP regulation | 37 | 3 | 0.016581 |
| **WP310** | mRNA processing | 460 | 12 | 0.034114 |
| **WP336** | Fatty Acid Biosynthesis | 22 | 2 | 0.040802 |
| **WP4344** | Sphingolipid Metabolism | 25 | 2 | 0.051524 |
| **WP403** | Wnt Signaling Pathway | 60 | 3 | 0.057581 |
| **WP6** | Integrin-mediated Cell Adhesion | 100 | 4 | 0.058736 |
| **WP543** | Synthesis and Degradation of Ketone Bodies | 5 | 1 | 0.071488 |
| **WP523** | Regulation of Actin Cytoskeleton | 152 | 5 | 0.071828 |
| **WP350** | p38 MAPK Signaling Pathway | 36 | 3 | 6,05E-10 |
| **WP151** | IL-5 Signaling Pathway | 69 | 3 | 0.004006 |
| **WP493** | MAPK signaling pathway | 159 | 4 | 0.006085 |
| **WP387** | IL-6 signaling Pathway | 99 | 3 | 0.010936 |
| **WP373** | IL-3 Signaling Pathway | 100 | 3 | 0.011240 |
| **WP2841** | Focal Adhesion-PI3K-Akt-mTOR-signaling pathway | 325 | 5 | 0.016252 |
| **WP297** | IL-7 Signaling Pathway | 44 | 2 | 0.018147 |
| **WP1261** | ErbB signaling pathway | 46 | 2 | 0.019741 |

## 1.3 Comparative analysis of DEGs in Aβo-treated, 3x Tg-AD and AD oligodendrocytes

Finally, we wondered whether the disease-associated gene signatures identified *in vitro* and in the 3xTg-AD mouse model were also altered in oligodendrocytes derived from AD patients. To this end, we selected published datasets obtained from oligodendrocyte-lineage cells derived from early-stage human AD and control subjects (Mathys et al., 2019) and performed a comparative analysis. 370 genes were common to the three conditions (4%), which are mainly involved in cytoplasmic translation and

mitochondrial metabolism (ATP metabolic process, oxidative phosphorylation and mitochondrial ATP synthesis). When comparing which DEGs follow the same trend in all three conditions, we only found 53 genes up- (1%) and none downregulated **(Figure 12C)**. The upregulated GOs showed pathways related to cytoskeleton and positive regulation of protein localization among others.

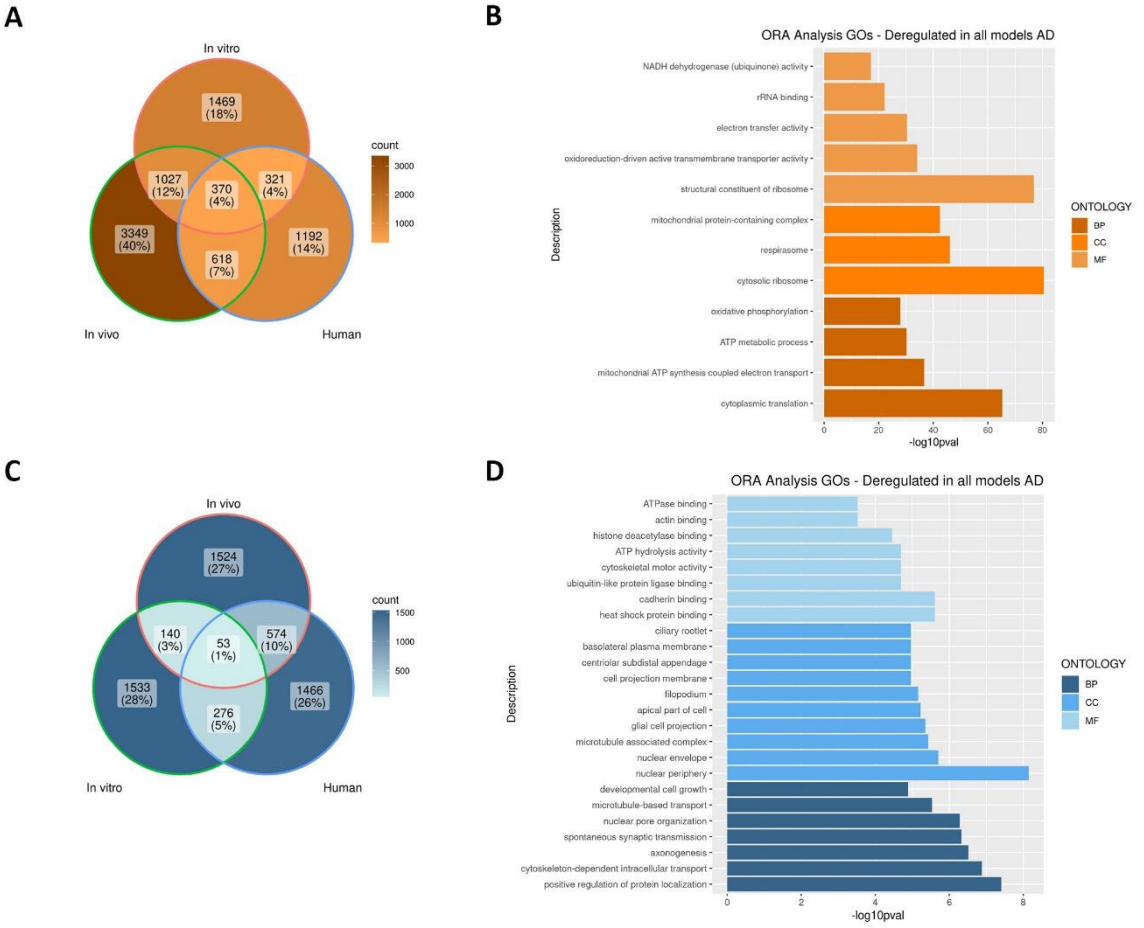


***Figure 12. Comparative transcriptomic analysis of oligodendrocytes in vitro, 3xTg-AD mice and AD patients. (A)*** *Venn diagram depicting the overlap of DEGs in in vitro, 3xTg-AD and human AD patients. Percentage indicates the proportion of genes shared among datasets.* ***(B)*** *GO analysis of biological process (BP), cellular component (CC) and molecular function (MF) of DEGs.* ***(C)*** *Venn diagram depicting the overlap of DEGs upregulated in vitro, 3xTg-AD AND human AD patients. Percentage indicates the proportion of common DEGs.* ***(D)*** *Analysis of BPs, CCs and MFs of commonly upregulated DEGs.*

Pathway analyses revealed several pathways enriched in the three models and are related to energetics (Electron transport chain, oxidative phosphorylation, mitochondrial complex I assembly and glycolysis and gluconeogenesis), proteasome

(Parkin-Ubiquitin Proteasomal System pathway), translation (cytoplasmic ribosomal proteins) and mRNA processing among others **(Table 9)**. When looking at the upregulated pathways in the three conditions we can mention insulin signalling, mechanoregulation and cilium landscape. Interestingly, genes involved in myelination (*Itgb1, App, hnrnpa2b1 and Bace1*), cytoskeleton (*Actb, Rock2* and *Dync1l2*) and iron homeostasis (*Fth1, Iscu*) are some of the most remarkable deregulated genes in the three models.

Taken together, these results suggest that the most affected pathways in oligodendrocytes in AD are linked to RNA metabolism, myelination and energy metabolism.

***Table 9.*** *Pathway of DEGs in oligodendrocytes in the three models: in vitro, 3xTg-AD mice and human samples (orange) and pathways upregulated (blue).*

| geneSet | description | size | overlap | pValue |
|---|---|---|---|---|
| **WP477** | *Cytoplasmic Ribosomal Proteins* | *91* | *36* | *<2.2E-12* |
| **WP111** | *Electron Transport Chain (OXPHOS system in mitochondria)* | *105* | *24* | *1.55E-15* |
| **WP4324** | *Mitochondrial complex I assembly model OXPHOS system* | *105* | *24* | *1.55E-11* |
| **WP623** | *Oxidative phosphorylation* | *62* | *11* | *1.42E-10* |
| **WP3888** | *VEGFA-VEGFR2 Signalling Pathway* | *438* | *28* | *6.80E-09* |
| **WP534** | *Glycolysis and Gluconeogenesis* | *45* | *6* | *0.00184* |
| **WP3630** | *NAD metabolism, sirtuins and aging* | *11* | *3* | *0.00343* |
| **WP2359** | *Parkin-Ubiquitin Proteasomal System pathway* | *70* | *7* | *0.00418* |
| **WP314** | *Fas Ligand (FasL) pathway and Stress induction of Heat Shock Proteins (HSP) regulation* | *44* | *5* | *0.00879* |
| **WP411** | *mRNA Processing* | *133* | *8* | *0.04093* |
| **WP481** | *Insulin Signalling* | *161* | *4* | *0.00864* |
| **WP4534** | *Mechanoregulation and pathology of YAP/TAZ via Hippo and non-Hippo mechanisms* | *48* | *2* | *0.02454* |
| **WP4352** | *Ciliary landscape* | *220* | *4* | *0.02463* |

# PART II: Effect of $A\beta_{1-42}$ oligomers in RNA metabolism and local translation

Several studies have identified ribonucleoproteins or RNA binding proteins (RBP)- and other RNA-related molecules altered in AD (Rybak-Wolf & Plass, 2021). RNA binding proteins are the main regulators of gene expression at the RNA level, including transcription, processing, transport and degradation (Han, Tang, & Smith, 2010). Interestingly, our RNA-seq analysis revealed several pathways related to RNA metabolism as altered in oligodendrocytes exposed to Aβ, suggesting that RBPs alteration could affect RNA processing and gene expression profiles in oligodendrocytes. From all the RBPs identified in our study, we focused on hnRNP A2, which is a key heterogeneous nuclear ribosomal nucleoprotein that regulates splicing events in Alzheimer's disease (AD) (Berson et al., 2012). Besides, it also regulates the RNA transport and translation of two important myelin proteins: MBP and MOBP (Hoek et al., 1998).

## 2.1 Hippocampus of Alzheimer's disease patients present an increase of hnRNP A2 at early stages

Previous studies focusing on neurons revealed reduced expression of hnRNP A2 in the entorhinal cortex of AD patients (Berson et al., 2012) but increased expression in the hippocampus (Mizukami et al., 2005). Nevertheless, nothing has been described regarding oligodendrocytes. Therefore, we proceeded to evaluate the expression of hnRNP A2 in oligodendrocytes in human *post mortem* hippocampal samples from healthy subjects and AD patients. Samples were classified according to Braak stages (II, III, IV, VI) (Braak and Braak, 1995). Human hippocampal tissue sections were immunostained for hnRNP A2 and a specific marker for oligodendrocyte lineage cells, Olig2. Then, hnRNP A2 intensity was measured in oligodendrocyte nuclei. We observed an increase of hnRNP A2 in Braak II and III stages compared to controls (control 145.9±5.13, Braak II 168.5±3.62 and Braak III 168.5±3.62; arbitrary units, a.u.). In contrast, no changes were observed at later stages (Braak IV 135.3±3.66 and Braak III 152.9±4.38; a.u.). **(Figure 13A, B)**.

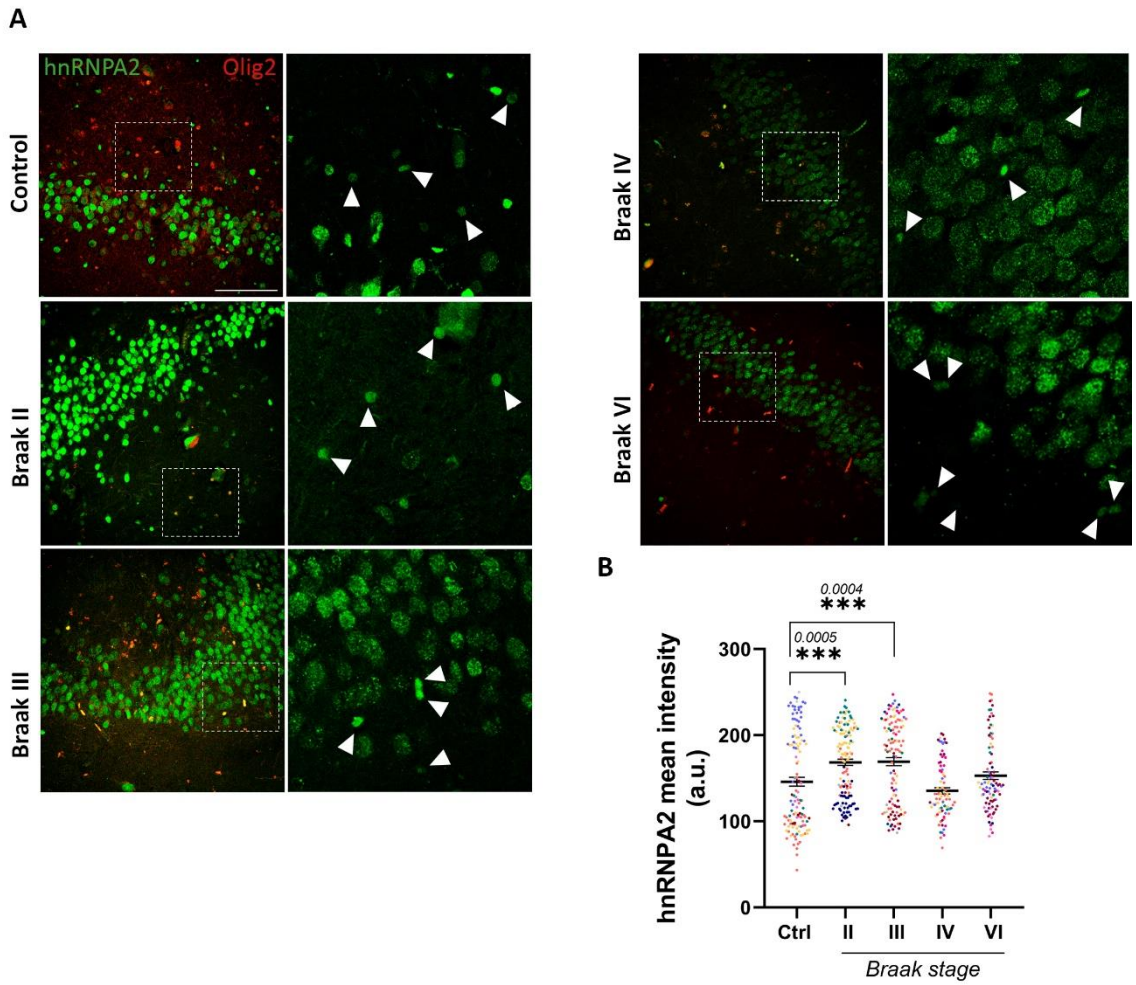


***Figure 13. hnRNP A2 is upregulated in oligodendrocytes in early stages of AD. (A)*** *Representative confocal images of Olig2 (red) and hnRNP A2 (green) in the hippocampus from controls and AD patients at Braak II-VI stages.* ***(B)*** *Quantification of hnRNP A2 intensity in Olig2+ cells in the human hippocampus. Scale bar, 100 µm. Data indicate the means ± S.E.M and coloured dots represent individual cells in each human sample, ***p<0.001, AD compared to control cases. Statistical significance was drawn by two-tailed ordinary one-way ANOVA followed by Dunnett post-hoc test.*

## 2.2 hnRNP A2 is overexpressed in hippocampus of 3xTg-AD and Aβo-injected mice

To further assess hnRNP A2 changes in oligodendrocytes, we used the AD 3xTg-AD mouse model. Specifically, we analysed the levels of hnRNP A2 in the hippocampus of 6- and 18-month-old mice. At 6 months, mice exhibited intraneuronal Aβ peptide in the cortex and hippocampus but not neurofibrillary tangles (Oddo et al., 2003).

Coronal tissue sections were immunostained for hnRNP A2 and Olig2. At 6 months, we observed an increase in the mean intensity of hnRNP A2 immunolabelling in the 3xTg-AD mouse CA3 (WT 18715±2077 vs 3xTg-AD 27554±2020; a.u.) and dentate gyrus of the hippocampus (WT 17241±1643 vs 3xTg-AD 27219±2421; a.u.) but not in the CA1 region (WT 15276±1595 vs 3xTg-AD 20659±2209) **(Figure 14A, B)**. However, no significant changes were found in the CA3 (WT 69900±16414 vs 3xTg-AD 76753±14117; a.u.), CA1 (WT 48862±4853 vs 3xTg-AD 46890±9238; a.u.) nor dentate gyrus (WT 93970±15600 vs 3xTg-AD 70710±19060; a.u.) in 18-month-old mice **(Figure 14C, D)**.

To determine whether Aβo could be causing the increased expression of hnRNP A2 in oligodendrocytes *in vivo*, we next measured the mean intensity of immunolabelling in mice that had received an Aβo intrahippocampal injection (10 μM). Control and Aβo-injected mouse coronal tissues were immunostained for hnRNP A2 and Olig2. Similarly to 3xTg-AD mice, hnRNP A2 expression analyses of the hippocampus in Aβo-injected mice showed a significant increase of hnRNP A2 intensity in oligodendrocytic nuclei, specifically in the dentate gyrus (control 140772±9011 vs Aβ-injected 171787±8360) compared to control mice **(Figure 14E, F)**.

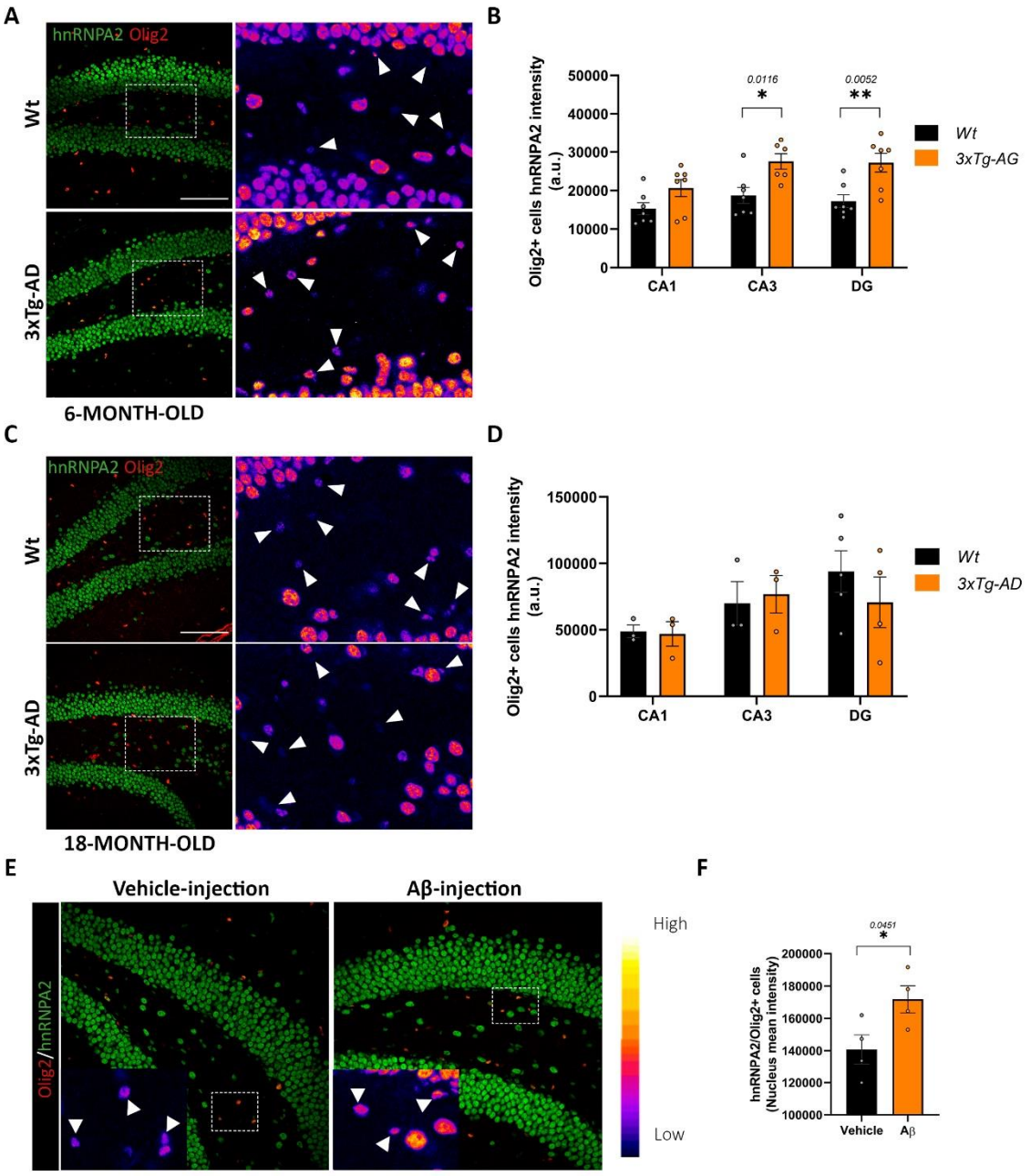


***Figure 14. hnRNP A2 is upregulated in 3xTg-AD mice and Aβ$_{1-42}$ oligomers-injected mice. (A)*** *Representative confocal images of Olig2 (red) and hnRNP A2 (green) in the dentate gyrus of 6-month-old and 18-month-old mice.* ***(B, C)*** *Quantification of hnRNP A2 intensity in Olig2+ cells in the hippocampus.* ***(D)*** *Representative confocal images of Olig2 (red) and hnRNP A2 (green) in the dentate gyrus of vehicle and Aδ-injected mice.* ***(E)*** *Quantification of hnRNP A2 intensity in Olig2+ cells in the dentate gyrus. Scale bar 100 µm. Data indicate means ±S.E.M and dots represent individual animals, *p<0.05, **p<0.01, compared to Wt or vehicle-injected mice. Statistical significance was drawn by two-tailed unpaired Student t-test.*

## 2.3 $A\beta_{1-42}$ oligomers upregulate the expression of hnRNP A2 in cultured oligodendrocytes

*In vitro,* hnRNP A2 shuttles between the nucleus and the cytoplasm where it participates in the translation regulationof mRNAs containing a specific cis-acting element, A2RE. To determine whether Aβo could alter hnRNP A2 expression at both mRNA and protein levels, we used primary oligodendrocyte cultures derived from rat cortices. We first isolated OPCs from glia mixed culture and cells were cultured in Sato+ differentiation medium for 3 DIV. OLs were then treated with 1 µM Aβ oligomers for 3 or 24 **(Figure 15A)**. We first observed a significant increase in mRNA level of hnRNP A2 after 3 h of Aβo-treatment (control 2.060±0.7519 vs Aβo 3.451±0.5751, a.u.) **(Figure 15B).**

Next, to measure protein levels and asses the localization of hnRNP A2, we performed western blot and immunocytochemistry analysis, respectively. Western blot analyses showed a 44.5%±12.45 increase in hnRNP A2 levels after 24 h compared to 100% of control (144.5%± 12.45 vs 100% of control) **(Figure 15C, D)**. On the other hand, immunofluorescence analysis revealed that hnRNP A2 is abundantly present in the nucleus and additionally shows a granular pattern in the processes of oligodendrocytes **(Figure 15E)**. As hnRNP A2 shuttles to the cytoplasm, we wondered whether Aβo could be promoting this shift. Thus, we measured the total area occupied by hnRNP A2 in the cytoplasm per cell and observed a significant increase after 24 h of Aβo-treatment (control 21.16±2.032 vs Aβo 26.95±2.346) **(Figure 15E, F)**.

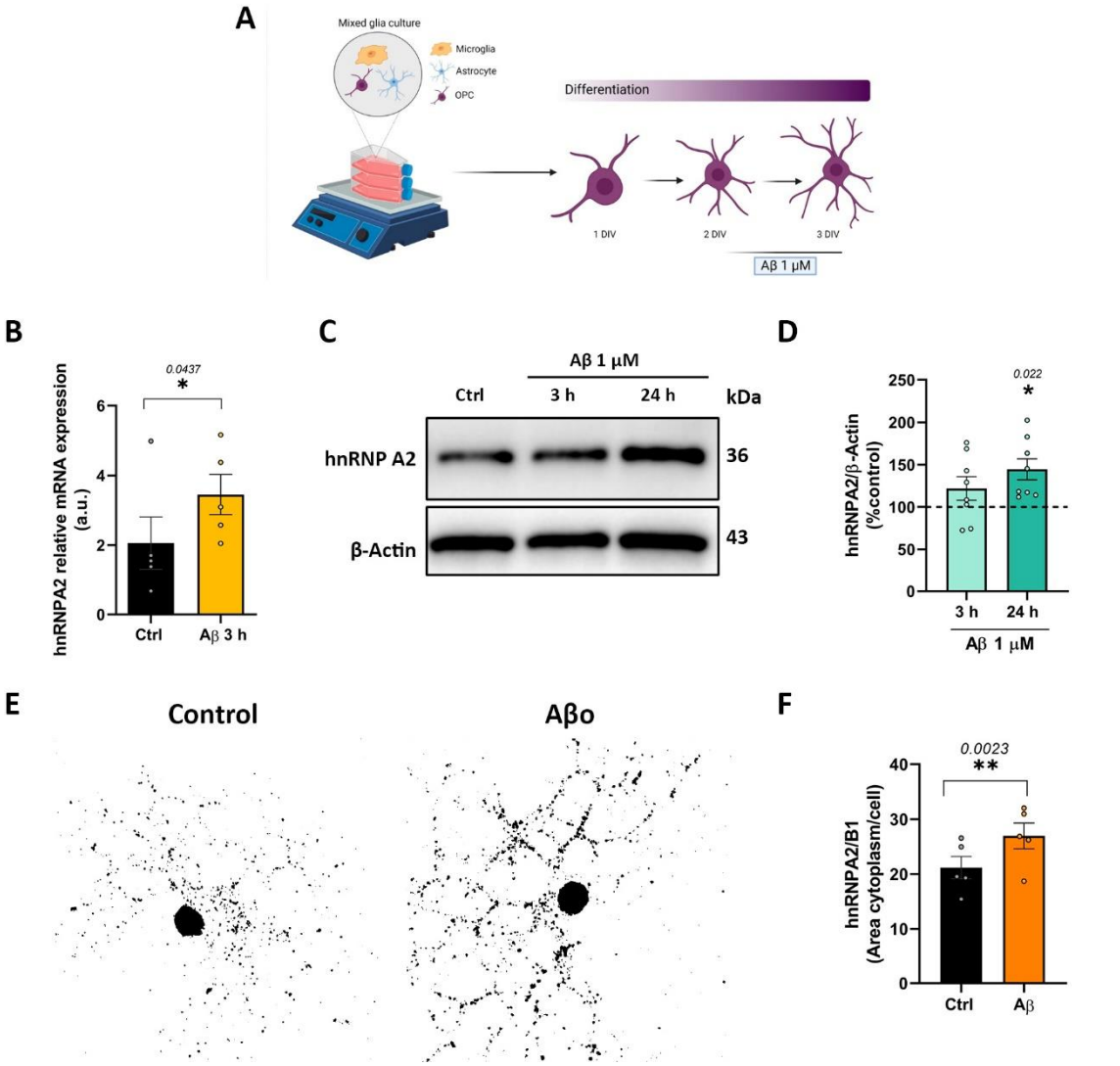


***Figure 15. Aβ$_{1-42}$ oligomers upregulate hnRNPA2. (A)*** *Cells (3 DIV) were treated with Aβ 1 μM for 3 and 24 hours.* ***(B)*** *RT-qPCR analysis of hnRNP A2 in A-treated and controlcontrol cells.* ***(C, D)*** *hnRNP A2 expression and relative quantification in oligodendrocyte cell extracts normalized to β-actin.* ***(E)*** *Representative micrographs of hnRNP A2 in control and Aβo-treated oligodendrocytes.* ***(F)*** *Histogram depicting changes in the area occupied by hnRNP A2. Data indicate means ± S.E.M and dots represent independent experiments, *p<0.05, **p<0.01, compared to control cells. Statistical significance was drawn by two-tailed paired Student t-test and one-way ANOVA followed by Dunnett post-hoc test.*

## 2.4 Aβ$_{1-42}$ oligomers changes hnRNP A2 interactome

hnRNP A2 has multiple effects on RNA processing (alternative splicing, transport, stability and degradation) through its binding to specific RNA sequences. Despite the importance of this protein in health and disease, little is known about its interactome.

Thus, we first analised the RNAs bound to hnRNP A2 in oligodendrocytes in order to gain insight into possible functions of this protein in oligodendrocyte biology

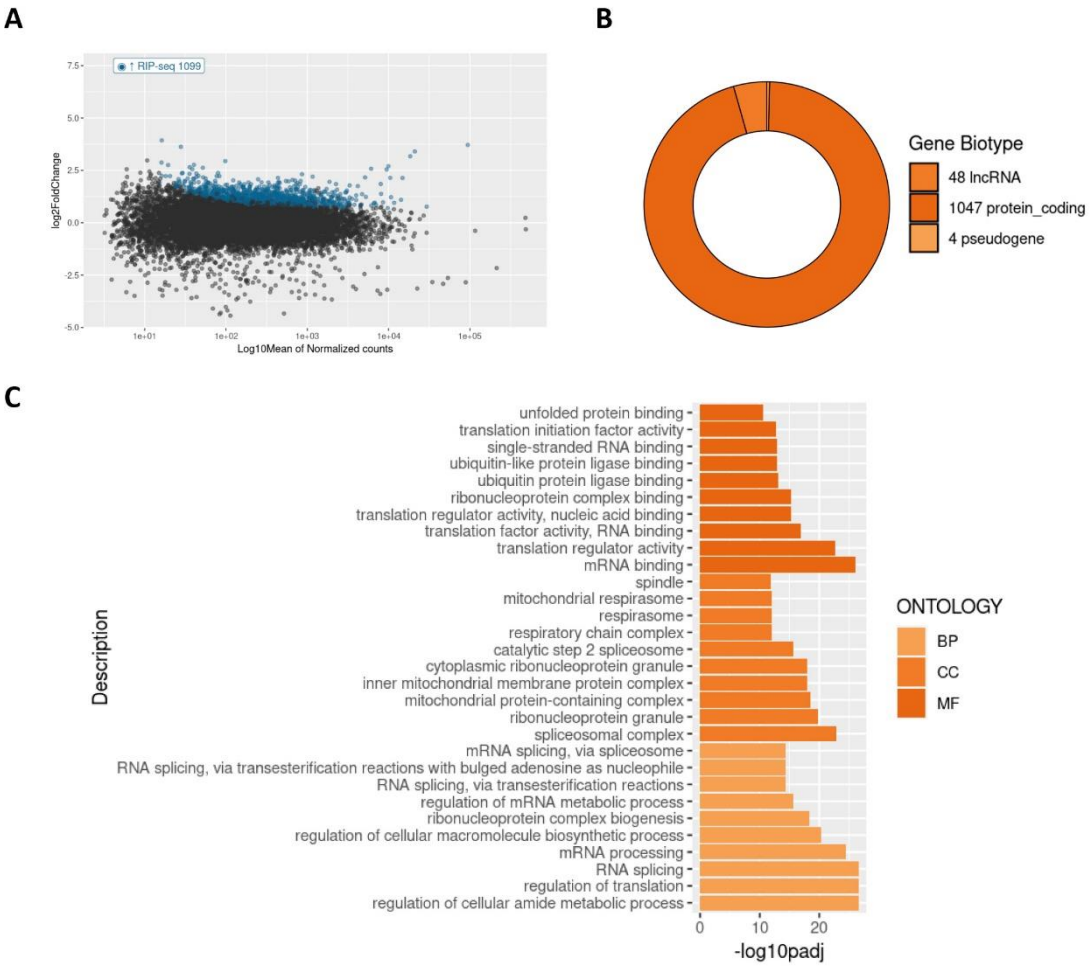


***Figure 16. hnRNP A2 interactome in oligodendrocytes. (A)*** *MA plot of hnRNP A2 RIP-seq data. For each transcript, the average signal (measured as log10 mean of normalized counts) against the RIP-seq log2 Fold Enrichment (RIP versus IgG) was plotted. Significantly enriched targets are highlighted in blue.* ***(B)*** *Classification of hnRNP A2-associated RNAs. The majority of identified targets are protein-coding genes, but long intervening noncoding RNAs (lincRNAs) and pseudeogenes were also present.* ***(C)*** *Functional annotation of enriched hnRNP A2 target genes. The barplot displays enriched classes from Gene Ontology terms (BP, biological process; CC, cellular component; MF, molecular function). The length of each bar is proportional to the statistical significance of the enrichment.*

To that aim, we performed RIP-seq using anti-hnRNP A2 and isotype control antibodies in primary cultured oligodendrocytes treated with 1 µM Aβo for 24 h. RIP is an antibody-based technique used to identify RNA-protein interactions. Thus, hnRNP A2 was immunoprecipitated together with its associated mRNAs. RIP-seq results showed that

1099 transcripts were significantly enriched in the immunoprecipitated hnRNP A2 complex in control oligodendrocytes **(Figure 16A)**. 95% of RNAs were protein coding, while 5% were long non-coding (lnRNAs) and pseudogenes **(Figure 16B)**. We then performed GO Term enrichment (Clusterprofiler software) and Wikipathway analysis. Gene ontology analyses revealed that among the most abundant interacting mRNAs, there were several factors involved in mitochondria metabolism (such as *Ndufa5, Cox3, Cytb, COX2* and *Nd4*), ribonucleoprotein complex biogenesis (such as *Abce1, Bicd1, Brix1, Xpo1* and *Snrpc*), mRNA metabolism (such as *Ybx1, Clk1, Ddx1, Srsf10, Rbmx, Hnrnph2, Srsf7* and *Hnrnpk*) and translational control (such as *Eif1a, Pabpc1, Eef1b2, Eif4a1* and *Eef1g*) **(Figure 16C)**. Additionally, Wikipathway analysis revealed pathways related to lipid metabolism (Cholesterol biosynthesis, cholesterol metabolism and fatty acid biosynthesis), proteasome degradation and TNF-alpha NF-kB signalling pathway **(Table 9)**. Interestingly, hnRNP A2 interacts with *hnrnpa2/b1*, suggesting an autoregulatory role.

***Table 9.*** *Pathways regulated by hnRNP A2 in control conditions.*

| *geneSet* | *description* | *size* | *Overlap* | *pValue* |
|---|---|---|---|---|
| **WP529** | *mRNA Processing* | *112* | *25* | *2,82E-07* |
| **WP149** | *Translation Factors* | *45* | *15* | *6,96E-06* |
| **WP59** | *Electron Transport Chain* | *93* | *20* | *1,43E-10* |
| **WP302** | *Proteasome Degradation* | *48* | *11* | *2,03E-12* |
| **WP461** | *Cholesterol Biosynthesis* | *15* | *6* | *2,31E-11* |
| **WP457** | *TNF-alpha NF-kB Signaling Pathway* | *174* | *24* | *3,33E-12* |
| **WP1283** | *Oxidative phosphorylation* | *60* | *12* | *4,09E-11* |
| **WP30** | *Cytoplasmic Ribosomal Proteins* | *108* | *15* | *0.004196* |
| **WP632** | *Cholesterol metabolism* | *23* | *5* | *0.015002* |
| **WP504** | *Fatty Acid Biosynthesis* | *19* | *4* | *0.032454* |

Next, we wanted to see if Aβo was able to alter hnRNP A2 interactome and consequently, alter RNA metabolism. Thus, we compared the Aβo-treated oligodendrocyte interactome to the control interactome. Surprisingly, hnRNP A2 interacts with less RNAs in upon Aβo exposure compared to control conditions:only 684 RNAs were identified **(Figure 17A)**. From all of them, 655 (58%) genes interact in the same way as control cells while 29 (3%) show higher interaction in Aβo treated cells and 448 (40%) mRNAs interact more in control conditions **(Figure 17B)**. The genes with lesser with hnRNP A2 in Aβo-treated cells compared to controls are involved in RNA

metabolism (for example *Hnrnpk, Hnrnph1, Sf3b1, Hnrnpa2b1 and Dhx9*), mitochondria (*Ndufb9, Atp5pd, Ndufa5, Atp5mg, Uqcrfs1, Ndufc2 and Cox6c)* and translation (*Pabpc1, Eef1b2 and Eef1g*), while the ones that associate more with hnRNP A2 in Aβo-treated oligodendrocytes are related to metal ion binding (*Gse3, Osgelpl1, Mbnl2, Prnp, Ppp2r3c, Slc38a9* and *Znf708*) **(Figure 17C)**.

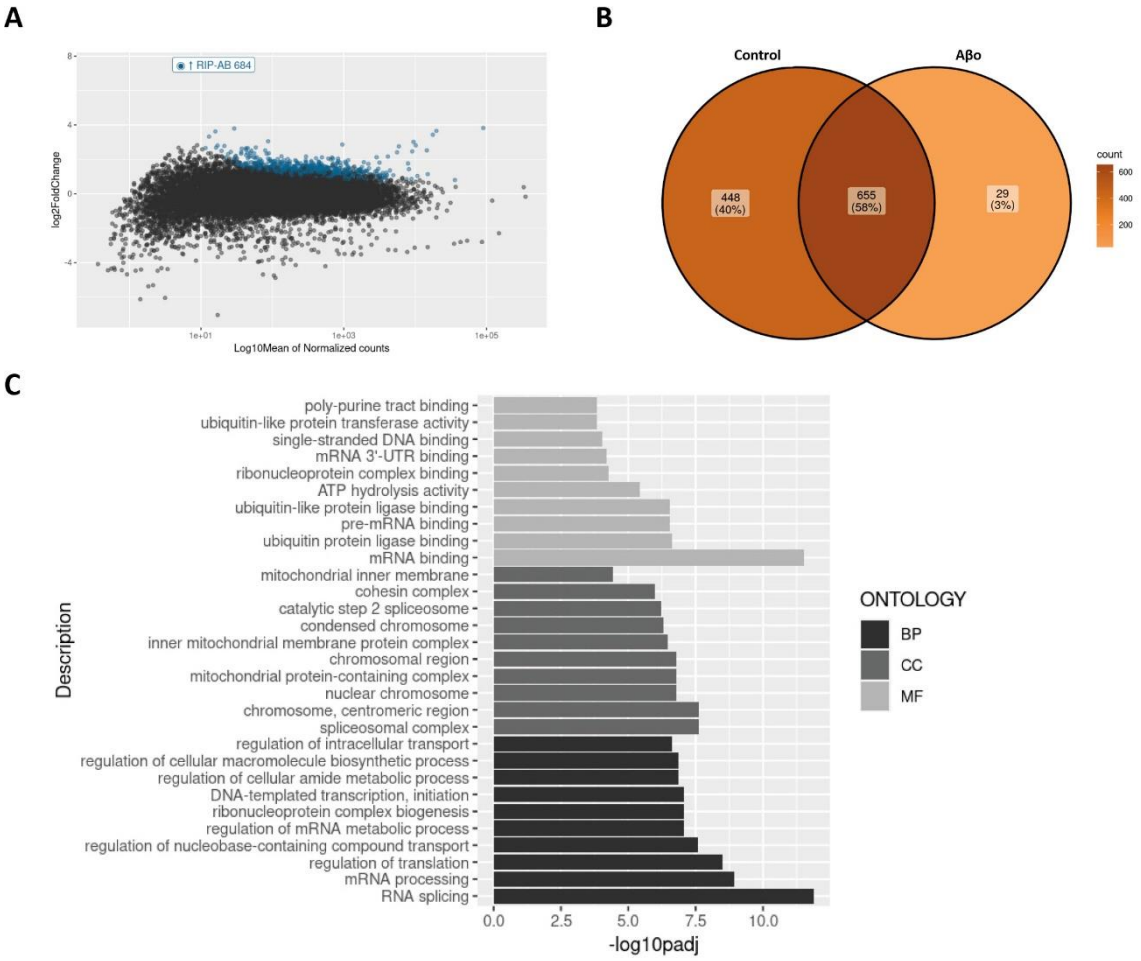


***Figure 17. Aβ$_{1-42}$ oligomers change the hnRNP A2 interactome. (A)*** *MA plot of hnRNP A2 RIP-seq for Aβo-treated cells.* ***(B)*** *Venn diagram of transcripts that specific to vehicle and Aβ-treated cells and commonly shared by both experimental conditions****. (C)*** *Functional annotation enrichment analysis of downregulated hnRNP A2 target RNAs in Aβ-treated cells. The barplot displays enriched classes from Gene Ontology terms (BP, biological process; CC, cellular component; MF, molecular function). The length of each bar is proportional to the statistical significance of the enrichment.*

## 2.5 Aβ oligomers promote interaction between hnRNPA2 and *Mbp/Mobp* mRNA

We had previously shown that Aβ oligomers upregulate local translation of MBP via integrin β1 and Fyn kinase signalling (Quintela-Lopez et al., 2019). hnRNP A2 is a major component of mRNA transport granules in oligodendrocytes and binds to a *cis*-acting element in in the 3' untranslated region of *Mbp* and *Mobp* (Ainger et al., 1993; Carson, Worboys, Ainger, & Barbarese, 1997). Together with the mRNAs, hnRNP A2 forms a supramolecular complex that it is then transported to the myelin compartment where the mRNAs are locally translated. Therefore, we wondered whether upregulation of hnRNP A2 and its altered interactome could be affecting local translation of MBP and MOBP.

First, we assessed if the interaction between hnRNP A2 and *Mbp* or *Mobp* was modified by Aβo. To address this, we performed RIP with anti-hnRNP A2 and isotype control antibodies **(Figure 18A)**. Anti-IgG was used to assess the specificity of the antibody and the effectiveness of the pull down. RIP analysis of mRNA levels by RT-qPCR revealed a significant enrichment of *Mbp* (control 0.2117±0.2064 vs Aβo 0.5081±0.3158) and *Mobp* (control 0.3082±0.1447 vs Aβo 0.6270±0.3131) mRNAs in RIP fractions of Aβo-treated cells compared to control cells, while in the input there were not significant changes (Mbp control 1.744±0.5058 vs Aβo 1.522±0.2864; Mobp control 1.574±0.7259 vs Aβo 1.301±0.4673) **(Figure 18B, C)**. Importantly, we observed very little expression of *Mbp* (0.01785±0.01412) and *Mobp* (0.02301±0.01262) in the control condition with the anti-IgG. Finally, to determine if the enrichment is specific for *Mbp* and *Mobp,* we used *Tau*, which has also been reported to bind to hnRNP A2 (Behar, Marx, Sadot, Barg, & Ginzburg, 1995). No significant changes were observed in the RIP fractions (control 0.1749±0.1473, Aβo 0.1739±0.1331 and IgG 0.001438±0.0006) nor in the input (control 1.645±0.1953 vs Aβo 2.013±0.2466) **(Figure 18D)**.

Overall, these results suggest that Aβo promotes specifically the interaction between hnRNP A2 and *Mbp*/*Mobp* mRNA in oligodendrocytes.

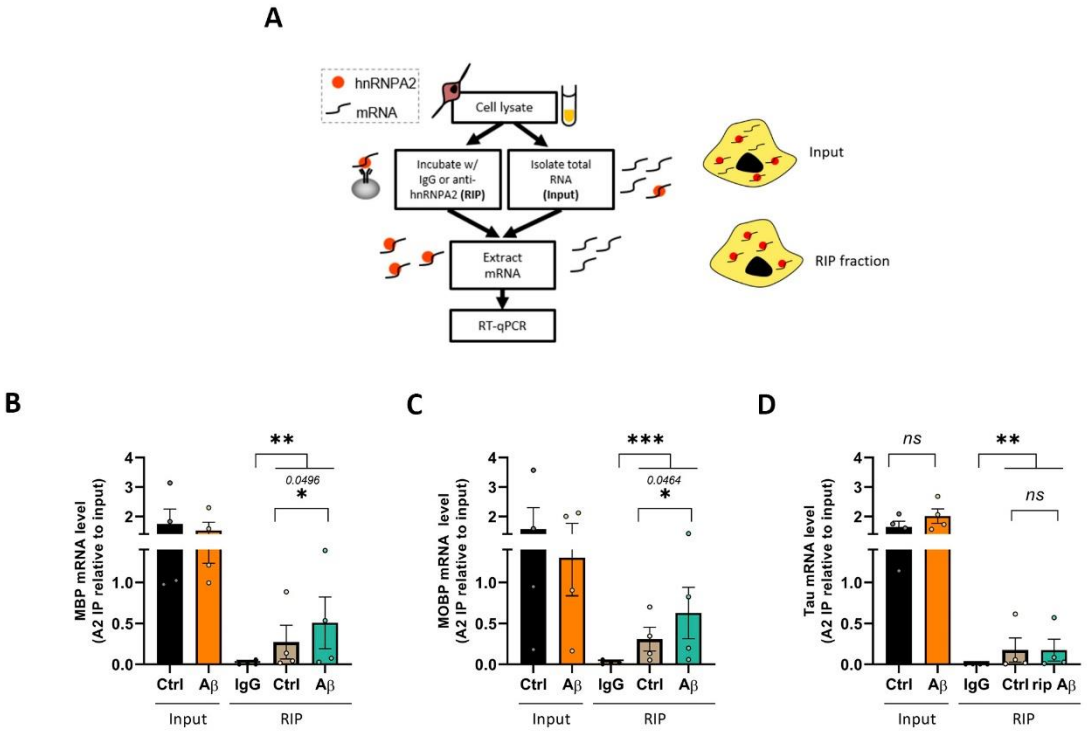


***Figure 18. Aβ$_{1-42}$ oligomers promote interaction between hnRNP A2 and Mbp and Mobp mRNA. (A)*** *Diagram illustrating hnRNPA2-RIP workflow. Control IgG and antibodies against hnRNPA2 were employed for RIP from oligodendrocyte lysates.* ***(B, C, D)*** *Analysis of Mbp, Mobp and Tau mRNAs levels by RT qPCR. Data indicate the means ± S.E.M and dots represent independent experiments, *p<0.05, **p<0.01, ***p<0.001 compared to control cells. Statistical significance was drawn by two-tailed paired Student´s t-test.*

## 2.6 Aβ$_{1-42}$ oligomers promote phosphorylation of hnRNPA2 triggering *Mbp* and *Mobp* local translation

In order to initiate translation, hnRNPA2 needs to be disassembled from the mRNA granule. hnRNP A2 disassembly occurs through its phosphorylation in its Tyr residues by the tyrosine-protein kinase Fyn, which needs to get activated (White et al., 2018). We have already observed that Aβo activate Fyn by binding to the ITGβ1 (Quintela-Lopez et al., 2019). Therefore, we next wondered if A□o could be promoting hnRNP A2 phosphorylation.

To determine if Fyn activation by A□o increases the phosphorylation of hnRNP A2 we performed an immunoprecipitation assay followed by western blot using an anti-pTyr (PY99) and isotype control antibodies **(Figure 19A, B).** Data showed that, after 15 minutes of A□o treatment, the levels of phosphorylated hnRNP A2 were significantly

higher than those obtained in the control (0.04298±0.007 vs 0.08557±0.0167, respectively).

Next, to determine whether these changes in hnRNP A2 levels and phosphorylation promotes translation of *Mbp* and *Mobp* mRNA, we performed puromycin together with PLA (Puro-PLA) and examined translation. Using an antibody against MBP or MOBP and another against puromycin, we can detect *de novo* synthesis of the proteins of interest. Moreover, this technique gives the opportunity to assess the localization of the synthesis within the cell. Puromycin is an antibiotic which inhibits protein synthesis causing premature polypeptide chain termination during translation. Thus, the levels of puromycin-labelled peptides reflects the overall rate of protein synthesis, making puromycin a powerfull tool to measure changes in protein synthesis rates. To visualise oligodendrocytic processes, cytoskeleton was made visible with phalloidin, which binds to F-actin.

We measured PLA intensity in the primary processes, which are the processes emerging from the soma and total processes to see if the localization differs **(Figure 19C)**. Aβo-treated oligodendrocytes exhibited significantly more local translation of MBP both in primary (control 1625088±636696 vs Aβo 2628083±764320) and total processes (control 543407±185673 vs Aβo 897499±219650) **(Figure 19D, E)**. In the case of MOBP local translation, results were not as clear as previous ones: despite the fact that Aβo presented an enhanced local translation of MOBP in primary processes (control 64370±28499 vs Aβo 1403583±1040424), no significant difference was observed for the total processes (control 426037±272836 vs Aβo 555533±373571) **(Figure 19E, F)**. Anysomycin (40 µM) was added 20 minutes before puromycin and used as a negative control due to the fact that it inhibits translation initiation by binding to the peptidyl transferase domain of the 60S ribosomal subunit. As showed in the puro-PLA images, cells preincubated with anisomycin, did not show any $PLA^+$ puncta, confirming that the puncta that we observed in the puro-PLA were translation dependent.

Combined, these observations suggest that Aβo promotes *Mbp* and *Mobp* translation in oligodendroglial processes by phosphorylating hnRNP A2.

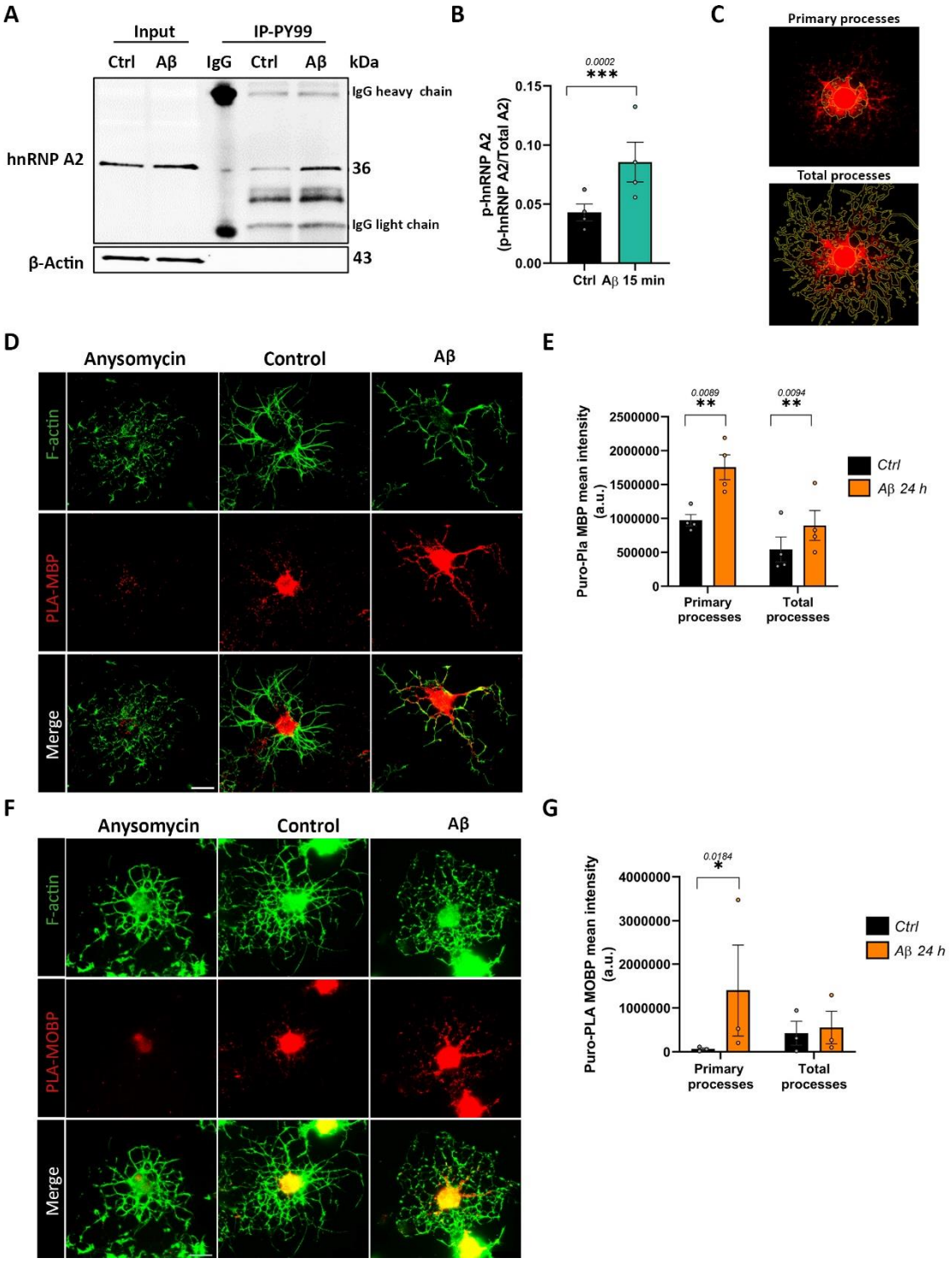


***Figure 19. Aβ$_{1-42}$ oligomers trigger local translation through phosphorylation of hnRNPA2. (A)****.Western blot of pTYR-IP and IgG to detect hnRNP A2 phosphorylation.* ***(B)*** *Histogram depicting the phosphorylation of hnRNP A2 normalized to total hnRNP A2 from input.* ***(C)*** *The intensity of MBP and MOBP puro-PLA-positive puncta in bins of 10 µm ranging from the soma was measured in primary and total processes.* ***(D, E)*** *Representative images from puro-PLA for MBP and its quantification in primary and total processes.* **(F, G)** *Representative images from puro-PLA for MOBP and its quantification in primary and total processes. Scale bar, 10 µm. Data indicate means ±S.E.M and dots represent independent experiments, *p<0.05,*

***p<0.01, ***p<0.001 compared to control cells. Statistical significance was drawn by two-tailed paired Student´s t-test.*

## 2.7 Aβ$_{1-42}$ oligomers change *Mbp* and *Mobp* RNA granule number and dynamics

*Mbp* and *Mobp* mRNAs need to be assembled into granules and transported to the periphery with the contribution of different hnRNPs. As we observed that both local translation and hnRNP A2 expression were increased upon Aβ treatment, we wondered if Aβo could have an effect in other hnRNPs expression levels. To address this, we analysed the mRNA and protein levels of the different hnRNPs (hnRNP F, hnRNP E1, hnRNP K) found in *Mbp* and *Mobp* RNA granules. We did not observe any significant changes for any of them at mRNA nor protein levels **(Figure 20A, B, C)**.

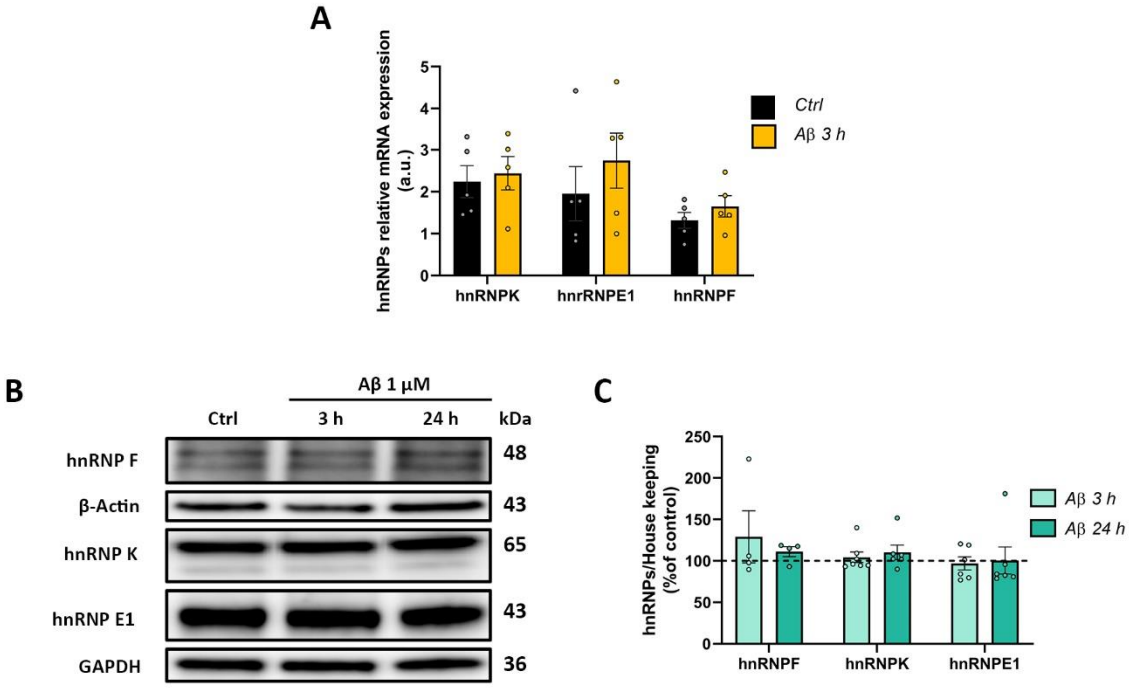


***Figure 20. Aβ$_{1-42}$ oligomers do not change hnRNP F, K nor E1. (A)*** *RT-qPCR analysis of hnRNPS in treated and control cells.* ***(B, C)*** *hnRNPs western blot and relative quantification in total cell extracts from oligodendrocytes. Data indicate means ± S.E.M and dots represent independent experiments. Statistical significance was drawn by two-tailed paired Student´s t-test and one-way ANOVA followed by Dunnett post-hoc test.*

mRNA granules are highly dynamic structures that undergo different remodelling steps before mRNA translation takes place. In the first step, hnRNP A2 binds to *Mbp* and *Mobp* mRNAs in the nucleus, which are then exported to the cytoplasm. In the cytoplasm,

hnRNP A2 binds to different hnRNPs: hnRNP E1, which inhibits translation during mRNA transport, and hnRNP F, which regulates MBP and MOBP synthesis. Once in the periphery, hnRNP E1 exchanges for hnRNP K, which is a prerequisite for the targeting of the mRNA to the myelin sheath and the initiation of translation (White *et al*., 2008; Laursen *et al*., 2011; Torvund-Jensen *et al*., 2014). Therefore, we can define two different granule complexes: the inactive granules (containing hnRNP E1, A2 and F) and the active granules (containing hnRNP K, A2 and F) **(Figure 21A)**.

Since we observed an upregulation of hnRNP A2, MBP and MOBP in the processes of oligodendrocytes, we asked whether the upregulation could be due to a change in the RNA granule number and dynamics. First, by immunocytochemistry we wanted to determine the localization of the different granule components in the oligodendrocyte. We observed that hnRNP K, hnRNP F, hnRNP E1 and hnRNP A2 are present predominantly in the nuclei but also have a granular pattern in the soma and processes of the oligodendrocytes. Specifically, hnRNP A2 is expressed throughout the cell, hnRNP K and hnRNP F are located more predominantly in the processes and hnRNP E1 is more abundant in the soma **(Figure 21B)**.

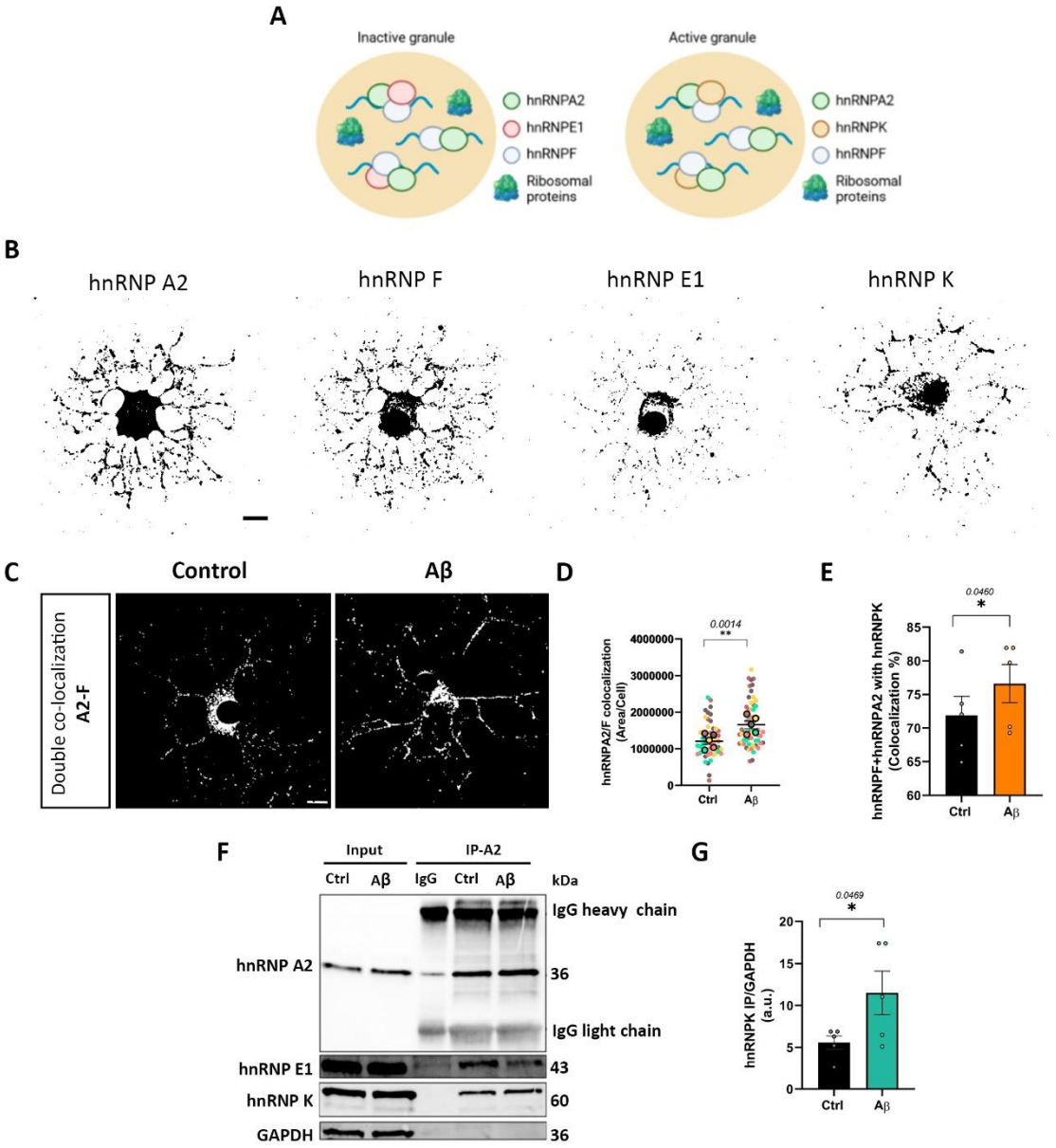


***Figure 21. Aβ$_{1-42}$ oligomers alter mRNA granule dynamics. (A)*** *Photograph illustrating the two different granule complexes: inactive and active.* ***(B)*** *Representative micrographs showing the localisation of the different hnRNPs.* ***(C, D)*** *Double colocalization images of hnRNP A2 and hnRNP F. 1 µM Aβ significantly increases hnRNPA2/F colocalization.* ***(E)*** *Graphs show that 70% of all granules contain hnRNPK (active granules) and Aβ treated cells contain 5 % more active granules.* ***(F, G)*** *hnRNP A2 CO-IP with the different hnRNPs found in the granules. 1 µM Aβ exposure significantly increases hnRNPK within the granule. Data indicate means ± S.E.M and bigger dots represent the mean of independent experiments and smaller dots represent individual cells, *p<0.05, **p<0.01 compared to control cells. Statistical significance was drawn by two-tailed paired Student´s t-test.*

Next, we quantified the double co-localization of hnRNP A2 and hnRNP F, to identify active and inactive granules. Interestingly, we found more granules containing both

components in Aβo-treated cells (control 1207778±90958 vs Aβo 1655855±108033; a.u.) **(Figure 21C, D)**, suggesting an increase in granule number. Then, we measured the percentage of granules containing hnRNP K and found that more than 70% of hnRNP A2-F complexes co-localized with hnRNP K and that Aβo-treated cells had a significant increase in the total hnRNP A2-F-K granules compared to control cells (71.87%±2.845 vs 76.60%±2.845, respectively) **(Figure 21E)**.

We also validated the granule components by co-immunoprecipitation assay with anti-hnRNP A2 antibody. In fact, hnRNP A2 co-precipitated with both hnRNP E1 and hnRNP K, as shown previously by immunocytochemistry. Quantification of granule components by western blot showed a significant increase in hnRNP K levels in Aβo-treated oligodendrocytes compared to control (5.588±0.8006 vs 11.49±2.602, respectively) **(Figure 21F, G)**.

Altogether, these results indicate that Aβo increase the number of RNA granules and modify their content by favouring the molecular composition that facilitates mRNA translation.

## 2.8 $A\beta_{1-42}$ oligomers upregulate late maturation stage markers MBP, MOBP and MOG *in vitro*

Next, we wanted to determine if Aβo could affect the expression of other myelin-related proteins, besides from upregulating localized translation, and thus regulate oligodendrocyte differentiation. The differentiation stages of oligodendroglia are determined by the expression of lineage-specific cell markers. While Olig2 is maintained throughout the entire oligodendroglia lineage, CNPase expression begins in late progenitors, immature and mature oligodendrocytes express MBP, MOBP and MAG and in their final stage, oligodendrocytes express MOG (Kuhn, Gritti, Crooks, & Dombrowski, 2019).

Initially, we measured PLP, CNPase, MOG, MAG, MBP and MOBP levels at the RNA level by RT-qPCR and at the protein levels by western blot. We did not observe any significant differences in neither *Plp, Cnp, Mog nor Mag* (**Figure 22A**) at mRNA levels. However, we observed that levels of *Mbp* (1.260±0.2195 vs 2.648±0.7077, respectively) and *Mobp*

(0.7096±0.1658 vs 0.8470±0.2007, respectively) mRNA increased after 3 hours of Aβo-treatment compared to control **(Figure 22A)**. On the other hand, expression analysis of different myelin-related proteins by western blot showed that MBP (150%±13.45), MOBP (138.3%±17.46) and MOG (111.6%±3.908) levels significantly increased after 24 hours of Aβo-treatment compared to 100% of control **(Figure 22B, C, D, E)**.

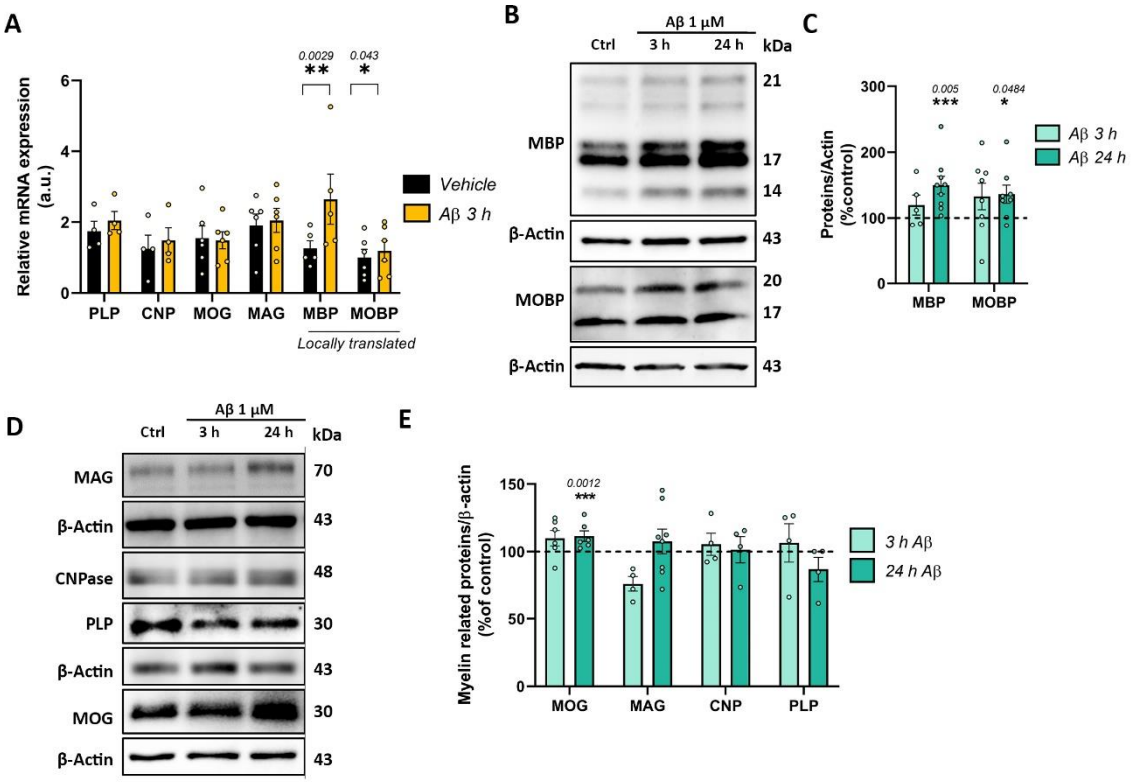


***Figure 22. Aβ$_{1-42}$ oligomers upregulate myelin-related proteins at mRNA and protein levels. (A)*** *RT-qPCR analysis of different myelin-related proteins in treated and ccontrol cells.* ***(B, C)*** *MBP and MOBP expression and relative quantification in treated and control oligodendrocyte cell extracts.* ***(D, E)*** *Different myelin related protein expression and relative quantification in treated and control oligodendrocyte cell extracts. Data are represented as means ± S.E.M and dots indicate independent experiments, *p<0.05, **p<0.01, ***p<0.001 compared to control cells. Statistical significance was drawn by two-tailed paired Student´s t-test and one-way ANOVA followed by Dunnett post-hoc test.*

As a way to evaluate the impact of the previous results in cell maturation, we performed assays using nanofibers. The ability of oligodendrocytes to differentiate and form myelin sheaths in PDL-coated nanofibers has been reported before (Bechler, Byrne, & Ffrench-Constant, 2015; Lee et al., 2012). That is, this experiment gave us the opportunity to examine oligodendrocyte maturation in a neuron-free model for myelination study. Aβo-treated oligodendrocytes showed increased MBP (11193±1424 vs 14469±3092,

respectively) and MOG (6521±558.2 vs 8417±473.8) fluorescence intensity levels compared to controls **(Figure 23A, B)**. These data validated the effect of A in promoting oligodendrocyte maturation in a culture system to study myelination.

Overall, these results suggest that Aβo upregulate proteins known to be locally synthesised, MBP and MOBP, as well as markers of mature oligodendrocytes MOG.

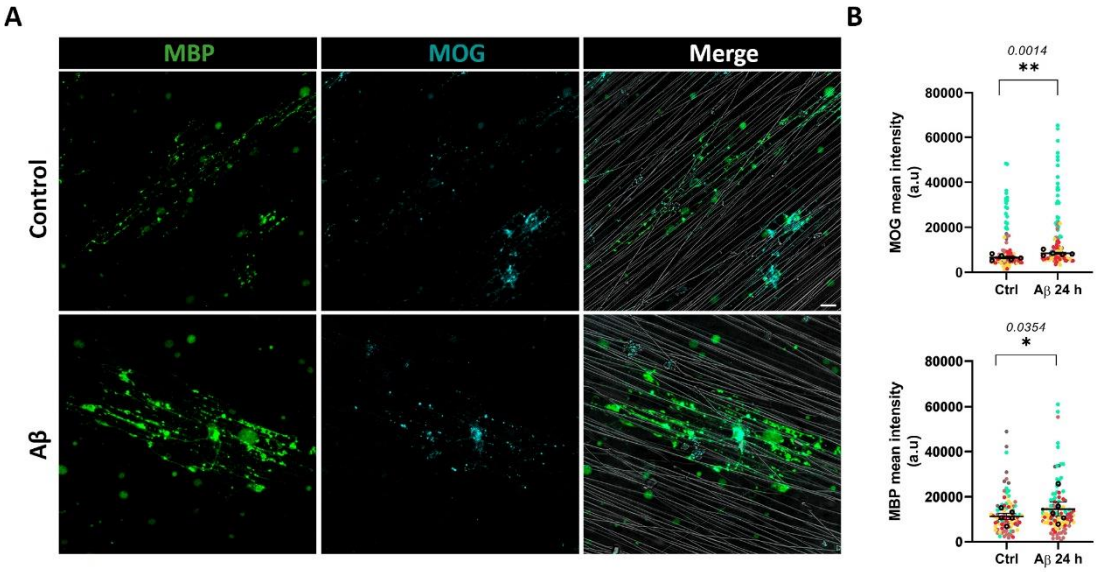


***Figure 23. Aβ$_{1-42}$ oligomers upregulate MBP and MOG in oligodendrocyte 3D culture. (A)*** *Representative micrographs of oligodendrocytes grown in nanofibers showing double-immunostaining for oligodendrocyte linage marker MBP (green) and MOG (cyan)* ***(B)*** *Analysis of MBP and MOG fluorescence intensity after 1 µM of Aβo for 24 h. Scale bar, 20 µm. Data indicate the means ± S.E.M and bigger dots represent the mean of independent experiments and smaller dots represent individual cells, *p<0.05, **p<0.01, compared to control cells. Statistical significance was drawn by two-tailed paired Student´s t-test.*

## 2.9 Adult AD transgenic mice exhibit increased levels of MBP and MOBP in the hippocampus and in myelin extracts

We next sought to determine whether the expression of MBP, MOBP and MOG change in 3xTg-AD mouse model. For that purpose, we analysed the levels of these proteins in the hippocampus and in the myelin fractions of 6-month-old 3xTg-AD mice. It is well described that one of the first areas of the brain affected in Alzheimer's disease is the hippocampus. Compared to the corpus callosum, the turnover of oligodendrocytes is higher in the grey matter of the human brain (Yeung et al., 2014). Previous data have shown that MBP expression is positively associated with Aβo levels in the hippocampus

in 18-month-old mice (Quintela et al., 2019) but it is unknown whether myelin-proteins are dysregulated in early stages of AD pathology in the 3xTg-AD mouse.

Analysis of MBP, MOBP and MOG levels showed a significant increase of MBP (1.911±0.2575 vs 3.300±0.411, respectively) and MOBP (2.1283±0.062 vs 3.097±0.2928, respectively) levels but not of MOG (4.155±0.8029 vs 2.512±0.4147, respectively) in 3xTg-AD mice compared to wild type mice **(Figure 24A, B)**. In contrast, in myelin fractions only MBP was increased in 3xTg-AD mice compared to wild type (2.736±0.036 vs 3.654±0.3696, respectively) **(Figure 24C, D)**. Interestingly, in total fractions of the hippocampus the major isoforms of MBP are the 17, 18 and 21.5 kDa isofroms, whereas in myelin fractions the 14, 17, and 18 kDa isoforms are predominant as previously described (Karthigasan, Garvey, Ramamurthy, & Kirschner, 1996).

Together, these results demonstrate that the 3xTg-AD hippocampus presents increased MBP and MOBP levels at early stages of AD and besides, myelin contains more MBP.

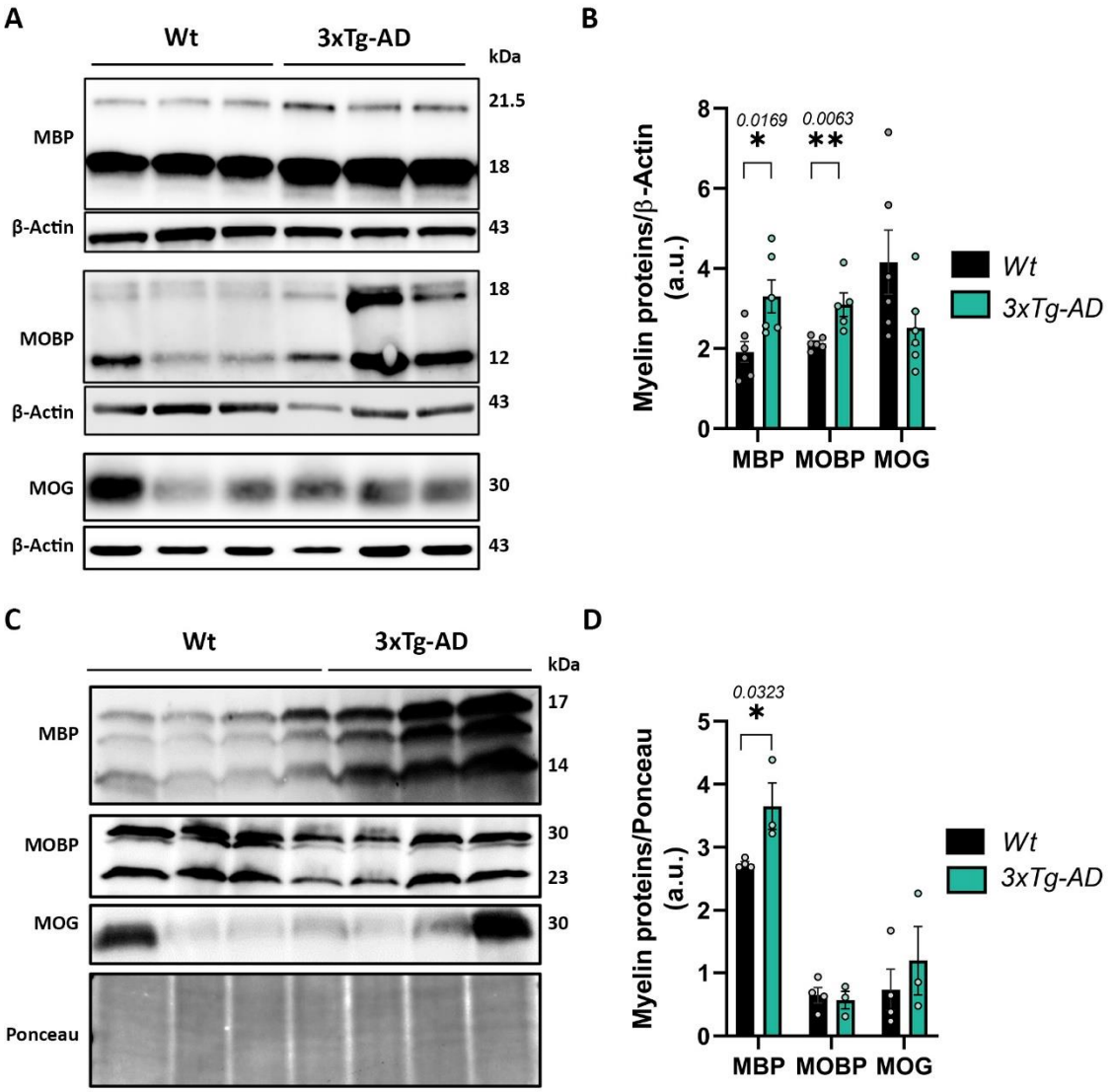


***Figure 24. 3xTg-AD mice exhibit increased levels of MBP and MOBP. (A, B)*** *MBP, MOBP and MOG expression and relative quantification of hippocampal lysates of 6-month-old 3xTg-AD mice compared to WT.* ***(C, D)*** *MBP, MOBP and MOG expression and relative quantification of the myelin extract of 6-month-old 3xTg-AD and Wt mice. Data indicate means ± S.E.M and dots represent individual animals *p<0.05, **p<0.01 compared to Wt. Statistical significance was drawn by two-tailed unpaired Student´s t-test.*

## 2.10 Overexpression of MBP changes oligodendrocyte homeostasis

### 2.10.1 MBP overexpression inhibits calcium influx into the cell

MBP is a multifunctional protein that interacts with lipids and a variety of proteins (Smirnova et al., 2021). It was previously described that overexpression of MBP significantly reduces $Ca^{2+}$ influx into oligodendrocytes by modulating voltage-operated

$Ca^{2+}$ channels (VGCCs) and thereby affecting $Ca^{2+}$ responses in the cell (Smith et al., 2011).

Thus, to determine if the Aβ-dependent MBP upregulation, and not Aβo itself induced an effect on VOCCs we recorded intracellular $Ca^{2+}$ levels upon KCl stimulation (25 mM) while silencing *Mbp* in the presence or absence of Aβo. First, we confirmed that the *Mbp* gene expression was reduced with an *Mbp*-targeting siRNA when compared to a control siRNA **(Figure 25A, B)**. The *Mbp*-targeting siRNA decreased the 21 kDa isoform by 38.78%±10.14, while the 17 and 18 kDa isoforms decreased by 19.49%±10.50 **(Figure 25C)**. Additionally, in cells treated with the control siRNA Aβo-treated oligodendrocytes showed an increase in MBP 21 kDa 121.6%±7.782 and 17-18 kDa isoforms 132.1±11.92, which was blocked when MBP was silenced **(Figure 25A, C)**. Recordings of intracellular calcium levels in oligodendrocytes showed a decrease in calcium influx in Aβo-treated cells (0.448±0.043 vs 0.2091±0.024), which was partially recovered by silencing *Mbp* (0.5967±0.056 vs 0.3966±0.032) **(Figure 25D, F)**. Besides, we observed a decrease in the area under the curve (AUC) in Aβo-treated cells (313.7±5.494 vs 272.8±7.495) that was fully recovered when *Mbp* was silent (300.7±8.374 vs 289.1±8.365) **(Figure 25G)**.

These results indicate that MBP overexpression, mainly the 17 and 18 kDa isoforms, partially inhibits the calcium influx through VGCCs, however Aβ might inhibit calcium dynamics through independent mechanisms which do not rely on MBP expression.

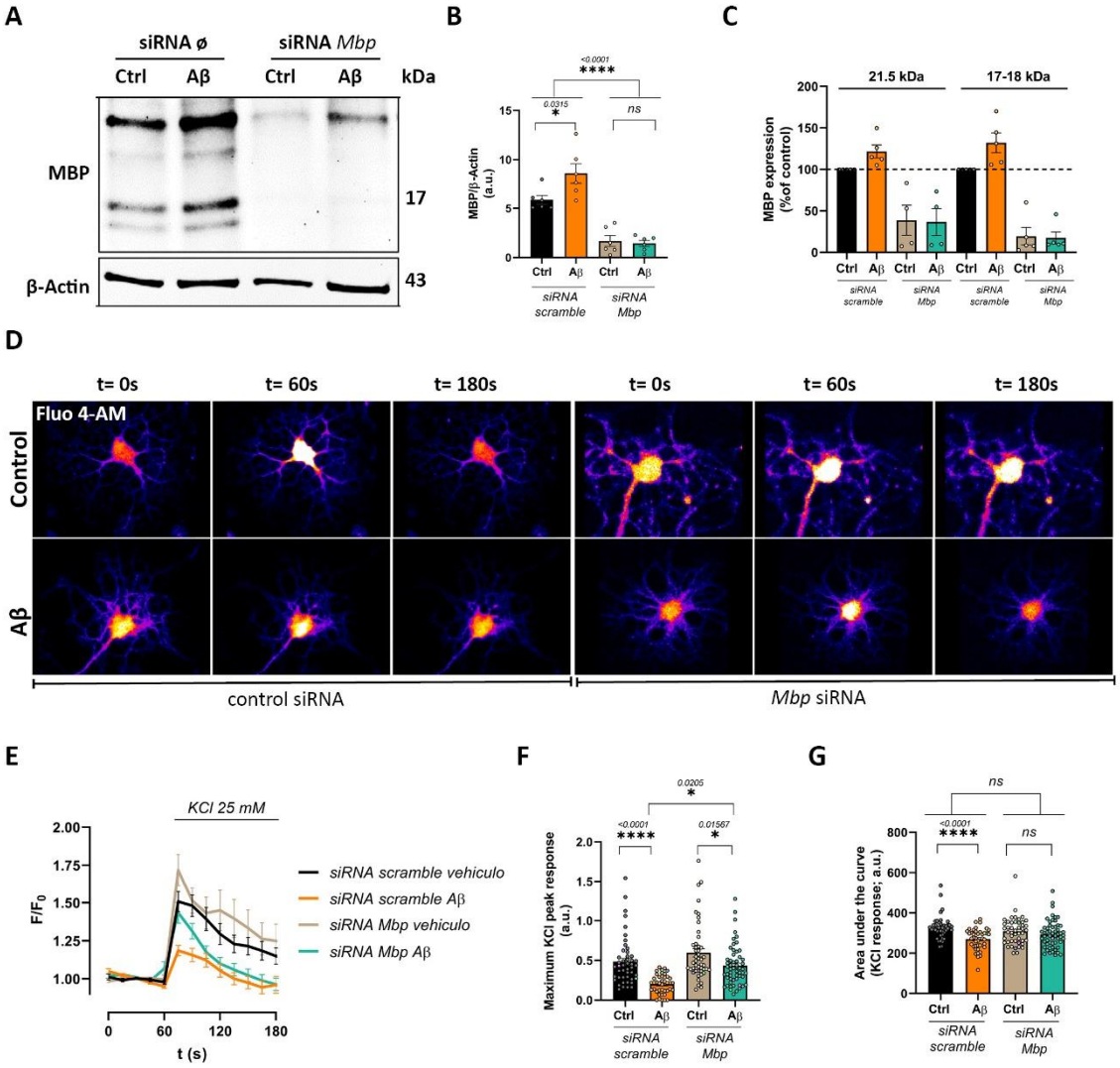


***Figure 25. MBP overexpression inhibits KCl-induced $Ca^{2+}$influx into the cell. (A-C)*** *Western blot and analysis of MBP expression levels following Aϐ exposure in oligodendrocytes treated with siRNA scramble and siRNA Mbp are shown.* ***(D, E)*** *Cells transfected with either scramble siRNA or Mbp siRNA were loaded with Fluo-4AM and exposed to Aϐ for 24 h. Time course of intracellular calcium levels were recorded before and after KCl 25 mM stimulus by confocal microscopy.* ***(F, G)*** *Bar graphs show the and maximum peak and the area under the curve of KCl response in the different conditions. Data indicate means ±S.E.M and dots represent independent experiments in WB and cells in the case of calcium analysis, *p<0.05, ****p<0.0001, compared to control cells. Statistical significance was drawn by ordinary two-way ANOVA followed by Tukey post-hoc test.*

### 2.10.2 $A\beta_{1-42}$ oligomers inhibits calcium influx high KCl-induced depolarization in oligodendrocytes of hippocampal organotypic slices

To further address if Aβo could change calcium homeostasis we used rat hippocampal organotypic cultures as a more complex cellular system. Hippocampal organotypic cultures have been used as models to investigate mechanisms underlying neurodegenerative disease and to explore treatment strategies to tackle them as they partially maintain tissue architecture, anatomical relations and network connections (Stoppini, Buchs, & Muller, 1991). To label oligodendrocytes, organotypic slices were transduced by rAAV8-MBP-GFP and produced GFP protein was observed as early as 72 h after infection. The GFP fluorescence was located in the cytoplasma and nucleus as well as the processes of olig2+ oligodendcroyte cells, but not in NeuN+ neurons and GFAP+ astrocytes. **(Figure 26A)**. Then, we treated rat hippocampal slices after 7 DIV with Aβ at 1 µM for 48 h **(Figure 26B)**, and we recorded intracellular $Ca^{2+}$ levels upon KCl stimulation (50 mM) using puff technique. We clearly observed that Aβo induced a significant decrease in the maximum peak and AUC (0.09034±0.002 vs 0.03368±0.006) **(Figure 26C, D)**, suggesting a decrease the influx of $Ca^{2+}$ through voltage-gated calcium channels.

Altogether, these data suggest that Aβo altered VGCC affecting the calcium influx into the cell.

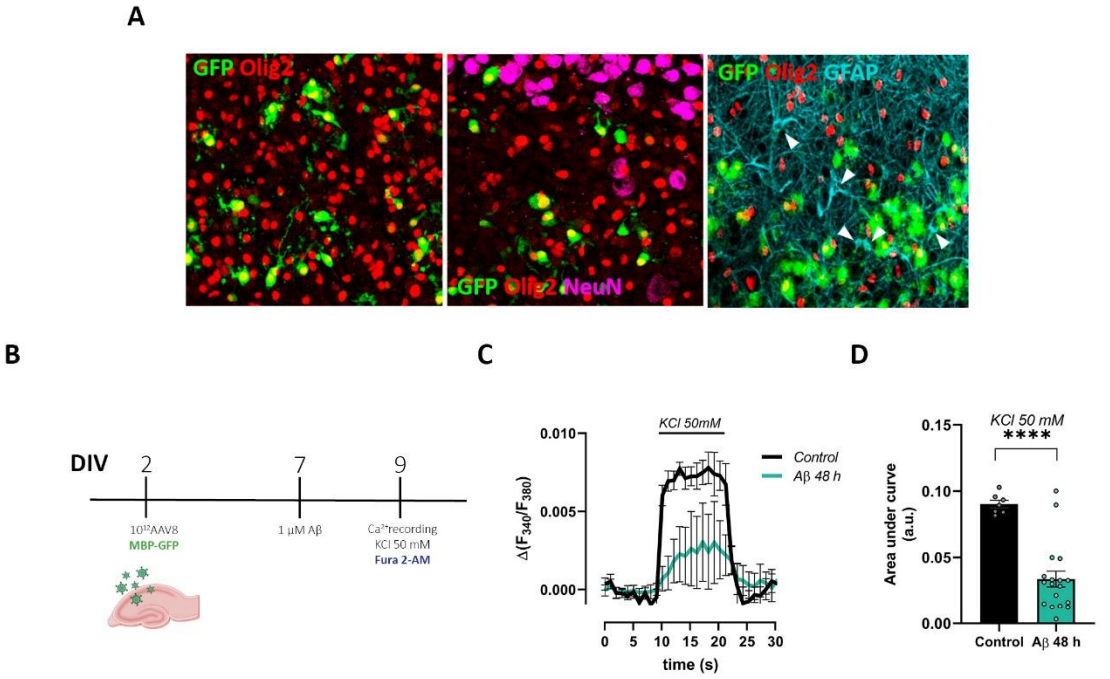


***Figure 26. Aβ$_{1-42}$ oligomers inhibits intracellular calcium influx in oligodendrocytes of hippocampal organotypic slices. (A)*** *Representative confocal z-stacks projections of hippocampal organotypic slices infected with AAV8-MBP-GFP (green) immunostained with Olig2 (red), NeuN (magenta) and GFAP (cyan). Note that only olig2 colocalized with GFP.* ***(B)*** *Scheme of the experimental approach.* ***(C)*** *Cells were loaded with Fura 2-AM and KCl-induced intracellular calcium levels were recorded.* ***(D)*** *Histogram depicting area under the curve (AUC) obtained by KCl 50mM application in vehicle-and Aβo-treated hippocampal organotypic slices. Data indicate means ±S.E.M and dots represent individual cells, ****p<0.0001, compared to vehicle-treated organotypic oligodendrocytes. Statistical significance was drawn by two-tailed unpaired Student´s t-test.*

### 2.10.3 MBP overexpression promotes protein synthesis

One of the largest group of proteins that interacts with MBP belongs to proteins involved in the protein synthesis machinery, as well as in the spatial and temporal regulation of translation (Smirnova, E.V. *et al*., 2021). To analyse the potential role of MBP in translation, we treated cultured oligodendrocytes with Aβ using a control siRNA and a *Mbp*-targeting siRNA. 10 minutes before protein extraction, we treated oligodendrocytes with puromycin (2 µM). Interestingly, western blot analysis showed that Aβo increased global protein synthesis (1.439±0.046 vs 2.177±0.2082, respectively) and this was blocked by silencing MBP (1.872±0.1347 vs 1.808±0.1058, respectively)

**(Figure 27A, B)**. In order to get a clue on how MBP levels could be altering translation, we performed immunofluorescence analysis to visualise where exactly in the cell was puromycin incorporating. We observed a significant increase specifically in the processes of Aβo treated cells compared to controls (2.502±0.1625 vs 3.206±0.3088, respectively) **(Figure 27C, D)**. Of note, we observed the increase where MBP is found, reinforcing the hypothesis that the MBP may play a role in protein synthesis. Surprinsingly, we observe a non-significant trend toward to increase in puromycin when *Mbp* was silenced in both control and Aβo-treated cells.

Then, as we observed a MBP increase in the 3xTg-AD hippocampus and myelin, we wondered if hippocampal oligodendrocytes have changes in protein synthesis dynamics. First, we analysed puromycin incorporation in the myelin-enriched fractions and observed a trend towards an increase in the 3xTg-AD compared to controls **(Figure 27E, F)**. Then, we treated acute slices from wild type and 3xTg-AD mice with puromycin (10 µM). We immunostained the acute slices with Olig2 and puromycin **(Figure 27G)** and we measured the fluorescence intensity of puromycin in $Olig2^+$ cells. Analyses showed that translation in oligodendrocytes was significantly increased in the 3xTg-AD mice hippocampal acute slices (120672±16857 vs 182662±8593, respectively) **(Figure 18H)**.

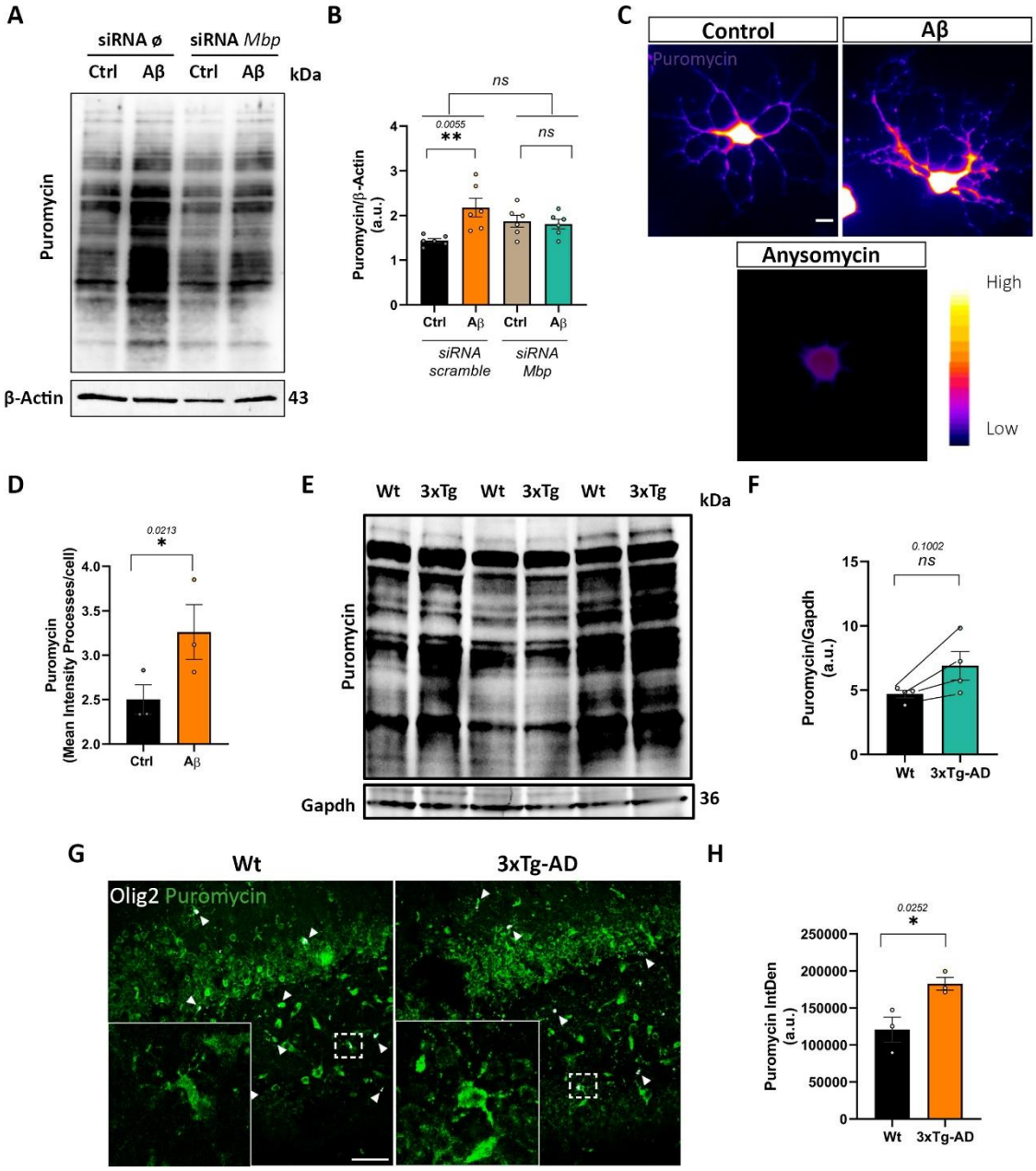


***Figure 27. MBP promotes protein translation. (A, B)*** *Puromycin levels were analysed by western blot after exposure of Aβ for 24 h in cells transfected with scramble siRNA or Mbp-targeting siRNA.* ***(C, D)*** *Puromycin levels were analysed by western blot in myelin-enriched fractions from Wt and 3xTg-AD mice.* ***(E, F)*** *Representative immunofluorescence micrographs and quantification of hippocampal acute slices of Wt and 3xTg-AD mice. Immunostaining for oligodendrocyte marker Olig2 (white) and puromycin (green).Scale bar, 100 µm. Data indicate means ±S.E.M and dots represent individual animals or independent experiments, *p<0.05, **p<0.01, compared to controls. Statistical significance was drawn by two-tailed unpaired Student´s t-test and ordinary two-way ANOVA followed by Tukey post-hoc test.*

# PART III: Effect of $A\beta_{1-42}$ oligomers on actin dynamics and myelination

## 3.1 Effect of $A\beta_{1-42}$ oligomers on actin dynamics *in vitro*

Actin dynamics is a key factor in the basic functions of oligodendrocytes as it is involved in processes such as migration, differentiation and myelination (Brown & Macklin, 2019). Changes in the balance of polymerization and depolymerisation could affect the cytoskeleton of these cells with physiological impact on the function of the CNS. Aberrations in actin dynamics have been described in *in vitro* neuronal models and in animal models of AD, however, there are no studies describing changes of the cytoskeleton of oligodendrocytes in this disease. Moreover, we observed altered expression of genes associated with cytoskeleton in our RNA-seq experiments. Therefore, we analysed the possible effects of Aβ in the cytoskeleton dynamics of oligodendrocytes.

### 3.2.1 $A\beta_{1-42}$ oligomers alters oligodendrocyte morphology

It was previously described that oligodendrocytes undergo stereotyped morphological changes as they differentiate, from an arborized morphology to a more lamellar like structure. Moreover, as the cell is adopting a more mature state, F-actin is lost while MBP is increased and interestingly, its expression by oligodendrocytes and in myelin occurs simultaneously with actin disassembly **(Figure 28)** (Zuchero *et al.*, 2015).

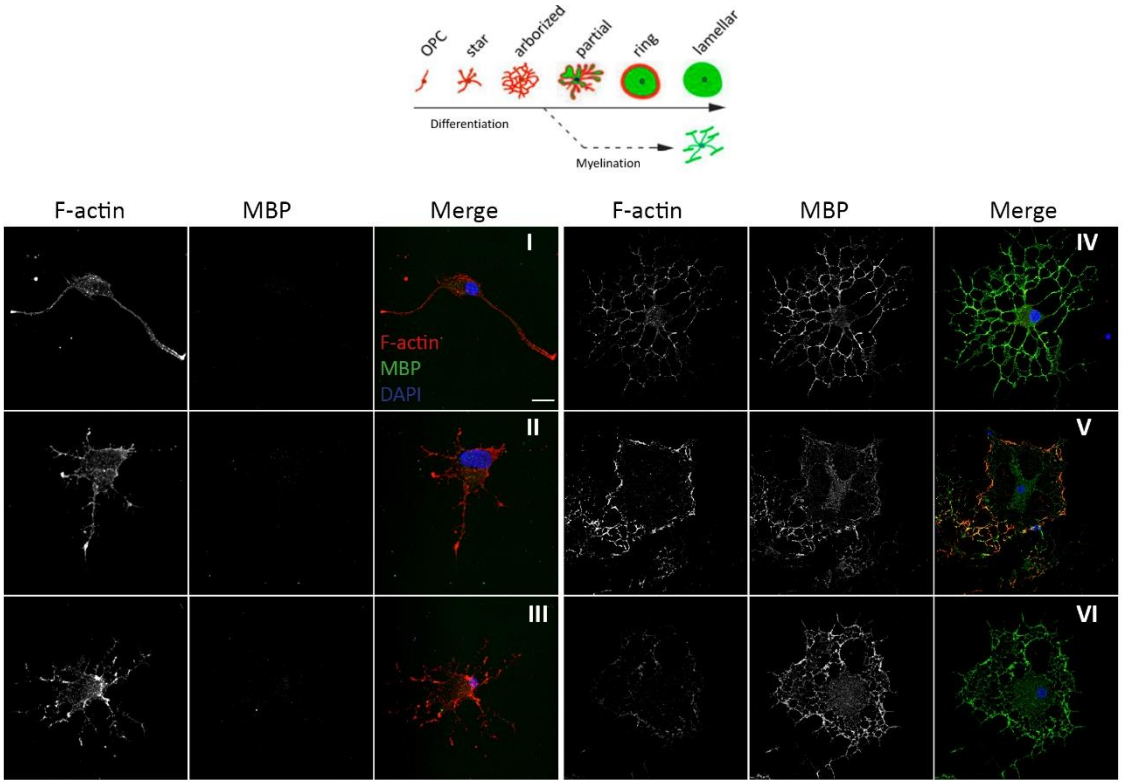


***Figure 28. Schematic model of morphology change during OPC differentiation in vitro.*** *Oligodendrocytes (OLs) were fixed after 1, 3 and 6 days in vitro (DIV) with the representation of the different morphologies during differentiation: I, OPC; II; Starry; III; Arborized; IV; Partial; V, Annular; VI, Lamellar. OLs were immunostained for F-actin filaments (phalloidin, red), MBP (Green) and nuclei (DAPI, blue). Scale bar, 10 µm. Figure adapted from Zuchero et al., 2015.*

First, we checked whether Aβo could alter actin cytoeskeletonan thus, affect oligodendrocyte morphology. Therefore, we stained oligodendrocytes with Phalloidin-Texas red (F-actin) together with tubulin and we measured the complexity of the cell by Sholl analysis. A significant increase in the number of Sholl rings crossing were observed for F-actin in Aβo-treated oligodendrocyte relative to control, indicating that Aβo increase the complexity of oligodendroglial morphology **(Figure 29B)**. In contrast, we did not observe any significant differences between both conditions in the number of sholl rings crossing for tubulin **(Figure 29C)**. These data indicate that Aβo induces morphological changes presumably by altering actin filaments but not microtubules.

Next, to analyse morphological differentiation in more detail in a 3D environment, we cultured oligodendrocytes in PCL nanofibers. Oligodendrocytes align and wrap around nanofibers adopting a morphology similar to that in physiological conditions. We stained the cells for MBP and quantified different parameters such as cell length, width, process

number and process length. We found that Aβo decrease the mean cell length (209.5±10.56 vs 181.7±10.49, respectively) but do not change the width or the total process number **(Figure 29E, F, G)**.

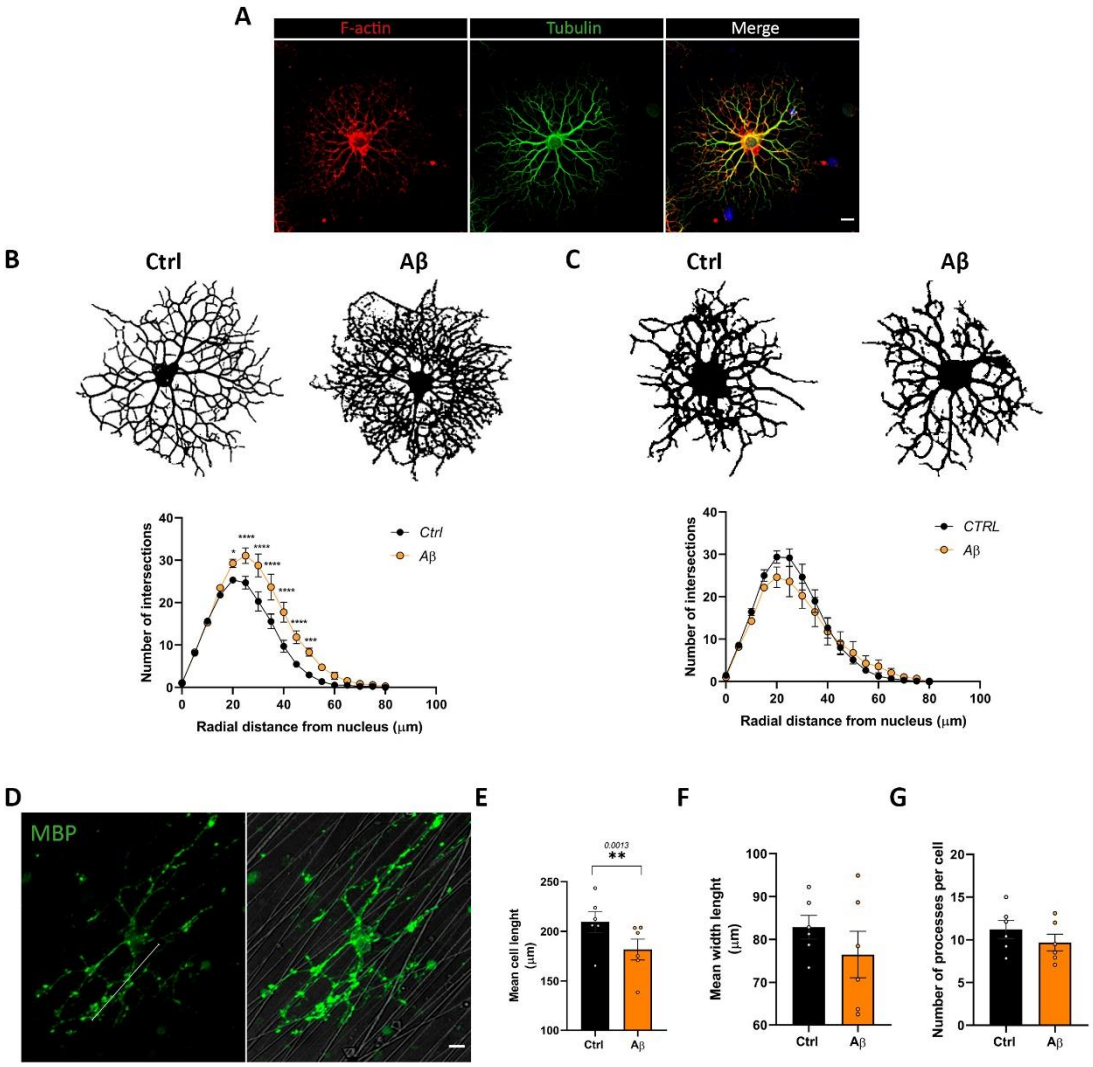


***Figure 29. Aβ$_{1-42}$ oligomers dysregulate the actin-cytoskeleton. (A)*** *Representative micrographs of F-actin (phalloidin, red) and tubulin (green) distribution in cultured oligodendrocytes* ***(B)*** *Representative image of Sholl analysis (black) and quantification for F-actin in oligodendrocytes treated with 1 µM of Aβ for 24 h.* ***(C)*** *Representative image of Sholl analysis (black) and quantification for tubulin in oligodendrocytes treated with 1 µM of Aβ for 24 h.* ***(D)*** *Representative maximum projection of oligodendrocyte grown in nanofibers and immunostained for MBP (Green). White arrow shows the process length.Histograms depicting mean cell length* ***(E)****, mean cell width* ***(F)*** *and number of processes per cell* ***(G)****. Scale bar, 10 µm. Data indicate means ± SEM and dots represent idependent experiments, p*<0.05, p**<0.01 compared to control cells. Statistical differences between groups were assessed by not paired one-way ANOVA with Sidak post-hoc test.*

### 3.2.2 Aβ$_{1-42}$ oligomers stimulate actin dynamics

To understand whether the observed effect of Aβo on cytoskeleton morphology and dynamics could be due to an increase in stabilized microfilaments, we performed experiments of fluorescence recovery after photobleaching (FRAP). FRAP was performed on oligodendrocytes at 2 and 3 DIV virally infected with Lifeact-GFP. Lifeact is a small peptide, which stains F-actin structures in eukaryotic cells and tissues. For the analysis, photo-bleaching was applied at the leading edge of oligodendrocyte processes and fluorescence recovery was recorded for each condition in subsequent seconds **(Figure 30A, B, C)**.

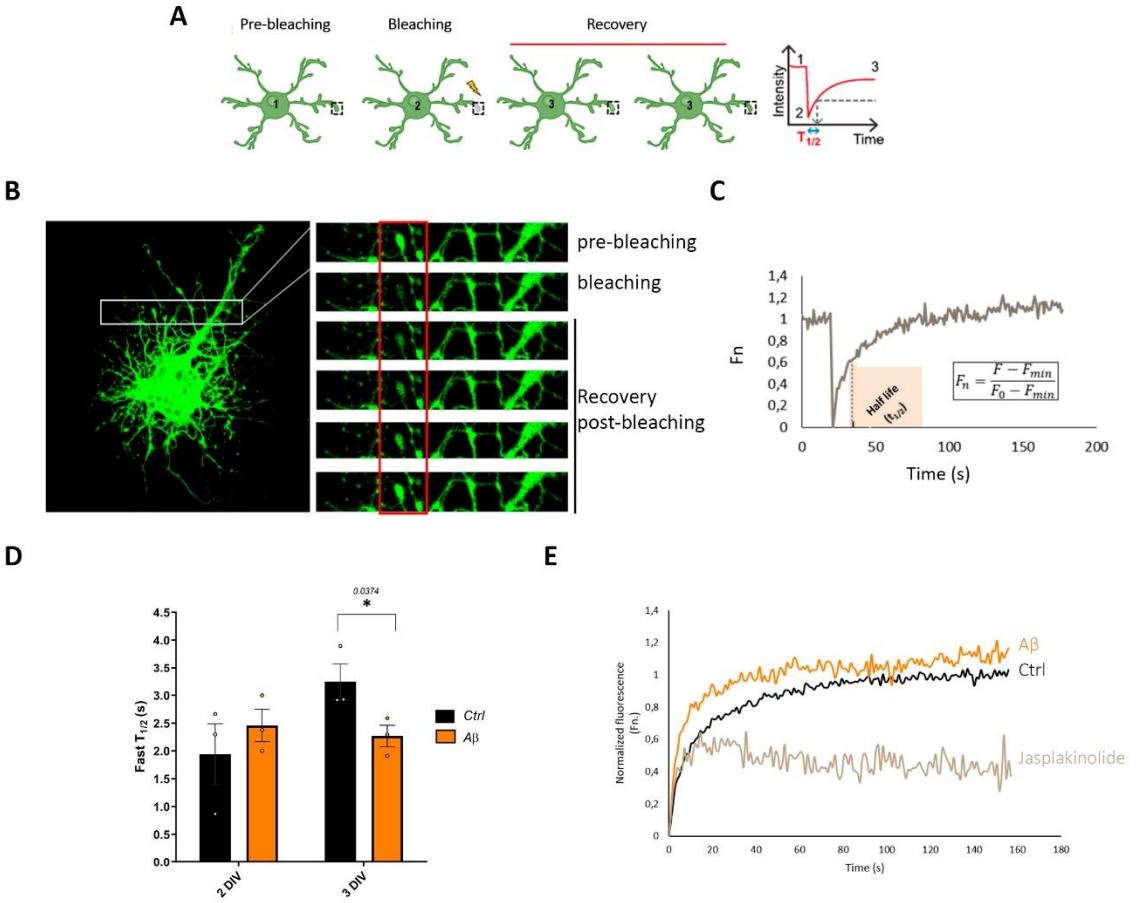


***Figure 30. Aβ$_{1-42}$ oligomers changes actin dynamics. (A)*** *Diagram showing the different phases of FRAP. Pre-photobleaching; 2. Laser photobleaching and 3. Fluorescence recovery. ROI was performed on the growth cone of the OL processes.* ***(B)*** *Representative FRAP image of a 3 DIV control OL transduced with LifeAct (1:100, for 16 hours). Growth cones were photobleached and fluorescence recovery time was measured.* ***(C)*** *Fluorescence recovery intensity curve was using the equation in the box and half-life parameter ($t_{1/2}$).* ***(D, E)*** *Recovery curves of fluorescence in control (black), Aβ-treated (orange) and Jasplakinolide-treated (brown) OLs. 2-3 cells were visualised per condition in each experiment and within*

*each cell 3-5 different spots were quantified. Data indicate mean± SEM and dots represent independent experiments, *p < 0.05 compared to control cells. Statistical significance was drawn by two-tailed paired Student t-test.*

At 2 DIV the recovery of fluorescence expressed as Fast $T_{1/2}$ was similar in Aβo-treated and control control oligodendrocytes (1.943 ± 0.5475s for control and 2.459 ± 0.2911s for Aβo-treated cells). In contrast, at 3 DIV changes were observed, mainly in the first half of the curve, suggesting significant differences in the rate of actin polymerization with and without treatment (3.247 ± 0.3254s for control and 2.266 ± 0.1955s for Aβo-treated cells). Jasplakinolide stabilizes the filaments and promotes filamentous assembly of actin, thus it was used as a negative control **(Figure 30D, E)**. These data indicate actin polymerization occurs faster in oligodendrocytes treated with Aβ-peptide.

### 3.2.3 $A\beta_{1-42}$ oligomers alter F and G-actin ratio and cofilin phosphorylation

A good insight in the status of actin dynamics is to measure the ratio between monomeric globular actin (G-actin) and filamentous actin (F-actin) in cells. Therefore, we determined the levels of G- and F-actin by biochemical and immunofluorescence-based assays in control, Aβ and Latrunculin B (LatB) treated oligodendrocytes. LatB is an inhibitor of actin polymerization that interacts with G-actin in a 1:1 ratio to inhibit polymerization into F-actin *in vitro.* Both approaches revealed an increase in the amount of F-actin at the expense of G-actin in Aβ-treated cells compared to control (2.489±0.07 vs 3.264±0.2668, respectively), suggesting an increase of F-actin. Additionally, LatB treated cell turned F and G-actin to a more 1:1 ratio (1.431±0.2417) **(Figure 31A, C, D)**.

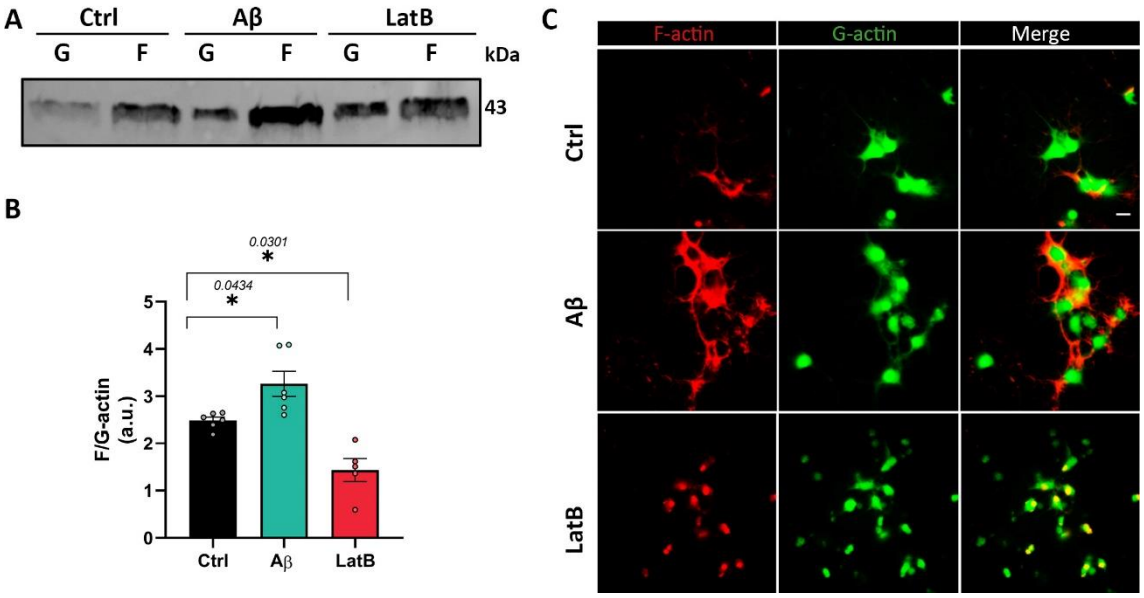


***Figure 31. Aβ$_{1-42}$ oligomers changes F/G actin ratio. (A)*** *Western blot of G-and F-actin from vehicle-, Aβ and LatB -treated cells.* ***(B)*** *Histogram depicting changes in F/G actin ratio in vehicle-, Aβ and LatB-treated cells.* ***(C)*** *Representative immunofluorescence micrograph for F-actin filaments (phalloidin, red) and G-actin (DNAase I, green). Scale bar, 10 µm. Data indicate mean± SEM and dots represent independent experiments, *p < 0.05, compared to controls. Statistical significance was drawn by one-way ANOVA followed by Dunnett post-hoc test.*

In order to investigate the molecular pathway underlying Aβo-induced changes in actin dynamics, we focused on the actin binding protein family. ADF/Cofilin that is one of the proteins involved in actin turnover and it is enriched in oligodendrocytes. It has been described that the activity of ADF/Cofilin is responsible for generating low F/G actin ratios in oligodendrocytes (Nawaz et al., 2015). ADF/Cofilin can be in two different states depending on its phosphorylation state: it becomes activated when it is dephosphorylated and inhibited when it is phosphorylated. Thus, we measured its activation status upon Aβo-treatment at different time points: 15 minutes, 3 hours and 24 hours. Western blot analysis showed a significant increase in the phosphorylation status after 15 minutes of Aβo insult which then stabilizes over time (Ctrl 0.721±0.104; Aβ 15 min 1.053±0.091; Aβ 3 h 0.6694±0.085; Aβ 24 h 0.5129±0.088) **(Figure 32A, B)**.

Overall, these data suggest that Aβo alters oligodendrocyte morphology by altering the actin dynamics.

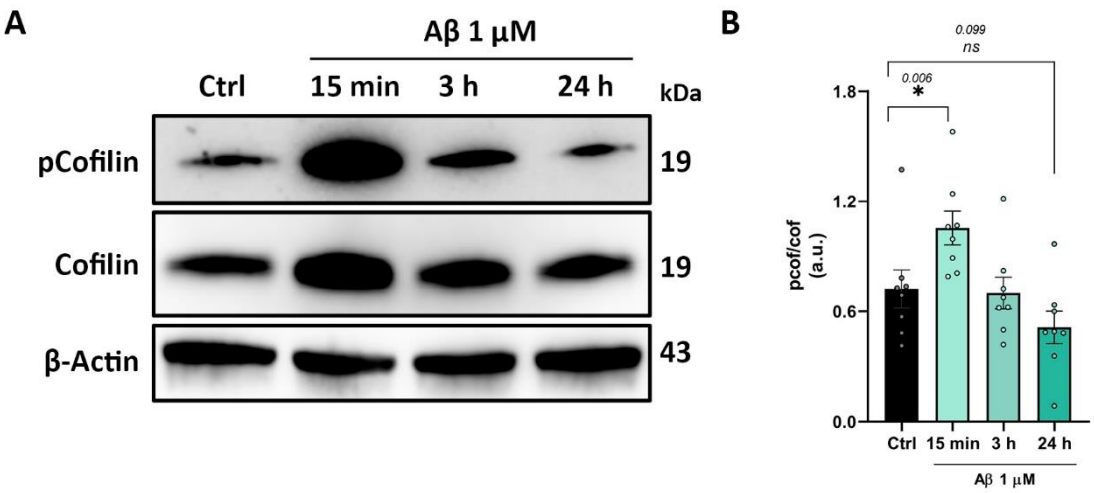


***Figure 32. Aβ$_{1-42}$ oligomers alter acting binding proteins. (A)*** *Western blot of cofilin and p-cofilin from vehicle and Aβ-treated cells at different time points; 15 min, 3 h and 24 h.* ***(B)*** *Histogram of p-cofilin levels normalized to total cofilin. Data indicate mean± SEM and dots represent independent experiments, *p < 0.05, compared to control cells. Statistical significance was drawn by one-way ANOVA followed by Dunnett post-hoc test.*

## 3.3 Effect of Aβ$_{1-42}$ oligomers in myelination *in vivo*

Myelination of axons in the CNS is essential for the rapid propagation of action potentials. Moreover, myelin degeneration and white matter loss are events in AD that lead to cognitive deficits. As we found several pathways associated with myelination altered in Aβ-treated oligodendrocytes and in 3xTg-AD oligodendrocytes in our RNA-seq analysis, we wondered if Aβ could have an effect in myelination *in vivo*.

### 3.3.1 3xTg-AD mice hippocampus present thicker myelin

In our lab it was previously described that 3xTg-AD mice present a thicker myelin in the corpus callosum at 6, 12 and 18-months-old (in progress). As the hippocampus is one of the first affected areas in AD and we had already observed a marked increase in the synthesis of MOBP and MBP, we wondered if myelin could be altered in 6-months-old 3xTg-AD mice. To explore this hypothesis, we carried out electron microscopy imaging in dentate gyrus of WT and 3xtg-AD mice. We calculated myelin thickness by measuring the *g-ratio* value. Remarkably, dentate gyrus myelin showed a significant decrease in the g-ratio of 3xTg-AD in comparison with WT, indicating an increase in myelin thickness **(Figure 33A, B)**.

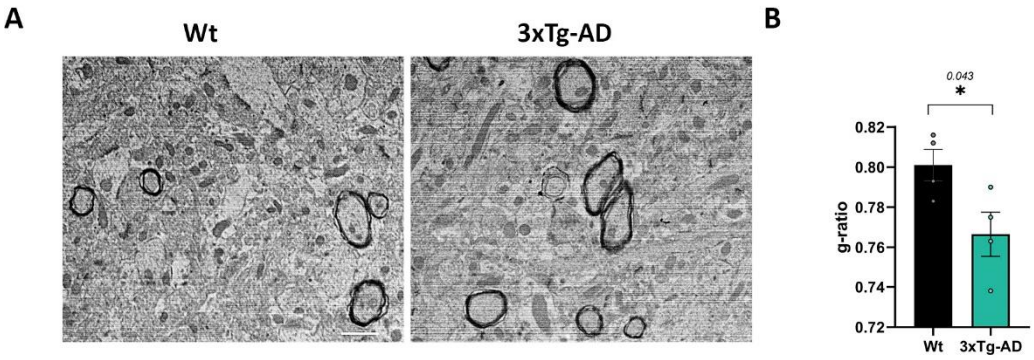


***Figure 33. 3xTg-AD mice hippocampus has thicker myelin at 6-months-old. (A)*** *Representative electron micrographs of dentate gyrus cross-sections from WT and 3xTg-AD at 6 months.* ***(B)*** *Histogram showing g-ratio value in WT and 3xTg-AD mice. Scale bar, 1 µm. Data indicate means ± SEM and dots represent individual animals, p*<0.05, compared to Wt mice. Statistical significance was drawn by two-tailed unpaired Student´s t-test.*

### 3.2.2 Aβ-injected zebrafish larvae present changes in myelination

Little is known about the role of Aβ on myelination. The zebrafish model is an animal model in which myelination can be observed *in vivo*. Since zebrafish postnatal development is fast and larvae are transparent, this model is ideal to track myelination in vivo upon Aβ exposure. In addition, it expresses an orthologue of the murine and human *MBP*, *Mbpa*.

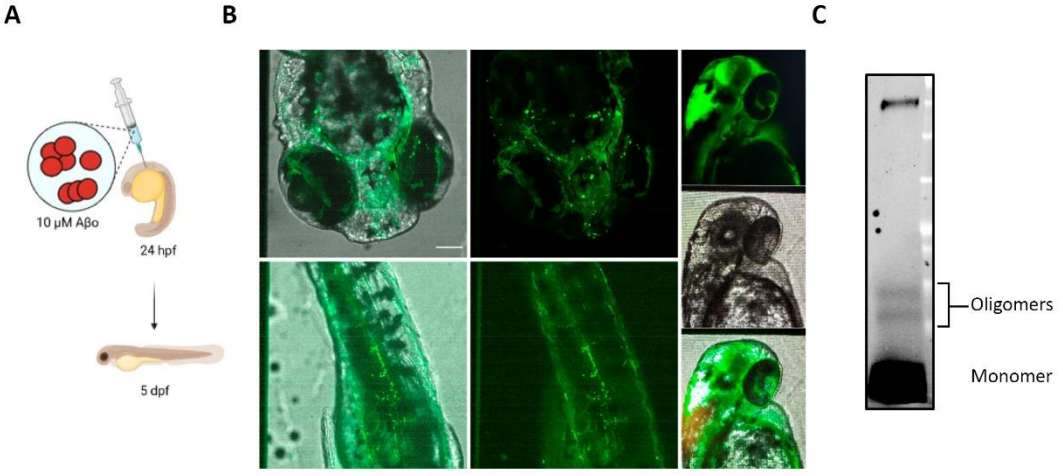


***Figure 34. Aβo-labelled injection into zebrafish. (A)*** *Scheme of the experimental approach; 10 µm of Aβo were injected in the hindbrain of zebrafish larvae and wait until 5 dpf to perform experiments.* ***(B)*** *Representative fluorescence images of labelled- Aβo injection in larvae****. (C)*** *Western blot of Aβ species in the injected mixture; monomers and different types of oligomers. Scale bar, 1 mm.*

Therefore, we analysed the effect of Aβo on myelination in zebrafish larvae. To carry these experiments out, we injected 10 µM Aβo or vehicle intraventricularly in the embryos at 24 hours post-fertilization (hpf) and waited until 3 and 5 days post fertilization (dpf) to perform the experiments. Initially, we verified that the injection was being done correctly by injecting labelled Aβo. We could clearly see that the labelled-Aβo spreads all over the brain and the spinal cord **(Figure 34A, B, C)**. Once we checked the injection efficiency, we studied the effect of Aβo on myelination by immunohistochemistry and *in vivo* imaging.

#### 3.2.2.1 $A\beta_{1-42}$ -injected zebrafish larvae show changes in RNA expression in the spinal cord

In order to identify possible changes in oligodendrocyte differentiation we first performed RNAscope FISH assays in the spinal cord for different oligodendroglial markers; *Myrf, Mbpa* and *Sox10*. We measured the area occupied by the probes and observed a significant decrease of *Myrf* in Aβo-injected zebrafish (153.1±19.58 vs 31.27±7.456, respectively) while the other two markers seem to be unchanged **(Figure 34A, B, C ,D)**. In the spinal cord, the majority of oligodendrocytes develop from cells originally located in the ventral zone, that migrate to the dorsal zone where they proliferate and differentiate into oligodendrocytes (Lee et al., 2010).

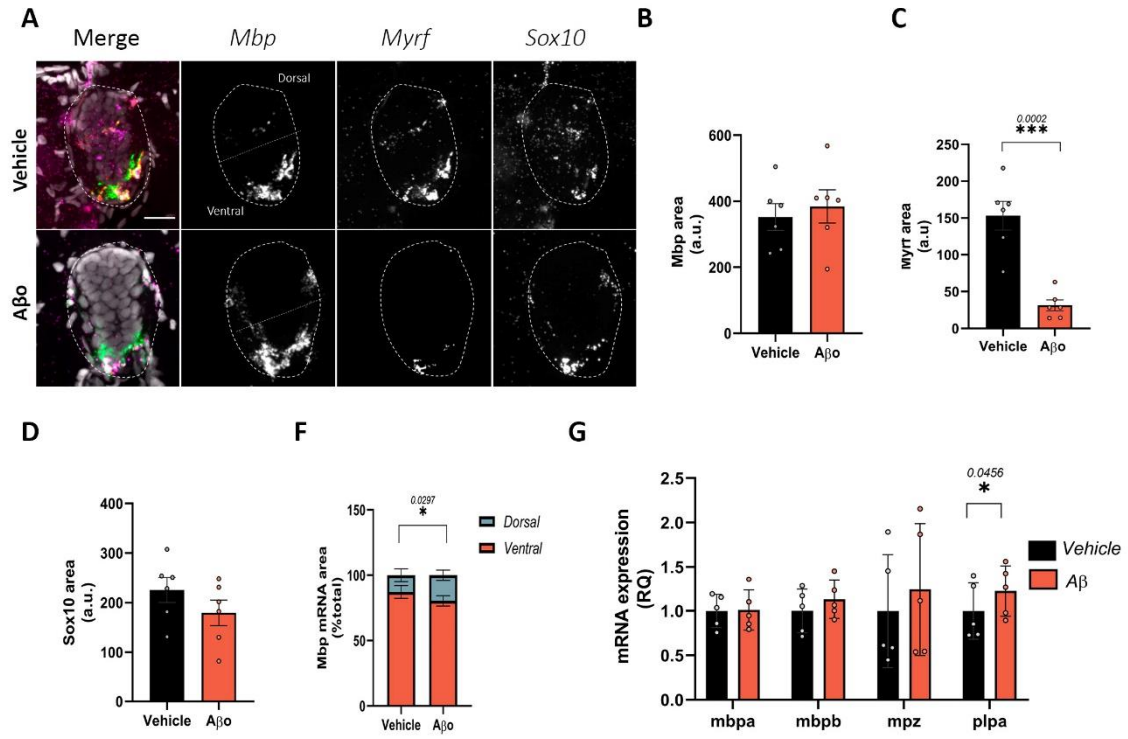


***Figure 35. Aβo-injected zebrafish larvae show changes in mRNA levels and distribution. (A)*** *Representative confocal images of spinal cord cross sections showing Mbp, Myrf and Sox10 mRNA fluorescence intensity in vehicle-and Aβo-injected zebrafish.* ***(B, C, D)*** *RNAscope analysis of mRNAs area in spinal cord.* ***(F)*** *Quantification of Mbp mRNA distribution in ventral and dorsal areas.* ***(G)*** *RT-qPCR analysis of total mbpa/b, mpz and plpa mRNA in vehicle-and Aβo-injected zebrafish. Scale bar, 20 µm. Data indicate means ± SEM and dots represent individual larvae, p*<0.05, p<***0.001 compared to vehicle-injected zebrafish larvae. Statistical significance was drawn by two-tailed unpaired Student´s t-test.*

Therefore, we checked whether oligodendrocytes were migrating more towards to the dorsal zone to differentiate. We measured the area occupied by *Mbpa* in the dorsal and the ventral zone and observed a significant shift towards the dorsal area in Aβo-injected zebrafish compared to vehicle-injected zebrafish **(Figure 35F)**. Moreover, we also performed RT-qPCR for *Mbpa, Mbpb, Mpz* and *Plpa*, and detected a significant increase of *plpa* in Aβo-injected zebrafish (0.9998±0.1317 vs 1.208±0.1288, respectively) **(Figure 35G)**.

### 3.2.2.2 Aβo- injected zebrafish larvae have more sheaths per oligodendrocyte

Once we observed that Aβo could affect the differentiation stage of oligodendrocytes, we next wondered if this could alter myelin sheath number and length *in vivo*. To

examine myelin sheaths in individual oligodendrocytes, we transiently expressed *mbpa:egfp-caax* by microinjection into 1-cell stage zebrafish embryos, which express membrane-tethered EGFP-CAAX in the myelin tracts of the larvae **(Figure 36E)**. We did not observe any changes in sheath length but we detected a significant increase in sheath number in Aβo-injected zebrafish compared to vehicle-injected zebrafish (7.704±0.629 vs 10.06±0.4997, respectively) **(Figure 36A, B, C)**.

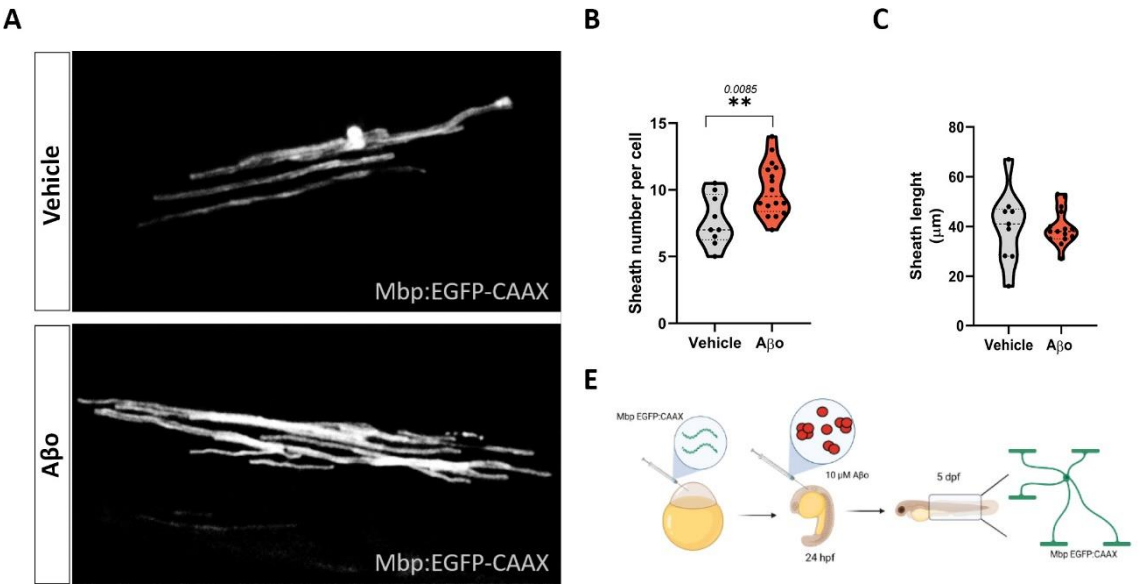


***Figure 36. Aβo-injected zebrafish larvae have more sheath number per cell. (A)*** *Representative live-images of oligodendrocytes in spinal cord of vehicle- and Aβ-injected zebrafish larvae.* ***(B)*** *Histogram depicting sheath number per cell.* ***(C)*** *Histogram depicting individual sheath length.* ***(E)*** *Scheme of the experimental approach; mbp:egfp-caax was injected in embryos and at 24 hpf 10 µm of Aβo were injected in the hindbrain of zebrafish larvae and wait until 5 dpf to perform experiments. Data indicate means ± SEM and dots represent individual larvae, p<**0.01 compared to vehicle-injected zebrafish larvae. Statistical significance was drawn by two-tailed unpaired Student´s t-test.*

### 3.2.2.3 Aβo-injected zebrafish present alterations in myelination

Finally, we asked ourselves if changes in sheath number, distribution and mRNAs of myelin-related proteins could alter myelination. To that end, we performed EM of the spinal cord of the zebrafish larvae and analysed the dorsal and ventral areas. We first measured the *g-ratio* of the Mauthner cells, giant reticulospinal neurons with unique specializations for rapid responses, and observed a significant decrease of the *g-ratio* in

Aβo-injected zebrafish, indicating an increment in myelin thickness (0.8942±0.007 vs 0.8549±0.009, respectively) **(Figure 37B, C)**.

Then we measured myelinated axons in the ventral area and observed a non-significant trend towards a decrease. **(Figure 37B, E)**. In contrast, in the dorsal area we observed a significant increase of myelinated axons in Aβo-injected zebrafish compared to vehicle-injected zebrafish (92.46±19.66 vs 146.2±11.53, respectively) **(Figure 37D, F)**.

Overall, these results demonstrated that Aβo modify oligodendrocyte differentiation and myelin structure *in vivo*.

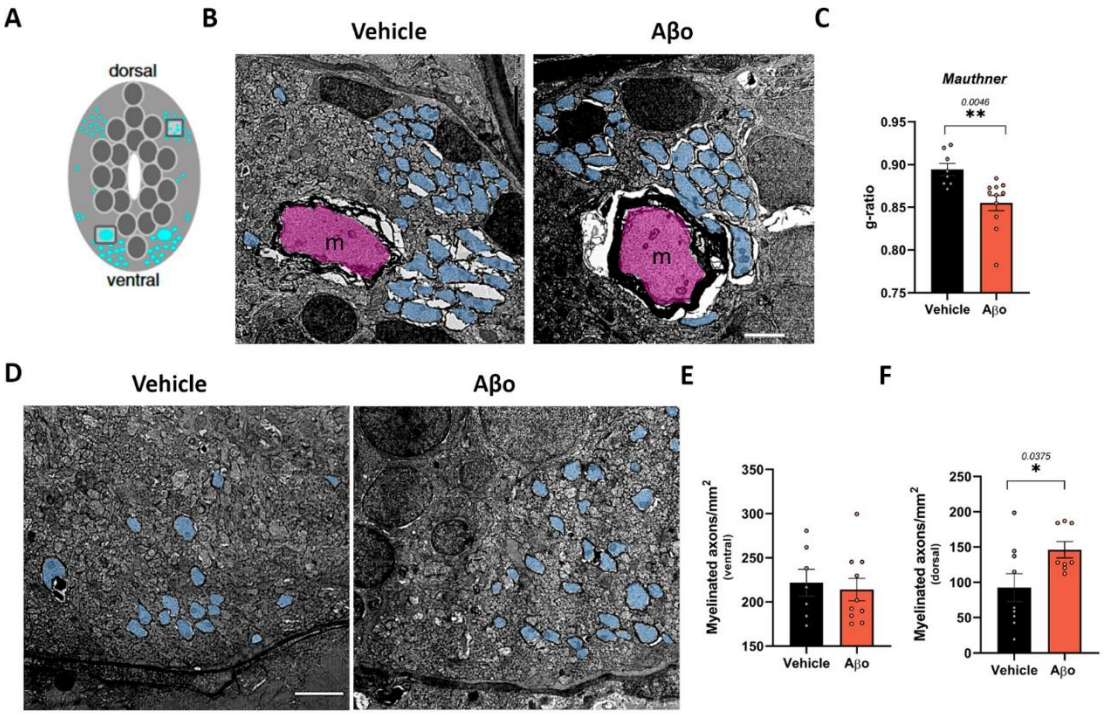


***Figure 37. Aβo-injected zebrafish larvae show changes in myelination. (A)*** *Schematic cross-section of spinal cord illustrating the ventral and dorsal areas.* ***(B)*** *Representative electron micrographs of ventral spinal cords of vehicle- or Aβo-treated larvae at 8 dpf. Myelinated axons are shaded in blue and Mauthner cell axons in pink.* ***(C)*** *Histogram showing g-ratio value in Mauthner cells from vehicle-and Aβo-injected zebrafish.* ***(D)*** *Representative electron micrographs of the dorsal spinal cord from vehicle-and Aβo-injected zebrafish at 8 dpf. Myelinated axons are shaded in blue.* ***(E, F)*** *Histograms showing % of myelinated axons in dorsal and in ventral areas from vehicle-and Aβo-injected zebrafish. Scale bar, 2 µm. Data indicate means ± SEM and dots represent individual larvae, p*<0.05, compared to vehicle-injected zebrafish larvae. Statistical significance was drawn by two-tailed unpaired Student´s t-test.*

# PART IV: Description and effect of EVs derived from control and Aβ treated oligodendrocytes

## 4.1 $A\beta_{1-42}$ oligomers stimulate extracellular vesicle release in oligodendrocytes

Previous studies have shown that oligodendrocytes secrete relatively large amounts of EVs carrying a multitude of proteins, like myelin related proteins (PLP, CNP, MOG and MBP) as well as RNAs (Krämer-Albers et al., 2007). EVs have been suggested to play a central role in the spreading and progression of neurodegenerative diseases (Howitt & Hill, 2016). Therefore, since we observed in the RNA-seq that one of the most upregulated pathways is related with vesicle transport and localization, we wondered whether Aβ could stimulate the secretion of extracellular vesicles (EVs). To test this possibility, primary cultured oligodendrocytes were treated with 1 µM of Aβo for 24 hours and EVs were isolated from culture media by ultracentrifugation. Western blot analysis showed that EV marker TSG-101 levels were significantly increased in Aβo-treated cells (0.807±0.363 for control vs 1.953±0.28 for Aβo), enhanced EV secretion **(Figure 38A, B)**. Moreover, western blot analysis of myelin proteins revealed higher MBP levels in EVs derived from Aβo-treated cells (3.454±0.1073 vs 7.909±0.7095, respectively) **(Figure 38A, C)**. Similarly, nanoparticle-tracking analysis (NTA) showed a significant increase in vesicle secretion in Aβo-treated oligodendrocytes **(Figure 38D)**.

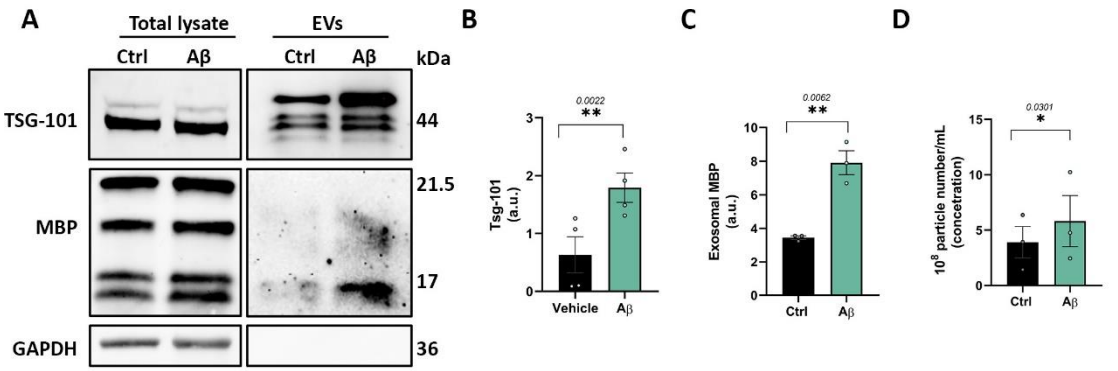


***Figure 38. $A\beta_{1-42}$ oligomers stimulate the release of oligodendrocyte EVs containing MBP. (A)*** *Western Blot of MBP, GAPDH and TSG-101 in total lysate and EVs isolated by ultracentrifugation from culture media of cultured oligodendrocytes treated with 1 µM Aβ for 24 h.* ***(B)*** *Quantification of EV marker TSG-101 by western blot.* ***(C)*** *Quantification of MBP levels in EVs by western blot.* ***(D)*** *Nanoparticle tracking analysis of EVs derived from culture media of cultured oligodendrocytes treated with Aβ 1 µM for 24 h. Data indicate*

*means ±S.E.M. and dots represent independent experiments, **p<0.01 compared to control cells. Statistical significance was drawn by two-tailed paired Student´s t-test.*

Prior to their secretion into to the extracellular space, EVs need to be transported by molecular motor proteins such as, dynactin, kinesin and dynein **(Figure 39A)**. Thus, we next wondered if we could have an altered transport of the vesicles in Aβo-treated oligodendrocytes. We performed RT-qPCR and western blot analysis for dynactin and dynein. We did not observ any alterations at mRNA levels **(Figure 39B, E)**. Nonetheless, we observed increased levels of dynactin in Aβo-treated oligodendrocytes compared to controls at protein levels (1.873±0.1654 vs 2.187±0.1361) **(Figure 39C, D).** Overall, these results suggest that Aβo drive the secretion of EVs into the extracellular space.

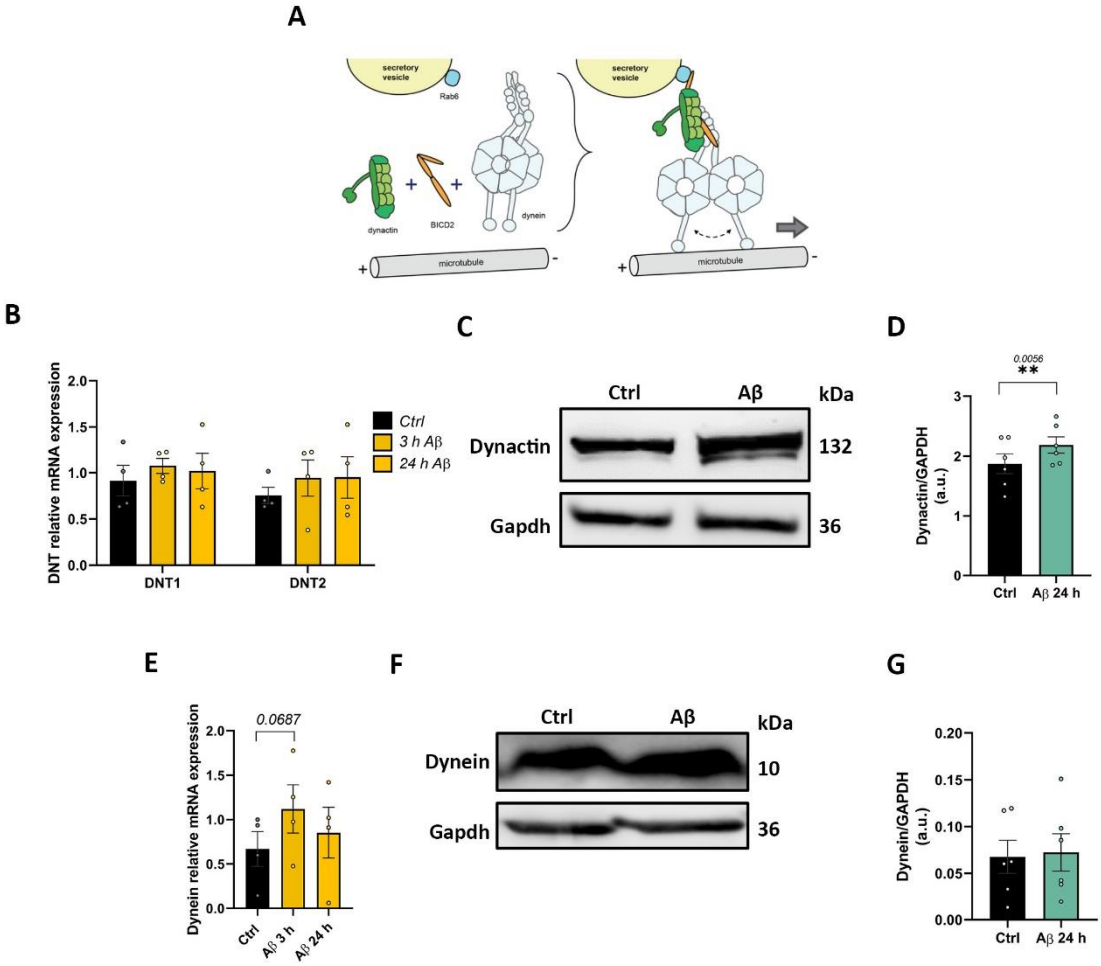


***Figure 39. Aβ$_{1-42}$ oligomers upregulate motor protein dynactin. (A)*** *Model of regulation of processive dynein/dynactin motility by cargo adaptors.* ***(B)*** *RT-qPCR analysis of Dynactin1 (DNT1) AND 2 (DNT2) in oligodendrocytes treated with 1 µM for 3h and 24 h.* ***(C, D)*** *Dynactin expression and relative quantification in total cell extracts from oligodendrocytes treated with Aβ 1 µM for 24 h.* ***(E)*** *RT-qPCR analysis of Dynein*

*in oligodendrocytes treated with 1 µM for 3h and 24 h.* ***(C, D)*** *Dynein expression and relative quantification in total cell extracts from oligodendrocytes treated with Aβ 1 µM for 24 h. Data indicate means ±S.E.M. and dots represent independent experiments, **p<0.01 compared to control cells. Statistical significance was drawn by two-tailed paired Student´s t-test and one-way ANOVA followed by Dunnett post-hoc test.*

## 4.2 Impact of oligodendroglial EVs on neurons

EVs were initially considered as vesicles that enabled the discard of obsolete molecules but increasing evidence suggest EVs play important roles in intercellular communication. As we observed increased secretion EVs of Aβo-treated oligodendrocytes, we wondered if these could have an effect on neurons.

It has been described that oligodendrocyte-derived EVs mediate neuroprotection, improve neuronal homeostasis and support axonal transport and maintenance (Frühbeis et al., 2020; Howitt & Hill, 2016). Therefore, we wonder if under pathological conditions oligodendroglial EVs could affect neuronal functions. As we have previous data that Aβo-treated astrocytes derived EVs increased global translation in neurons neurites (Gamarra et al., 2021), we wondered if oligodendrocyte-derived EVs from Aβo-treated cells could also affect translation. Therefore, primary hippocampal neurons (10 DIV) were treated with fresh media, and EVs derived from control and Aβo-treated oligodendrocytes EVs for 24 h. Prior fixation, cells were treated with puromycin (2 µM) for 10 minutes **(Figure 40A)**.

First, we wanted to check if neurons were able to capture EVs released from oligodendrocytes. To that end, isolated EVs were stained using a red dye (PKH26 red fluorescence labelling, Sigma-Aldrich) and we observed EVs outside and inside the neurons in the soma and processes **(Figure 40B)**. Then, we performed immunofluorescence analysis and observed EVs derived from Aβo-treated oligodendrocytes increased puromycin intensity in the soma of neurons compared to those derived from control oligodendrocytes, suggesting that EVs from Aβo-treated cells increase translation in neurons (fresh media 13339±5797; control±4135; Aβo 18550±4596) **(Figure 40C, D)**.

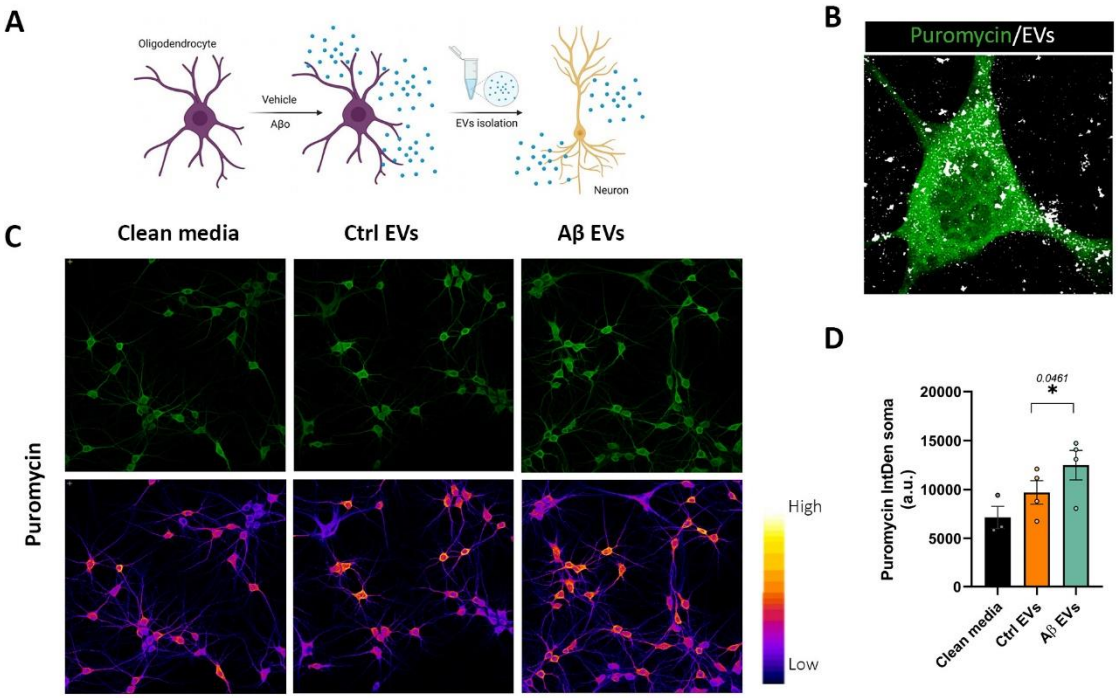


***Figure 40. EVs secreted by Aβo-treated oligodendrocyte increase protein synthesis. (A)*** *Diagram illustrating the experimental approach.* ***(B)*** *Representative micrographs showing puromycin (green) and labelled-EVs (white) within the neurons.* ***(C)*** *Representative micrographs showing puromycin (green and fire) immunostaining in hippocampal neurons treated with fresh media, EVs from Ctrl OL and from OLs treated with Aβ for 24 h.* ***(D)*** *Analysis of puromycin integrated density in the soma of neurons. Data indicate means ±S.E.M. and dots represent independent experiments, **p<0.05. Statistical significance was drawn by one-way ANOVA followed by Tukey post-hoc test.*

Mounting evidence has revealed that EVs are a key modulator of synaptic activity under physiological and pathological conditions. Thus, having shown an increased release of EVs from oligodendrocytes by Aβo and that these EVs increase translation in neurons, we wondered if derived from control and Aβo-treated oligodendrocytes could modify synapses. To test this possibility, we quantified pre-and post-synaptic markers in primary hippocampal neurons (21 DIV). We found that pre-synaptic protein synaptophysin puncta was increased in neurites treated with control EVs, albeit in neurons treated with Aβ-derived EVs synaptophysin levels were similar to those of control treatments (fresh media 8575±0.3205; control 11.01±0.3083; Aβo 9.808±0.3172) **(Figure 41A, B)**. Meanwhile, no changes were observed in the post-synaptic marker homer in neurons in any of the conditions **(Figure 41A, C)**. Altogether,

the data suggest that oligodendroglial EVs affect synapses when released by control but not by Aβo-treated oligodendrocytes.

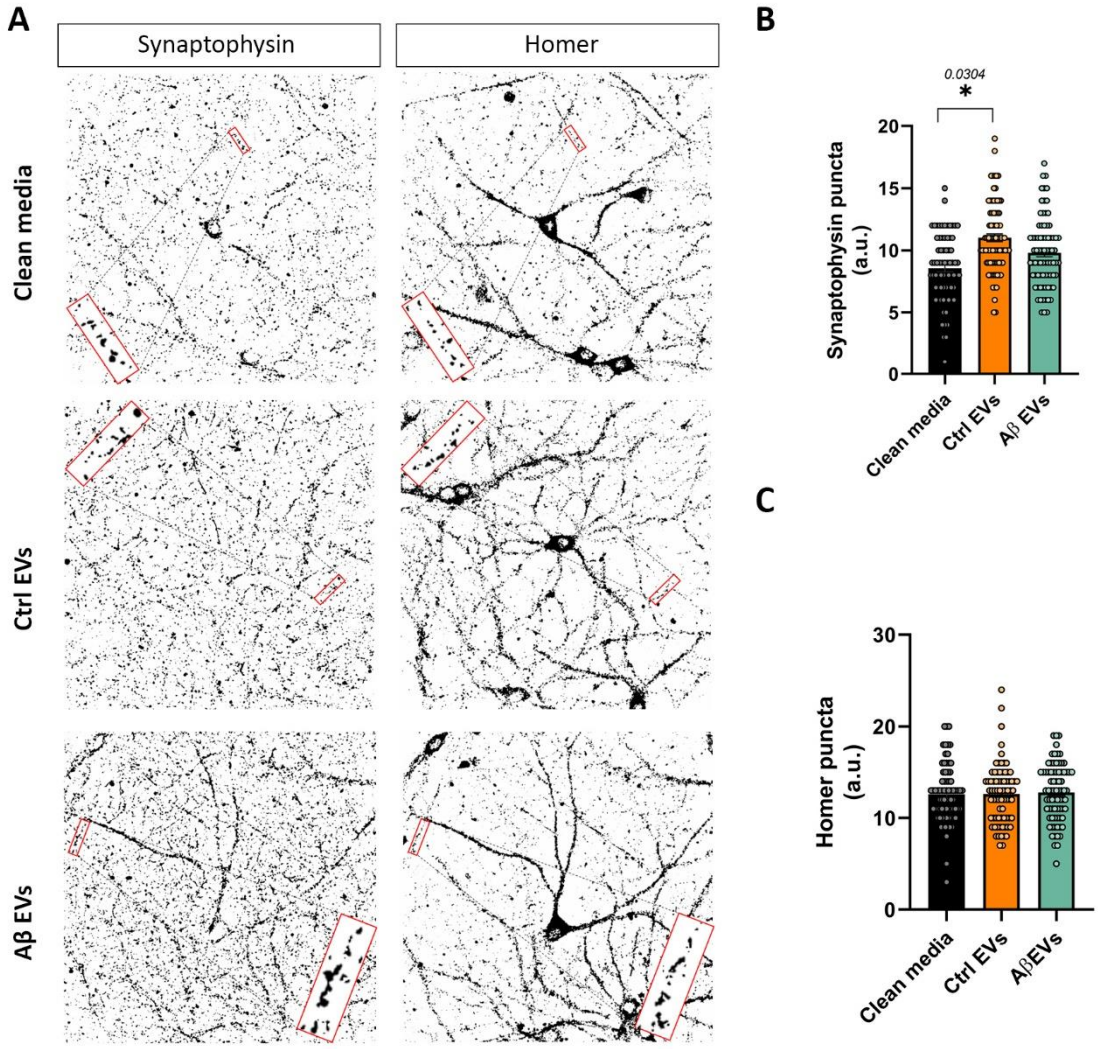


***Figure 41. EVs derived from control oligodendrocytes increase synaptophysin expression in neurons. (A)*** *Representative micrographs of synaptohysin and homer synaptic markers in hippocampal neurons treated with fresh media and EVs from ctrl OLs and Aβ-treated OLs for 24 h.* ***(B)*** *Histogram depicting quantification of synaptophysin puncta in neurites.* ***(C)*** *Histogram depicting quantification of homer puncta in neurites. Data indicate means ±S.E.M. and dots represent individual synapses, **p<0.05, compared to clean media. Statistical significance was drawn by nested one-way ANOVA followed by Dunnett post-hoc test.*

Aβ is derived from the intracellular proteolytic processing of the membrane protein, amyloid precursor protein (APP). Recent studies have highlighted of the secretory pathway and the Golgi apparatus as a major location for APP processing and Aβ production and secretion. Thus, we next wanted to check if oligodendrocyte-derived EVs

could promote exocytosis in neurons. To this end, we added BODIPY FL $C_5$-ceramide to cultured neurons. At high concentrations, BODIPY FL $C_5$-ceramide forms excimers with an emission maximum of 620 nm but fluoresces green (515 nm) at lower concentrations (Pagano, Martin, Kang, & Haugland, 1991). This unique property causes intense red labelling of the trans-Golgi network and Golgi-derived vesicles. Upon fusion with the plasma membrane, the BODIPY label rapidly dissipates in the membrane causing the dissociation of the excimers resulting in decreased fluorescence at 620 nm. Therefore, the decrease of 620 nm emission indicates higher exocytosis. We observed a significant decrease of far red fluorescence (620 nm) in neurons treated with EVs derived from control oligodendrocytes, suggesting an increased exocytosis, whereas EVs from Aβo-treated cells showed no effect **(Figure 42A, B)**.

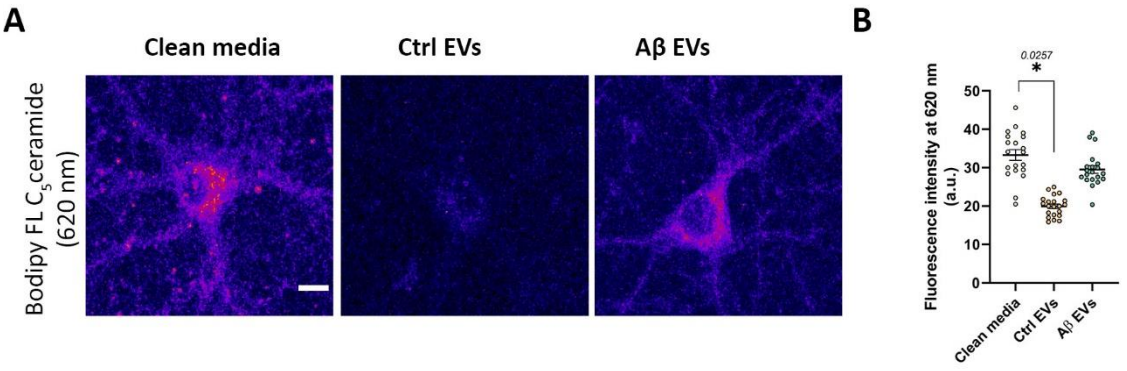


***Figure 42. Control oligodendrocytes derived EVs increase exocytosis. (A)*** *Representative micrographs showing bodipy at 620 nm (fire) immunostaining in hippocampal neurons treated with fresh media, EVs derived from Ctrl oligodendrocytes and from Aβ-treated oligodendrocytes for 24 h.* ***(B)*** *Analysis of fluorescence intensity in the soma of neurons. Data indicate means ±S.E.M. and dots represent independent experiments. Scale bar, 10 µm. Statistical significance was drawn by Nested one-way ANOVA followed by Dunnett post-hoc test.*

Exosomal Aβ was reported first by Rajendran et al. (Rajendran et al., 2006), who observed that N2a cells expressing the Swedish APP mutant (N2a/$APP_{swe}$) secrete EVs containing Aβ. Given that oligodendrocyte EVs modulate Golgi apparatus-derived vesicles and that the Golgi in turn regulates Aβ production, we wondered whether EVs could alter the Aβ secretion. To this end, we used the cell line N2a/$APP_{swe}$ that continuously generates $Aβ_{1-42}$ and we treated cells with fresh media, and EVs derived from control oligodendrocyte and from Aβo-treated oligodendrocytes for 24 h. First, we

addressed whether EVs were toxic for neurons. We performed a viability assays and observed no differences between the three experimental conditions tested **(Figure 43A)**. Next, we measured extracellular $A\beta_{1-42}$ levels by ELISA. We found that $A\beta_{1-42}$ was significantly increased in supernatants from neurons treated with both EVs derived from control and Aβo -reated oligodendrocytes EVs compared to those treated with fresh media (fresh media 2.530E-07±0.2194E-07, control EVs2.853E-07±0.2113E-07, Aβo EVs 3.070E-07±0.2372E-07) **(Figure 43B)**. When comparing between control and Aβo-derived EVs we observed a trend towards an increase in the case of neurons treated with Aβo. We also measured intracellular $A\beta_{1-42}$ and found no significant differences between the three experimental groups **(Figure 43C)**.

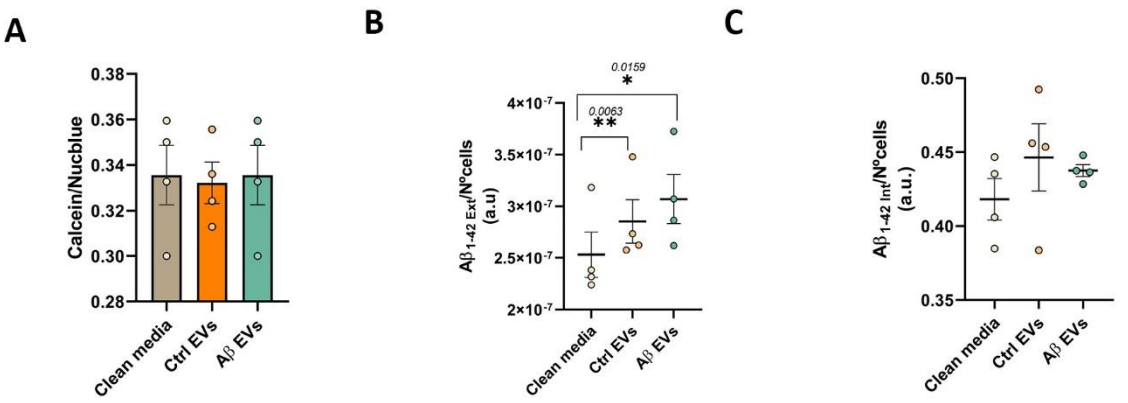


***Figure 43. Oligodendrocyte EVs increase Aβ$_{1-42}$ secretion in N2a/APP$_{swe}$ neurons. (A)*** *Cell viability quantification by Calcein-AM assay in neurons treated with fresh media, and EVs derived from Ctrl OLs and Aβo-treated OLs for 24 h* ***(B)*** *Quantification of extracellular Aβ$_{1-42}$ by high-sensitivity ELISA.* ***(C)*** *Quantification of intracellular Aβ$_{1-42}$ by high-sensitivity ELISA. Data indicate means ±S.E.M. and dots represent independent experiments, *p<0.05, **p<0.01. Statistical significance was drawn by one-way ANOVA followed by Tukey post-hoc test.*

# DISCUSSION

Emerging evidences support the importance of white matter degeneration in AD. Several studies indicate that myelin and oligodendrocyte aberrations are associated with the characteristic increased Aβ peptide levels of AD (Dean et al., 2017; Roher et al., 2002). In human AD, OL alterations precede neuronal impairment, and the loss of OLs may lead to cognitive deficits (Behrendt et al., 2013; Zhan et al., 2014; Zhan et al., 2015). Moreover, thicker myelin and increased oligodendrogenesis caused by amyloidosis has been observed in adult mouse brain not long ago (Ferreira et al., 2020). However, the mechanisms by which OLs become dysfunctional and lead to AD pathology have remained unknown. In this study, we report that Aβ oligomers alters several aspects of oligodendrocytes biology.

## 1. Oligodendrocytes show alterations in energy and cholesterol metabolism

Several transcriptomic analyses have been done in AD patients in the last years (Grubman et al., 2019; Mathys et al., 2019; Morabito et al., 2021; Zhou et al., 2020). In all of them, oligodendrocytes showed alterations in several functions, including myelination, neural activity sensing and immune function (Murdock & Tsai, 2023). Spatial transcriptomic analyses (Chen et al., 2020) show that oligodendrocytes have a different transcriptomic response in plaque environment suggesting that soluble Aβ peptide alters the oligodendrocyte response in the disease. In agreement with these

analyses, we have shown that 24 h treatment with Aβ oligomers leads to altered oligodendrocyte transcriptome.

Interestingly, observed that one of the most upregulated pathways is associated with myelination like cholesterol metabolism and biosynthesis, hexose metabolism and one carbon metabolism. Myelin is composed mainly by lipids (cholesterol, phospholipids and glycolipids). Cholesterol is one of the most abundant lipids in myelin sheaths comprising the 26%. Of note, among the top risk genes for sporadic AD, *APOE, TREM2, APOJ, PICALM, ABCA1*, and *ABCA7* are all directly involved in lipid trafficking or metabolism and likewise, a key regulator of cholesterol metabolism, *SREBP2* is also genetically associated with altered AD risk (Yin, 2022). A recent studys described that ApoE, the strongest risk for AD, impairs myelination via cholesterol dysregulation in oligodendrocytes (Blanchard et al., 2022). Moreover, uncontrolled cholesterol synthesis in the brain is also associated with worsened AD-related phenotypes (Barbero-Camps, Fernandez, Martinez, Fernandez-Checa, & Colell, 2013). On the other side, hexoses are sources for glycans, which are involved in post-translational modifications particularly relevant in the development and function of the nervous system. In addition, MOG, an important protein of the myelin sheath is glycosylated. In that regard, it has been observed that AD patients present an abnormal glycan profile, (Haukedal & Freude, 2021).

In the same line, other pathway deregulated in Aβo-treated oligodendrocytes is related with energy metabolism. Beyond pathological hallmarks involving Aβ and tau, AD brains are characterized by metabolic abnormalities encompassing glucose hypometabolism, mitochondrial dysfunction, oxidative stress, and lipid dyshomeostasis (Yin, 2022). In fact, lipid-related abnormalities are among the initial neuropathological findings identified by Alois Alzheimer in 1907 (Alzheimer, Stelzmann, Schnitzlein, & Murtagh, 1995). OLs are a key cell type in the regulation of lipid homeostasis in the brain and have been shown to prefer glycolysis over oxidative phosphorylation in spite of their high energetic demands (Rone et al., 2016). Disruption in OL glycolysis due to mitochondrial dysfunction is thought to contribute to AD (Zhang et al., 2020). In this regard, it seems that Aβo favour fatty acid oxidation and downregulate oxidative phosphorylation and electron transport

chain. These data suggest a metabolic sshift towards β-oxidation that could be due to a dysfunction in the mitochondria. In fact, recent evidence indicates that mitochondria dysfunction increases β-oxidation in neurons (Audano et al., 2019). When comparing in vivo and in vitro results, we have observed contradictory results. In fact, in vitro we have detected a downregulation of oxidative phosphorylation in oligodendrocytes exposed to Aβo, while this pathway is increased in 3xTg-AD is compared to WT mice. These opposite results could be due to the time of exposure to Aβ oligomers in oligodendrocytes, given that in vivo it is chronic and in vitro it is more acute.

Altogether, these results suggest that myelination process is boosted with Aβo. At the same time, it appears that Aβo alter mitochondria, probably rendering them dysfunctional. Therefore, it is possible to hypothesise that cells needing a greater energy demand to cope with the newly established homeostasis (new energetic demands) might be switching to β-oxidation of fatty acids. These changes in energy metabolism could affect myelination and axon metabolic support.

## 2. Oligodendrocytes show alterations in hnRNP A2 and RNA metabolism

We have observed that mRNA metabolism is deregulated *in vitro* in cultured oligodendrocytes and *in vivo* in 3xTg-AD and AD patient´s brains. RNA-binding proteins interact with RNA by forming RBP complexes and regulating several aspects of RNA metabolism processes such as pre-mRNA splicing, transcription and translation regulation. In AD, RNA processing alterations arise due to changes in the expression, location, and relative abundance of the isoforms of the RBPs expressed, and/or by mutations in the sequence or expression of the genes they regulate (Rybak-Wolf & Plass, 2021). Impaired RNA processing in neurons of the AD brain have been reported before (Rybak-Wolf & Plass, 2021). Amongst the most abundant RBPs are the members of the heterogeneous nuclear ribonucleoproteins hnRNP A/B family, namely hnRNP A1 and A2/B1. HnRNPA2 plays a central role in pre-mRNA processing, transport and translation of important myelin proteins, including MBP and MOBP. In AD patients, hnRNP A2 is downregulated in the entorhinal cortex (Berson et al., 2012), but upregulated in the hippocampus of mild and severe AD cases (Mizukami et al., 2005), suggesting region

specific responses in AD pathology. Notably, hnRNP A2 depletion results in the production of a more active β-secretase (BACE1) isoform, thus promoting the accumulation of Aβ-plaques (Kolisnyk et al., 2017).

In our study, we observed that oligodendrocytes present intense hnRNP A2 immunoreactivity in hippocampal sections of control and AD-patients. When comparing the Braak stages, we observed increased levels of hnRNP A2 in oligodendrocytes in the hippocampus of mild AD cases that decrease to control levels in severe AD. We also measured hnRNP A2 levels in oligodendrocytes in the hippocampus of 6 and 18 months-old 3xTg-AD mice as well as in that of Aβo-injected mice.. Hippocampal hnRNP A2 expression was analysed in detail, revealing increased levels only in the CA3 and the dentate gyrus, while levels in the CA1 remained unchanged. These data suggest that Aβ-dependent A2 increase in oligodendrocytes is transient liekely due to compensatory mechanisms.

Although hnRNP A2 is believed to have numerous functions, its role in the CNS is poorly understood. The cytoplasmic roles of hnRNPA2 protein in AD are not characterized but understanding the hnRNP A2-regulated transcriptome and function is necessary for elucidating its role in AD. In this study, we demonstrated that hnRNP A2 is upregulated by Aβo in primary cultured oligodendrocytes. In addition, we described that its interactome changes with Aβo. In control conditions, we showed that hnRNP A2 regulate genes associated with RNA biology, involved in RNA metabolism, processing and splicing, ribonucleoprotein complex biogenesis and translation regulation. Nevertheless, Aβo weakened the interaction of more than half of the mRNAs. Reduced RNA binding by A2/B1 results in either production of alternatively spliced protein isoforms, or nonsense-mediated decay of mRNA with retained intronic sequences (Thibault et al., 2021). Therefore, it is likely to think that changes in the interactions of hnRNP A2 due to Aβo could have significant downstream effects on the cellular transcriptome and proteome.

HnRNP A2 plays a regulatory role in translation through their RNA binding activities. HnRNP A2 is known to bind to AU-rich elements (AREs), to either repress translation or

promote mRNA degradation, but A2 is also known as internal ribosomal entry site (IRES)-transactivating factors (ITAF) and binds to mRNA IRESes to facilitate cap-independent translation (Thibault et al., 2021). Thus, it is plausible that weaker A2-RNA binding leads to altered translation and mRNA processing, a possibility which is in line with our observations from RNA-seq analyses. Alternatively, another intriguing possibility is that hnRNP A2 binds to other RBPs in response to Aβo, changing changing the way they interact with RNAs.

We found that RNAs encoding proteins involved in metal ion binding has a higher interaction in Aβo-treated oligodendrocytes. Metal ions homeostasis is essential for maintaining normal brain functions. In AD patients, changes in the dynamic balance of metal ions in the brain are closely related to Aβ deposition and tau accumulation. Moreover, hnRNP A2 has been shown to modulate copper homeostasis (McCann, Hasan, Padilla-Benavides, Roy, & Lutsenko, 2022). Therefore, Aβo could be altering ion homeostasis in oligodendrocytes through hnRNP A2.

Of note, among the many targets of A2 is its own mRNA.(McGlincy et al., 2010). It has been already described that overexpression of hnRNP A2 resultes in down-regulation of Hnrnpa2 by nonsense-mediated mRNA decay (NMD), a key mechanism for regulating normal gene expression by clearing faulty transcripts. Interestingly, very recently it has been described that Tau induces deficits in NMD, impairing RNA processing in the brain and contributing to downstream neuronal loss (Zuniga et al., 2022). In our study, we showed that in oligodendrocytes exposed to Aβo have higher A2 protein and mRNA levels and that the interaction of hnRNP A2 with its own mRNA weakens, suggesting loss of self-regulation.

Evidence shows that brain-derived neurotrophic factor (BNDF) upregulates hnRNP A2 expression in neurons (Jung et al., 2020). Interestingly, in oligodendrocytes BNDF activates Fyn to promote myelination (Peckham et al., 2016) and coincidentally, Aβo also activates Fyn promoting oligodendrocyte differentiation (Quintela-Lopez et al., 2019). Hence, although it is not clear how Aβo upregulate hnRNP A2 in oligodendrocytes, we can present several possible modes of action: first, Aβo may activate the transcription of hnrnpa2 mRNA. The interaction between Aβo and ITGβ1 receptor activates Fyn kinase

triggering several signalling pathways leading to activation of transcription factors (Peckham et al., 2016). Second, as Aβo promotes MBP synthesis and there is a temporal correlation between the increase in cytoplasmic A2-positive granules when the level of Mbp mRNA is at its peak levels (Maggipinto et al., 2004), it is likely to think that oligodendrocytes upregulate hnRNP A2 to cope with the increase of Mbp mRNA. Third, it is possible that Aβo interferes in some way with NMD, decreasing its mRNA degradation and increasing stability.

Taken together, these data indicate that the gain of hnRNP A2 by Aβo could be ultimately leading to RNA metabolism impairment.

## 3. Aβ oligomers promote local translation of MBP and MOBP by modifying RNA granule dynamics

Local protein synthesis in myelin compartments is spatio-temporally regulated in response to neuronal stimulation and provides a reservoir pool for the myelin renew. The localization of *Mbp* and *Mobp* mRNA depends largely on its association with hnRNP A2 and the formation of RNA transport granules. We had previously shown that low concentrations of Aβo promote the synthesis of MBP (Quintela-Lopez et al., 2019). Fyn tirosine kinase is known to stimulate *Mbp* and *Mobp* transcription and local translation to mediate oligodendrocyte maturation (Krämer-Albers & White, 2011; Schäfer, Müller, Luhmann, & White, 2016; Umemori et al., 1999). Moreover, *in vitro* and in animal models, Fyn has been described to be a downstream target of Aβ (Boehm, 2013; Quintela-Lopez et al., 2019). Interestingly, Fyn phosphorylates the granule proteins hnRNP A2 and hnRNP F and stimulates the translation of *Mbp* and *Mobp* (Schafer, Muller, Luhmann, & White, 2016; White et al., 2008; White et al., 2012).

In the present study, we provide the first evidence suggesting that Aβo promotes local translation of *Mbp* and *Mobp* by altering mRNA granule number and dynamics, through hnRNP A2 regulation. Using immunocytochemistry techniques, we found a substantial increase in granule number containing hnRNP A2 and F, as well as active granules upon Aβ treatment. Moreover, by immunoprecipitation assays, we showed higher association

between hnRNP A2 and *Mbp* and *Mobp* mRNAs, in addition to higher hnRNP A2 phosphorylation.

We used a recently described technique, Puro-PLA (tom Dieck et al., 2015), to directly visualize newly synthesized MBP and MOBP proteins. It is worth mentioning that despite both proteins being locally produced in oligodendocyte´s peripheral processes in response to Aβ, *Mbp* and *Mobp* increased translation pattern is different: *Mbp* local translation is more intense in both in large and thin processes while MOBP synthesis mainly occurs in large oligodendroglia processes. This is consistent with the differential synthesis pattern of MBP and MOBP previously described (Montague et al., 1998). Interestingly, Fyn kinase can be detected mainly in larger processes and smaller veins passing through membrane sheaths (Osterhout, Wolven, Wolf, Resh, & Chao, 1999) allowing the assumption that these are the primary sites of *Mbp* and *Mobp* translation. Interestingly, our data specifically showed higher expression expression levels of MBP and MOBP and not of other proteins in response to Aβ.

Previous studies implicate different hnRNPs in the transport and translation of MBP and MOBP (Muller, Bauer, Schafer, & White, 2013; Schäfer et al., 2016). The interaction between hnRNP A2 and *Mbp* and *Mobp* mRNAs is crucial for the assembly of specific RNA granules and for the transport to the periphery of oligodendrocytes (Munro et al., 1999). We showed that Aβo increase cytoplasmic hnRNP A2. Previous studies suggest that overall level of hnRNP A2 increases in oligodendrocytes as they differentiate into MBP-positive cells, and that this augmentation is reflected primarily in the cytoplasmic pool of hnRNP A2 present in the form of granules (Maggipinto et al., 2004). In addition, we also observed an increased in granules containing hnRNP K. Exchange of hnRNP E1 for hnRNP K, has been suggested to be a prerequisite for the targeting of the mRNA to the myelin sheath, or for the recruitment of protein factors required for the initiation of translation (Torvund-Jensen, Steengaard, Reimer, Fihl, & Laursen, 2014). Thus, having more granules containing hnRNP K would suggest that more granules are approaching its final destination and thus, translating.

Taken together, these data indicate that Aβo alters local protein synthesis by altering RNA granule composition and dynamics though Fyn mediated pathways. Specifically,

Fyn kinase activated by Aβ oligomers would induce *Mbp* and *Mobp* mRNA local translation by phosphorylating hnRNP A2, in every compartment where mRNA granules are present. At the same time, it would also induce *Hnrnpa2*, *Mpb* and *Mobp* transcription.

## 4. MBP and MOBP are upregulated in adult triple transgenic mice

Alzheimer's disease is a multifactorial neurodegenerative disorder with several target proteins contributing to its aetiology. Several animal models have been used to mimic AD disorder and to gain insight into its pathological features. Nonetheless, none of them have been able to recapitulate all the hallmarks. The 3xTg-AD mice have brought a great advance in AD research since they develop both amyloid plaques and neurofibrillary tangles in patterns and brain regions reminiscent of human AD. In turn, this model acquires extracellular Aβ deposits prior to tangle formation, which is consistent with the amyloid cascade hypothesis.

Our previous data showed an upregulation of MBP in the corpus callosum and the hippocampus in 12 and 18-month 3×Tg-AD mice without any significant differences in axonal damage (Quintela-Lopez, 2018). In the present report, we analysed the expression of mature oligodendrocytes markers (MOG, MBP and MOBP) in the hippocampus of 6-month 3xTg-AD mice, as it is one of the first affected areas in the diseased brain. Here, we show a marked increase in MBP and MOBP expression, with goes in accordance with our *in vitro* findings. Similarly, a study demonstrated MBP upregulation in the hippocampus of 2-month-old APP/PS1 transgenic mice (Wu et al., 2017). In addition, we have also observed and increased in MBP expression in myelin-enriched fractions of 6-month-old 3xTg-AD mice. Interestingly, MBP production is suggested to modulate WM plasticity in response to learning-induced neuronal activity by regulating the myelin sheath thickness (Martini & Schachner, 1997). Our data indicate that upregulation of MBP and MOBP occurs in 3xTg-AD in early stages of the pathology, preceding axonal damage and likely being associated to primary white matter changes related with AD.

Hypothetically, these changes in myelin proteins are precededby AD-related pathophysiological mechanisms. However, it is possible that a compensatory response to brain damage is also occurring. In this mouse model, demyelination in specific areas such as the hippocampus and the entorhinal cortex has been observed in 6-month-old 3xTg-AD mice (Desai et al., 2009; Vanzulli et al., 2020). Although, we cannot completely rule out this hypothesis, strong evidence point out that changes in the oligodendroglial lineage observed in AD mice may be caused by the activity of Aβ peptide.

In this regard, white matter abnormalities have been reported in the 3xTg-AD and APP/PS1 transgenic mice correlating with elevated levels of intracellular Aβ prior to the manifestation of plaque and tangle pathology (Desai et al., 2010; Wirths et al., 2006). Accordingly, we had previously reported a positive correlation between MBP upregulation and Aβ levels in the hippocampus of 18-month-old transgenic mice (Quintela-Lopez, 2018). In addition, we detected alterations in MBP and MOBP synthesis at a time point when high amounts of Aβ oligomers and few amyloid plaques are reported, and no signs of concomitant Tau pathology is observed (Oddo et al., 2006). More interestingly, Desai and coworkers described elevated CC1+ mature cells in the hippocampus of 3xTg-AD, which were reduced by injection with an anti-$A\beta_{1-42}$ engineered intrabody, indicating a direct effect of Aβ in oligodendrocyte survival or differentiation (Desai et al., 2010). Moreover, very recently, elevated newly synthesized myelin in APP/PS1 mice has been shown (Chen et al., 2021), suggesting that oligodendrocytes respond to Aβ by synthesizing more myelin proteins, which could be a protective mechanism. Overall, these results indicate that impaired oligodendrocyte differentiation observed in the triple transgenic mouse model is mainly triggered by Aβ oligomers.

Triple transgenic mice harbour three mutations: human mutated Tau (htaup301L), human amyloid precursor protein with Swedish mutation (hAPPSwe) and human mutated presenilin-1 (hPS1M146V). hAPPSwe and htaup301L mutant transgenes are expressed exclusively in neurons, while hPS1M146V can be ubiquitously expressed, including in oligodendrocytes. PS1 is the catalytic component of γ-secretase complex, mainly known for its role in the amyloidogenic processing of APP (Scheuner et al., 1996).

Previous studies have also described that γ- secretase is involved in oligodendrocyte maturation but contradictory results have been reported in oligodendrocyte primary cells and in co-cultures with neurons (Lai and Feng, 2004; Watkins et al., 2008). In addition, this familial AD mutation has been shown to increase oligodendrocyte vulnerability to several insults associated with AD, including Aβ (Pak et al., 2003; Desai et al., 2011). In this regard, our results are in accordance with observations in the oligodendrocyte lineage in APP/PS1 mice (Behrendt et al., 2013; Wu et al., 2017), a mouse model of AD in which both mutations are exclusively expressed in neurons, which helps to exclude direct effects of the PS1 mutations in oligodendrocytes. In conclusion, evidence suggests that Aβ-related insults impact oligodendrocytes independently from of PS1 mutant expression, although PS1 mutation may exacerbate Aβ effects.

## 5. MBP upregulation inhibit calcium influx in cells and promote translation

It has been reported that MBP upregulation inhibits VGCCs, decreasing the calcium influx into oligodendrocytes (Smith et al., 2011). The influx of $Ca^{2+}$ through membrane channels is a crucial step in signal transduction pathways involved in regulating growth, maturation, and functional plasticity. Additionally, increased intracellular calcium levels stimulate MBP synthesis in oligodendrocytes (Friess et al., 2016). Here, we demonstrate that Aβo inhibit the calcium influx into the cell, which is partially recovered by siRNA-mediated MBP downregulation. In addition, we have also shown that Aβo inhibit calcium entry into oligodendrocytes in hippocampal organotypic cultures. Since calcium entry stimulates MBP synthesis (Friess et al., 2016) and MBP in turn inhibits calcium entry, our results could suggest a self-regulatory mechanism in which MBP inhibits VGCCs to regulate its own synthesis. The accumulation of MBP in the membrane would inhibit or decrease the number of VGCC in the membrane as reported before (Smith et al., 2011), thereby affecting to the calcium entry through these channels.

Nevertheless, as we do not see a complete recovery of calcium upon MBP downregulation, we can conclude that Aβo might inhibit calcium entry by additional mechanisms. As previously described (Quintela-Lopez et al., 2019), Aβo increase the basal levels of $Ca^{2+}$ in oligodendrocytes via ryanodine receptors located in endoplasmic

reticulum. Thus, it is possible that Aβo initially facilitate calcium entry from intracellular pools via ryanodine receptors resulting in a rise in cytosolic calcium levels. Increased intracellular $Ca^{2+}$ levels may affect oligodendrocytes excitability to extracellular responses. These results are in line with a study showing that brains of AD mouse models chronically exposed to Aβ oligomers and fibrils, have increased resting calcium levels due to a concomitant dysregulation of extracellular calcium entry and intracellular calcium buffering systems (Kuchibhotla et al., 2008). Therefore, as we have observed an increase of MBP in the hippocampus of 3xTg-AD mice, it is likely to think that calcium homeostasis could also be affected *in vivo* by the aberrant accumulation of MBP by inhibiting VGCCs. Altogether, we have observed that Aβ peptide destabilizes $Ca^{2+}$ homeostasis and may make oligodendrocytes less vulnerable to environmental stimuli that elevate intracellular $Ca^{2+}$ levels.

Aberrant protein accumulation is a unifying feature of neurodegenerative disorders that can be explained by increased protein synthesis, increased protein stability or decreased degradation. Because we had already observed that Aβo lead to increased MBP and MOPB synthesis we wondered if Aβ could have a global effect in this process.. We analysed *de novo* protein synthesis in cultured oligodendrocytes in response to Aβo. To directly monitor protein synthesis, we used the SUnSET assay (Schmidt, Clavarino, Ceppi, & Pierre, 2009), which utilises incorporation of puromycin to directly reflect the rate of mRNA translation *in vitro*. Previous studies have provided circumstantial evidence that micromolar (subtoxic) doses of $A\beta_{1\text{-}42}$ enhance protein translation in neurons (Gamarra, Blanco-Urrejola, Batista, Imaz, & Baleriola, 2020; Ghosh et al., 2020; Li & Gotz, 2017; Schmidt et al., 2009; Westmark et al., 2011). In this regard, we demonstrated that Aβo increase global protein synthesis by a pathway involving MBP. Interestingly, MBP interacts with core proteins of the 40S and 60S ribosome subunits (Smirnova et al., 2021) and thus MBP itself could regulate translation. Hence, it could be possible that MBP acts as an anchor for the two subunits, thereby promoting translation. In fact, our results revealed a significant increase of global proteins synthesis Aβo-treated cells, that it is lost when MBP is silenced. In addition, we also showed a significant increase in protein synthesis in oligodendrocytes from 3xTg-AD mice hippocampus acute slices where we previously showed a MBP upregulation as well.

## 6. Aβ oligomers alter oligodendrocyte cytoskeleton through reorganization of actin cytoskeleton

The actin cytoskeleton is critical to maintain cell morphology and multiple cellular processes, including differentiation and myelination (Brown & Macklin, 2019). During the development of the CNS, OPCs are responsible for extending a network of processes to contact axons and initiate myelination. In this action, the dynamics of the cytoskeleton is vital, and any alteration in both the formation and repair of myelin generates neurodegenerative diseases such as AD. In addition, Hirano bodies, intracellular inclusions containing actin and actin binding proteins, are a prominent feature of the AD brain (Mitake, Ojika, & Hirano, 1997).

In this work, we show that oligodendrocytes change their actin dynamics in response to Aβo. Specifically, we have focused on cofilin, a essential actin reguatory protein that accelerates actin assembly dynamics. Interestingly, we demonstrate that acute Aβo treatment induces cofilin phosphorylation and increases F-actin levels. Similarly, studies performed in Aβo-treated primary neurons demonstrated that activation of Rac1 and Cdc42, downstream targets of Fyn that induce actin polymerization, (Mendoza-Naranjo, Gonzalez-Billault, & Maccioni, 2007), and phosphorylation of cofilin (Rush et al., 2018), leads to an increase in the concentration of F-actin. Interestingly, MBP binds to F-actin in a 1:1 ratio and induces the formation of ordered bundles of F-actin filaments (Bary ko & Dobrowolski, 1984). Our work shows that the rate of actin polymerisation significantly increases in response to Aβo in cultured oligodendrocytes at 3 DIV and not at 2 DIV. This may be because the cells are not yet sufficiently differentiated and do not express MBP in sufficient quantities to release the F-actin depolymerising proteins.

From this, several hypotheses can be generated about the mechanisms involved in actin polymerisation in oligodendrocytes in AD. We suggest the following scenario: stimulation of oligodendrocytes with Aβo induces the activation of Rac1, as previously described (Manterola et al., 2013; Mendoza-Naranjo et al., 2007) possibly through the Fyn pathway activation (Quintela-Lopez et al., 2019), which leads to a transient increase

in the level of P-cofilin and F-actin assembly. In later stages, upregulated MBP would compete with actin depolymerising proteins (gelsolin and cofilin) for the binding to the membrane lipid PI(4,5)P2 (Zuchero et al., 2015). Therefore, Aβo-mediated MBP increased could cause a higher release of these depolymerising proteins, increasing the polymerisation and, consequently, increasing the dynamics of the process. As a whole we can conclude that Aβo enhance actin dynamics, increase F-actin and promote the branching, ultimately governing oligodendrocyte morphology.

F-actin localizes to the leading edge of oligodendrocytes during myelin wrapping, leading to the expansion of the cytoplasm that protrudes underneath previous myelin wraps and between those wraps and the axon, driving membrane formation around the axon. F-actin is immediately depolymerized, allowing for myelin compaction behind the leading edge. In RNA-seq analysis we identified mRNAs encoding for proteins involved in actin-related pathways as altered upon Aβ treatments. Additionally, we have reported altered increased myelin thickness in the corpus callosum of 6-, 12- and 18-month-old 3xTg-AD mice (Quintela-Lopez, 2018) and in the hippocampus of 6-months-old 3xTg-AD . Importantly, amyloidosis has been associated with thicker myelin (Ferreira et al., 2020). Therefore, a possible mechanism explaining thicker myelin could be due to an increase of polymerizing forces of F-actin pushing out membrane protrusions that squeeze in between the axon and the myelin sheath, together with the subsequent disassembly of F-actin by more MBP enabling it to locally activate actin disassembly at sites of MBP compaction to drive myelin wrapping. Nevertheless, we previously observed that the hypermyelinated fibres conduct less efficient, suggesting that it could be detrimental for axon conduction. Thus, the mechanism describe could be a defence mechanism that in time it gets detrimental for the neuron.

Overall, we demonstrate that Aβo changes oligodendrocyte morphology by altering the actin cytoskeleton in oligodendrocytes. Our current results provide important molecular links between Aβ and actin dynamics, which can potentially lead to myelin dysfunctions in Alzheimer's disease.

## 7. Aβ oligomers enhance myelination *in vivo*

Increasing evidence suggests that damage to myelin may be an important component of AD and myelin impairments have been suggested to lead to neuronal dysfunction and cognitive decline. Nevertheless, is undefined if Aβo can modulate myelination *in vivo*. In recent years, zebrafish have become well established for the study of oligodendrocyte biology and myelination *in vivo*.

Therefore, we analysed the effect of Aβo in myelination using zebrafish. In this study, we demonstrated Aβo increase number of sheaths per oligodendrocyte. Notably, we identified *Mbp* transcript to be accumulated in the dorsal region of the spinal cord, suggesting that Aβo promotes the migration of oligodendrocytes. Moreover, we show that *Myrf,* a key transcription factor of myelin proteins*,* is downregulated in Aβo-injected zebrafish. Importantly, as the oligodendrocytes mature, they lost them transcriptional activity suggesting Aβo could be promoting differentiation of oligodendrocytes. In this regard, we have also see a global increase of *Plp1*, one of the most abundant proteins in the myelin from the CNS. Accordingly, we showed an increase of myelinated axons in dorsal area of the spinal cord in addition to thicker myelin of Mauthner cell. Mauthner cells are a pair of resticulospinal neurons involved in fish escape behaviours that are essential for survival. Previous data suggested that Aβo-injected zebrafish avoided the aversive stimulus less effectively than animals injected with vehicle (Nery et al., 2014). Therefore, the aberrant hypermyelination observed in Aβo-injected zebrafish could cause the behaviour observed. Overall, these results strongly suggest that Aβo is able to alter myelination *in vivo*.

## 9. Aβ oligomers promote extracellular vesicle release in oligodendrocytes with functional consequences in neurons

Similar to neurons, oligodendrocytes are able to secrete extracellular vesicles triggered by neuronal activity. Oligodendrocytes EVs contained myelin proteins like PLP, CNP and MBP (Krämer-Albers et al., 2007). Neurons endocytose these vesicles conferring neuroprotection and improving neuronal homeostasis (Kramer-Albers, 2020). In

addition, it can also have an autocrine/paracrine effect by modulating morphological differentiation of oligodendrocytes and myelin formation (Bakhti, Winter, & Simons, 2011). With the ability of EV to transport cargo packaged by the originating cell, their role in the pathogenesis of neurological conditions, particularly neurodegenerative diseases associated with misfolded proteins, has become a growing area of interest. However, no study has so far investigated if Aβo treated oligodendrocyte EVsEVs can have an impact in the disease start and propagation.

Therefore, we set out to investigate whether Aβo could alter EVs release and whether these EVs could potentially affect neuron functions. Our analysis revealed that Aβo increment the release of EVs and besides, these vesicles contain more MBP. Then we wonder whether oligodendrocytes derived-EVs could affect neurons. Previous results suggest that Aβo-treated astrocyte derived-EVs increase protein synthesis in neurites (Gamarra et al., 2021). Likewise, we observed that EVs derived form Aβo-treated oligodendrocytes increased translation in the soma of neurons. This is no new since previously it has been shown that oligodendroglial EVsEVs alter neuronal gene expression (Frohlich et al., 2014). Through horizontally transferring proteins, lipids, and nucleic acids, EVs can modulate synaptic activities rapidly by controlling neurotransmitter release or progressively by regulating neural plasticity including synapse formation. Therefore, we next analysed the effect of oligodendrocyte-derived EVs in synapsis. Our analysis revealed no significant changes in postsynaptic marker, homer, but significant increase in presynaptic marker synaptophysin only in control oligodendrocyte-derived EVs. Loss of presynaptic proteins is thought to be one of the earliest (and most clinically relevant) changes in human AD with some reports indicating it precedes extensive postsynaptic changes. Moreover, overexpression of synaptophysin has been observed to enhance neurotransmitter secretion (Alder, Kanki, Valtorta, Greengard, & Poo, 1995). Therefore, these results could indicate that oligodendrocytes enhance the neurotransmitter release altering neuron response.

As we show that OL derived-EVs could affect neurotransmitter secretion, we next sought to determine if they could enhance exocytosis as a way to respond to oligodendrocytes. We observed a significant accumulation of Bodipy-ceramide after incubation in clean

medium and Aβ-OL derived EVs but a decrease in control-OL derived EVs, suggesting that oligodendrocytes enhance exocytosis in physiological conditions likely as a mean of reciprocal communication. Bodipy-Ceramide is accumulated in Golgi vesicle network and interestingly, $A\beta_{1-42}$ is made in the trans-golgi network and packaged into secretory vesicles. Hence, since we show changes in accumulation of Bodipy-ceramide we wonder if oligodendrocytes could trigger the secretion of $A\beta_{1-42}$. In opposition to what we expected, we noticed that both control and Aβo-treated OL derived EVs significantly stimulated $A\beta_{1-42}$ secretion to the extracellular space. The finding that oligodendroglial EVs influence Aβo secretion provides mechanistic insight into how oligodendrocyte EVs can contribute to Aβ plaque burden.

Altogether, these results suggest that Aβo-treated and control oligodendrocyte derived EVs impact in translation, synapsis and Aβ secretion. It would be interesting to study how oligodendrocyte EVs affect the aforementioned functions.

## 10. Concluding remarks

Overall, the data reported in this Thesis provide broader knowledge about the effect of Aβo in oligodendrocyte´s functions. We have described MBP as a possible hub regulating physiological functions of oligodendrocytes and how this can be exacerbated in AD. Our data suggest that Aβ may be mimicking laminin-1 receptor located in the axon (by binding to ITGβ1 as described previously, Quintela-López et al., 2019), thereby promoting myelination and possibly causing a shift in the oligodendroglial lineage to more mature oligodendrocytes and changes in morphology **(Figure 44)**. Such a maturational change could reduce the number of OPCs, as seen before in AD models (Chacon de la Rocha et al., 2020; Vanzulli et al., 2020), leading to a loss of source of mature oligodendrocytes. However, the functions of OPCs are not limited to oligodendrogenesis, since very recently, a role of oligonendrocytes in synapse engulfment during circuit during circuit remodeling in mice has been reported (Auguste et al., 2022). Furthermore, recent studies from our laboratory corroborate this hypothesis, as we showed in 3xTg-AD mice and Wt animals that received Aβ injections show a higher population of mature oligodendrocytes and consequently a lower

population of immature oligodendrocytes (Balantzategi et al., 2021). Therefore, one might speculate that these changes in lineage dynamics might leave the brain with less manoeuvrability to respond to demyelination together with a loss of functions of OPCs with consequences in brain homeostasis.

This multidisciplinary study highlights an underappreciated involvement of oligodendrocyte lineage cells in the pathophysiology of AD and suggests that targeting the signalling pathways activated by Aβ in oligodendrocyte and myelin might be a therapeutic strategy to ameliorate memory performance in the early stages of AD and prevent, or at least slow down, the neurodegenerative process that progressively takes place during AD progression.

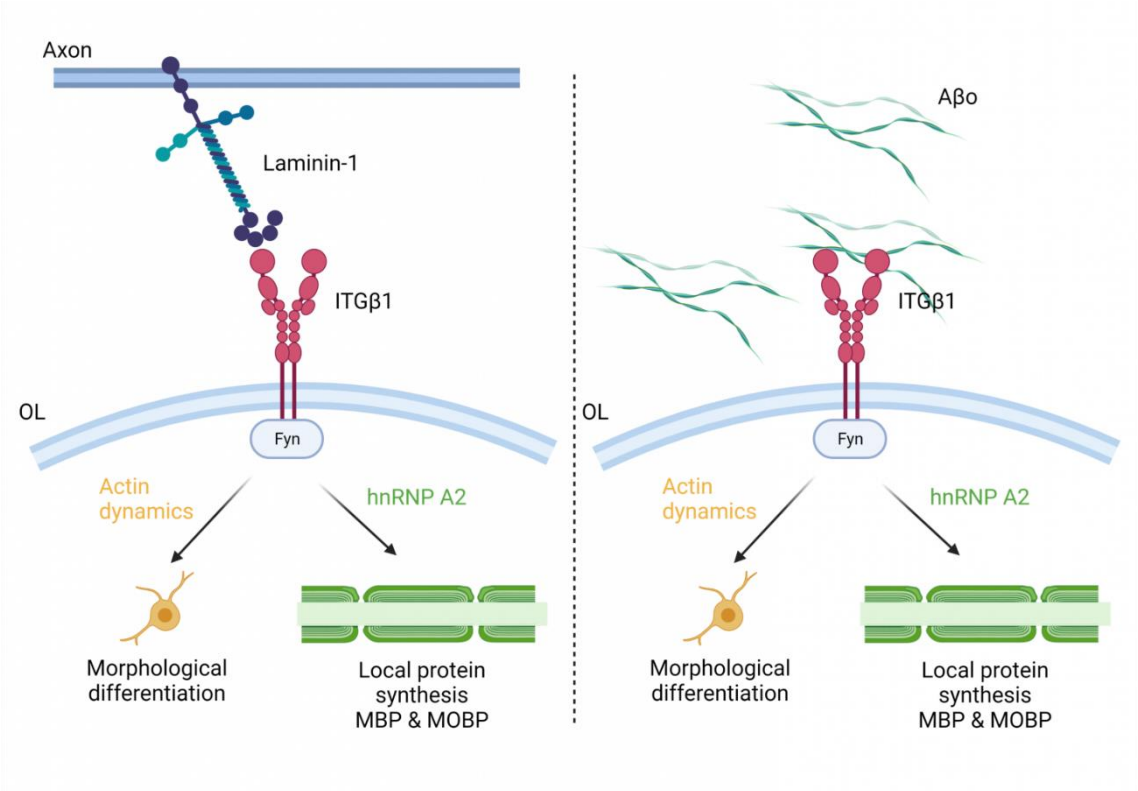


***Figure 44. Aβ-signalling pathway underlying local protein synthesis and morphological differentiation.*** *Model diagram showing in the left part the one activated by neurons and in the right part the one activated by Aβo.*

# CONCLUSIONS

1. Amyloid β oligomers promote changes in RNA metabolism by likely deregulating RNA-binding proteins.
2. AD patients show increase expression of hnRNP A2 in oligodendrocytes at early stages.
3. Amyloid β oligomers upregulate hnRNP A2 granule component and alter its interactome.
4. Amyloid β oligomers induce MBP and MOBP local translation by modulating their mRNA granule number and dynamics.
5. MBP upregulation inhibits calcium influx into cell and promotes protein translation.
6. Amyloid β oligomers alters myelination and maturation of oligodendrocytes in zebrafish.
7. Amyloid β oligomers alters actin dynamics promoting their arborisation.
8. Amyloid β oligomers enhance extracellular vesicle secretion with consequences in neuron functions.

Altogether, the results included in this doctoral thesis suggest that amyloid β oligomers can alter transcriptomics and proteomics in oligodendrocytes and therefore modulate important oligodendroglial functions, like RNA metabolism, protein translation and calcium homeostasis. These multi effects can contribute to the disease onset and progression of AD pathology.

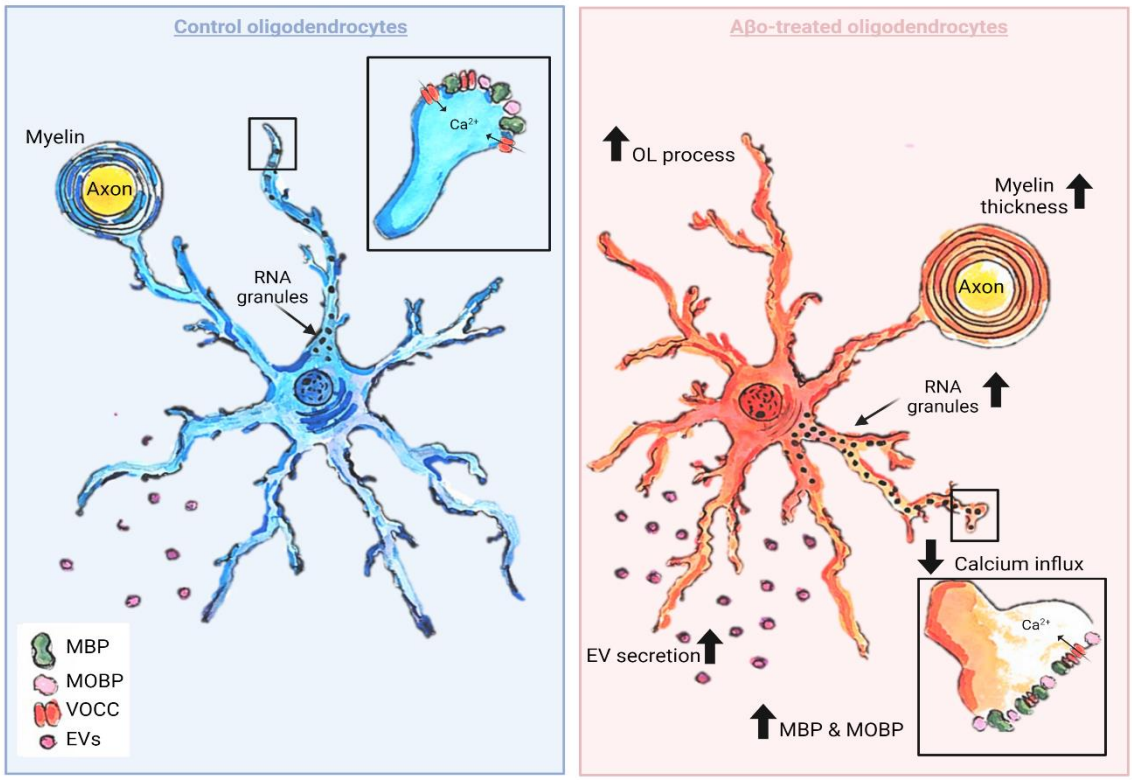


**Figure 43.** Scheme showing effect of soluble Aβ oligomers in oligodendrocytes.

# REFERENCES


Aber, E. R., Griffey, C. J., Davies, T., Li, A. M., Yang, Y. J., Croce, K. R., et al. (2022). Oligodendroglial macroautophagy is essential for myelin sheath turnover to prevent neurodegeneration and death. Cell Reports, 41(3), 111480. doi:S2211-1247(22)01330-4

Afshari, F. S., Chu, A. K., & Sato-Bigbee, C. (2001). Effect of cyclic AMP on the expression of myelin basic protein species and myelin proteolipid protein in committed oligodendrocytes: Differential involvement of the transcription factor CREB. Journal of Neuroscience Research, 66(1), 37-45. doi:10.1002/jnr.1195

Ainger, K., Avossa, D., Morgan, F., Hill, S. J., Barry, C., Barbarese, E., et al. (1993). Transport and localization of exogenous myelin basic protein mRNA microinjected into oligodendrocytes. The Journal of Cell Biology, 123(2), 431-441. doi:94012987 [pii]

Alder, J., Kanki, H., Valtorta, F., Greengard, P., & Poo, M. M. (1995). Overexpression of synaptophysin enhances neurotransmitter secretion at xenopus neuromuscular synapses. The Journal of Neuroscience, 15(1), 511-519. doi:10.1523/JNEUROSCI.15-01-00511.1995

Almeida, R. G. (2018). The rules of attraction in central nervous system myelination. Frontiers in Cellular Neuroscience, 12, 367. doi:10.3389/fncel.2018.00367 [doi]

Alzheimer, A., Stelzmann, R. A., Schnitzlein, H. N., & Murtagh, F. R. (1995). An english translation of alzheimer's 1907 paper, "uber eine eigenartige erkankung der hirnrinde". Clinical Anatomy (New York, N.Y.), 8(6), 429-431. doi:10.1002/ca.980080612

Amata, I., Maffei, M., & Pons, M. (2014). Phosphorylation of unique domains of src family kinases. Frontiers in Genetics, 5, 181. doi:10.3389/fgene.2014.00181 [doi]

Anders, S., Pyl, P. T., & Huber, W. (2015). HTSeq--a python framework to work with high-throughput sequencing data. Bioinformatics (Oxford, England), 31(2), 166-169. doi:10.1093/bioinformatics/btu638

Audano, M., Pedretti, S., Crestani, M., Caruso, D., De Fabiani, E., & Mitro, N. (2019). Mitochondrial dysfunction increases fatty acid beta-oxidation and translates into

impaired neuroblast maturation. FEBS Letters, 593(22), 3173-3189. doi:10.1002/1873-3468.13584

Bakhti, M., Aggarwal, S., & Simons, M. (2014). Myelin architecture: Zippering membranes tightly together. Cellular and Molecular Life Sciences: CMLS, 71(7), 1265-1277. doi:10.1007/s00018-013-1492-0

Bakhti, M., Winter, C., & Simons, M. (2011). Inhibition of myelin membrane sheath formation by oligodendrocyte-derived exosome-like vesicles. The Journal of Biological Chemistry, 286(1), 787-796. doi:10.1074/jbc.M110.190009

Balantzategi, U., Quintela-Lopez, T., Gaminde-Blasco, A., Hernandez, N., Zugaza, J. L., Matute, C., Ruiz, A., Alberdi, E. (2021). The role of Aβ oligomers in the myelin regulatory factor MYRF regulation and oligodendrocyte differentiation. Glia, meeting abstract.

Balderrama-Gutierrez, G., Liang, H., Rezaie, N., Carvalho, K., Forner, S., Matheos, D., Rebboah, E., Green, K.N., Tenner, A.J., LaFerla, F., & Mortazavi, A. Single-cell and nucleus RNA-seq in a mouse model of AD reveal activation of distinct glial subpopulations in the presence of plaques and tangles. (2021). bioRxiv. doi: 10.1101/2021.09.29.462436

Bamburg, J. R. (1999). Proteins of the ADF/cofilin family: Essential regulators of actin dynamics. Annual Review of Cell and Developmental Biology, 15, 185-230. doi:10.1146/annurev.cellbio.15.1.185

Banker, G., & Goslin, K. (1988). Developments in neuronal cell culture. Nature, 336(6195), 185-186. doi:10.1038/336185a0 [doi]

Barbero-Camps, E., Fernandez, A., Martinez, L., Fernandez-Checa, J. C., & Colell, A. (2013). APP/PS1 mice overexpressing SREBP-2 exhibit combined abeta accumulation and tau pathology underlying Alzheimer's disease. Human Molecular Genetics, 22(17), 3460-3476. doi:10.1093/hmg/ddt201

Bartzokis, G. (2011). Alzheimer's disease as homeostatic responses to age-related myelin breakdown. Neurobiology of Aging, 32(8), 1341-1371. doi:10.1016/j.neurobiolaging.2009.08.007

Bartzokis, G., Cummings, J. L., Sultzer, D., Henderson, V. W., Nuechterlein, K. H., & Mintz, J. (2003). White matter structural integrity in healthy aging adults and patients with Alzheimer disease: A magnetic resonance imaging study. Archives of Neurology, 60(3), 393-398. doi:10.1001/archneur.60.3.393

Bartzokis, G., Lu, P. H., Geschwind, D. H., Edwards, N., Mintz, J., & Cummings, J. L. (2006). Apolipoprotein E genotype and age-related myelin breakdown in healthy individuals: Implications for cognitive decline and dementia. Archives of General Psychiatry, 63(1), 63-72. doi:10.1001/archpsyc.63.1.63

Bartzokis, G., Lu, P. H., Geschwind, D. H., Tingus, K., Huang, D., Mendez, M. F., et al. (2007). Apolipoprotein E affects both myelin breakdown and cognition: Implications for age-related trajectories of decline into dementia. Biological Psychiatry, 62(12), 1380-1387. doi:10.1016/j.biopsych.2007.03.024

Baryko, B., & Dobrowolski, Z. (1984). Ca2+-calmodulin-dependent regulation of F-actin-myelin basic protein interaction. European Journal of Cell Biology, 35(2), 327-335.

Bauer, N. M., Moos, C., van Horssen, J., Witte, M., van der Valk, P., Altenhein, B., et al. (2012). Myelin basic protein synthesis is regulated by small non-coding RNA 715. EMBO Reports, 13(9), 827-834. doi:10.1038/embor.2012.97

Baumann, N., & Pham-Dinh, D. (2001). Biology of oligodendrocyte and myelin in the mammalian central nervous system. Physiological Reviews, 81(2), 871-927. doi:10.1152/physrev.2001.81.2.871

Bechler, M. E., Byrne, L., & Ffrench-Constant, C. (2015). CNS myelin sheath lengths are an intrinsic property of oligodendrocytes. Current Biology: CB, 25(18), 2411-2416. doi:S0960-9822(15)00890-8

Behar, L., Marx, R., Sadot, E., Barg, J., & Ginzburg, I. (1995). Cis-acting signals and trans-acting proteins are involved in tau mRNA targeting into neurites of differentiating neuronal cells. International Journal of Developmental Neuroscience: The Official Journal of the International Society for Developmental Neuroscience, 13(2), 113-127. doi:10.1016/0736-5748(95)00001-w

Behrendt, G., Baer, K., Buffo, A., Curtis, M. A., Faull, R. L., Rees, M. I., et al. (2013). Dynamic changes in myelin aberrations and oligodendrocyte generation in chronic amyloidosis in mice and men. Glia, 61(2), 273-286. doi:10.1002/glia.22432

Bernstein, B. W., & Bamburg, J. R. (2010). ADF/cofilin: A functional node in cell biology. Trends in Cell Biology, 20(4), 187-195. doi:10.1016/j.tcb.2010.01.001

Berson, A., Barbash, S., Shaltiel, G., Goll, Y., Hanin, G., Greenberg, D. S., et al. (2012). Cholinergic-associated loss of hnRNP-A/B in Alzheimer's disease impairs cortical splicing and cognitive function in mice. EMBO Molecular Medicine, 4(8), 730-742. doi:10.1002/emmm.201100995

Blanchard, J. W., Akay, L. A., Davila-Velderrain, J., von Maydell, D., Mathys, H., Davidson, S. M., et al. (2022). APOE4 impairs myelination via cholesterol dysregulation in oligodendrocytes. Nature, 611(7937), 769-779. doi:10.1038/s41586-022-05439-w

Boehm, J. (2013). A 'danse macabre': Tau and fyn in STEP with amyloid beta to facilitate induction of synaptic depression and excitotoxicity. The European Journal of Neuroscience, 37(12), 1925-1930. doi:10.1111/ejn.12251

Boggs, J. M. (2006). Myelin basic protein: A multifunctional protein. Cellular and Molecular Life Sciences: CMLS, 63(17), 1945-1961. doi:10.1007/s00018-006-6094-7

Borit, A., & McIntosh, G. C. (1981). Myelin basic protein and glial fibrillary acidic protein in human fetal brain. Neuropathology and Applied Neurobiology, 7(4), 279-287. doi:10.1111/j.1365-2990.1981.tb00099.x

Braak, H., & Braak, E. (1995). Staging of Alzheimer's disease-related neurofibrillary changes. Neurobiology of Aging, 16(3), 271-284. doi:10.1016/0197-4580(95)00021-6

Brown, T. L., & Macklin, W. B. (2019). The actin cytoskeleton in myelinating cells. Neurochemical Research, 10.1007/s11064-0. doi:10.1007/s11064-019-02753-0

Canedo-Antelo, M., Serrano, M. P., Manterola, A., Ruiz, A., Llavero, F., Mato, S., et al. (2018). Inhibition of casein kinase 2 protects oligodendrocytes from excitotoxicity by attenuating JNK/p53 signalling cascade. Frontiers in Molecular Neuroscience, 11, 333. doi:10.3389/fnmol.2018.00333

Carson, J. H., Worboys, K., Ainger, K., & Barbarese, E. (1997). Translocation of myelin basic protein mRNA in oligodendrocytes requires microtubules and kinesin. Cell Motility and the Cytoskeleton, 38(4), 318-328. doi:10.1002/(SICI)1097-0169

Chacon-De-La-Rocha, I., Fryatt, G., Rivera, A. D., Verkhratsky, A., Raineteau, O., Gomez-Nicola, D., et al. (2020). Accelerated dystrophy and decay of oligodendrocyte precursor cells in the APP/PS1 model of Alzheimer's-like pathology. Frontiers in Cellular Neuroscience, 14, 575082. doi:10.3389/fncel.2020.575082

Chamberlain, K. A., Huang, N., Xie, Y., LiCausi, F., Li, S., Li, Y., et al. (2021). Oligodendrocytes enhance axonal energy metabolism by deacetylation of mitochondrial proteins through transcellular delivery of SIRT2. Neuron, 109(21), 3456-3472.e8. doi:10.1016/j.neuron.2021.08.011

Chen, J., Liu, K., Hu, B., Li, R., Xin, W., Chen, H., et al. (2021). Enhancing myelin renewal reverses cognitive dysfunction in a murine model of Alzheimer's disease. Neuron, 109(14), 2292-2307.e5. doi:10.1016/j.neuron.2021.05.012

Chen, W., Lu, A., Craessaerts, K., Pavie, B., Sala Frigerio, C., Corthout, N., et al. (2020). Spatial transcriptomics and in situ sequencing to study Alzheimer's disease. Cell, 182(4), 976-991.e19. doi:10.1016/j.cell.2020.06.038

Chen, Y., Balasubramaniyan, V., Peng, J., Hurlock, E. C., Tallquist, M., Li, J., et al. (2007). Isolation and culture of rat and mouse oligodendrocyte precursor cells. Nature Protocols, 2(5), 1044-1051. doi:10.1038/nprot.2007.149

Chia, L. S., Thompson, J. E., & Moscarello, M. A. (1984). X-ray diffraction evidence for myelin disorder in brain from humans with Alzheimer's disease. Biochimica Et Biophysica Acta, 775(3), 308-312. doi:0005-2736(84)90185-8

Colman, D. R., Kreibich, G., Frey, A. B., & Sabatini, D. D. (1982). Synthesis and incorporation of myelin polypeptides into CNS myelin. The Journal of Cell Biology, 95(2 Pt 1), 598-608. doi:10.1083/jcb.95.2.598

Crotty, P., Sangrey, T., & Levy, W. B. (2006). Metabolic energy cost of action potential velocity. Journal of Neurophysiology, 96(3), 1237-1246. doi:10.1152/jn.01204.2005

Czopka, T., Ffrench-Constant, C., & Lyons, D. A. (2013). Individual oligodendrocytes have only a few hours in which to generate new myelin sheaths in vivo. Developmental Cell, 25(6), 599-609. doi:S1534-5807(13)00287-6

Dahlgren, K. N., Manelli, A. M., Stine, W. B., Baker, L. K., Krafft, G. A., & LaDu, M. J. (2002). Oligomeric and fibrillar species of amyloid-beta peptides differentially affect neuronal viability. The Journal of Biological Chemistry, 277(35), 32046-32053. doi:10.1074/jbc.M201750200

Damoiseaux, J. S., Smith, S. M., Witter, M. P., Sanz-Arigita, E. J., Barkhof, F., Scheltens, P., et al. (2009). White matter tract integrity in aging and Alzheimer's disease. Human Brain Mapping, 30(4), 1051-1059. doi:10.1002/hbm.20563

de la Fuente, A. G., Queiroz, R. M. L., Ghosh, T., McMurran, C. E., Cubillos, J. F., Bergles, D. E., et al. (2020). Changes in the oligodendrocyte progenitor cell proteome with ageing. Molecular & Cellular Proteomics, 19(8), 1281-1302. doi:10.1074/mcp.RA120.002102

de la Monte, S. M. (1989). Quantitation of cerebral atrophy in preclinical and end-stage Alzheimer's disease. Annals of Neurology, 25(5), 450-459. doi:10.1002/ana.410250506

Dean, D. C., Hurley, S. A., Kecskemeti, S. R., O'Grady, J. P., Canda, C., Davenport-Sis, N. J., et al. (2017). Association of amyloid pathology with myelin alteration in preclinical Alzheimer disease. JAMA Neurology, 74(1), 41-49. doi:10.1001/jamaneurol.2016.3232

Desai, M. K., Mastrangelo, M. A., Ryan, D. A., Sudol, K. L., Narrow, W. C., & Bowers, W. J. (2010). Early oligodendrocyte/myelin pathology in Alzheimer's disease mice constitutes a novel therapeutic target. The American Journal of Pathology, 177(3), 1422-1435. doi:10.2353/ajpath.2010.100087

Desai, M. K., Sudol, K. L., Janelsins, M. C., Mastrangelo, M. A., Frazer, M. E., & Bowers, W. J. (2009). Triple-transgenic Alzheimer's disease mice exhibit region-specific abnormalities in brain myelination patterns prior to appearance of amyloid and tau pathology. Glia, 57(1), 54-65. doi:10.1002/glia.20734

Dobin, A., Davis, C. A., Schlesinger, F., Drenkow, J., Zaleski, C., Jha, S., et al. (2013). STAR: Ultrafast universal RNA-seq aligner. Bioinformatics (Oxford, England), 29(1), 15-21. doi:10.1093/bioinformatics/bts635

Domingues, H. S., Cruz, A., Chan, J. R., Relvas, J. B., Rubinstein, B., & Pinto, I. M. (2018). Mechanical plasticity during oligodendrocyte differentiation and myelination. Glia, 66(1), 5-14. doi:10.1002/glia.23206

Elbaz, B., & Popko, B. (2019). Molecular control of oligodendrocyte development. Trends in Neurosciences, 42(4), 263-277. doi:S0166-2236(19)30002-5

Ferreira, S., Pitman, K. A., Wang, S., Summers, B. S., Bye, N., Young, K. M., et al. (2020). Amyloidosis is associated with thicker myelin and increased oligodendrogenesis in the adult mouse brain. Journal of Neuroscience Research, 98(10), 1905-1932. doi:10.1002/jnr.24672

Fessel, J. (2022). Reversing Alzheimer's disease dementia with clemastine, fingolimod, or rolipram, plus anti-amyloid therapy. Alzheimer's & Dementia: Translational Research & Clinical Interventions, 8(1), e12242. doi:10.1002/trc2.12242

Fields, R. D. (2008). White matter in learning, cognition and psychiatric disorders. Trends in Neurosciences, 31(7), 361-370. doi:10.1016/j.tins.2008.04.001

Fields, R. D. (2015). A new mechanism of nervous system plasticity: Activity-dependent myelination. Nature Reviews. Neuroscience, 16(12), 756-767. doi:10.1038/nrn4023

Fornasiero, E. F., Mandad, S., Wildhagen, H., Alevra, M., Rammner, B., Keihani, S., et al. (2018). Precisely measured protein lifetimes in the mouse brain reveal differences across tissues and subcellular fractions. Nature Communications, 9(1), 4230. doi:10.1038/s41467-018-06519-0

Friess, M., Hammann, J., Unichenko, P., Luhmann, H. J., White, R., & Kirischuk, S. (2016). Intracellular ion signalling influences myelin basic protein synthesis in oligodendrocyte precursor cells. Cell Calcium, 60(5), 322-330. doi:10.1016/j.ceca.2016.06.009

Fröhlich, D., Kuo, W. P., Frühbeis, C., Sun, J., Zehendner, C. M., Luhmann, H. J., et al. (1983). Research. Research, 369(1652), 20130510. Retrieved from https://www.ncbi.nlm.nih.gov/pmc/articles/PMC4142031/

Frohlich, D., Kuo, W. P., Fruhbeis, C., Sun, J., Zehendner, C. M., Luhmann, H. J., et al. (2014). Multifaceted effects of oligodendroglial EVs on neurons: Impact on neuronal

firing rate, signal transduction and gene regulation. Philosophical Transactions of the Royal Society of London. Series B, Biological Sciences, 369(1652), 20130510. doi: 10.1098/rstb.2013.0510. doi:10.1098/rstb.2013.0510

Frühbeis, C., Kuo-Elsner, W. P., Müller, C., Barth, K., Peris, L., Tenzer, S., et al. (2020). Oligodendrocytes support axonal transport and maintenance via exosome secretion. PLoS Biology, 18(12), e3000621. doi:10.1371/journal.pbio.3000621

Fruhbeis, C., Kuo-Elsner, W. P., Muller, C., Barth, K., Peris, L., Tenzer, S., et al. (2020). Oligodendrocytes support axonal transport and maintenance via exosome secretion. PLoS Biology, 18(12), e3000621. doi:10.1371/journal.pbio.3000621

Frykman, S., Teranishi, Y., Hur, J., Sandebring, A., Yamamoto, N. G., Ancarcrona, M., et al. (2012). Identification of two novel synaptic gamma-secretase associated proteins that affect amyloid beta-peptide levels without altering notch processing. Neurochemistry International, 61(1), 108-118. doi:10.1016/j.neuint.2012.03.016

Gamarra, M., Gonzalez, E., Azkargorta, M., Falcon, J. M., Elortza, F., & Baleriola, J. (2021). Astrocyte-derived extracellular vesicles modulate local translation in neurons. Paper presented at the Glia, 69. pp. E295-E296.

Gamarra, M., Blanco-Urrejola, M., Batista, A. F. R., Imaz, J., & Baleriola, J. (2020). Object-based analyses in FIJI/ImageJ to measure local RNA translation sites in neurites in response to Abeta1-42 oligomers. Frontiers in Neuroscience, 14, 547. doi:10.3389/fnins.2020.00547

Garnier-Crussard, A., Bougacha, S., Wirth, M., Dautricourt, S., Sherif, S., Landeau, B., et al. (2022). White matter hyperintensity topography in Alzheimer’s disease and links to cognition. Alzheimer's & Dementia: The Journal of the Alzheimer's Association, 18(3), 422-433. doi:10.1002/alz.12410

Ghosh, A., Mizuno, K., Tiwari, S. S., Proitsi, P., Gomez Perez-Nievas, B., Glennon, E., et al. (2020). Alzheimer's disease-related dysregulation of mRNA translation causes key pathological features with ageing. Translational Psychiatry, 10(1), 192-7. doi:10.1038/s41398-020-00882-7

Grubman, A., Chew, G., Ouyang, J. F., Sun, G., Choo, X. Y., McLean, C., et al. (2019). A single-cell atlas of entorhinal cortex from individuals with Alzheimer's disease reveals cell-type-specific gene expression regulation. Nature Neuroscience, 22(12), 2087-2097. doi:10.1038/s41593-019-0539-4

Han, S. P., Tang, Y. H., & Smith, R. (2010). Functional diversity of the hnRNPs: Past, present and perspectives. The Biochemical Journal, 430(3), 379-392. doi:10.1042/BJ20100396

Harauz, G., & Boggs, J. M. (2013). Myelin management by the 18.5-kDa and 21.5-kDa classic myelin basic protein isoforms. Journal of Neurochemistry, 125(3), 334-361. doi:10.1111/jnc.12195

Harauz, G., Ladizhansky, V., & Boggs, J. M. (2009). Structural polymorphism and multifunctionality of myelin basic protein. Biochemistry, 48(34), 8094-8104. doi:10.1021/bi901005f

Harauz, G., & Musse, A. A. (2007). A tale of two citrullines--structural and functional aspects of myelin basic protein deimination in health and disease. Neurochemical Research, 32(2), 137-158. doi:10.1007/s11064-006-9108-9

Hardy, J. A., & Higgins, G. A. (1992). Alzheimer's disease: The amyloid cascade hypothesis. Science (New York, N.Y.), 256(5054), 184-185. doi:10.1126/science.1566067

Hartline, D. K. (2008). What is myelin? Neuron Glia Biology, 4(2), 153-163. doi:10.1017/S1740925X09990263

Haukedal, H., & Freude, K. K. (2021). Implications of glycosylation in Alzheimer's disease. Frontiers in Neuroscience, 14, 625348. doi:10.3389/fnins.2020.625348

Hector, A., & Brouillette, J. (2021). Hyperactivity induced by soluble amyloid-beta oligomers in the early stages of Alzheimer's disease. Frontiers in Molecular Neuroscience, 13, 600084. doi:10.3389/fnmol.2020.600084

Herbert, A. L., Fu, M., Drerup, C. M., Gray, R. S., Harty, B. L., Ackerman, S. D., et al. (2017). Dynein/dynactin is necessary for anterograde transport of mbp mRNA in oligodendrocytes and for myelination in vivo. Proceedings of the National Academy of

Sciences of the United States of America, 114(43), E9153-E9162. doi:10.1073/pnas.1711088114

Hirschfeld, L. R., Risacher, S. L., Nho, K., & Saykin, A. J. (2022). Myelin repair in Alzheimer's disease: A review of biological pathways and potential therapeutics. Translational Neurodegeneration, 11(1), 47. doi:10.1186/s40035-022-00321-1

Hoch-Kraft, P., White, R., Tenzer, S., Krämer-Albers, E., Trotter, J., & Gonsior, C. (2018). Dual role of the RNA helicase DDX5 in post-transcriptional regulation of myelin basic protein in oligodendrocytes. Journal of Cell Science, 131(9), jcs204750. doi:10.1242/jcs.204750

Hoek, K. S., Kidd, G. J., Carson, J. H., & Smith, R. (1998). hnRNP A2 selectively binds the cytoplasmic transport sequence of myelin basic protein mRNA. Biochemistry, 37(19), 7021-7029. doi:bi9800247

Horiuchi, M., Maezawa, I., Itoh, A., Wakayama, K., Jin, L., Itoh, T., et al. (2012). Amyloid β1-42 oligomer inhibits myelin sheet formation in vitro. Neurobiology of Aging, 33(3), 499-509. doi:10.1016/j.neurobiolaging.2010.05.007

Howitt, J., & Hill, A. F. (2016). EVs in the pathology of neurodegenerative diseases. The Journal of Biological Chemistry, 291(52), 26589-26597. doi:10.1074/jbc.R116.757955

Hu, X., Hicks, C. W., He, W., Wong, P., Macklin, W. B., Trapp, B. D., et al. (2006). Bace1 modulates myelination in the central and peripheral nervous system. Nature Neuroscience, 9(12), 1520-1525. doi:10.1038/nn1797

Hughes, A. N., & Appel, B. (2020). Microglia phagocytose myelin sheaths to modify developmental myelination. Nature Neuroscience, 23(9), 1055-1066. doi:10.1038/s41593-020-0654-2

Inano, S., Takao, H., Hayashi, N., Abe, O., & Ohtomo, K. (2011). Effects of age and gender on white matter integrity. AJNR. American Journal of Neuroradiology, 32(11), 2103-2109. doi:10.3174/ajnr.A2785

Jantaratnotai, N., Ryu, J. K., Kim, S. U., & McLRNAon, J. G. (2003). Amyloid beta peptide-induced corpus callosum damage and glial activation in vivo. Neuroreport, 14(11), 1429-1433. doi:10.1097/00001756-200308060-00005

Jung, Y., Seo, J., Ryu, H. G., Kim, D., Lee, K., & Kim, K. (2020). BDNF-induced local translation of GluA1 is regulated by HNRNP A2/B1. Science Advances, 6(47), eabd2163. doi: 10.1126/sciadv.abd2163. Print 2020 Nov. doi:10.1126/sciadv.abd2163

Jungbauer, L. M., Yu, C., Laxton, K. J., & LaDu, M. J. (2009). Preparation of fluorescently-labeled amyloid-beta peptide assemblies: The effect of fluorophore conjugation on structure and function. Journal of Molecular Recognition: JMR, 22(5), 403-413. doi:10.1002/jmr.948

Karthigasan, J., Garvey, J. S., Ramamurthy, G. V., & Kirschner, D. A. (1996). Immunolocalization of 17 and 21.5 kDa MBP isoforms in compact myelin and radial component. Journal of Neurocytology, 25(1), 1-7. doi:10.1007/BF02284781

Kavroulakis, E., Simos, P. G., Kalaitzakis, G., Maris, T. G., Karageorgou, D., Zaganas, I., et al. (2018). Myelin content changes in probable Alzheimer's disease and mild cognitive impairment: Associations with age and severity of neuropsychiatric impairment. Journal of Magnetic Resonance Imaging: JMRI, 47(5), 1359-1372. doi:10.1002/jmri.25849 [doi]

Kimberly, W. T., Zheng, J. B., Guénette, S. Y., & Selkoe, D. J. (2001). The intracellular domain of the beta-amyloid precursor protein is stabilized by Fe65 and translocates to the nucleus in a notch-like manner. The Journal of Biological Chemistry, 276(43), 40288-40292. doi:10.1074/jbc.C100447200

Kitada, M., & Rowitch, D. H. (2006). Transcription factor co-expression patterns indicate heterogeneity of oligodendroglial subpopulations in adult spinal cord. Glia, 54(1), 35-46. doi:10.1002/glia.20354

Kolisnyk, B., Al-Onaizi, M., Soreq, L., Barbash, S., Bekenstein, U., Haberman, N., et al. (2017). Cholinergic surveillance over hippocampal RNA metabolism and Alzheimer's-like pathology. Cerebral Cortex (New York, N.Y.: 1991), 27(7), 3553-3567. doi:10.1093/cercor/bhw177

Kosturko, L. D., Maggipinto, M. J., D'Sa, C., Carson, J. H., & Barbarese, E. (2005). The microtubule-associated protein tumor overexpressed gene binds to the RNA trafficking protein heterogeneous nuclear ribonucleoprotein A2. Molecular Biology of the Cell, 16(4), 1938-1947. doi:10.1091/mbc.E04-08-0709

Kosturko, L. D., Maggipinto, M. J., Korza, G., Lee, J. W., Carson, J. H., & Barbarese, E. (2006). Heterogeneous nuclear ribonucleoprotein (hnRNP) E1 binds to hnRNP A2 and inhibits translation of A2 response element mRNAs. Molecular Biology of the Cell, 17(8), 3521-3533. doi:10.1091/mbc.E05-10-0946

Kramer-Albers, E. (2020). Extracellular vesicles in the oligodendrocyte microenvironment. Neuroscience Letters, 725, 134915. doi:10.1016/j.neulet.2020.134915

Krämer-Albers, E., Bretz, N., Tenzer, S., Winterstein, C., Möbius, W., Berger, H., et al. (2007). Oligodendrocytes secrete EVs containing major myelin and stress-protective proteins: Trophic support for axons? Proteomics. Clinical Applications, 1(11), 1446-1461. doi:10.1002/prca.200700522

Krämer-Albers, E., & White, R. (2011). From axon-glial signalling to myelination: The integrating role of oligodendroglial fyn kinase. Cellular and Molecular Life Sciences: CMLS, 68(12), 2003-2012. doi:10.1007/s00018-010-0616-z

Kuchibhotla, K. V., Goldman, S. T., Lattarulo, C. R., Wu, H., Hyman, B. T., & Bacskai, B. J. (2008). Abeta plaques lead to aberrant regulation of calcium homeostasis in vivo resulting in structural and functional disruption of neuronal networks. Neuron, 59(2), 214-225. doi:10.1016/j.neuron.2008.06.008

Kuhn, S., Gritti, L., Crooks, D., & Dombrowski, Y. (2019). Oligodendrocytes in development, myelin generation and beyond. Cells, 8(11), 1424. doi:10.3390/cells8111424

Lam, M., Takeo, K., Almeida, R. G., Cooper, M. H., Wu, K., Iyer, M., et al. (2022). CNS myelination requires VAMP2/3-mediated membrane expansion in oligodendrocytes. Nature Communications, 13(1), 5583-4. doi:10.1038/s41467-022-33200-4

Lanoiselée, H., Nicolas, G., Wallon, D., Rovelet-Lecrux, A., Lacour, M., Rousseau, S., et al. (2017). APP, PSEN1, and PSEN2 mutations in early-onset Alzheimer disease: A genetic screening study of familial and sporadic cases. PLoS Medicine, 14(3), e1002270. doi:10.1371/journal.pmed.1002270

Lau, S., Cao, H., Fu, A. K. Y., & Ip, N. Y. (2020a). Single-nucleus transcriptome analysis reveals dysregulation of angiogenic endothelial cells and neuroprotective glia in Alzheimer's disease. Proceedings of the National Academy of Sciences of the United States of America, 117(41), 25800-25809. doi:10.1073/pnas.2008762117

Lau, S., Cao, H., Fu, A. K. Y., & Ip, N. Y. (2020b). Single-nucleus transcriptome analysis reveals dysregulation of angiogenic endothelial cells and neuroprotective glia in Alzheimer's disease. Proceedings of the National Academy of Sciences of the United States of America, 117(41), 25800-25809. doi:10.1073/pnas.2008762117

Lee, J., Padmanabhan, A., Shin, J., Zhu, S., Guo, F., Kanki, J. P., et al. (2010). Oligodendrocyte progenitor cell numbers and migration are regulated by the zebrafish orthologs of the NF1 tumor suppressor gene. Human Molecular Genetics, 19(23), 4643-4653. doi:10.1093/hmg/ddq395

Lee, S., Leach, M. K., Redmond, S. A., Chong, S. Y. C., Mellon, S. H., Tuck, S. J., et al. (2012). A culture system to study oligodendrocyte myelination processes using engineered nanofibers. Nature Methods, 9(9), 917-922. doi:10.1038/nmeth.2105 [doi]

Li, C., & Gotz, J. (2017). Somatodendritic accumulation of tau in Alzheimer's disease is promoted by fyn-mediated local protein translation. The EMBO Journal, 36(21), 3120-3138. doi:10.15252/embj.201797724

Liu, A., Li, J., Marin-Husstege, M., Kageyama, R., Fan, Y., Gelinas, C., et al. (2006). A molecular insight of Hes5-dependent inhibition of myelin gene expression: Old partners and new players. The EMBO Journal, 25(20), 4833-4842. doi:10.1038/sj.emboj.7601352

Long, J. M., & Holtzman, D. M. (2019). Alzheimer disease: An update on pathobiology and treatment strategies. Cell, 179(2), 312-339. doi:10.1016/j.cell.2019.09.001

Love, M. I., Huber, W., & Anders, S. (2014). Moderated estimation of fold change and dispersion for RNA-seq data with DESeq2. Genome Biology, 15(12), 550-8. doi:550

Lyons, D. A., Naylor, S. G., Scholze, A., & Talbot, W. S. (2009). Kif1b is essential for mRNA localization in oligodendrocytes and development of myelinated axons. Nature Genetics, 41(7), 854-858. doi:10.1038/ng.376

Maggipinto, M., Rabiner, C., Kidd, G. J., Hawkins, A. J., Smith, R., & Barbarese, E. (2004). Increased expression of the MBP mRNA binding protein HnRNP A2 during oligodendrocyte differentiation. Journal of Neuroscience Research, 75(5), 614-623. doi:10.1002/jnr.20014

Manterola, L., Hernando-Rodriguez, M., Ruiz, A., Apraiz, A., Arrizabalaga, O., Vellon, L., et al. (2013). 1-42 beta-amyloid peptide requires PDK1/nPKC/rac 1 pathway to induce neuronal death. Translational Psychiatry, 3(1), e219. doi:10.1038/tp.2012.147

Marisca, R., Hoche, T., Agirre, E., Hoodless, L. J., Barkey, W., Auer, F., et al. (2020). Functionally distinct subgroups of oligodendrocyte precursor cells integrate neural activity and execute myelin formation. Nature Neuroscience, 23(3), 363-374. doi:10.1038/s41593-019-0581-2

Marques, S., Zeisel, A., Codeluppi, S., van Bruggen, D., Mendanha Falcão, A., Xiao, L., et al. (2016a). Oligodendrocyte heterogeneity in the mouse juvenile and adult central nervous system. Science (New York, N.Y.), 352(6291), 1326-1329. doi:10.1126/science.aaf6463

Marques, S., Zeisel, A., Codeluppi, S., van Bruggen, D., Mendanha Falcão, A., Xiao, L., et al. (2016b). Oligodendrocyte heterogeneity in the mouse juvenile and adult central nervous system. Science (New York, N.Y.), 352(6291), 1326-1329. doi:10.1126/science.aaf6463

Martini, R., & Schachner, M. (1997). Molecular bases of myelin formation as revealed by investigations on mice deficient in glial cell surface molecules. Glia, 19(4), 298-310.

Mastrangelo, M. A., & Bowers, W. J. (2008). Detailed immunohistochemical characterization of temporal and spatial progression of Alzheimer's disease-related pathologies in male triple-transgenic mice. BMC Neuroscience, 9, 81-81. doi:10.1186/1471-2202-9-81

Mathys, H., Davila-Velderrain, J., Peng, Z., Gao, F., Mohammadi, S., Young, J. Z., et al. (2019). Single-cell transcriptomic analysis of Alzheimer's disease. Nature, 570(7761), 332-337. doi:10.1038/s41586-019-1195-2

McCann, C. J., Hasan, N. M., Padilla-Benavides, T., Roy, S., & Lutsenko, S. (2022). Heterogeneous nuclear ribonucleoprotein hnRNPA2/B1 regulates the abundance of the copper-transporter ATP7A in an isoform-dependent manner. Frontiers in Molecular Biosciences, 9, 1067490. doi:10.3389/fmolb.2022.1067490

McGlincy, N. J., Tan, L., Paul, N., Zavolan, M., Lilley, K. S., & Smith, C. W. J. (2010). Expression proteomics of UPF1 knockdown in HeLa cells reveals autoregulation of hnRNP A2/B1 mediated by alternative splicing resulting in nonsense-mediated mRNA decay. BMC Genomics, 11, 565-565. doi:10.1186/1471-2164-11-565

McNamara, N. B., Munro, D. A. D., Bestard-Cuche, N., Uyeda, A., Bogie, J. F. J., Hoffmann, A., et al. (2022). Microglia regulate central nervous system myelin growth and integrity. Nature, doi:10.1038/s41586-022-05534-y

Mendoza-Naranjo, A., Gonzalez-Billault, C., & Maccioni, R. B. (2007). Abeta1-42 stimulates actin polymerization in hippocampal neurons through Rac1 and Cdc42 rho GTPases. Journal of Cell Science, 120(Pt 2), 279-288. doi:10.1242/jcs.03323

Meschkat, M., Steyer, A. M., Weil, M., Kusch, K., Jahn, O., Piepkorn, L., et al. (2022). White matter integrity in mice requires continuous myelin synthesis at the inner tongue. Nature Communications, 13(1), 1163. doi:10.1038/s41467-022-28720-y

Miller, R. H. (2018). Calcium control of myelin sheath growth. Nature Neuroscience, 21(1), 2-3. doi:10.1038/s41593-017-0043-7

Min, Y., Kristiansen, K., Boggs, J. M., Husted, C., Zasadzinski, J. A., & Israelachvili, J. (2009). Interaction forces and adhesion of supported myelin lipid bilayers modulated by myelin basic protein. Proceedings of the National Academy of Sciences of the United States of America, 106(9), 3154-3159. doi:10.1073/pnas.0813110106

Mirra, S. S., Heyman, A., McKeel, D., Sumi, S. M., Crain, B. J., Brownlee, L. M., et al. (1991). The consortium to establish a registry for Alzheimer's disease (CERAD). part II.

standardization of the neuropathologic assessment of Alzheimer's disease. Neurology, 41(4), 479-486. doi:10.1212/wnl.41.4.479

Mitake, S., Ojika, K., & Hirano, A. (1997). Hirano bodies and alzheimer's disease. *The Kaohsiung Journal of Medical Sciences, 13*(1), 10-18.

Mitew, S., Kirkcaldie, M. T. K., Halliday, G. M., Shepherd, C. E., Vickers, J. C., & Dickson, T. C. (2010). Focal demyelination in alzheimer's disease and transgenic mouse models. Acta Neuropathologica, 119(5), 567-577. doi:10.1007/s00401-010-0657-2

Mizukami, K., Ishikawa, M., Iwakiri, M., Ikonomovic, M. D., Dekosky, S. T., Kamma, H., et al. (2005). Immunohistochemical study of the hnRNP A2 and B1 in the hippocampal formations of brains with Alzheimer's disease. Neuroscience Letters, 386(2), 111-115. doi:10.1016/j.neulet.2005.05.070

Möbius, W., Cooper, B., Kaufmann, W. A., Imig, C., Ruhwedel, T., Snaidero, N., et al. (2010). Electron microscopy of the mouse central nervous system. Methods in Cell Biology, 96, 475-512. doi:10.1016/S0091-679X(10)96020-2

Montague, P., Barrie, J. A., Thomson, C. E., Kirkham, D., McCallion, A. S., Davies, R. W., et al. (1998). Cytoskeletal and nuclear localization of myelin oligodendrocytic basic protein isoforms. The European Journal of Neuroscience, 10(4), 1321-1328. doi:10.1046/j.1460-9568.1998.00143.x

Moore, S., Meschkat, M., Ruhwedel, T., Trevisiol, A., Tzvetanova, I. D., Battefeld, A., et al. (2020). A role of oligodendrocytes in information processing. Nature Communications, 11(1), 5497-7. doi:10.1038/s41467-020-19152-7

Morabito, S., Miyoshi, E., Michael, N., Shahin, S., Martini, A. C., Head, E., et al. (2021). Single-nucleus chromatin accessibility and transcriptomic characterization of Alzheimer's disease. Nature Genetics, 53(8), 1143-1155. doi:10.1038/s41588-021-00894-z

Mukherjee, C., Kling, T., Russo, B., Miebach, K., Kess, E., Schifferer, M., et al. (2020). Oligodendrocytes provide antioxidant defense function for neurons by secreting ferritin heavy chain. Cell Metabolism, 32(2), 259-272.e10. doi:10.1016/j.cmet.2020.05.019

Muller, C., Bauer, N. M., Schafer, I., & White, R. (2013). Making myelin basic protein - from mRNA transport to localized translation. Frontiers in Cellular Neuroscience, 7, 169. doi:10.3389/fncel.2013.00169

Müller, C., Schäfer, I., Luhmann, H. J., & White, R. (2015). Oligodendroglial argonaute protein Ago2 associates with molecules of the mbp mRNA localization machinery and is a downstream target of fyn kinase. Frontiers in Cellular Neuroscience, 9, 328. doi:10.3389/fncel.2015.00328

Müller, U. C., Deller, T., & Korte, M. (2017). Not just amyloid: Physiological functions of the amyloid precursor protein family. Nature Reviews. Neuroscience, 18(5), 281-298. doi:10.1038/nrn.2017.29

Munro, T. P., Magee, R. J., Kidd, G. J., Carson, J. H., Barbarese, E., Smith, L. M., et al. (1999). Mutational analysis of a heterogeneous nuclear ribonucleoprotein A2 response element for RNA trafficking. The Journal of Biological Chemistry, 274(48), 34389-34395. doi:10.1074/jbc.274.48.34389

Murdock, M. H., & Tsai, L. (2023). Insights into Alzheimer's disease from single-cell genomic approaches. Nature Neuroscience, doi:10.1038/s41593-022-01222-2

Nasrabady, S. E., Rizvi, B., Goldman, J. E., & Brickman, A. M. (2018a). White matter changes in Alzheimer's disease: A focus on myelin and oligodendrocytes. Acta Neuropathologica Communications, 6(1), 22. doi:10.1186/s40478-018-0515-3

Nasrabady, S. E., Rizvi, B., Goldman, J. E., & Brickman, A. M. (2018b). White matter changes in Alzheimer's disease: A focus on myelin and oligodendrocytes. Acta Neuropathologica Communications, 6(1), 22-3. doi:10.1186/s40478-018-0515-3 [doi]

Nave, K. (2010). Myelination and support of axonal integrity by glia. Nature, 468(7321), 244-252. doi:10.1038/nature09614

Nave, K., & Werner, H. B. (2014). Myelination of the nervous system: Mechanisms and functions. Annual Review of Cell and Developmental Biology, 30, 503-533. doi:10.1146/annurev-cellbio-100913-013101

Nawaz, S., Sanchez, P., Schmitt, S., Snaidero, N., Mitkovski, M., Velte, C., et al. (2015). Actin filament turnover drives leading edge growth during myelin sheath formation in the central nervous system. Developmental Cell, 34(2), 139-151. doi:10.1016/j.devcel.2015.05.013

Nery, L. R., Eltz, N. S., Hackman, C., Fonseca, R., Altenhofen, S., Guerra, H. N., et al. (2014). Brain intraventricular injection of amyloid-beta in zebrafish embryo impairs cognition and increases tau phosphorylation, effects reversed by lithium. PloS One, 9(9), e105862. doi:10.1371/journal.pone.0105862

Nie, X., Falangola, M. F., Ward, R., McKinnon, E. T., Helpern, J. A., Nietert, P. J., et al. (2019). Diffusion MRI detects longitudinal white matter changes in the 3xTg-AD mouse model of Alzheimer's disease. Magnetic Resonance Imaging, 57, 235-242. doi:10.1016/j.mri.2018.12.003

A novel fluorescent ceramide analogue for studying membrane traffic in animal cells: Accumulation at the golgi apparatus results in altered spectral properties of the sphingolipid precursor.(1991). The Journal of Cell Biology, 113(6), 1267-1279. Retrieved from https://www.ncbi.nlm.nih.gov/pmc/articles/PMC2289039/

Oddo, S., Caccamo, A., Shepherd, J. D., Murphy, M. P., Golde, T. E., Kayed, R., et al. (2003). Triple-transgenic model of Alzheimer's disease with plaques and tangles: Intracellular abeta and synaptic dysfunction. Neuron, 39(3), 409-421. doi:10.1016/s0896-6273(03)00434-3

Oddo, S., Caccamo, A., Tran, L., Lambert, M. P., Glabe, C. G., Klein, W. L., et al. (2006). Temporal profile of amyloid-beta (abeta) oligomerization in an in vivo model of alzheimer disease. A link between abeta and tau pathology. The Journal of Biological Chemistry, 281(3), 1599-1604. doi:10.1074/jbc.M507892200

Osterhout, D. J., Wolven, A., Wolf, R. M., Resh, M. D., & Chao, M. V. (1999). Morphological differentiation of oligodendrocytes requires activation of fyn tyrosine kinase. The Journal of Cell Biology, 145(6), 1209-1218. doi:10.1083/jcb.145.6.1209

Ovadi, J., & Orosz, F. (2009). An unstructured protein with destructive potential: TPPP/p25 in neurodegeneration. BioEssays: News and Reviews in Molecular, Cellular and Developmental Biology, 31(6), 676-686. doi:10.1002/bies.200900008

Pagano, R. E., Martin, O. C., Kang, H. C., & Haugland, R. P. (1991). A novel fluorescent ceramide analogue for studying membrane traffic in animal cells: Accumulation at the golgi apparatus results in altered spectral properties of the sphingolipid precursor. The Journal of Cell Biology, 113(6), 1267-1279. doi:91258396

Parente, D. B., Gasparetto, E. L., da Cruz, L. C. H., Domingues, R. C., Baptista, A. C., Carvalho, A. C. P., et al. (2008). Potential role of diffusion tensor MRI in the differential diagnosis of mild cognitive impairment and Alzheimer's disease. AJR. American Journal of Roentgenology, 190(5), 1369-1374. doi:10.2214/AJR.07.2617

Peckham, H., Giuffrida, L., Wood, R., Gonsalvez, D., Ferner, A., Kilpatrick, T. J., et al. (2016). Fyn is an intermediate kinase that BDNF utilizes to promote oligodendrocyte myelination. Glia, 64(2), 255-269. doi:10.1002/glia.22927

Philips, T., & Rothstein, J. D. (2017). Oligodendroglia: Metabolic supporters of neurons. The Journal of Clinical Investigation, 127(9), 3271-3280. doi:10.1172/JCI90610

Quintela-Lopez, T., Ortiz-Sanz, C., Serrano-Regal, M. P., Gaminde-Blasco, A., Valero, J., Baleriola, J., et al. (2019). Abeta oligomers promote oligodendrocyte differentiation and maturation via integrin beta1 and fyn kinase signaling. Cell Death & Disease, 10(6), 445-8. doi:10.1038/s41419-019-1636-8

Rajendran, L., Honsho, M., Zahn, T. R., Keller, P., Geiger, K. D., Verkade, P., et al. (2006). Alzheimer's disease beta-amyloid peptides are released in association with EVsEVs. Proceedings of the National Academy of Sciences of the United States of America, 103(30), 11172-11177. doi:10.1073/pnas.0603838103

Raju, C. S., Göritz, C., Nord, Y., Hermanson, O., López-Iglesias, C., Visa, N., et al. (2008). In cultured oligodendrocytes the A/B-type hnRNP CBF-A accompanies MBP mRNA bound to mRNA trafficking sequences. Molecular Biology of the Cell, 19(7), 3008-3019. doi:10.1091/mbc.e07-10-1083

Recuero, M., Serrano, E., Bullido, M. J., & Valdivieso, F. (2004). Abeta production as consequence of cellular death of a human neuroblastoma overexpressing APP. FEBS Letters, 570(1-3), 114-118. doi:10.1016/j.febslet.2004.06.025

Roher, A. E., Weiss, N., Kokjohn, T. A., Kuo, Y., Kalback, W., Anthony, J., et al. (2002). Increased A beta peptides and reduced cholesterol and myelin proteins characterize white matter degeneration in Alzheimer's disease. Biochemistry, 41(37), 11080-11090. doi:10.1021/bi026173d

Ruiz, A., Alberdi, E., & Matute, C. (2014). CGP37157, an inhibitor of the mitochondrial na+/Ca2+ exchanger, protects neurons from excitotoxicity by blocking voltage-gated Ca2+ channels. Cell Death & Disease, 5(4), e1156. doi:10.1038/cddis.2014.134

Rush, T., Martinez-Hernandez, J., Dollmeyer, M., Frandemiche, M. L., Borel, E., Boisseau, S., et al. (2018). Synaptotoxicity in Alzheimer's disease involved a dysregulation of actin cytoskeleton dynamics through cofilin 1 phosphorylation. The Journal of Neuroscience : The Official Journal of the Society for Neuroscience, 38(48), 10349-10361. doi:10.1523/JNEUROSCI.1409-18.2018

Rybak-Wolf, A., & Plass, M. (2021a). RNA dynamics in Alzheimer's disease. Molecules, 26(17), 5113. doi:10.3390/molecules26175113

Rybak-Wolf, A., & Plass, M. (2021b). RNA dynamics in Alzheimer's disease. Molecules (Basel, Switzerland), 26(17), 5113. doi: 10.3390/molecules26175113.

Sachdev, P. S., Zhuang, L., Braidy, N., & Wen, W. (2013). Is alzheimer's a disease of the white matter? Current Opinion in Psychiatry, 26(3), 244-251. doi:10.1097/YCO.0b013e32835ed6e8

Samanta, J., & Kessler, J. A. (2004). Interactions between ID and OLIG proteins mediate the inhibitory effects of BMP4 on oligodendroglial differentiation. Development (Cambridge, England), 131(17), 4131-4142. doi:10.1242/dev.01273

Samanta, J., & Salzer, J. L. (2015). Myelination: Actin disassembly leads the way. Developmental Cell, 34(2), 129-130. doi:S1534-5807(15)00457-8

Sánchez-Gómez, M. V., Serrano, M. P., Alberdi, E., Pérez-Cerdá, F., & Matute, C. (2018). Isolation, expansion, and maturation of oligodendrocyte lineage cells obtained from rat neonatal brain and optic nerve. Methods in Molecular Biology (Clifton, N.J.), 1791, 95-113. doi:10.1007/978-1-4939-7862-5_8

Schäfer, I., Müller, C., Luhmann, H. J., & White, R. (2016). MOBP levels are regulated by fyn kinase and affect the morphological differentiation of oligodendrocytes. Journal of Cell Science, 129(5), 930-942. doi:10.1242/jcs.172148

Schafer, I., Muller, C., Luhmann, H. J., & White, R. (2016). MOBP levels are regulated by fyn kinase and affect the morphological differentiation of oligodendrocytes. Journal of Cell Science, 129(5), 930-942. doi:10.1242/jcs.172148

Schmidt, E. K., Clavarino, G., Ceppi, M., & Pierre, P. (2009). SUnSET, a nonradioactive method to monitor protein synthesis. Nature Methods, 6(4), 275-277. doi:10.1038/nmeth.1314

Selkoe, D. J., Brown, B. A., Salazar, F. J., & Marotta, C. A. (1981). Myelin basic protein in alzheimer disease neuronal fractions and mammalian neurofilament preparations. Annals of Neurology, 10(5), 429-436. doi:10.1002/ana.410100505

Selkoe, D. J. (1991). The molecular pathology of Alzheimer's disease. Neuron, 6(4), 487-498. doi:10.1016/0896-6273(91)90052-2

Selkoe, D. J., & Hardy, J. (2016). The amyloid hypothesis of Alzheimer's disease at 25 years. EMBO Molecular Medicine, 8(6), 595-608. doi:10.15252/emmm.201606210

Skaper, S. D., Evans, N. A., Evans, N. A., Rosin, C., Facci, L., & Richardson, J. C. (2009). Oligodendrocytes are a novel source of amyloid peptide generation. Neurochemical Research, 34(12), 2243-2250. doi:10.1007/s11064-009-0022-9

Smirnova, E. V., Rakitina, T. V., Ziganshin, R. H., Arapidi, G. P., Saratov, G. A., Kudriaeva, A. A., et al. (2021). Comprehensive atlas of the myelin basic protein interaction landscape. Biomolecules, 11(11), 1628. doi:10.3390/biom11111628

Smith, G. S. T., Paez, P. M., Spreuer, V., Campagnoni, C. W., Boggs, J. M., Campagnoni, A. T., et al. (2011). Classical 18.5-and 21.5-kDa isoforms of myelin basic protein inhibit

calcium influx into oligodendroglial cells, in contrast to golli isoforms. Journal of Neuroscience Research, 89(4), 467-480. doi:10.1002/jnr.22570

Snaidero, N., Mobius, W., Czopka, T., Hekking, L. H. P., Mathisen, C., Verkleij, D., et al. (2014). Myelin membrane wrapping of CNS axons by PI(3,4,5)P3-dependent polarized growth at the inner tongue. Cell, 156(1-2), 277-290. doi:S0092-8674(13)01530-4

Snaidero, N., & Simons, M. (2014). Myelination at a glance. Journal of Cell Science, 127(Pt 14), 2999-3004. doi:10.1242/jcs.151043

Snaidero, N., Velte, C., Myllykoski, M., Raasakka, A., Ignatev, A., Werner, H. B., et al. (2017). Antagonistic functions of MBP and CNP establish cytosolic channels in CNS myelin. Cell Reports, 18(2), 314-323. doi:S2211-1247(16)31760-0

Söderberg, O., Gullberg, M., Jarvius, M., Ridderstråle, K., Leuchowius, K., Jarvius, J., et al. (2006). Direct observation of individual endogenous protein complexes in situ by proximity ligation. Nature Methods, 3(12), 995-1000. doi:10.1038/nmeth947

Song, J., Goetz, B. D., Baas, P. W., & Duncan, I. D. (2001). Cytoskeletal reorganization during the formation of oligodendrocyte processes and branches. Molecular and Cellular Neurosciences, 17(4), 624-636. doi:10.1006/mcne.2001.0974

Sperber, B. R., & McMorris, F. A. (2001). Fyn tyrosine kinase regulates oligodendroglial cell development but is not required for morphological differentiation of oligodendrocytes. Journal of Neuroscience Research, 63(4), 303-312. doi:10.1002/1097-4547

Stadelmann, C., Timmler, S., Barrantes-Freer, A., & Simons, M. (2019a). Myelin in the central nervous system: Structure, function, and pathology. Physiological Reviews, 99(3), 1381-1431. doi:10.1152/physrev.00031.2018

Stadelmann, C., Timmler, S., Barrantes-Freer, A., & Simons, M. (2019b). Myelin in the central nervous system: Structure, function, and pathology. Physiological Reviews, 99(3), 1381-1431. doi:10.1152/physrev.00031.2018

Stoppini, L., Buchs, P. A., & Muller, D. (1991a). A simple method for organotypic cultures of nervous tissue. Journal of Neuroscience Methods, 37(2), 173-182. doi:10.1016/0165-0270(91)90128-m

Stoppini, L., Buchs, P. A., & Muller, D. (1991b). A simple method for organotypic cultures of nervous tissue. Journal of Neuroscience Methods, 37(2), 173-182. doi:10.1016/0165-0270(91)90128-m

Stricker, N. H., Schweinsburg, B. C., Delano-Wood, L., Wierenga, C. E., Bangen, K. J., Haaland, K. Y., et al. (2009). Decreased white matter integrity in late-myelinating fiber pathways in Alzheimer's disease supports retrogenesis. NeuroImage, 45(1), 10-16. doi:10.1016/j.neuroimage.2008.11.027

Teipel, S. J., Bayer, W., Alexander, G. E., Zebuhr, Y., Teichberg, D., Kulic, L., et al. (2002). Progression of corpus callosum atrophy in alzheimer disease. Archives of Neurology, 59(2), 243-248. doi:10.1001/archneur.59.2.243

Thakurela, S., Garding, A., Jung, R. B., Muller, C., Goebbels, S., White, R., et al. (2016). The transcriptome of mouse central nervous system myelin. Scientific Reports, 6, 25828. doi:10.1038/srep25828

Thal, D. R., Rüb, U., Orantes, M., & Braak, H. (2002). Phases of A beta-deposition in the human brain and its relevance for the development of AD. Neurology, 58(12), 1791-1800. doi:10.1212/wnl.58.12.1791

Thibault, P. A., Ganesan, A., Kalyaanamoorthy, S., Clarke, J. W. E., Salapa, H. E., & Levin, M. C. (2021). hnRNP A/B proteins: An encyclopedic assessment of their roles in homeostasis and disease. Biology, 10(8), 712. doi: 10.3390/biology10080712.

Thomason, E. J., Escalante, M., Osterhout, D. J., & Fuss, B. (2020). The oligodendrocyte growth cone and its actin cytoskeleton: A fundamental element for progenitor cell migration and CNS myelination. Glia, 68(7), 1329-1346. doi:10.1002/glia.23735

tom Dieck, S., Kochen, L., Hanus, C., Heumuller, M., Bartnik, I., Nassim-Assir, B., et al. (2015). Direct visualization of newly synthesized target proteins in situ. Nature Methods, 12(5), 411-414. doi:10.1038/nmeth.3319

Torvund-Jensen, J., Steengaard, J., Reimer, L., Fihl, L. B., & Laursen, L. S. (2014). Transport and translation of MBP mRNA is regulated differently by distinct hnRNP proteins. Journal of Cell Science, 127(Pt 7), 1550-1564. doi:10.1242/jcs.140855

Transport and localization of exogenous myelin basic protein mRNA microinjected into oligodendrocytes. (1993). The Journal of Cell Biology, 123(2), 431-441. Retrieved from https://www.ncbi.nlm.nih.gov/pmc/articles/PMC2119827/

Tripathi, R. B., Jackiewicz, M., McKenzie, I. A., Kougioumtzidou, E., Grist, M., & Richardson, W. D. (2017). Remarkable stability of myelinating oligodendrocytes in mice. Cell Reports, 21(2), 316-323. doi:10.1016/j.celrep.2017.09.050

Truong, P. H., Ciccotosto, G. D., Merson, T. D., Spoerri, L., Chuei, M. J., Ayers, M., et al. (2019). Amyloid precursor protein and amyloid precursor-like protein 2 have distinct roles in modulating myelination, demyelination, and remyelination of axons. Glia, 67(3), 525-538. doi:10.1002/glia.23561

Umemori, H., Kadowaki, Y., Hirosawa, K., Yoshida, Y., Hironaka, K., Okano, H., et al. (1999). Stimulation of myelin basic protein gene transcription by fyn tyrosine kinase for myelination. The Journal of Neuroscience: The Official Journal of the Society for Neuroscience, 19(4), 1393-1397. doi:10.1523/JNEUROSCI.19-04-01393.1999

Umemori, H., Sato, S., Yagi, T., Aizawa, S., & Yamamoto, T. (1994). Initial events of myelination involve fyn tyrosine kinase signalling. Nature, 367(6463), 572-576. doi:10.1038/367572a0

Vanzulli, I., Papanikolaou, M., De-La-Rocha, I. C., Pieropan, F., Rivera, A. D., Gomez-Nicola, D., et al. (2020a). Disruption of oligodendrocyte progenitor cells is an early sign of pathology in the triple transgenic mouse model of Alzheimer's disease. Neurobiology of Aging, 94, 130-139. doi:10.1016/j.neurobiolaging.2020.05.016

Vanzulli, I., Papanikolaou, M., De-La-Rocha, I. C., Pieropan, F., Rivera, A. D., Gomez-Nicola, D., et al. (2020b). Disruption of oligodendrocyte progenitor cells is an early sign of pathology in the triple transgenic mouse model of Alzheimer's disease. Neurobiology of Aging, 94, 130-139. doi:10.1016/j.neurobiolaging.2020.05.016

Viola, K. L., & Klein, W. L. (2015). Amyloid β oligomers in Alzheimer's disease pathogenesis, treatment, and diagnosis. Acta Neuropathologica, 129(2), 183-206. doi:10.1007/s00401-015-1386-3

von Jonquieres, G., Mersmann, N., Klugmann, C. B., Harasta, A. E., Lutz, B., Teahan, O., et al. (2013). Glial promoter selectivity following AAV-delivery to the immature brain. PloS One, 8(6), e65646. doi:10.1371/journal.pone.0065646

von Rotz, R. C., Kohli, B. M., Bosset, J., Meier, M., Suzuki, T., Nitsch, R. M., et al. (2004). The APP intracellular domain forms nuclear multiprotein complexes and regulates the transcription of its own precursor. Journal of Cell Science, 117(Pt 19), 4435-4448. doi:10.1242/jcs.01323

Wang, S., & Young, K. M. (2014). White matter plasticity in adulthood. Neuroscience, 276, 148-160. doi:10.1016/j.neuroscience.2013.10.018

Waxman, S. G. (1997). Axon-glia interactions: Building a smart nerve fiber. Current Biology: CB, 7(7), 406. doi:10.1016/s0960-9822(06)00203-x

Waxman, S. G., & Ritchie, J. M. (1993). Molecular dissection of the myelinated axon. Annals of Neurology, 33(2), 121-136. doi:10.1002/ana.410330202

Westmark, C. J., Westmark, P. R., O'Riordan, K. J., Ray, B. C., Hervey, C. M., Salamat, M. S., et al. (2011). Reversal of fragile X phenotypes by manipulation of AbetaPP/abeta levels in Fmr1KO mice. PloS One, 6(10), e26549. doi:10.1371/journal.pone.0026549

White, R., Gonsior, C., Bauer, N. M., Kramer-Albers, E., Luhmann, H. J., & Trotter, J. (2012a). Heterogeneous nuclear ribonucleoprotein (hnRNP) F is a novel component of oligodendroglial RNA transport granules contributing to regulation of myelin basic protein (MBP) synthesis. The Journal of Biological Chemistry, 287(3), 1742-1754. doi:10.1074/jbc.M111.235010

White, R., Gonsior, C., Bauer, N. M., Kramer-Albers, E., Luhmann, H. J., & Trotter, J. (2012b). Heterogeneous nuclear ribonucleoprotein (hnRNP) F is a novel component of oligodendroglial RNA transport granules contributing to regulation of myelin basic protein (MBP) synthesis. The Journal of Biological Chemistry, 287(3), 1742-1754. doi:10.1074/jbc.M111.235010

White, R., Gonsior, C., Kramer-Albers, E., Stohr, N., Huttelmaier, S., & Trotter, J. (2008). Activation of oligodendroglial fyn kinase enhances translation of mRNAs transported in hnRNP A2-dependent RNA granules. The Journal of Cell Biology, 181(4), 579-586. doi:10.1083/jcb.200706164

Williamson, J. M., & Lyons, D. A. (2018). Myelin dynamics throughout life: An ever-changing landscape? Frontiers in Cellular Neuroscience, 12, 424. doi:10.3389/fncel.2018.00424

Wu, Y., Ma, Y., Liu, Z., Geng, Q., Chen, Z., & Zhang, Y. (2017a). Alterations of myelin morphology and oligodendrocyte development in early stage of Alzheimer's disease mouse model. Neuroscience Letters, 642, 102-106. doi:10.1016/j.neulet.2017.02.007

Wu, Y., Ma, Y., Liu, Z., Geng, Q., Chen, Z., & Zhang, Y. (2017b). Alterations of myelin morphology and oligodendrocyte development in early stage of Alzheimer's disease mouse model. Neuroscience Letters, 642, 102-106. doi:10.1016/j.neulet.2017.02.007

Xu, J., Chen, S., Ahmed, S. H., Chen, H., Ku, G., Goldberg, M. P., et al. (2001). Amyloid-β peptides are cytotoxic to oligodendrocytes. The Journal of Neuroscience, 21(1), RC118. doi:10.1523/JNEUROSCI.21-01-j0001.2001

Yeung, M. S. Y., Zdunek, S., Bergmann, O., Bernard, S., Salehpour, M., Alkass, K., et al. (2014). Dynamics of oligodendrocyte generation and myelination in the human brain. Cell, 159(4), 766-774. doi:10.1016/j.cell.2014.10.011

Yin, F. (2022). Lipid metabolism and Alzheimer's disease: Clinical evidence, mechanistic link and therapeutic promise. The FEBS Journal, doi:10.1111/febs.16344

Young, K., Psachoulia, K., Tripathi, R., Dunn, S., Cossell, L., Attwell, D., et al. (2013). Oligodendrocyte dynamics in the healthy adult CNS: Evidence for myelin remodelling. Neuron, 77(5), 873-885. doi:10.1016/j.neuron.2013.01.006

Yu, Y., Herman, P., Rothman, D. L., Agarwal, D., & Hyder, F. (2018). Evaluating the gray and white matter energy budgets of human brain function. Journal of Cerebral Blood Flow and Metabolism: Official Journal of the International Society of Cerebral Blood Flow and Metabolism, 38(8), 1339-1353. doi:10.1177/0271678X17708691

Zhan, X., Jickling, G. C., Ander, B. P., Stamova, B., Liu, D., Kao, P. F., et al. (2015). Myelin basic protein associates with AβPP, Aβ1-42, and amyloid plaques in cortex of Alzheimer's disease brain. Journal of Alzheimer's disease: JAD, 44(4), 1213-1229. doi:10.3233/JAD-142013

Zhan, X., Jickling, G. C., Ander, B. P., Liu, D., Stamova, B., Cox, C., et al. (2014). Myelin injury and degraded myelin vesicles in Alzheimer's disease. Current Alzheimer Research, 11(3), 232-238. doi:10.2174/1567205011666140131120922

Zhang M., Zhang J., Zhang W., Yao Z. (2018). Demyelination takes place prior to neuronal damage following intracerebroventricular injection of amyloid-beta oligomer. Neuropsychiatry, 8, 1770–1785. doi:10.4172/NEUROPSYCHIATRY.1000519

Zhang, P., Kishimoto, Y., Grammatikakis, I., Gottimukkala, K., Cutler, R. G., Zhang, S., et al. (2019). Senolytic therapy alleviates Aβ-associated oligodendrocyte progenitor cell senescence and cognitive deficits in an Alzheimer's disease model. Nature Neuroscience, 22(5), 719-728. doi:10.1038/s41593-019-0372-9

Zhang, X., Wang, R., Hu, D., Sun, X., Fujioka, H., Lundberg, K., et al. (2020). Oligodendroglial glycolytic stress triggers inflammasome activation and neuropathology in Alzheimer’s disease. Science Advances, 6(49), eabb8680. doi: 10.1126/sciadv.abb8680

Zhao, L. N., Long, H. W., Mu, Y., & Chew, L. Y. (2012a). The toxicity of amyloid beta oligomers. International Journal of Molecular Sciences, 13(6), 7303-7327. doi:10.3390/ijms13067303

Zhao, L. N., Long, H., Mu, Y., & Chew, L. Y. (2012b). The toxicity of amyloid β oligomers. International Journal of Molecular Sciences, 13(6), 7303-7327. doi:10.3390/ijms13067303

Zheng, H., & Koo, E. H. (2011). Biology and pathophysiology of the amyloid precursor protein. Molecular Neurodegeneration, 6(1), 27. doi:10.1186/1750-1326-6-27

Zhou, Y., Song, W. M., Andhey, P. S., Swain, A., Levy, T., Miller, K. R., et al. (2020a). Human and mouse single-nucleus transcriptomics reveal TREM2-dependent and

TREM2-independent cellular responses in Alzheimer's disease. Nature Medicine, 26(1), 131-142. doi:10.1038/s41591-019-0695-9

Zhou, Y., Song, W. M., Andhey, P. S., Swain, A., Levy, T., Miller, K. R., et al. (2020b). Human and mouse single-nucleus transcriptomics reveal TREM2-dependent and TREM2-independent cellular responses in Alzheimer's disease. Nature Medicine, 26(1), 131-142. doi:10.1038/s41591-019-0695-9

Zuchero, J. B., Fu, M., Sloan, S. A., Ibrahim, A., Olson, A., Zaremba, A., et al. (2015). CNS myelin wrapping is driven by actin disassembly. Developmental Cell, 34(2), 152-167. doi:S1534-5807(15)00400-1

Zuniga, G., Levy, S., Ramirez, P., De Mange, J., Gonzalez, E., Gamez, M., et al. (2022). Tau-induced deficits in nonsense-mediated mRNA decay contribute to neurodegeneration. Alzheimer's & Dementia: The Journal of the Alzheimer's Association, doi:10.1002/alz.12653